Master Thesis in Geosciences

Liverpool Land Lamprophyres

A petrographical and geochemical study

Dag Erlend Førsund

UNIVERSITY OF OSLO

FACULTY OF MATHEMATICS AND NATURAL SCIENCES

Liverpool Land Lamprophyres

A petrographical and geochemical study

Dag Erlend Førsund

Master Thesis in Geosciences

Discipline: Tectonics, petrology and geochemistry

Department of Geosciences

Faculty of Mathematics and Natural Sciences

UNIVERSITY OF OSLO

February 1, 2010

Tutor(s): Professor Arild Andresen
This work is published digitally through DUO – Digitale Utgivelser ved UiO
http://www.duo.uio.no
It is also catalogued in BIBSYS (http://www.bibsys.no/english)

Cover photo: Alkaline lamprophyric dyke from Liverpool Land.

Acknowledgements

I would like to thank my supervisor, Professor Arild Andresen for bringing me along to Liverpool Land, NW Greenland, and proposing this thesis. The expedition to Liverpool Land and the following work has been a great experience. His thorough review is also highly appreciated.

Professor Else-Ragnhild Neumann and post-doc Anders Mattias Lundmark deserve special thanks for always being available for questions and discussions when I needed. I appreciate that Mattias also have worked with lamprophyres and the discussions we had about our findings. Lars Eivind Augland and Tom Andersen are thanked for always being enthusiastic and helpful when I have asked for help.

I am very thankful to Dr. Muriel Erambert who supervised me in the EMP-lab and has always been helpful when needed. Gunborg Bye Fjeld and Mufak Naoroz are thanked for teaching me procedures for preparation of samples.

Marit Sørlie, always helpful in the library in the Department of Geosciences, thank you very much. Berit Løken Berg, I thank you for rescuing me during the late phase of my thesis when I needed to use the SEM, a very fascinating machine by the way.

I would also like to thank friends and fellow students for providing a good working environment, for being supportive and for all the lunch-breaks.

Last but not least, I would like to thank my parents and two sisters who have given me so much inspiration and always have been very supportive.

Contents

1 Introduction

The geologic evolution of the North-Atlantic region is characterized by crustal extension following the Late-Silurian to Early Devonian Caledonian orogeny (Wilson et al., 2004). Seismic studies of the continental margin outside Norway and E Greenland demonstrate that extension was not a continuous process but took place in pulses with formation of rift basins (Dore et al., 1999). Based on the seismic data it is well documented that major episodes of crustal extension and normal faulting took place in the Late Jurassic (prominent), Early Cretaceous, and in the Tertiary (Dore et al., 1999). Based on onshore geological data, including data on the exhumation history of Caledonian rocks – several pulses of extension or continuous extension affected the North Atlantic Region also in the Devonian, as well as in the Permian (Steltenpohl et al., 2004).

The structural grain associated with the various rifting events changed orientation with time, a feature easily seen when looking at the present configuration of the continental margins relative to the orientation of the older basin bounding faults. With respect to the mid-Norwegian margin, the direction of extension was NE-SW during the Devonian orogenic collapse, E-W in Permian and Late Jurassic time, NW-SE in early Cretaceous time, and arguably NNW-SSE during break-up (Lundin, 2008; Timmerman et al., 2009).

Magmatic activity related to crustal extension is well documented in the North Sea and surrounding areas (e.g. Oslo Rift), dominantly of Permian age (Neumann et al., 2004), but appears to be poorly documented in the northern part of the North Atlantic region. An important exception to this is the Tertiary volcanism associated with continental break-up and formation of oceanic crust between Norway and Greenland (Tegner et al., 2008). Minor volumes of post-Caledonian igneous rocks have however also been identified in the coastal areas of western Norway and Northeast Greenland.

Færseth et al. (1976) mapped several alkaline dykes (including lamprophyres) in Sunnhordland and three emplacement ages has been determined, 275 Ma, 220 Ma, and 160 Ma respectively, based on K-Ar thermochronology. Of these the 220 Ma event seems to be most common. The dykes are controlled by NNW-SSE trending faults which form part of a general joint and fault system of a similar orientation which dominates the tectonic structure of western Norway. The igneous activity had a trend towards increasing alkalinity and enrichment in rare earth elements (Faerseth et al., 1976).

Torsvik et al. (1997) have also assessed post-Caledonian mafic dykes in the Sunnfjord area. The dolerite dykes studied by Torsvik et al. (1997) appear to be of mid-late Permian age and are probably contemporaneous with the geochemically similar Sotra dykes (262 ± 6 Ma).

Pre -Tertiary post-Caledonian rocks are also known from NE Greenland where mafic dikes and dike swarms are known from many localities. E.g. 500-1000 m structurally below the Eleonore Bay Supergroup the protolith is a folded supracrustal sequence (Krummedal Sequence?) intruded by mafic dykes (Andresen et al., 1995).

Purpose of study

This study focuses on the mineralogy and geochemistry of lamprophyric dykes from Liverpool Land, North-Eastern Greenland. It also includes $^{40}Ar/^{39}Ar$ thermochronology results by Buchanan (2008).

Professor Arild Andresen has done extensive work in the Fjord Region and on Liverpool Land, East Greenland. The summer of 2006 several lamprophyric dykes were sampled by Buchanan (2008) and Augland (2007). In the summer of 2008 more lamprophyric dykes were sampled. Dr. Mark Anderson , Plymouth University and Professor Arild Andresen, University of Oslo, along with students Hans Kristian Daviknes and Dag Erlend Førsund sampled the dykes for palaeomag and bulk rock chemistry. According to professor Arild Andresen there has been no previous work done on these rocks and they are therefore very interesting.

The main objectives are:

1. Bulk rock chemistry of major- and trace elements.
2. A petrographic description of thin sections of samples with a petrographic microscope.
3. Electron-microprobe work on selected thin sections.

Field work and analytical methods

We spent three weeks on Liverpool Land in July 2008 doing field work for various projects. With Constable Point as a base several localities on Liverpool Land were visited using a helicopter as transportation. The weather was very nice with temperatures between from 0 – 15°C. Field work in relation to the lamprophyric dykes was not the main objective for this expedition and is not a vital part of this thesis.

In the field a hand held Garmin GPS was used to record positions at the localities we visited. A Silva 360 compass was used to record structural data. Reconnaissance work was aided by geological maps from Grønlands Geologiske Undersøgelse. A Casio Elixim digital camera was used to document observations in the field. For subsequent analytical work PANalytical Axios Wavelength Dispersive X-ray Fluorescence Spectrometer (WD-XRF) to find bulk rock chemistry and a Cameca SX 100 Electron Microprobe (EMP) was used for mineral chemistry and imaging. In addition, the Secondary Electron Microprobe (SEM) was used for imaging and mineral identification because the EMP was busy at the time. Microsoft Office Excel 2007, Adobe Illustrator CS3, Adobe Photoshop CS3, Igpet 2008 and GCDkit 2.3 have been used to plot the results and edit the figures, tables and pictures presented in this thesis.

2 Geological setting

The closure of the Iapetus Ocean and the main collision between Baltica-Avalonia and Laurentia occurred in Late Silurian/Early Devonian times (Cocks and Torsvik, 2005; Higgins et al., 2004) forming the Caledonian Orogen. The Variscan orogeny was partly contemporaneous with the Caledonian orogeny but outlasted it with approximately 100 m.y. and is the result of collision between Laurentia-Baltica and Africa, following the closure of both the Iapetus and the European Paleozoic oceans at approximately 380 Ma (Matte, 1989). The remnants of the Variscan Orogen appear as a complex belt of highly deformed and metamorphosed rocks across central Europe and with a Carboniferous-Permian age foreland basin to the north (Northern Germany and North Sea) (Matte, 1989).

Magmatism in the UK started c. 350 m.y. ago (Tournisian) in a transtensional regime in the foreland of the Variscan Orogeny and continued into the mid-Permian, possibly terminating as late as c. 250 Ma (Timmerman, 2004; Upton et al., 2004). The Lower Rotliegend group (300 – 288 Ma) experienced large scale dextral wrench-deformation of the lithosphere and upwelling of the asthenosphere triggering extensive melt generation which caused a period of uplift and erosion at the end of the Westphalian (Maynard et al., 1997; Timmerman et al., 2009; Ziegler, 1990). The Lower Rotliegend is thus dominated by volcanic rocks but also include sedimentary rocks of fluvial and lacustrine origin (Martin et al., 2002). The UK part of the Lower Rotliegend comprise basalts and tuffs with interbedded mudstone and rare sandstone (Cameron, 1993). Between the Lower- and Upper Rotliegend Group there was a 20 Ma tectonically quiet period, with uplift and erosion of NW Europe, resulting in the development of the 'Saalian Unconformity' (Glennie, 1998).

Thermal subsidence following the Lower Rotliegend volcanic event creates the Northern – and Southern Permian basins which were filled up with continental clastic deposits deposited representing fluvial, aeolian, sabkha, and lacustrine environments (Glennie, 1998). The sea transgress in Late Permian times (Zechstein) and because of the warm climate and rate of subsidence the Zechstein Salts develop.

Within the Fennoscandian craton, located north of the basin, wrench tectonics was succeeded by roughly E-W extension during the Permian. The craton was decoupled from the Northern Permian Basin, where the stress regime changed from right-lateral wrenching to a more NE-SW directed extensional stress regime during post magmatic thermal relaxation (Timmerman et al., 2009). The wrenching and extension in the Northern – and Southern Permian Basins is interpreted to have created the Oslo Rift, Skagerrak-Kattegat rift area, Norwegian-Danish Basin, and the central North Sea. This is a good indication that the whole area was affected by the same regional tectono-magmatic phase (Heeremans and Faleide, 2004).

UK Post-Caledonian Magmatism

Late Caledonian calc-alkaline lamprophyre (minette) dykes in the eastern Southern Uplands of Scotland with a K – Ar biotite age of 400 ± 9 Ma form part of a dyke swarm nearly parallel to the

inferred Iapetus Suture (Shand et al., 1994). Carboniferous – Permian alkaline lamprophyres occur in thousands in the UK and Scotland (Baxter and Mitchell, 1984).

In the Dinantian (354 – 337 Ma) the Midland Valley of Scotland (MVS) was subject to a strike-slip transtensional tectonic regime and large volumes of alkaline magma erupted (Timmerman, 2004; Upton et al., 2004). In the Namurian and Westphalian, transtension and transpression controlled by dextral strike-slip was active in the MVS. This was accompanied by alkaline, transitional and tholeiitic magmatism across the British foreland. While the tholeiitic magmatism is considered to be short lived (301-295 Ma) the alkaline magmatism in the Stephanian outlasted it and continued into the Permian (Monaghan and Pringle, 2004).

Upton et al. (2004) suggests that the alkaline magmatism in the Dinantian (360-326 Ma) and Silesian (326-299 Ma) is triggered in response to phases of regional lithospheric extension. The most primitive magmas are predominately alkaline with trace-element and Sr-Nd isotopic characteristics similar to those of Ocean Island Basalts (OIB). Upton et al. (2004) also concludes that the short lived tholeiitic magmatic event in the latest Stephanian has a different origin. Heeremans and Faleide (2004) concludes that the Skagerrak, Kattegat and North Sea was characterized by a large volume of volcanics at c. 300 Ma and that the North Sea underwent a significant Permian – early Triassic rifting event accompanied by magmatism.

The Inge Volcanics Formation in the North Sea is the UK counterpart of the Lower Rotliegend and is dated to 299 by Heeremans et al. (2004) and interpreted to be part of the regional tholeiitic igneous event that occurred at the transition from the Carboniferous to the Permian. Martin et al. (2002) suggests that the tholeiitic magmatism started in early Westphalian times (311-308 Ma).

Norwegian Post-Caledonian Magmatism

Lamprophyre dykes from Ytterøy and Lerkehaug, near Steinkjer, Central Norwegian Caledonides has been reported by Mitchell and Roberts (1986). They associate the Lerkehaug lamprophyre with the 590-565 Ma rifting and alkaline-intrusive event recognized throughout northwestern Europe and Greenland. The Ytterøy lamprophyre age spectrum is complex and uncertain, but a 'total fusion' $^{40}Ar/^{39}Ar$ age of 370 Ma was obtained. Another age of 256 Ma was obtained by the Rb-Sr age but is interpreted as an overprint of hydrothermal activity related to Permian rift faulting.

Close to 100 post-Caledonian dikes in the Sunnhordland-Sotra region occur along N-S to NNW-SSE trending lineaments (that transect all ductile and many brittle tectonic structures in the region). Færseth et al. (1976) mapped 15 alkaline dykes in the Sunnhordland area and identified three age groups (K-Ar), 275 m. y., 220 m. y., and 160 m. y. respectively, 220 m. y. having the biggest population. The igneous activity had a trend towards increasing alkalinity and enrichment in rare earth elements (Faerseth et al., 1976). Torsvik et al. (1997) assessed dykes in the Sunnfjord area and his dolerite dykes of mid-late Permian (250 – 270 Ma) age are probably contemporaneous with the geochemically similar Sotra dykes (262 ± 6 Ma) (Lovlie and Mitchell, 1982). Torsvik et al. (1997) argue that collectively they attest to major Permo-Triassic rifting and a change from sub-alkaline (Permian) to alkaline (Triassic) magmatism.

Greenland Post-Caledonian Magmatism

Post-Caledonian granitoids are abundant in the North Atlantic Caledonides and Kalsbeek (2008) suggests that a more or less continuous belt may have been formed from Scotland through East Greenland. The Hurry Inlet Granite and the Hodal-Storefjord Monzodiorite situated in Liverpool Land have been investigated by Augland (2007) and Daviknes (2009). $^{40}Ar/^{39}Ar$ dating of lamprophyre dikes intruding extensional faults in the Eleonore Bay Supergroup in Ole Rømer Land gives an age of ca. 420 Ma and indicates that upper crustal extension was active in Late Silurian time (Hartz and Andresen, 1995).

Breakup and post-breakup magmatism is widespread and Rock (1991) presents in his book, 'Lamprophyres', six occurrences of calc alkaline tertiary lamprophyres along the coast of Northeast Greenland. Tegner et al. (2008) report coast-parallel dykes and other intrusions from the Wiedemann Fjord-Kronborg Gletscher (68°-70° N). Syenite, granite, gabbro, diorite, nephelinite, basanite, lamprophyre, and strongly undersaturated alkaline intrusions have been dated by the $^{40}Ar/^{39}Ar$ method and ages ranging from 56-35 Ma have been found (Tegner et al., 2008). The post-breakup magmatism is linked to reconfiguration of spreading ridges in the central Northeast Atlantic Ocean basin. This reconfiguration is also linked to splitting the Jan Mayen microcontinent away from the Blosseville Kyst (Tegner et al., 2008). While complete separation of the Jan Mayen microcontinent from the NE Atlantic margin happened around 20 Ma, a new kinematic model also suggests that separation started as early as 56 Ma (Gaina et al., 2009). Alkaline volcanic rocks related to rifting are also found on Jan Mayen suggested to be from similar sources as those from Iceland (Tronnes et al., 1999).

3 Geology of Liverpool Land

Liverpool Land (Figure 3-2) is dominated by Caledonian high-grade metamorphic rocks and intrusives, unconformably overlain by Permian and younger sedimentary rocks. The high grade gneisses are interpreted to represent an eastern continuation of the Caledonian nappes exposed in the Fjord Region further west. The protolith to the high-grade paragneisses present in the central and northern part of Liverpool Land is interpreted to correlate with the Late Mesoproterozoic Krummedal sequence. The latter is intruded by the Hurry Inlet Plutonic Complex and other smaller intrusive bodies (Andresen and Hartz, 1998; Augland, 2007). A major shear zone, the Gubbedalen Shear Zone, separates the orthogneisses and the Hurry Inlet Plutonic Complex from an eclogite bearing terrain making up the southern part of Liverpool Land (Augland, 2007). U-Pb dating revealed that there is at least two magmatic phases in the Hurry Inlet Plutonic Complex with ages of 445 Ma and 438 Ma, respectively (Augland, 2007).

The Hurry Inlet Plutonic Complex was first described by Coe and Cheney (1972) who identified four main facies, granodioritic to granitic in composition. They also described the contact between the Hurry Inlet Plutonic and the eclogite-bearing gneisses further south and considered it to be intrusive. Augland (2007), however, documented the presence of the Gubbedalen Shear Zone between the Hurry Inlet Plutonic Complex and the high grade gneisses further south. Augland (2007) have documented that the HP/UHP metamorphism in the eclogite-bearing footwall block dates to c. 399 Ma and has in a recent publication argued that Liverpool Land Eclogite Terrane represents a piece of Baltica (Augland et al. submitted).

Coe and Cheney (1972) also described minor basic intrusions from Liverpool Land believed to be of Tertiary age based on field observations. Three petrographic types were recognized, dolerites, lamprophyres and feldsparphyric basalts. They all have a north-south trend and no dyke intersections were observed. Accordingly no relative chronology was established within the suite. The lamprophyres appear to have a geographical relation to the Hurry Inlet Plutonic Complex, but Coe and Cheeney (1972) interpret this relation as structural and not genetic based on reports of other lamprophyres.

Three clusters of lamprophyre dikes have been sampled in Liverpool Land (this thesis) and the location of the sampling areas can be seen on the map in Figure 3-2. Two of these were sampled by Augland (2007) and Buchanan (2008) and preliminary ages and petrographic descriptions were published. Buchanan (2008) reports two NNE-SSW trending dykes (kersanites, see nomenclature in Figure 4-1), one sampled where the lamprophyre (M-14C) intruded the contact between the Krummedal Sequence and the Hodal-Storefjord Monzodiorite pluton (dated by Augland (2007) to 424 Ma), and one where the lamprophyre (M-21) intruded the Hodal-Storefjord Monzodiorite pluton. ^{40}Ar-^{39}Ar dating gave an age of 261.56±0.38 Ma (calculated with 1σ error and 95% confidence level) for sample M-14C and 263.93±0.93 Ma for sample M-21. The dykes cut the garnet biotite gneiss, the Hurry Inlet Granite and the Hodal-Storefjord Monzodiorite and contain abundant xenoliths of the host rock (Augland, 2007). Dolerite dykes intruding the Hodal-Storefjord Monzodiorite (and other rocks in the area) are presumably Tertiary and related to plateau lavas now exposed south of Scoresby Sund (Augland, 2007).

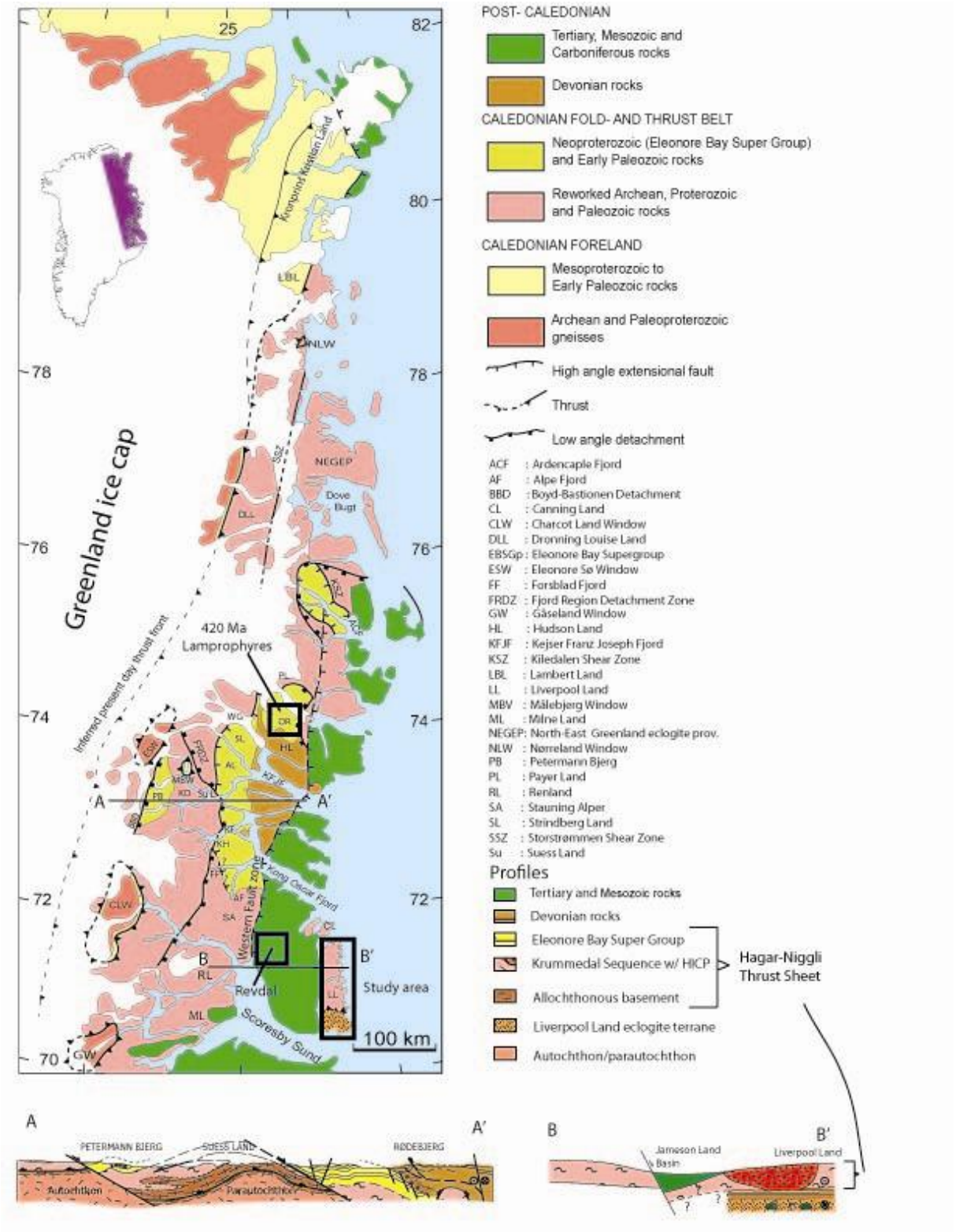

Figure 3-1: Figure modified from Augland (2007) showing the North Atlantic Caledonides. The 420 Ma lamprophyric dyke in Ole Rømer Land and the Tertiary lamprophyric dykes in Revdal has been marked.

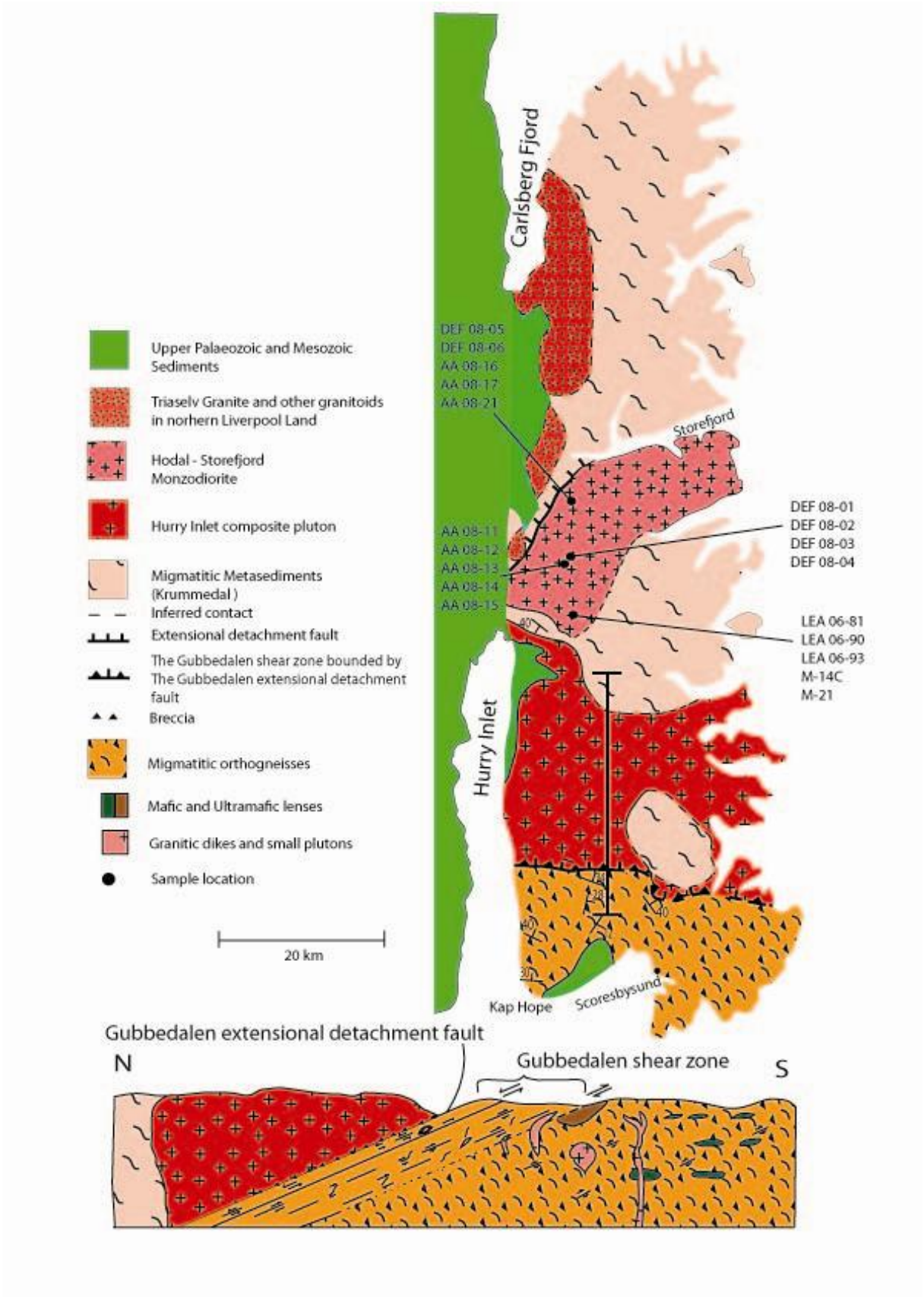

Figure 3-2: Map modified from Augland (2007) where the sampling areas have been marked.

4 Lamprophyres

4.1 History of lamprophyres

The term ”lamprophyre” was introduced to petrological literature by Gümbel in 1874. “Lampros porphyros” translates to “glistening porphyry” and describes the macroscopic appearance of a lamprophyre with its shining biotite phenocrystals in a fine grained matrix. In the early and mid 20th century many rocks which were difficult to classify was assigned to this group and given non-systematic names which made this group difficult to comprehend. In the 1970s the interest in lamprophyres escalated because of their supposed relation to gold and diamonds, the number of published articles increased enormously. In the 1990s the number of specimens analyzed also increased dramatically and the volume of analytical data from 1985-1990 exceeded the volume up to that time.

The International Union of Geological Sciences is a nongovernmental scientific organization founded in 1961. The Subcommission of the Systematics of Igneous Rocks was formed in 1970, under the IUGS Commission on Petrology to foster agreement on nomenclature and classification in petrology. Their first conclusions were published in A Classification of Igneous Rocks and Glossary of Terms 1. edition (Le Maitre, 1989). In this edition three groups of lamprophyres (calc-alkaline, alkaline and melilitic) were recognized and lamprophyres, lamproites, and kimberlites were placed under the heading “lamprophyric rocks”. The UML (Ultramafic Lamprophyres) group of Rock (1985) which included the melilitic rocks was not accepted and rocks like aillikite, damkjernite, and ouachitite were not included in the classification. The Preface of the book stated that this was provisional solution until a more satisfactory classification was established.

Nicholas Rock, one of the experts on lamprophyres, has made great contributions to the understanding of lamprophyric rocks (Rock, 1977; 1985; 1987; 1991) (these are only a handful of his extensive work on lamprophyres). After the IUGS coupled lamprophyres, lamproites, and kimberlites into one group Rock (1991) introduced the term “the lamprophyre clan” which now included five branches arguing that this was a natural conclusion to the work of Le Maitre (1989). His latest proposal for branches and rock names are given in Figure 4-1. Instead of the melilitic group of the IUGS, Rock (1991) included his own UML group (which includes the melilite group) in his own classification. This is thus the only complete classification so far and for years to come. Rock (1991) has also been a contributor to IUGS classification of lamprophyres (Lebas, 1989; Woolley et al., 1996) but not all of his proposals have been accepted.

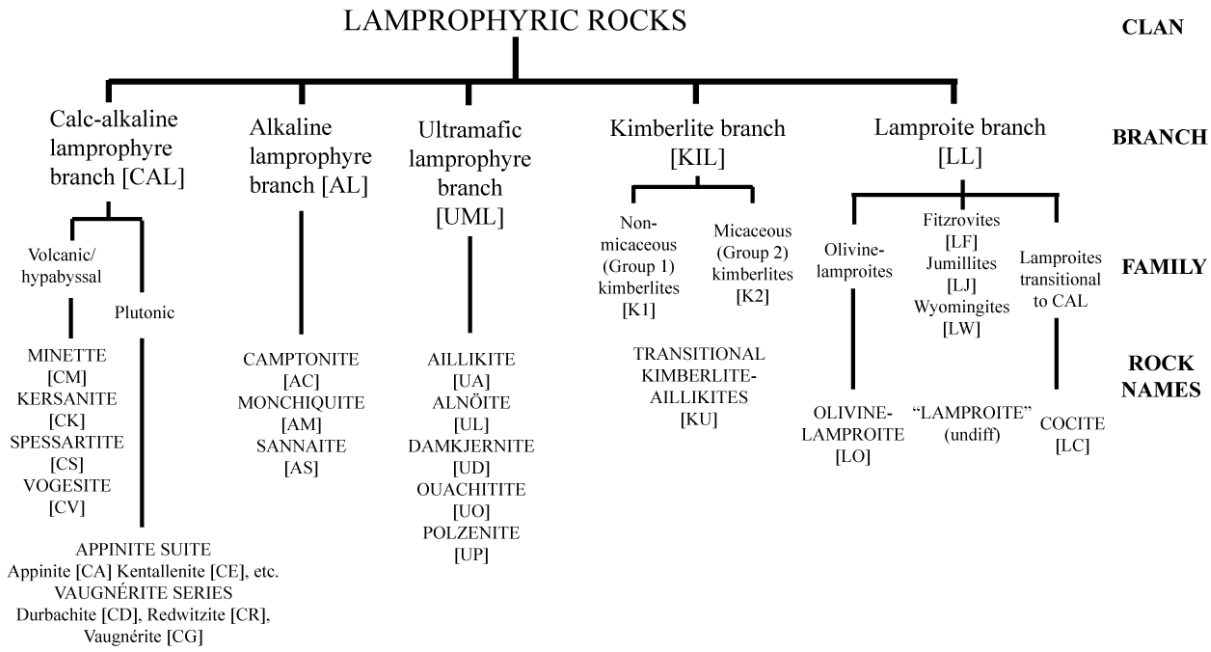

Figure 4-1: Nomenclature of lamprophyric rocks after Nicolas Rocks (1991).

There has been some discussion about Rocks (1991) lamprophyre clan because it is either inappropriate or incorrect because the term lamprophyre is devalued, whereas the classification of lamproites and kimberlites is not furthered. While Rock (1991) focuses on the complete geochemical and mineralogical gradation between lamproites and other lamprophyres Mitchell (1994) argues there is no genetic relation between some of the rocks in the clan and therefore no petrological purpose. A petrological clan is defined as a suite of comagmatic rocks that have been derived from a particular parental magma which has been produced repeatedly in time and space. Mitchell (1994) proposes "the lamprophyre facies" which might be more appropriate since the lamprophyre clan merely unites common magmas which crystallize under similar conditions.

Woolley (1996) tried to deal with the problem of the "lamprophyric rocks" by adding another flow chart in the classification scheme of Le Maitre (1989) to include lamproites, kimberlites and lamprophyres and the melilitic, kalsilitic and leucitic rocks. Once again the UML group of Rock (1985) was left out. This contribution was only meant as a proposal for discussion and was not to be regarded as the definitive statement on the topic.

The second and latest edition (Le Maitre, 2002) has dealt with some of the issues in Woolley's proposal (1996) but still has a few shortcomings concerning lamprophyres. The UML group of Rock (1985) has still not been accepted by the IUGS Subcommittee of Classification and the rocks alnöite and polzenite has been confined to the melilite-bearing rock classification. Hence ultramafic rocks without melilite cannot be classified according to the present IUGS classification.

In 2005 an attempt was made to integrate ultramafic lamprophyres into the IUGS Classification of Igneous Rocks (Tappe et al., 2005). A simplified version of Rocks (1985) UML group is presented as an addition to the IUGS Classification of Le Maitre (2002). As a consequence of this addition Tappe et al. (2005) also proposes an additional chemical criterion for sannaites where mineralogical definitions are inadequate to define sannaites and damtjernites. This last contribution by Tappe (2005) is

probably not the last contribution to the never ending discussion about the classification of “lamprophyric rocks”.

4.2 Classification and nomenclature

Because of the nature of the samples in question a classification which can handle ultramafic rocks without melilite is needed. The options narrow down to the latest version of Rock's (1991) classification or Tappe et al.'s (2005) addition to the IUGS classification.

The authors natural choice is to use the classification of Tappe (2005) which is built on the IUGS classification of Le Maitre (2002) along with a simplified version of Rocks UML group (1985). Discrimination criteria rely on mineral composition after (Mitchell and Roberts, 1986; Mitchell, 1995) and Tappe (2005; 2004). It is the complete classification of igneous rocks with a flow chart (Figure 4-2) to first determine the group in which the rock belongs and then follow a classification appropriate for this specific group. Step three (highlighted) will lead to Figure 4-3 if the rock is an ultramafic lamprophyre. Step nine will lead to Figure 4-4 if the rock is a calc-alkaline or alkaline lamprophyre.

There are still problems with the classification of Tappe (2005) which are mentioned in the ‘comments’. The coexistence of aillikites and sannaites has been described (Foley, 1984; Malpas et al., 1986) in Aillik Bay and implies the coexistence of ultramafic and alkaline lamprophyre magma types. However recent work (Tappe et al., 2006) has revealed that damtjernites are also present and form a mineral compositional and geochemical continuum with the aillikites and ‘sannaites’. This shows that ultramafic rocks grade into rocks with a felsic component higher than 10% and are clearly related by fractionation. This means that the ‘sannaites of Aillik Bay are really evolved damtjernites and that rocks from UML magmas could be misidentified as rocks from AL magmas in cases like this since they will not be picked up in step three of Figure 4-2 (Tappe et al., 2005). An additional chemical screen is proposed (41 wt% < SiO_2) to increase the probability of a rock classified as a sannaite really being related to alkaline lamprophyre magma type. Because of these new findings Tappe (2005) also mentions the need for the former UML rocks polzenite and ouachite which according to an extensive literate survey are the equivalents of evolved alnöites and damtjernites respectively. This emphasizes the need for further improvements in the classification of lamprophyres and considering geochemical and mineral compositional data from a larger sample suite whenever available (Tappe et al., 2005).

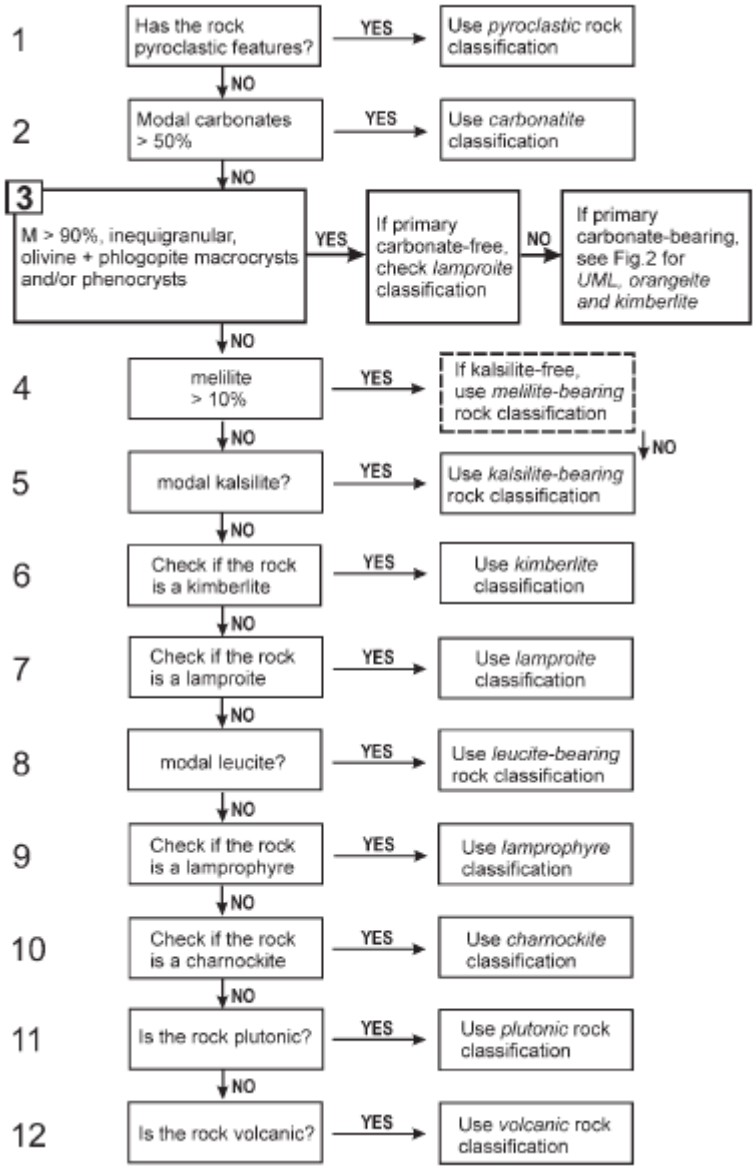

Figure 4-2: Flow chart from Tappe et al. (2005) illustrating the sequential system for the classification of igneous rocks following the IUGS scheme devised by Le Maitre (2002). Step 3 is highlighted and can distinguish between ultramafic lamprophyres (UML), kimberlite, orangeite and olivine lamproite. 'M' is defined as mafic and related minerals (i.e. including primary carbonate and apatite).

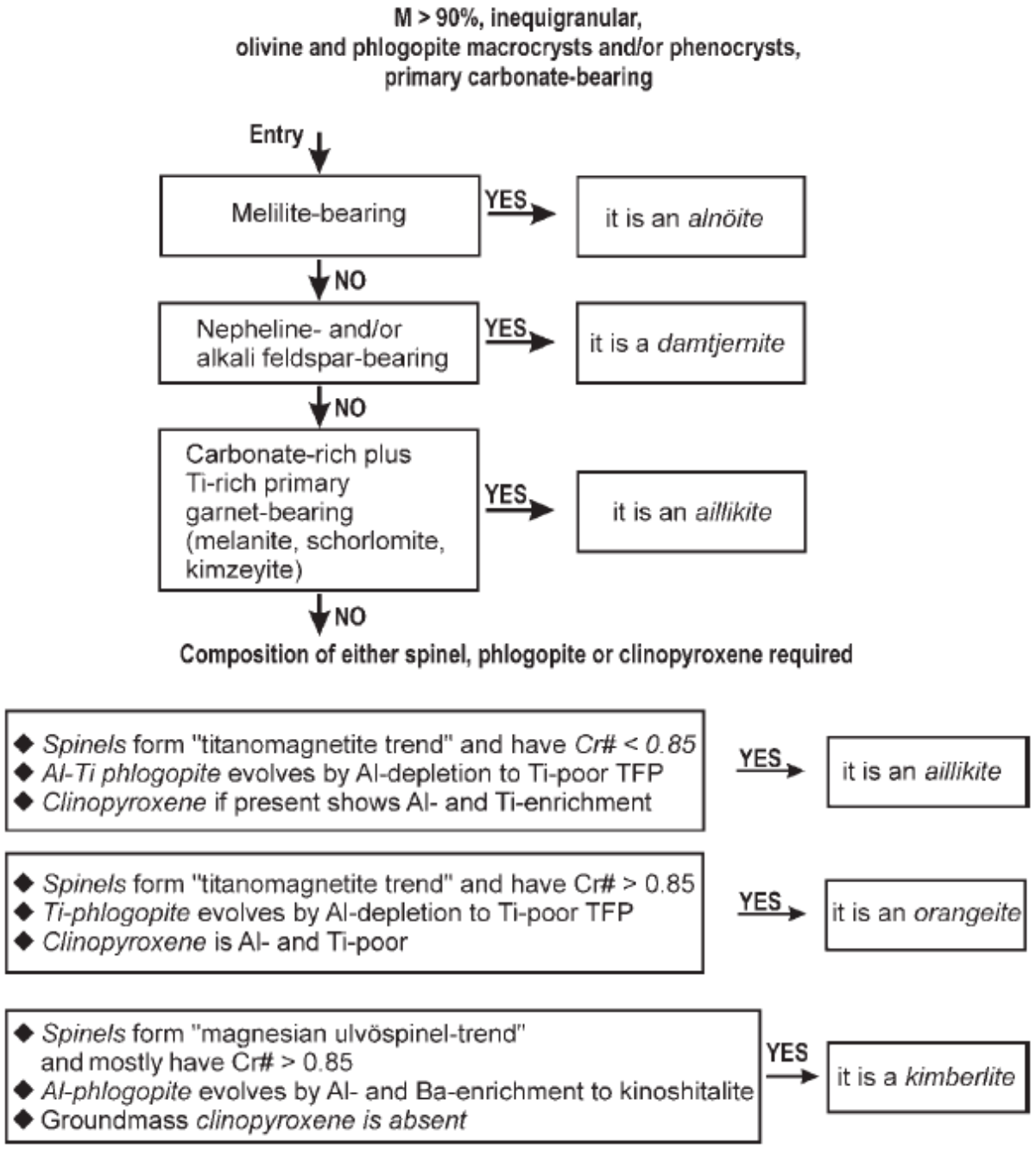

Figure 4-3: Flow chart illustrating how to distinguish between the three UML end-members (alnöite, damkjernite, aillikite), orangeite and kimberlite from Tappe (Tappe et al., 2005). Discrimination criteria that rely on mineral composition after (Mitchell and Roberts, 1986; Mitchell, 1995) and Tappe et al. (2005; 2004). Cr# (Cr-number) = atomic Cr/(Cr + Al); TFP, tetraferriphlogopite.

Light-coloured constituents		Predominant mafic minerals		
feldspar	foid	biotite > hornblende, ±diopsidic augite, (±olivine)	hornblende, diopsidic augite, ±olivine	brown amphibole, Ti-augite, olivine, biotite
or > pl	–	minette	vogesite	–
pl > or	–	kersantite	spessartite	–
or > pl	feld > foid	–	–	sannaite
pl > or	feld > foid	–	–	camptonite
–	glass or foid	–	–	monchiquite

or = alkali feldspar; pl = plagioclase; feld = feldspar; foid = feldspathoid.

Figure 4-4: Classification and nomenclature of calc-alkaline and alkaline lamprophyres based on their mineralogy (Le Maitre, 2002).

5 Field Occurrence

The samples were collected during an excursion to Liverpool Land (Figure 3-2), East Greenland, during three weeks in the summer of 2008. I was a field assistant, and was brought along to gain experience and maybe a possible thesis to work on when I came home. The other participants were Professor Arild Andresen, Dr. Mark Anderson, PhD Lars Eivind Augland and MsC Hans Kristian Daviknes. Dr. Mark Anderson was also interested in the lamprophyric dykes and sampled them for paleomag, with me and Hans Kristian as assistants. Hans Kristian was also doing field work for his own master thesis and was sampling granites for later dating. Lars Eivind Augland did field work and sampling for his own PhD, his second summer of field work on Greenland. Unfortunately I was sick when we were at the locality where most of the lamprophyric samples were taken and the observations are thus not very thorough. Some of the samples have been sampled by Arild Andresen and I have had a look on his notes. Lars Eivind Augland gave me three samples with GPS coordinates and I have used his thesis (Augland, 2007) for observations on field occurrence.

The lamprophyres occur in three clusters, each separated by around 5 kilometres (Figure 3-2). The cluster farthest to the south was not visited during this expedition and field observations and sampling has been done by Augland (2007) and Buchanan (2008). In labeling the samples have been given names with initials (AA = Arild Andresen; DEF = Dag Erlend Førsund; LEA = Lars Eivind Augland), year of sampling, and number, like DEF 08-01. The dyke from which a sample has been taken will be referred to with the sample name. The sampling areas and the rocks in which they intrude can be seen in the map of Liverpool Land in Figure 3-2. The dykes are subvertical, around 1 m thick and strike approximately N-S (Figure 5-4). Some dykes occur together as parallel dykes.

DEF 08-01, DEF 08-02, DEF 08-03 and DEF 08-04

The dykes, DEF 08-02, DEF 08-03 and DEF 08-04 show a lot of fractures and weathered surfaces. Rock fragments were covering a lot of the dykes and fresh rock samples were difficult to obtain (Figure 5-2 and Figure 5-3). Sample DEF 08-02 (Figure 5-1) is severely altered while the other samples show some alteration. Samples DEF 08-02, DEF 08-03 and DEF 08-04 are very fine grained with phenocrysts less than 1 mm across, dyke DEF 08-04 contain round carbonate aggregates with a diameter of up to 3 mm. The dyke DEF 08-01 is found in the same area but contain larger phenocrysts (up to 4 mm across) and elongated carbonate aggregates (up to 6 mm in length).

AA 08-11, AA 08-13 and AA 08-14

The dykes AA 08-11, AA 08-13 and AA 08-14 are found in the same area as the dykes DEF 08-01, DEF 08-02, DEF 08-03 and DEF 08-04. Sample AA 08-13 contain phenocrysts from 1 mm up to 1.4 cm across, samples AA 08-11 and AA 08-14 contain phenocrysts from 1-6 mm across. Sample AA 08-14 contain a crack filled with a brown mineral. Samples appear fresh in hand-specimen.

Amphibole phenocrysts were more abundant than biotite phenocrysts in these dykes (Andresen pers comm.). Dyke AA 08-11 consist of three parallel dykes of 1 m, 35 cm and 20 cm width. The rock looks like it has xenoliths of a dark mineral with a «glass looking» fracture. Fractures are oriented 020 and 050 (Andresen pers comm.).

DEF 08-05/DEF 08-06, AA 08-16, AA 08-17 and AA 08-21

The dykes DEF 08-05/DEF 08-06, AA 08-16, AA 08-17 and AA 08-21 are found in the same area (Figure 3-2). The dykes DEF 08-05/DEF 08-06, AA 08-16 and AA 08-17 has weathered surfaces but fresh rocks were easy to find (Figure 5-4). There were less loose rock fragments covering the dykes and they were less fractured than the dykes DEF 08-02, DEF 08-03 and DEF 08-04. Sample DEF 08-06 contain a large rounded xenolith (5 cm across) which contain a lot of feldspars (Figure 5-8). Large CPX, biotite and amphibole phenocrysts occur in a fine grained matrix of the dykes DEF 08-05/DEF 08-06, AA 08-16 and AA 08-17. Grain size varies a lot from mm size phenocrysts of CPX and biotite phenocrysts up to 4 cm biotite phenocrysts (Figure 5-7). The dyke DEF 08-05/DEF 08-06 contains zones of both coarse – and fine - grained rock. The centre of the dyke a coarse grained zone (Figure 5-5) with phenocrysts of mica and abundant felsic bubbles (Figure 5-6).

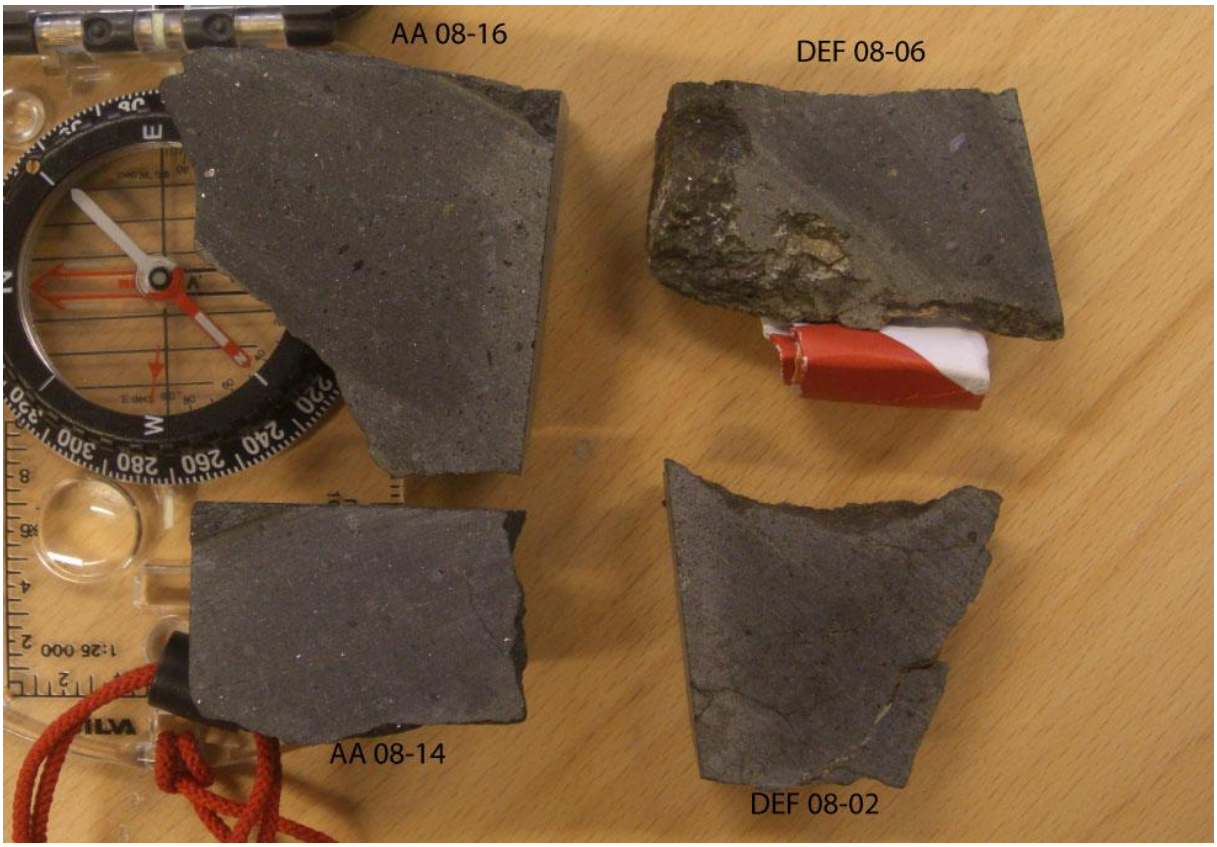

Figure 5-1: Photography of the samples AA 08-16, DEF 08-06, AA 08-14 and DEF 08-02. They exhibit varying grain size and sample DEF 08-02 has more fractures and brown alteration than the others. The compass to the left show a cm scale.

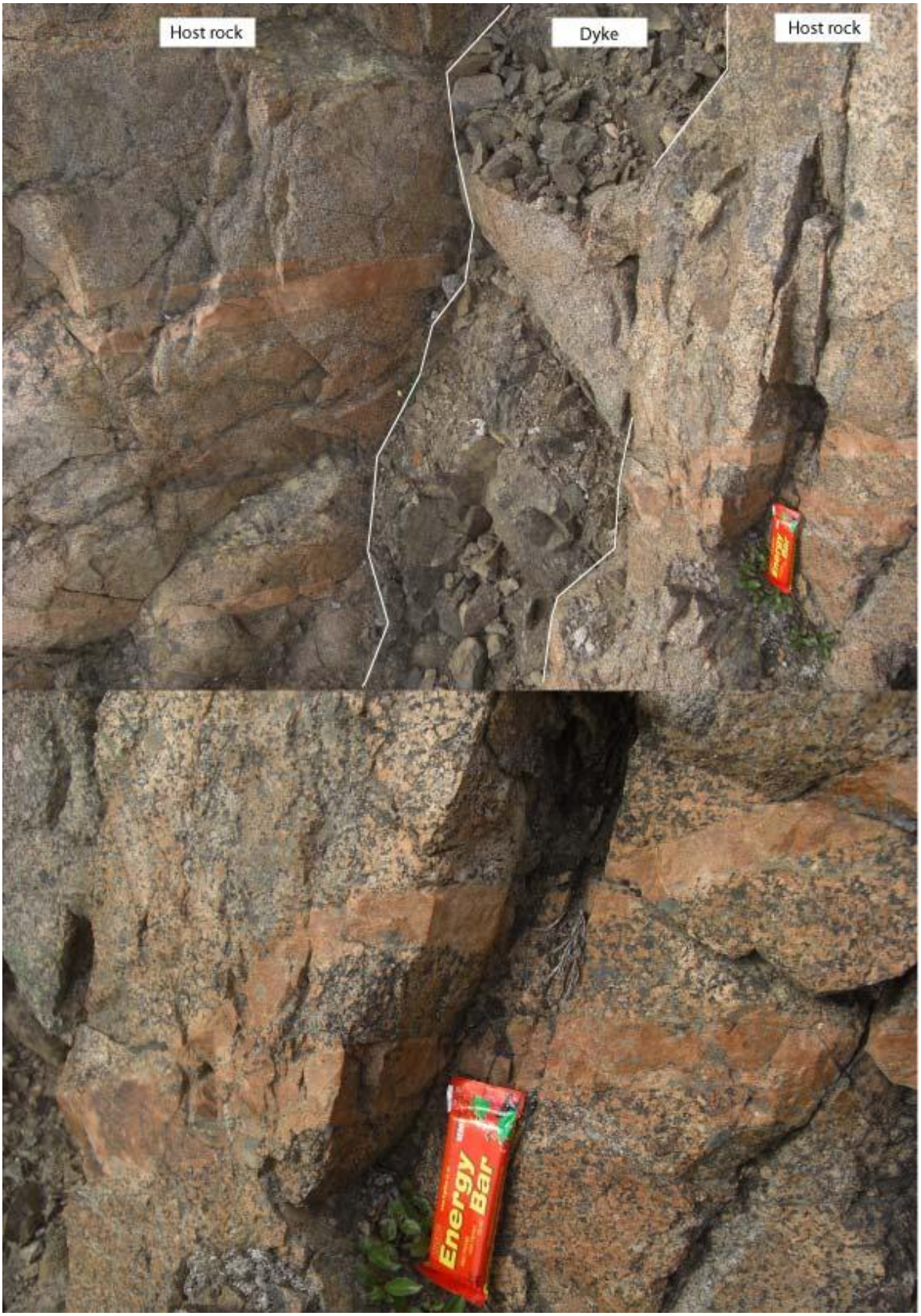

Figure 5-2: The upper photo is of the dyke where sample DEF 08-02 was sampled. The dyke has a lot of fractures and it is difficult to see any fresh surfaces. The dyke has intruded a monzodiorite body in Liverpool Land, East Greenland Caledonides. The lower photo is a close-up of the monzodiorite host rock. An energy bar has been used as scale, ca 15 cm.

Figure 5-3: Photo of the dyke where sample DEF 08-03 was sampled. The dyke has a lot of fractures and it is difficult to see any fresh surfaces. The dyke has intruded a monzodiorite body in Liverpool Land, East Greenland Caledonides.The geologist in the picture is Dr. Mark Anderson, Plymouth University.

Figure 5-4: An overview photo of the dyke where samples DEF 08-05 and DEF 08-05 were sampled. The distance to the partly covered red person is around 20 metres.

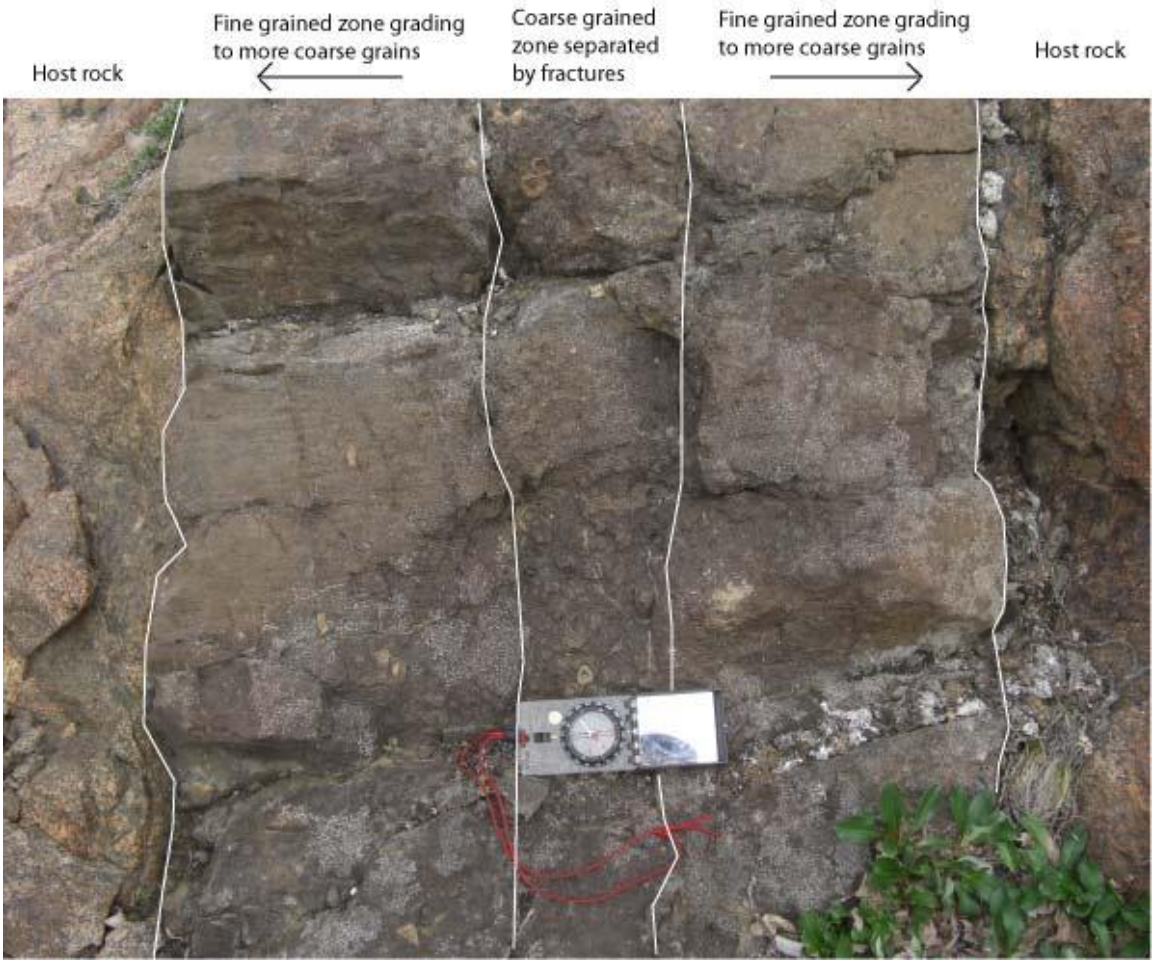

Figure 5-5: Photo of the dyke where samples DEF 08-05 and DEF 08-06 were sampled. Thin coarse grained zones are found at the edges and a thicker one in the middle of the dyke. The thick coarse grained zone is separated by fractures from the fine grained zones of the dyke. A compass of 10 cm length has been used as a scale.

Figure 5-6: A close-up photo of coarse grains and an aggregate/ocelli from the sampling area where samples DEF 08-05 and DEF 08-06 were sampled. The aggregate/ocelli is zoned, it as an eroded core, a felsic inner rim and a dark outer rim. A cm-scale is seen to the right in the photo.

Figure 5-7: Close-up photos from the sampling area of samples DEF 08-05 and DEF 08-06, cm-scales are seen at the top and at the bottom. The upper photo are of mica prints in the rock which were up to 4 cm across. The lower picture show a weathered surface from the same dyke.

Figure 5-8: Sample from dyke DEF 08-05/DEF 08-06 with a xenolith rich in feldspar. A cm scale can be seen at the bottom.

Sample	Latitude	Longitude	Strike	Use	Age	Classification
DEF 08-01	70° 55.308'N	22° 21.855'W	-	Petrography, bulk and mineral chemistry	-	Aillikite (UML)
DEF 08-02	70° 55.309'N	22° 21.730'W	350/68	Petrography and bulk chemistry	-	-
DEF 08-03	70° 55.357'N	22° 21.946'W	038/90	Petrography and bulk chemistry	-	-
DEF 08-04	70° 55.255'N	22° 22.001'W	-	Petrography and bulk chemistry	-	-
DEF 08-05 and DEF 08-06	70° 59.252'N	22° 20.862'W	336/90	Petrography, bulk and mineral chemistry	-	Sannaite (AL)
AA 08-11	70° 54.931'N	22° 22.157'W	-	Petrography and bulk chemistry	-	-
AA 08-12	70° 54.912'N	22° 22.395'W	355/90	Petrography, bulk and mineral chemistry	-	Dolerite?
AA 08-13	70° 54.930'N	22° 22.238'W	-	Petrography, bulk and mineral chemistry	-	Aillikite (UML)
AA 08-14	70° 54.930'N	22° 22.238'W	-	Petrography, bulk and mineral chemistry	-	-
AA 08-15	70° 55.055'N	22° 22.453'W	-	Petrography, bulk and mineral chemistry	-	Dolerite?
AA 08-16	70° 59.253'N	22° 20.851'W	330/90	Petrography, bulk and mineral chemistry	-	Sannaite (AL)
AA 08-17	70° 59.253'N	22° 20.851'W	330/90	Petrography, bulk and mineral chemistry	-	Sannaite (AL)
AA 08-21	70° 58.966'N	22° 22.091'W	-	Petrography and bulk chemistry	-	-
LEA 06-81	70° 52.941'N	22° 19.379'W	-	Petrography and bulk chemistry	-	-
LEA 06-90	70° 52.378'N	22° 19.178'W	-		-	-
LEA 06-93	70° 52.716'N	22° 20.026'W	-	Bulk chemistry	-	-
M-14C	70° 52.644'N	22° 20.091'W	-		262 Ma	Kersantite (CAL)
M-21	70° 52.696'N	22° 20.493'W	-		264 Ma	Kersantite (CAL)

Table 5-1: A table summary of GPS coordinates, strike of the dykes, their use, age, and classification. GPS coordinates and strike has been obtained by the geologist who sampled the sample, Dag Erlend Førsund (DEF), Arild Andresen (AA) and Lars Eiving Augland (LEA).

6 Petrography

6.1 Introduction

To study the varied textural and mineralogical traits observed in the field in Liverpool Land, NE Greenland 15 thin-sections were made for further examination. In labeling the thin-sections have been given names with initials (AA = Arild Andresen; DEF = Dag Erlend Førsund; LEA = Lars Eivind Augland), year of sampling, and number, like DEF 08-01. Furthermore the different types of phenocrysts, structures or areas of analysis have been given another number which is added to the sample name. Thus, a CPX phenocryst in sample AA 08-13 could have the name AA 08-13-6. To avoid confusion with the gradational composition between biotite and phlogopite I have decided to use the term biotite throughout the rest of the thesis.

Samples DEF 08-01, DEF 08-05, DEF 08-06, AA 08-11, AA 08-13, AA 08-14, AA 08-16, and AA 08-17 are porphyritic with phenocrysts (rough estimation, 10-30%) of CPX and biotite (in some) in a fine-grained matrix. Other phenocrysts like calcite and spinel have also been observed in a lesser degree, but are important when determining the type of lamprophyre in question. Based on the type and occurrence of phenocrysts and the composition of the matrix, the Liverpool Land lamprophyres I have analyzed are classified as either aillikites or sannaites.

Thin-section scans out of some of the important samples are shown below. The sample name can be seen on the top, important areas in the thin-sections have been given names according to the earlier explanation and are marked with rectangle boxes. Phenocrysts with single analysis are marked with an analysis number and a rectangle box. Other areas or phenocrysts are marked with rectangles and will be referred to in the text. In addition to showing areas of interest, the thin-section scans show the texture and composition of the samples which will be a good supplement to the petrographic descriptions ahead.

In these thin-section scans (Figure 6-1 - Figure 6-6), there are two aillikites and four sannaites. They are all dominated by different types CPX phenocrysts. With a closer look one can see that thin-sections from samples DEF 08-01, AA 08-13, and AA 08-14 have some CPX phenocrysts which show a dark clear green core, some are relatively large (2 mm in length). The thin-sections DEF 08-06, AA 08-16, and AA 08-17 also show green cores or rims, but these show a more subtle green, sometimes grading to brown and appear mixed in some cases. In these thin-sections the other CPX phenocrysts display more color variations than in the first three thin-sections. Colors like brown, yellow, pink, along with the light green cores are seen. These variations along with EMP analysis will be further looked into in chapter 8, Mineral Chemistry.

As can be seen in the caption text for each photo, there are mineralogical differences between the aillikites and sannaites. The sannaites are the only ones containing calcite as phenocrysts. They also show complex zoning patterns, biotite rimming grains and aggregates/ocelli, resorbed spinel, glomeroclasts and simple twinning.

Samples DEF 08-01, AA 08-13, and AA 08-14 also show similarities, but while DEF 08-01 and AA 08-13 are classified as aillikites, AA 08-14 is classified as a sannaite. These samples all show green CPX cores which are larger and greener than in the other samples. DEF 08-01 does not contain biotite phenocrysts, while AA 08-13 and AA 08-14 contain one and two, respectively.

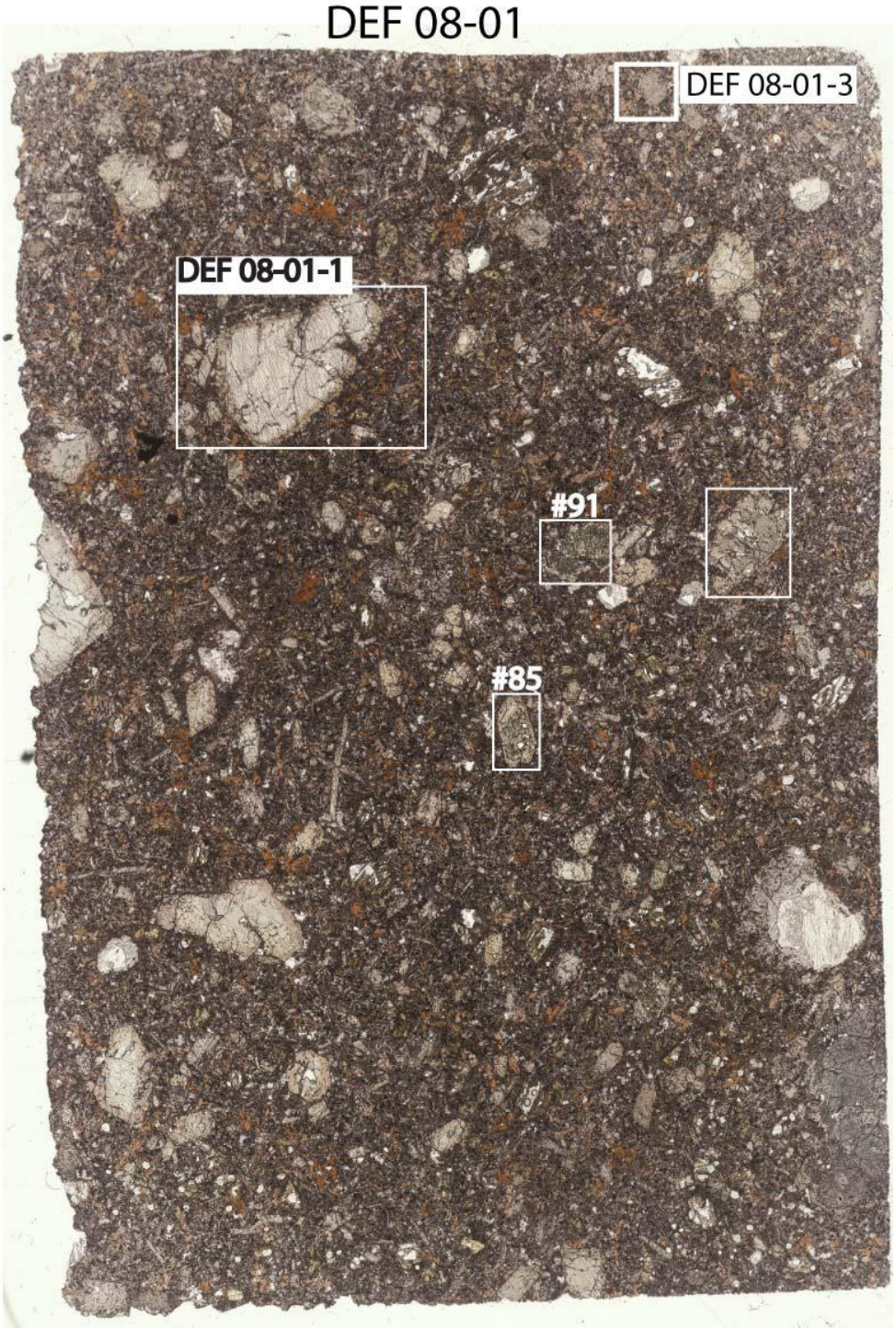

Figure 6-1: Thin-section scan of sample DEF 08-01 which is classified as an aillikite. Phenocrysts of CPX, Cr-spinel (one occurrence) in a fine grained matrix of CPX, biotite, spinel, analcite, and carbonate. CPX phenocryst profiles DEF 08-01-1 and DEF 08-01-3 can be seen in Figure 8-2, Figure 8-3, Figure 8-6 and Figure 8-7. Analyses results of #85 and #91 can be seen in Table 8-1.

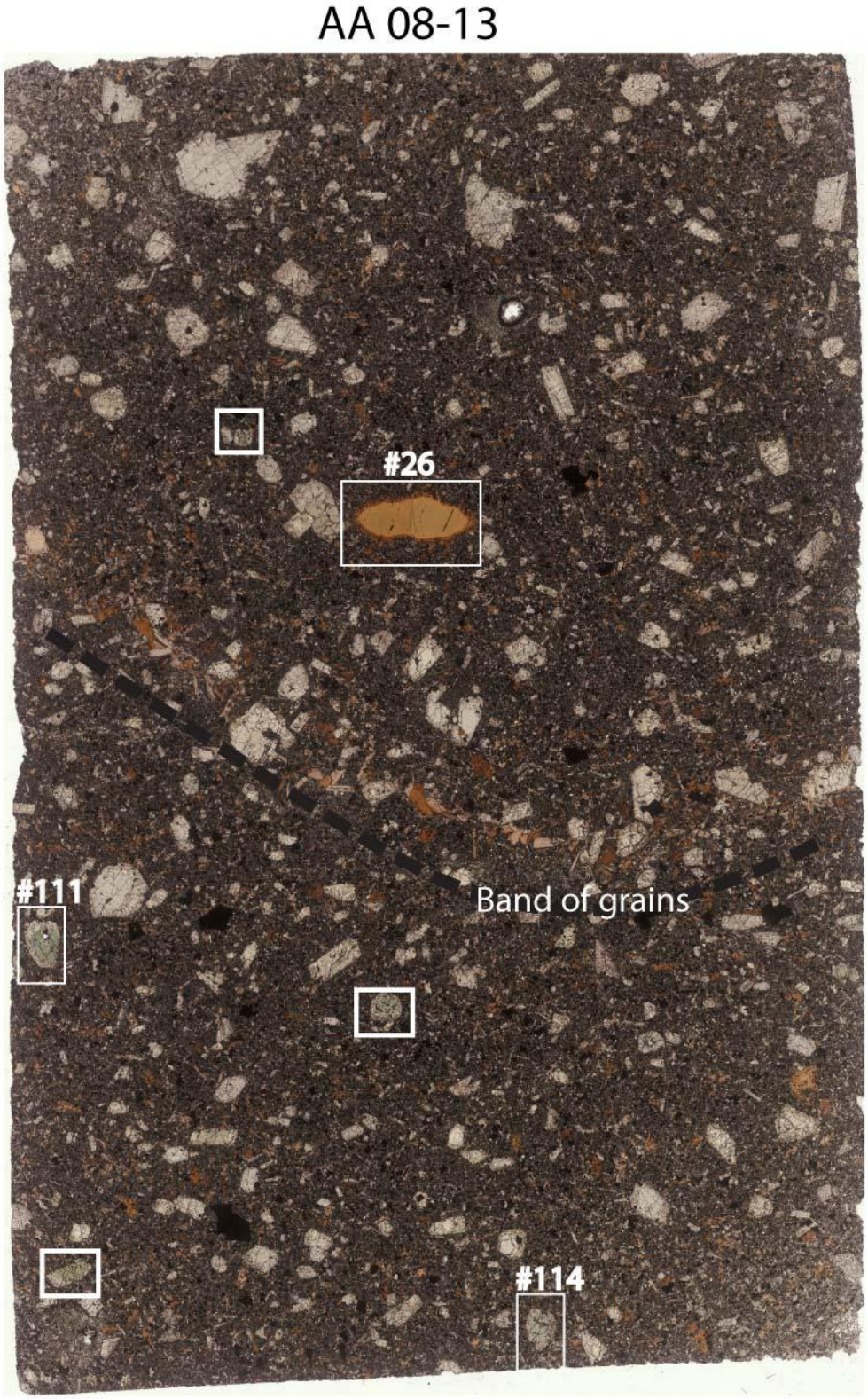

Figure 6-2: Thin-section scan of sample AA 08-13 which is classified as an aillikite. Phenocrysts of CPX, biotite, and spinel in a fine grained matrix of CPX, biotite, spinel, and analcite. Analyses results of #111 and #114 can be seen in Table 8-1. Analyses results from #26 can be seen in Appendix A under the subtitle; Biotite Single Spot EMP Analyses.

Figure 6-3: Thin-section scan of sample AA 08-14 which is classified as a sannaite. Phenocrysts of CPX, biotite, and spinel in a fine grained matrix of CPX, biotite, spinel, and analcite. Analyses results of #134 can be seen in Table 8-2.

Figure 6-4: Thin-section scan of sample DEF 08-06 which is classified as a sannaite. Phenocrysts of CPX, biotite, spinel, and calcite in a fine grained matrix of CPX, biotite, spinel, K-feldspar, and analcite. CPX phenocryst profiles DEF 08-06-4, DEF 08-06-5 and DEF 08-06-7 can be seen in Figure 8-8 - Figure 8-15. Biotite phenocryst profile DEF 08-06-02 can be seen in Figure 8-23 and Figure 8-24.

Figure 6-5: Thin-section scan of sample AA 08-16 which is classified as a sannaite. Phenocrysts of CPX, biotite, spinel, and calcite in a fine grained matrix of CPX, biotite, spinel, K-feldspar, analcite, and carbonate. Biotite phenocryst profiles AA 08-16-1 and AA 08-16-2 can be seen in Figure 8-21, Figure 8-22, Figure 8-25 and Figure 8-26.

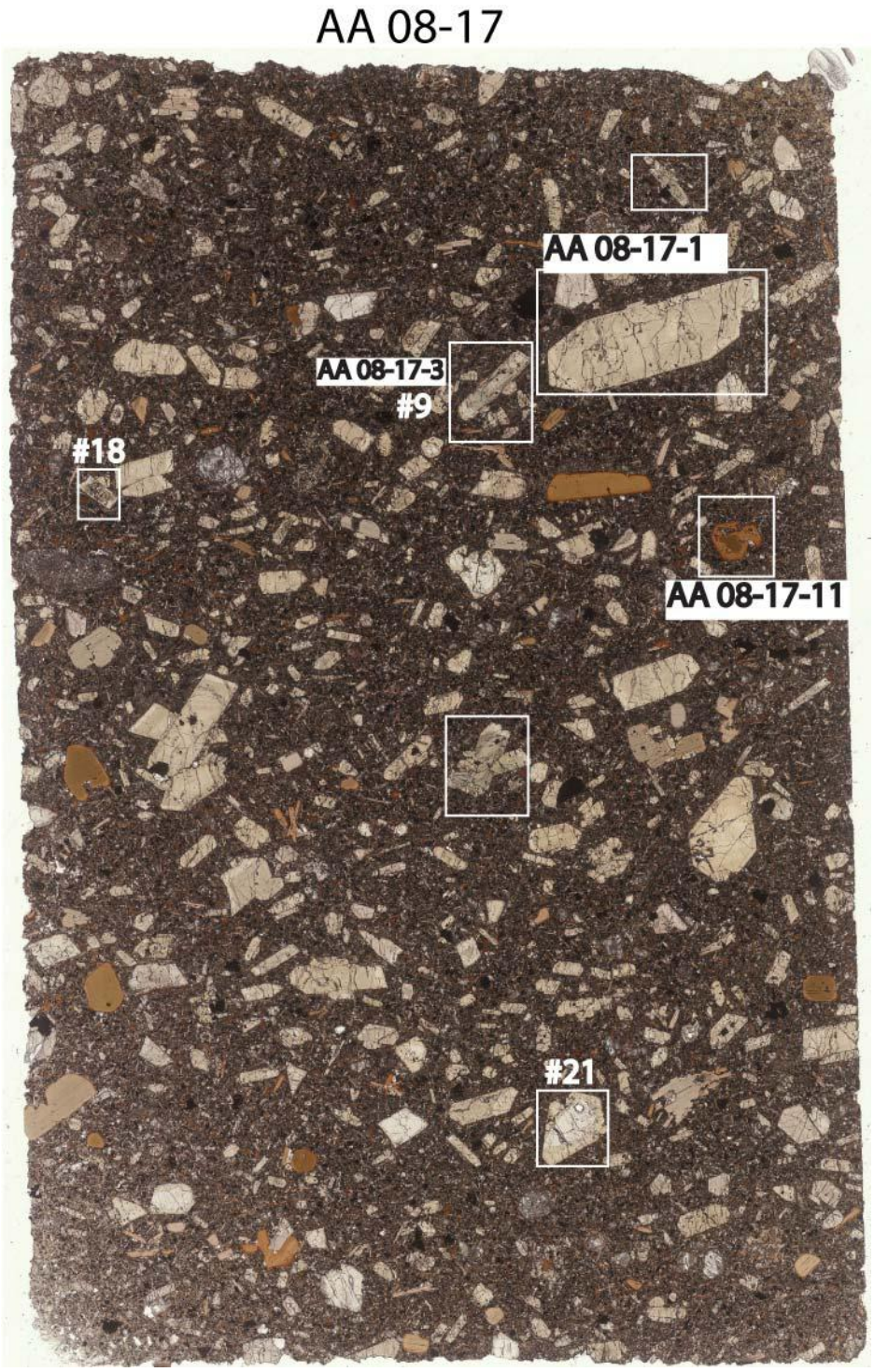

Figure 6-6: Thin-section scan of sample AA 08-17 which is classified as a sannaite. Phenocrysts of CPX, biotite, spinel, and calcite in a fine grained matrix of CPX, biotite, spinel, K-feldspar, analcite, and carbonate. CPX phenocryst profiles AA 08-17-1 and AA 08-17-3 can be seen in Figure 8-4, Figure 8-5, Figure 8-16 and Figure 8-17. Analyses #9, #18 and #21 can be seen in Table 8-2.

6.2 Minerals and textures

CLINOPYROXENE

CPX phenocrysts vary in size, shape, color, and other attributes. Most crystals are euhedral to subhedral, with an elongated shape (Figure 6-7 F). The longest axis in a CPX phenocryst varies from a few hundred µm up to 6 mm in length. Glomeroclasts are observed, some with few larger phenocrysts (Figure 6-7 G) and others with many smaller anhedral crystals. Acicular CPX crystals form radiating aggregates and are abundant some samples.

Different varieties in color are observed, grey cores with brown rims, green cores with grey rims, and grey cores with pink rims. AA 08-17-3 (Figure 6-7 F) is even more complicated with at least six different zones of grey, brown and green from the inner core to the outer rim. These different zones can be linked to different chemical compositions which will be further elaborated in chapter 8, Mineral Chemistry.

The cores in most grains show signs of resorbtion. The transition between the core and the outer rim is sometimes very irregular like AA 08-17-1 (Figure 6-7 D) and has a marked contrast in chemistry. Other grains have rounded cores as in AA 08-17-3 (Figure 6-7 F) and has a more gradational change in chemistry. The appearance of the rims of resorbed grains varies significantly.

Complex zoning is also observed, for example parallel stripes, patches, compositional zoning, hour-glass zoning (Figure 6-7 E), sector zoning (Figure 6-7 A), and irregular zoning. Simple twinning of CPX is observed in DEF 08-05, DEF 08-06, AA 08-16, and AA 08-17.

Inclusions are common in CPX phenocrysts, both primary and secondary. Spinel (Figure 6-7 B) and apatite (DEF 08-01-3) are often seen delineating surfaces between different compositions and are interpreted as primary inclusions. They are also found having high concentrations in different zones of phenocrysts. AA 08-17-3 (Figure 6-7 F) appears to have several small inclusions of spinel in the grey/green zone and in the outermost layer. A small euhedral biotite grain with six crystal faces is found inside a CPX phenocryst which has preserved the crystal shape of the biotite grain. Patches of carbonate/chlorite are found in several crystals, often related to cracks. Patches of chlorite (Figure 6-7 C), K-feldspar, and quartz have also been found, but are interpreted as secondary minerals.

Black overgrowth forming stripes or dots on CPX phenocrysts appear in sample AA 08-11. CPX phenocrysts in AA 08-14 contain dark green alteration zones with anomalous interference colors in cracks. CPX in AA 08-16 show a lot of alteration products. EMP-spot analyses did not give any good results but chlorite, carbonate and tremolite alteration is common alteration products of CPX (Rock, 1991).

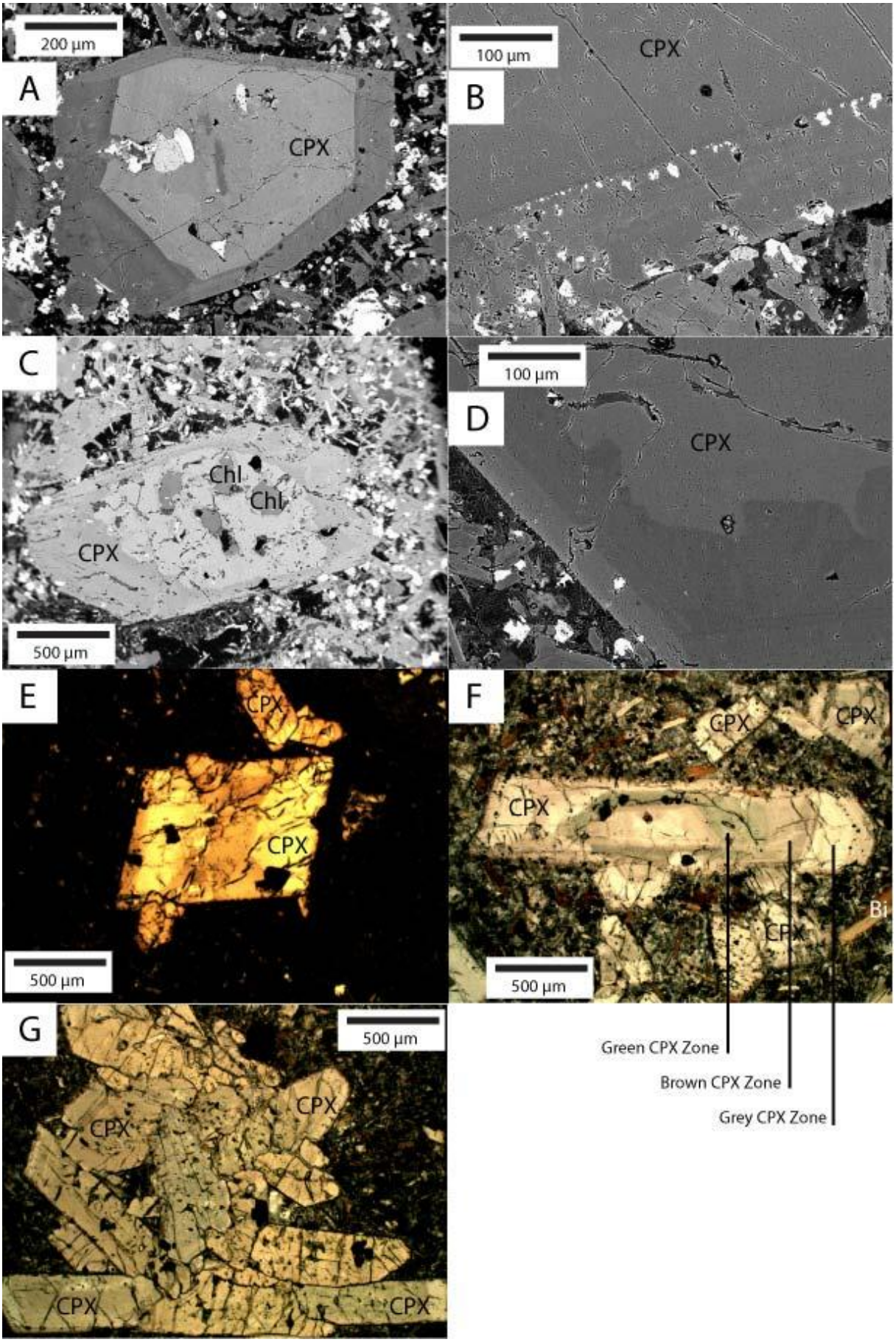
200 µm
A
CPX
100 µm
CPX
B
C
Chl
Chl
CPX
500 µm
100 µm
D
CPX
E
CPX
CPX
500 µm
F
CPX
CPX
CPX
CPX
Bi
500 µm
G
500 µm
CPX
CPX
CPX
CPX
CPX
Green CPX Zone
Brown CPX Zone
Grey CPX Zone

Figure 6-7: Images A-D are EMP BS-images, E-G are photomicrographs taken with crossed nicols. A) Sector zoning in CPX phenocryst AA 08-13-6, a common feature in lamprophyres (Rock, 1991). B) Opaque minerals delineating growth surfaces in CPX phenocrysts with different compositions in AA 08-13-1. C) Patches of chlorite in green core phenocryst DEF 08-01-4. D) CPX phenocryst AA 08-17-1 show an irregular resorbtion edge with marked chemical contrast. E) Hour-glass zoning in CPX phenocryst LEA 06-81-2. F) Complex zoning with opaque inclusions in AA 08-17-3 CPX phenocryst. G) A compact CPX glomeroclast DEF 08-06-8.

Biotite

Biotite phenocrysts in samples DEF 08-05, DEF 08-06, AA 08-16, AA 08-17 come in different sizes, the longest axis in a crystal may vary from just a few hundred µm to over 3 mm. Inclusions or lamellae of spinel (Figure 6-8 A) or CPX are common inside most biotite grains. Many biotite phenocrysts are bent or kinked (Figure 6-8 A), a phenomena typical for biotite phenocrysts in lamprophyres (Rock, 1991). Different types of zoning are seen in the biotite phenocrysts. Biotite phenocrysts with a light brown core and a thin darker brown rim (Figure 6-8 A) are found in most samples. Some biotite phenocrysts in samples AA 08-16 and AA 08-17 exhibit a dark brown core followed by a lighter brown inner rim and a darker brown outer rim (Figure 6-8 B). Most biotite phenocrysts show resorbtion which vary in appearance (Figure 6-8 A and B), similar to the CPX phenocryst resorbtion. Completely anhedral medium sized biotites found in these samples most likely represents resorbed biotite phenocrysts.

Whereas biotite phenocrysts are absent in DEF 08-01 and AA 08-11, samples AA 08-13 and AA 08-14 contain a few large resorbed biotites with inclusions or lamellae, these are some times kinked.

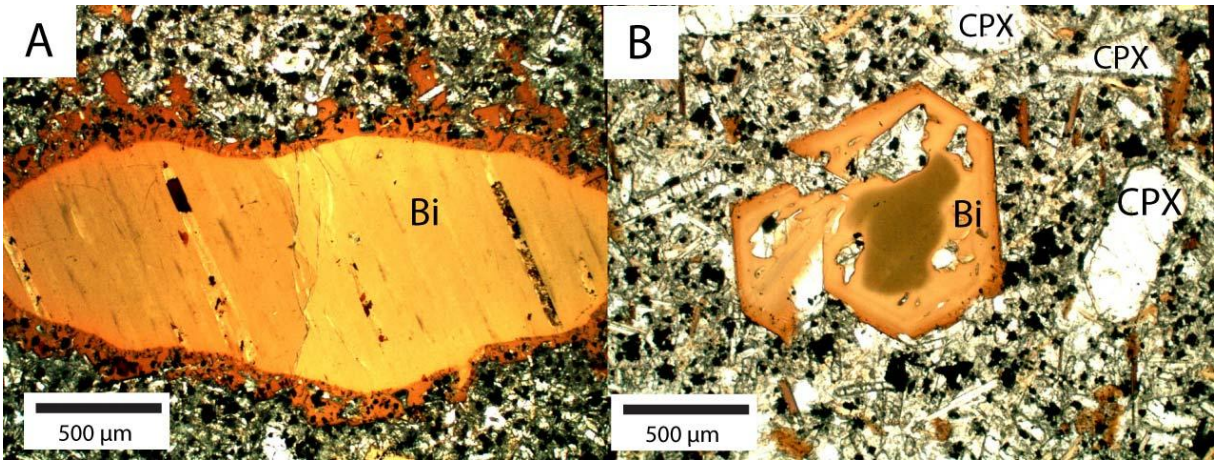

Figure 6-8: A) Photomicrograph taken with crossed nicols of a resorbed biotite phenocryst (AA 08-13-8) with lamellae of spinel. B) Photomicrograph taken with crossed nicols of a subhedral biotite phenocryst AA 08-17-11 with a resorbed dark inner core, a lighter brown inner rim and a brown outer rim.

Spinel

All samples in question contain some sort of spinel phenocryst, except samples DEF 08-01, AA 08-11 which contain very little. All samples appear to have resorbed spinel which can have a very varied appearance (Figure 6-9 E and F). Subhedral (Figure 6-9 D) and euhedral (Figure 6-9 B) crystals are also found. The almost euhedral spinel phenocryst AA 08-13-11 (Figure 6-9 B) might have kept its crystal

shape due to the protection provided by the CPX surrounding it while DEF 08-06-10 (Figure 6-9 C) was resorbed before the CPX grew on it. Spinel with hollow interiors are seen in Figure 6-9 A. Spinel is also found as lamellae in biotite phenocryst AA 08-13-8 (Figure 6-8 A).

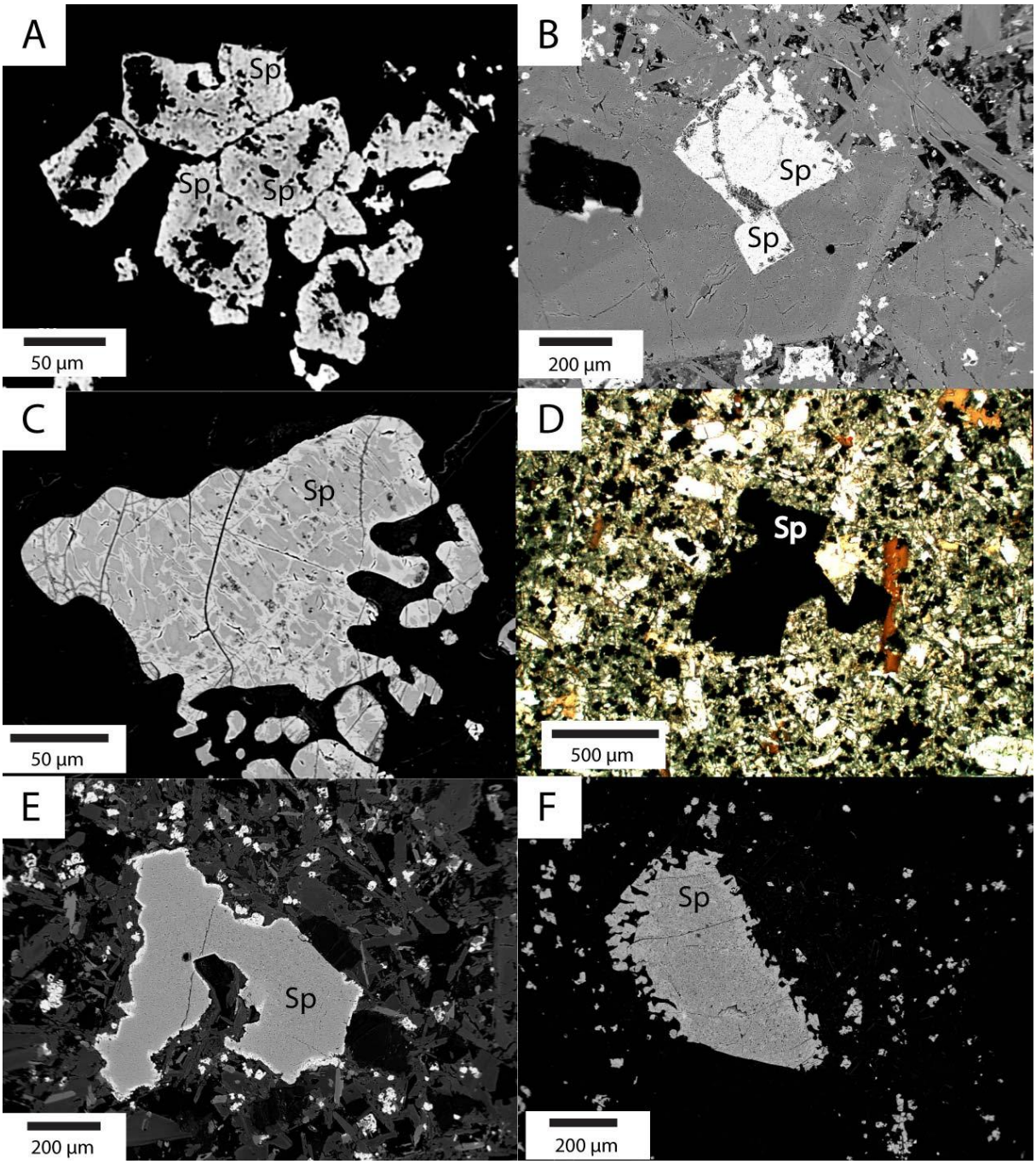

Figure 6-9: Images A, B, C, E and F are EMP BS-images, D is a photomicrograph taken with crossed nicols. A) Spinel grains (AA 08-13-4) with hollow interiors. B) A euhedral spinel phenocryst in CPX, AA 08-13-11. C) A resorbed spinel crystal in a CPX phenocryst (DEF 08-06-10). D) Image of spinel phenocryst (AA 08-13-10). E) A spinel phenocryst rich in Cr, Mg, Al, Ti, Fe (DEF 08-01-25). F) A spinel phenocryst (AA 08-17-14) rich in Ti and Fe with an Fe-rich rim and matrix.

Samples DEF 08-06, AA 08-16, and AA 08-17 contains phenocrysts of calcite (Figure 6-10 A). Sample DEF 08-01 contains an unknown mineral (Figure 6-10 B). Analyses of this mineral can be found in chapter 13, Appendix A.

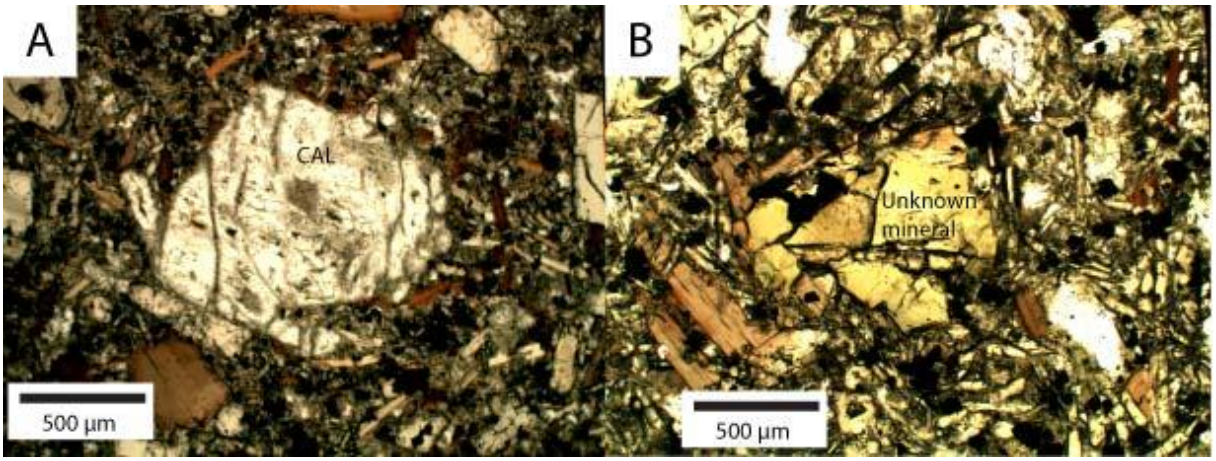

Figure 6-10: A) Photomicrograph of calcite phenocryst AA 08-17-20, taken with crossed nicols. B) Photomicrograph of fluid-rich mineral DEF 08-01-9, taken with crossed nicols.

Matrix

Most phenocrysts are easily identified with the help of the petrographic microscope. Identification of the minerals making up the fine-grained matrix is more difficult and is based on EMP. Thus, the matrix minerals have only been identified with certainty in a few samples. A selection of the EMP analyses has been included in Appendix A. Some minerals have only been analyzed and identified with non-quantitative analyses and will not be included in Appendix A.

CPX crystals seem to be the dominant mineral in the matrix. They vary in size between 30-200 µm and most grains are euhedral to subhedral. Most grains exhibit dark cores and lighter rims (when seen in BS images). Some are found rimming globular structures as aggregates/glomeroclasts (Figure 6-12 E).

Biotite grains are generally less common in the matrix and appear as small anhedral grains or lathlike crystals with a thin lighter colored rim, evenly spread throughout the thin section. In samples DEF 08-05, DEF 08-06, AA 08-16, and AA 08-17 biotite rimming grains and aggregates/ocelli are seen (Figure 6-12 B and D). In samples AA 08-14 and DEF 08-01 biotite grains vary more in size and the larger ones are anhedral and appear resorbed (also considered to be totally resorbed phenocrysts), some are also bent/kinked. AA 08-13 does not have biotite equally spread throughout the thin section, but a band of high biotite-concentration runs through the thin section.

The different samples have been classified according to the classification schemes in Chapter 1, Classification and nomenclature. DEF 08-01 and AA 08-13 have been classified as aillikites while AA 08-14, DEF 08-06, AA 08-16, and AA 08-17 has been classified as sannaites. DEF 08-05 is the same dyke as DEF 08-06 and is thus a sannaite. The classification is further supported by the bulk rock chemistry (Table 7-1 and Table 7-5) which shows that the dykes show a similar composition to alkaline - and ultramafic lamprophyres. In addition Figure 7-1 show a rock discrimination diagram by

Rock (1987) which show that the rocks are AL and UML. In addition, the samples M-14C and M-21 (Buchanan, 2008) have been classified as kersanites which are calc-alkaline lamprophyres.

In the sannaites (Figure 6-11 a), the voids between biotite - and CPX grains are filled with a mix of analcite, K-Feldspar, spinel, and calcite. In addition minor amounts of apatite, chlorapatite, titanite, pyrite and chalcopyrite has also been observed in most samples.

The aillikites has a matrix containing CPX and biotite with analcite and spinel filling the voids. An important difference between the sannaites and the aillikites is the lack K-feldspar in the aillikites and that they contain more than 90% mafic minerals (Figure 6-11 A).

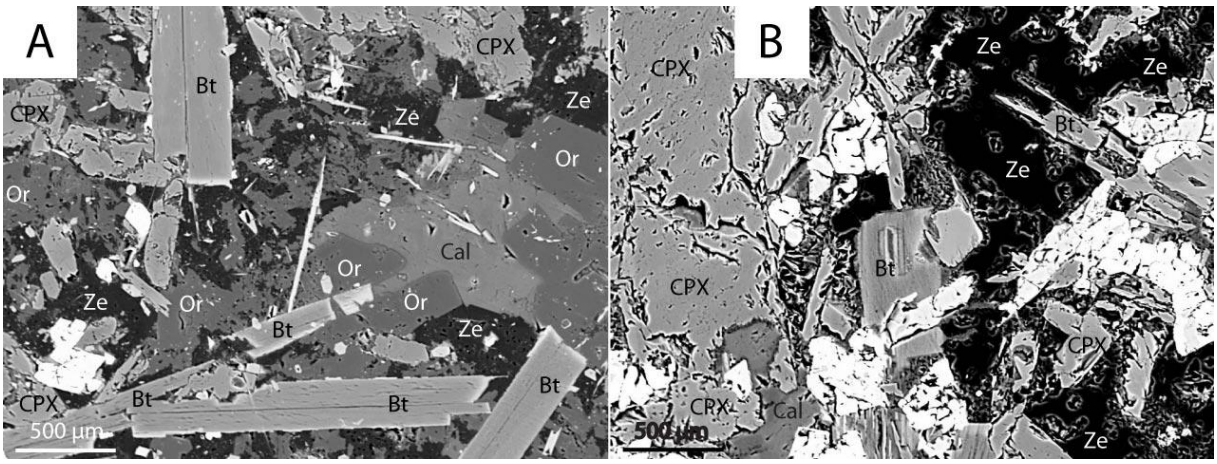

Figure 6-11: A) A BS-picture of sample area AA 08-17-16 which is an example of sannaite matrix. B) A BS-picture of sample area DEF 08-01-20 which is an example of aillikite matrix.

Aggregates/ocelli are found in the matrix in all samples and show great diversity. Figure 6-12 shows only a few of the different types of aggregates/ocelli observed. Some aggregates/ocelli contain calcite, others a mix of calcite and chlorite. Others have a matrix of e.g. analcite with acicular biotite, titanite and small apatite grains. The aggregate/ocelli in Figure 6-12 C appears to have two parts, the right part is analcite (qualitative energy dispersive X-ray spectroscopy (EDS) measurement) with matted needles of titanium-rich biotite (EDS), small CPX crystals, and small Fe-sulphides. The left part is a mix of K-feldspar, calcite (EDS) and chlorite (EDS) with no crystallographic features.

Azbej et al. (2006) recognize three different types of carbonate aggregates and propose explanations for their genesis:

The Type-I aggregates are globular in shape, contain primary aqueous fluid inclusions, lack major element zonation, and show tangentially aligned mica at the contact with the host rock (caused by expansion of gas bubbles in a partially crystallized magma (Phillips, 1973)). Based on microthermometric analyses and geothermometric calculations, it was concluded that these aggregates precipitated from aqueous hydrothermal solutions to fill vesicles in the crystallized (or partially crystallized) melt (Azbej et al., 2006). This observation is inconsistent with previous models that explain the genesis of such features by silicate-carbonate melt immiscibility (von Seckendorff et al., 2004).

Type-II aggregate also host primary fluid inclusions but show polygonal shape and lack oriented sheet silicates at their rims. Type-II aggregates were interpreted to have formed from hydrothermal fluids, similar to those forming Type-I aggregates, except that the carbonate phases precipitated in spaces previously formed by olivine phenocrysts (Azbej et al., 2006).

Type-III aggregates are interpreted as having a xenolithic – xenocrystic origin supported by their polygonal, irregular shape consistent with an origin as fragments from the conduits of the intruding lamprophyre melt. Another geochemical feature of the Type-III aggregate is that they contain Mg- and Fe-rich carbonate phases at the rims and Ca-rich carbonate cores. Compositional zoning in these aggregates is interpreted as the reaction between solid carbonate wall rock and hot lamprophyre melt, resulting in rapid melting and crystallization of carbonate xenoliths (Azbej et al., 2006). The rapid ascent to the surface of a lamprophyre after entrainment of carbonate wall-rock fragments (Rock, 1991) leave little time for complete assimilation and it is only the rim which show evidence of interaction with the host melts.

Aggregates comparable to the Type-I and Type-II aggregates can be seen in Figure 6-12, image B and D. A network of carbonate veins is often seen between the aggregates in thin-section, a feature also mentioned by Azbej et al. (2006), which he interprets as an indication that Type-I and Type-II aggregates originate from similar melts. A globular shape and tangentially aligned mica at the contact with the host rock is also seen in these samples. An obvious difference is that no dolomite is seen, but a similar zonation is seen with a calcite core and K-feldspar rim. An aggregate/ocelli (Figure 5-6) is seen in the field also show similarities to these aggregate/ocelli in thin-section. An eroded (presumably) calcite core, and a feldspar rich inner rim and a dark outer rim.

Some aggregates (e.g. Figure 6-12, image E) exhibit the polygonal, irregular shape similar to the Type-III aggregates. They do not however exhibit the compositional zoning seen in Type-III aggregates and does not contain the same mineral phases.

An alternative explanation for the different aggregates/ocelli include progressive partial equilibrations – crystallization of refractory minerals, melting and assimilation of fusible components – produces progressively more evolved and hydrous melts (Hamilton, 1994). The structure in Figure 6-12, image A could represent evolved and hydrous melts (Hamilton, 1994) because it shows similarities to the surrounding matrix, both in composition and grain size. The other structures of syenitic composition dominated by alkali feldspars could suggest mixing of coexisting melts that were immiscible due to different viscosities and high CO_2 contents (von Seckendorff et al., 2004).

An interesting phenomenon is seen in Figure 8-19, which show that the outer CPX grains show similar compositions as matrix CPX while the inner CPX analyses are depleted in TiO_2 and Al_2O_3 and have a higher SiO_2 content. The analyses 68# and 69# could reflect the primary composition of the xenoliths or late melts which are not enriched in Ti and Al while 70# and 71# show compositions with higher TiO_2 and Al_2O_3 contents similar to matrix CPX. These two analyses are unique in these samples; no other analyses show such low concentrations of TiO_2 and Al_2O_3.

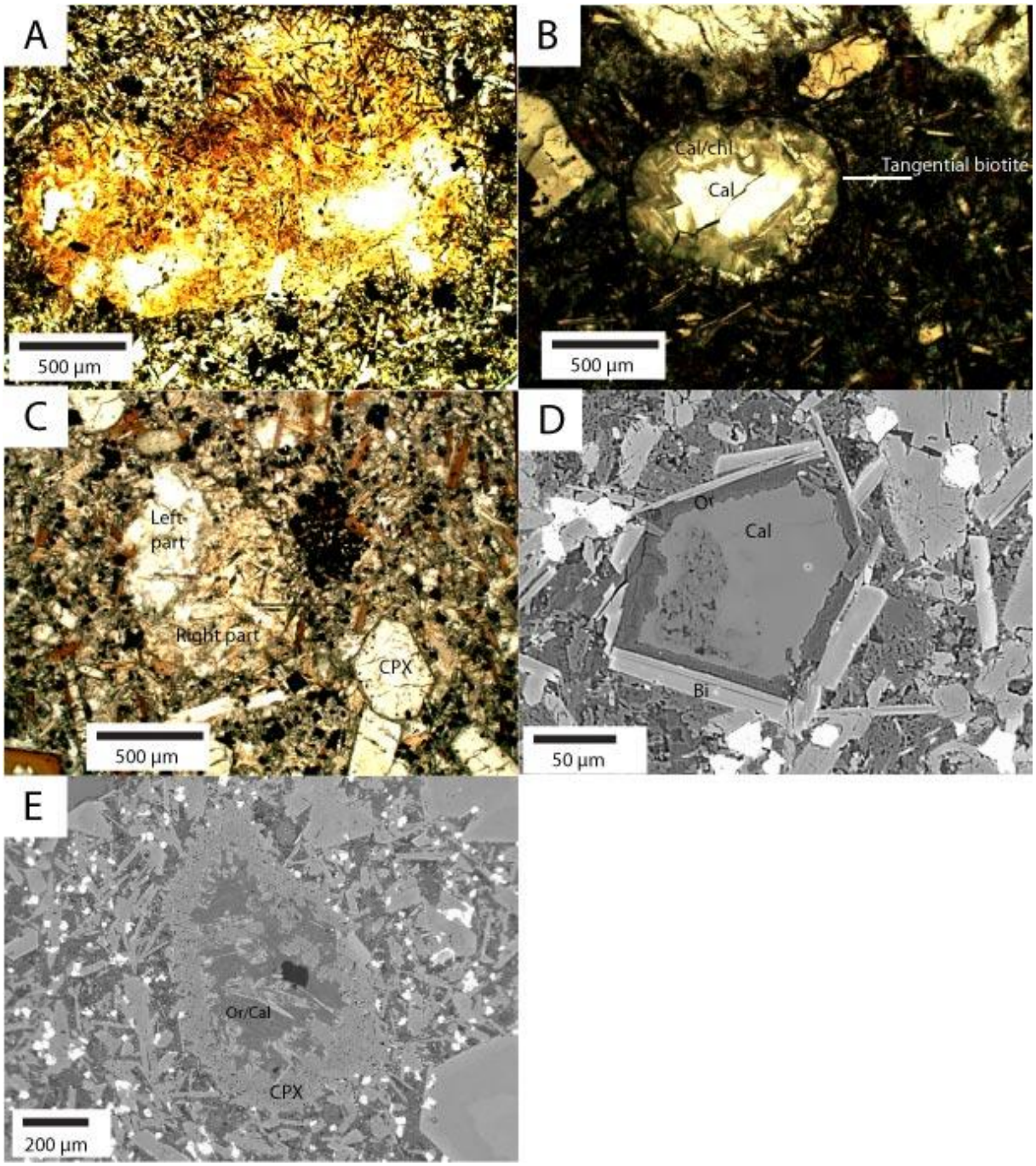

Figure 6-12: Images A, B and C are photomicrographs taken with crossed nicols, D is an EMP BS-image. A) A rounded aggregate/ocelli with complex mineralogy of analcite, biotite, titanite and apatite. B) A Type-I or Type-II aggregate (Azbej et al., 2006) with a core of calcite, a rim of mixed calcite and chlorite with tangentially aligned mica as a border to the host rock. C) A rounded aggregate/ocelli with two different mineralogies. D) A core of calcite rimmed by K-feldspar and lath-like biotite crystals, a Type-I or Type-II aggregate (Azbej et al., 2006). E) A mix of K-feldspar, calcite, apatite and quartz rimmed by an aggregate of CPX grains, Type-III aggregate (Azbej et al., 2006).

Other general observations

The thin-sections selected for EMP analyses were selected because of their fresh appearance and phenocryst assemblage. The other samples are variably altered and were not suitable for the objective of the analyses. E.g. sample DEF 08-02 which exhibit secondary calcite (Figure 6-13) sometimes mixed with chlorite.

The samples selected for EMP analyses were also the most porphyritic with up to 30 % phenocrysts (rough estimation). Samples DEF 08-02, DEF 08-03, DEF 08-04 and LEA 06-81 contain very few phenocrysts, some less than 5% (rough estimation).

Although CPX phenocrysts show alteration they are easy to distinguish and show similarities to CPX phenocryst assemblage in the analyzed samples. They do not however exhibit complex zoning patterns and green cores are not found in the samples which are not analyzed.

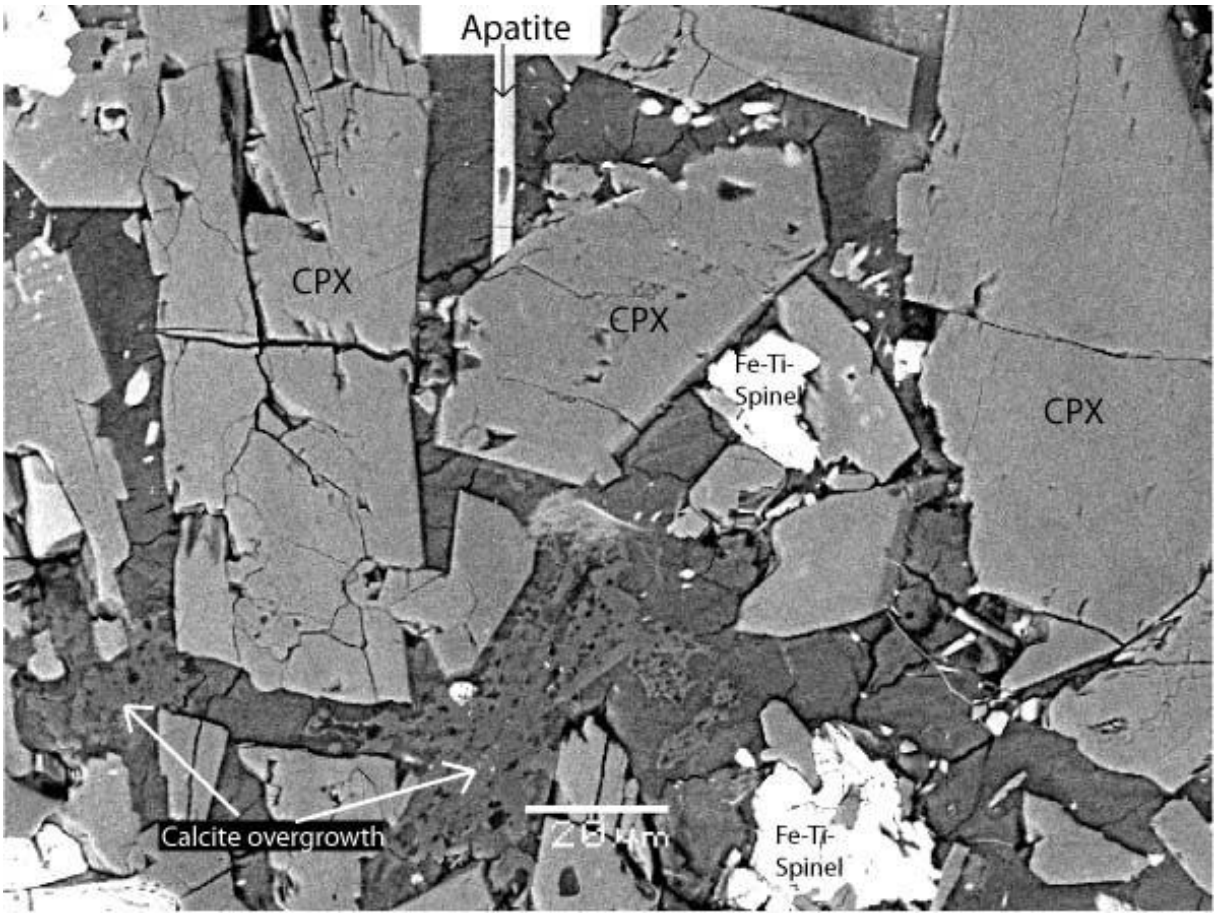

Figure 6-13: SEM BS-image showing calcite overgrowth in sample DEF 08-02. While this calcite appears secondary, the calcite in Figure 6-11 A which appear magmatic.

AA 08-12 and AA 08-15

Samples AA 08-12 and AA 08-15 differ texturally as well as compositionally from the other samples and has a very different mineralogy. AA 08-15 (Figure 6-14 A, B, C, and D) contain a few 200-500 µm phenocrysts of quartz along with round patches of chlorite. The matrix consists of K-feldspar, quartz,

chlorite, magnetite, and minor pyrite. Compared to the other samples, albite is the phenocryst stage and CPX fills the voids in between the albite phenocrysts in the poikilitic texture (Figure 6-14 A). Analysis of the matrix CPX can be seen in chapter 13, Appendix A, analysis #124, #125, #126, and #127.

AA 08-12 (Figure 6-14 E and F) contain a few 500 – 1000 µm albite phenocrysts along with circular patches of chlorite and some aggregates of opaque minerals. The matrix consists of crystals of albite, anorthite, orthoclase, chlorite, and magnetite.

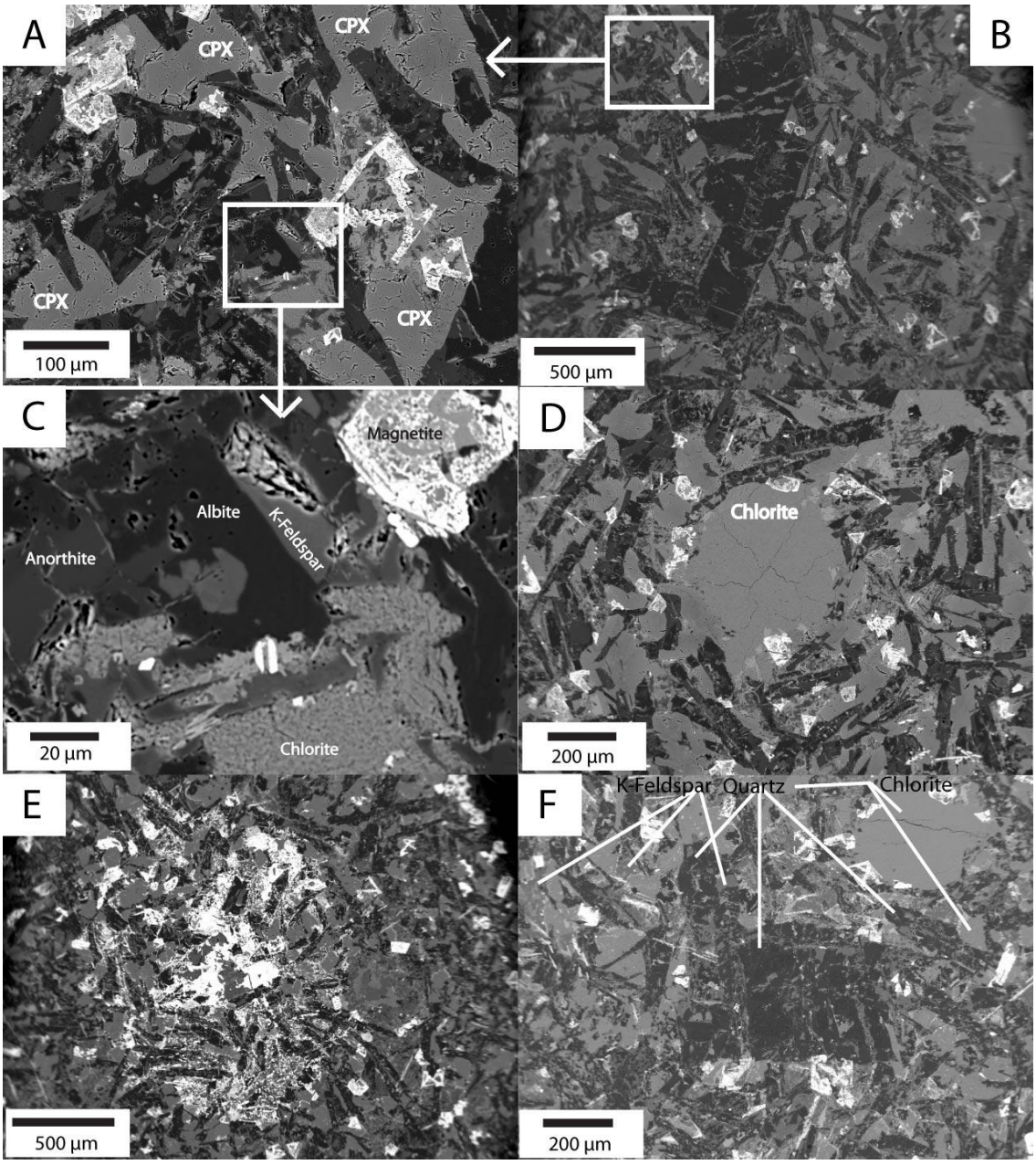

Figure 6-14: EMP BS-images of samples AA 08-12 and AA 08-15. A) Blow-up from image B) of analysis area AA 08-15-1b showing matrix CPX, feldspar, and spinel with a poikilitic texture. B) Image of albite phenocryst AA 08-15-1. C) Blow-up from image A) showing the mix of feldspars, chlorite, and magnetite in the matrix. D) Image of sample area AA 08-15-2 showing a circular chlorite patch. E) Image of sample area AA 08-12-4 showing a cluster of opaque minerals. F) Sample AA 08-12-2 showing a quartz phenocryst and chlorite, K-feldspar and quartz matrix.

7 Bulk Rock Chemistry

7.1 XRF

Analytical details, detection limit and uncertainties

Bulk rock analyses of 15 samples were performed at Geological Survey of Norway (NGU) in Trondheim on a PANalytical Axios Wavelength Dispersive X-ray Fluorescence Spectrometer (WD-XRF). The samples had already been crushed by a Jaw-crusher at the Department of Geosciences and were ready to be milled down in an agate-mill. For main element analysis sample material was burnt to get rid of organic material and then heated to a 1000 °C to predict loss of volatiles before melting. Glass beads were made by melting of 4.2 g Li2B4O7 + 0.6 g sample material. For analysis the PANalytical Axios 4 kW XRF (Rh-x-ray tube) was used. A table containing detection limit and uncertainties is pasted below.

LOWER DETECTION LIMIT (LLQ) AND UNCERTAINTIES FOR ANALYIS OF MAIN ELEMENTS (in %)

Element / Compound:	SiO_2	Al_2O_3	Fe_2O_3	TiO_2	MgO	CaO	Na_2O	K_2O	MnO	P_2O_5
LLQ:	0,5	0,02	0,01	0,01	0,04	0,01	0,1	0,01	0,01	0,01
$K_{ELEMENT}$ / $\%^{½}$	0,09	0,04	0,06	0,02	0,08	0,06	0,04	0,07	0,01	0,02

The uncertainties represent coverage factor 1 (68% confidence level),
by multiplying the uncertainty by 2 a confidence level of 95% is attained.

*) Are not accredited

BaO*	Cr_2O_3*	CuO*	HfO_2*	NiO*	PbO*	SrO*	V_2O_5*	ZnO*	ZrO_2*
0,03	0,02	0,01	0,02	0,01	0,01	0,04	0,02	0,01	0,02

For trace element analysis 9.6 g sample material + 2.4 g LicoWax (Hoechst C) was homogenized in a shaker. The mix was then transferred to a machine to press a pellet and was ready to be analyzed. For analysis the PANalytical Axios 4 kW x-ray spectrometer (Rh-x-ray tube) was used and analysis software used was ProTrace. Tables containing lower detection limit and analysis uncertainties are pasted below.

LOWER DETECTION LIMIT FOR TRACE ELEMENTS IN mg/kg (ppm) (except S, F and Cl in %)

Ag	As	Ba	Cd	Ce	Co	Cr	Cu	Ga	La	Mo	Nb	Nd	Ni	Pb
10	10	10	10	20	4	4	2	1	10	1	1	10	2	3

Rb	Sb	Sc	Sn	Sr	Th	U	V	W	Y	Yb	Zn	Zr	Cl	F

1	15	5	10	1	4	2	5	5	1	5	1	1	0,05	0,1

S	*Au**	*Bi**	*Br**	*Cs**	*Ge**	*Hf**	*Hg**	*I**	*Pt**	*Se**	*Sm**	*Ta**	*Te**	*Tl**
0,02		10	5	10	1	5	20	100		5	10	4	10	20

*) Are not accredited

Analysis uncertainty (coverage factor 1) :

Element	*Area of analysis /mg/kg*	Uncertainty
Co, Cr, Cu, Ga, Mo, Nb, Ni, Pb, Rb, Sr, Th, U, V, Y, Zn	< 50	< ± 10 % relative
	>50	< ± 5 % relative
Ag, As, Ba, Cd, La, Nd, Sc, Sn, W, Zr	< 50	< ± 20 % relative
	>50	< ± 10 % relative
Ce, Ge, Hf, Mn, Sb, Sm, Ta, Yb	< 50	< ± 30 % relative
	>50	< ± 15 % relative
Bi, Br, Cs, Hg, I, Se, Te	< 100	< ± 50 % relative
	>100	< ± 25 % relative
F, Cl, S, CaO, K_2O, Fe_2O_3, MgO, TiO_2	< 10000	< ± 50 % relative
	>10000	< ± 25 % relative
Al_2O_3, SiO_2, Na_2O, P		< ± 50 % relative

XRF Results of Major and Trace Elements

Sample id. *	SiO2 [%]	Al2O3 [%]	Fe2O3 [%]	TiO2 [%]	MgO [%]	CaO [%]	Na2O [%]	K2O [%]	MnO [%]	P2O5 [%]	L.O.I. [%]	Total main [%]	BaO* [%]	Cr2O3* [%]	CuO* [%]	HfO2* [%]	NiO* [%]	PbO* [%]	SrO* [%]	V2O5* [%]	ZnO* [%]	ZrO2* [%]
DEF 08-01	37,6	9,90	12,4	3,94	11,1	13,8	1,97	0,832	0,202	0,953	7,11	99,8	0,113	0,070	<0.01	<0.02	0,025	<0.01	0,160	0,076	0,011	0,047
DEF 08-02	40,0	11,0	15,0	4,74	8,33	11,3	2,05	2,26	0,229	0,867	4,06	100	0,119	0,037	<0.01	<0.02	0,022	<0.01	0,139	0,072	0,017	0,071
DEF 08-03	38,5	11,0	13,2	4,17	9,51	13,6	2,56	0,802	0,266	0,823	5,39	100	0,137	0,033	<0.01	<0.02	0,014	<0.01	0,123	0,078	0,013	0,052
DEF 08-04	38,2	10,7	13,5	4,23	9,76	14,8	2,38	0,323	0,216	0,800	5,22	100	0,063	0,031	<0.01	<0.02	0,012	<0.01	0,112	0,084	0,013	0,051
DEF 08-05	39,3	11,8	13,6	4,21	7,36	13,6	1,39	3,23	0,249	0,784	4,34	99,8	0,163	<0.02	0,011	<0.02	0,011	<0.01	0,138	0,093	0,013	0,043
AA 08-11	38,1	10,4	13,3	4,18	10,3	14,4	1,44	1,75	0,218	1,01	5,38	100	0,138	0,082	<0.01	<0.02	0,022	<0.01	0,164	0,081	0,018	0,051
AA 08-12	44,1	13,3	16,0	3,36	4,69	7,45	2,91	1,80	0,202	0,555	5,77	100	0,112	<0.02	<0.01	<0.02	<0.01	<0.01	0,100	0,076	0,016	0,045
AA 08-13	35,4	10,2	15,7	4,83	8,28	16,1	1,41	1,51	0,218	0,701	5,22	99,6	0,106	<0.02	0,011	<0.02	<0.01	<0.01	0,109	0,102	0,015	0,046
AA 08-14	36,8	11,6	15,2	4,37	6,81	14,3	1,26	2,65	0,203	0,823	5,39	99,4	0,133	<0.02	0,011	<0.02	<0.01	<0.01	0,166	0,095	0,015	0,051
AA 08-15	46,9	12,5	15,0	3,12	5,01	8,44	2,91	1,35	0,210	0,505	1,99	98,0	0,088	<0.02	<0.01	<0.02	<0.01	<0.01	0,100	0,077	0,016	0,042
AA 08-16	38,7	11,6	13,8	4,23	7,54	13,6	1,63	2,96	0,224	0,779	4,70	99,8	0,158	0,022	0,011	<0.02	0,012	<0.01	0,153	0,089	0,013	0,041
AA 08-17	39,7	11,5	13,2	4,33	7,75	14,0	1,60	2,91	0,279	0,764	4,21	100	0,161	0,025	0,011	<0.02	0,010	<0.01	0,123	0,090	0,012	0,042
AA 08-21	39,4	12,1	12,3	3,54	6,66	14,4	1,92	2,08	0,190	0,424	5,85	98,9	0,112	0,043	<0.01	<0.02	0,026	<0.01	0,121	0,064	0,014	0,036
LEA 06-81	39,1	12,4	14,5	4,16	7,00	12,6	1,38	3,19	0,310	0,843	4,40	99,8	0,126	<0.02	<0.01	<0.02	<0.01	<0.01	0,215	0,096	0,013	0,050
LEA 06-93	40,3	11,3	12,8	3,96	8,96	14,2	2,10	1,94	0,200	0,537	3,73	100	0,160	<0.02	0,012	<0.02	<0.01	<0.01	0,143	0,087	0,013	0,039

Table 7-1: XRF bulk rock major element analyses from NGU, Trondheim.

Sample id.	Ag	As	Ba	Cd	Ce	Co	Cr	Cu	Ga	La	Mo	Nb	Nd	Ni	Pb	Rb	Sb	Sc	Sn	Sr
	[mg/kg]	[mg/kg]	[mg/kg]	[mg/kg]	[mg/kg]	[mg/kg]	[mg/kg]	[mg/kg]	[mg/kg]	[mg/kg]	[mg/kg]	[mg/kg]	[mg/kg]	[mg/kg]	[mg/kg]	[mg/kg]	[mg/kg]	[mg/kg]	[mg/kg]	[mg/kg]
DEF 08-01	<10	<10	942	<10	202	60,6	434	80,6	17,2	87	1,7	120	93	160	<3	29,7	<15	28,8	<10	1090
DEF 08-02	<10	<10	1070	<10	179	63,9	257	46,7	22,8	83	3,7	96,4	88	151	<3	40,8	<15	23,0	<10	936
DEF 08-03	<10	<10	1200	<10	212	56,7	216	94,0	18,1	78	2,6	123	80	88,4	<3	21,8	<15	31,3	<10	858
DEF 08-04	<10	<10	593	<10	187	57,1	207	88,0	18,9	84	1,7	113	86	93,3	<3	10,7	<15	31,2	<10	762
DEF 08-05	<10	<10	1660	<10	178	59,2	134	114	17,6	64	3,4	94,7	71	65,7	<3	75,8	<15	28,8	<10	1030
AA 08-11	<10	<10	1190	<10	227	62,8	446	81,3	16,7	86	3,1	124	101	147	<3	46,7	<15	29,4	<10	1180
AA 08-12	<10	<10	852	<10	82	45,3	98,1	33,3	17,4	25	1,5	16,9	44	27,9	<3	38,1	<15	37,7	<10	709
AA 08-13	<10	<10	1090	<10	170	66,8	61,1	113	18,6	73	3,5	83,7	80	47,9	<3	45,9	<15	33,7	<10	817
AA 08-14	<10	<10	1270	<10	209	58,6	30,0	81,7	19,1	83	3,9	117	87	26,6	<3	66,2	<15	28,0	<10	1180
AA 08-15	<10	<10	768	<10	90	43,9	81,4	32,5	20,0	34	1,7	15,9	44	26,1	<3	30,9	<15	32,3	<10	688
AA 08-16	<10	<10	1560	<10	171	61,0	131	116	17,8	67	3,7	94,0	76	65,0	<3	66,6	<15	26,1	<10	1090
AA 08-17	<10	<10	1560	<10	158	59,7	141	115	18,0	62	3,7	88,2	70	70,5	<3	66,0	<15	34,1	<10	886
AA 08-21	<10	<10	1140	<10	109	61,4	281	42,2	17,9	54	3,5	71,7	44	185	<3	57,9	<15	23,3	<10	912
LEA 06-81	<10	<10	989	<10	209	53,3	13,9	87,2	19,4	79	1,9	117	89	19,6	<3	64,6	<15	29,2	<10	1610
LEA 06-93	<10	<10	1470	<10	159	56,5	75,6	126	17,2	67	2,0	82,2	60	58,8	<3	50,5	<15	36,5	<10	1080

Table 7-2: XRF bulk rock trace element analyses from NGU, Trondheim.

Th [mg/kg]	U [mg/kg]	V [mg/kg]	W [mg/kg]	Y [mg/kg]	Yb [mg/kg]	Zn [mg/kg]	Zr [mg/kg]	Cl [%]	F [%]	S [%]	Bi* [mg/kg]	Br* [mg/kg]	Cs* [mg/kg]	Ge* [mg/kg]	Hf* [mg/kg]	Se* [mg/kg]	Sm* [mg/kg]	Ta* [mg/kg]	Te* [mg/kg]	Tl* [mg/kg]
9,9	4,2	381	<5	26,5	<5	79,4	341	<0.05	<0.1	0,057	<10	<5	<10	<1	11,0	<5	<10	6,8	<10	<20
12,1	4,0	354	<5	38,4	<5	117	483	<0.05	<0.1	0,054	<10	<5	<10	<1	11,8	<5	14	7,1	<10	<20
11,6	3,5	403	<5	29,2	<5	99,2	359	<0.05	<0.1	0,064	<10	<5	10	<1	7,0	<5	14	7,1	<10	<20
10,3	3,7	404	<5	29,1	<5	95,3	349	<0.05	<0.1	0,062	<10	<5	<10	<1	9,6	<5	<10	7,4	11	<20
10,3	4,4	426	<5	26,4	<5	82,6	280	<0.05	<0.1	0,139	<10	<5	<10	<1	9,5	<5	<10	7,1	<10	<20
10,0	4,7	401	<5	28,7	<5	125	351	<0.05	<0.1	0,068	<10	<5	18	<1	9,3	<5	15	6,6	<10	<20
5,7	<2	358	<5	56,6	<5	129	304	<0.05	<0.1	0,043	<10	<5	<10	<1	10,1	<5	<10	<4	<10	<20
8,6	2,9	498	<5	25,7	<5	95,8	317	<0.05	<0.1	0,151	<10	<5	28	<1	11,0	<5	<10	4,6	<10	<20
11,9	4,9	455	<5	28,6	<5	98,1	349	<0.05	<0.1	0,183	<10	<5	21	<1	8,2	<5	<10	6,1	14	<20
5,0	<2	331	<5	54,0	<5	126	287	<0.05	<0.1	0,048	<10	<5	<10	<1	6,5	<5	<10	<4	<10	<20
9,8	4,6	429	<5	26,3	<5	86,5	281	<0.05	<0.1	0,128	<10	<5	<10	<1	8,6	<5	<10	5,1	<10	<20
9,5	2,9	440	<5	25,9	<5	84,7	279	<0.05	<0.1	0,123	<10	<5	<10	<1	7,5	<5	13	<4	<10	<20
8,1	3,6	291	<5	24,3	<5	90,9	256	<0.05	<0.1	0,061	<10	<5	<10	<1	7,7	<5	<10	4,3	<10	<20
12,5	6,5	453	<5	28,7	<5	97,4	336	<0.05	<0.1	0,124	<10	<5	<10	<1	8,8	<5	<10	6,0	10	<20
9,5	3,9	416	<5	22,8	<5	84,3	272	<0.05	<0.1	0,125	<10	<5	<10	<1	<5	<5	<10	4,5	<10	<20

Table 7-3: XRF bulk rock trace element analyses continued.

	Q	Or	Ab	An	Lc	Ne	Di	Hy	Ol	Il	Hm	Tn	Pf	Ap	Sum
DEF 08-01	0,00	4,92	10,15	15,71	0,00	3,53	26,15	0,00	10,88	0,43	12,40	0,00	6,32	2,26	92,75
DEF 08-02	0,00	13,36	17,35	14,14	0,00	0,00	16,07	0,00	9,32	0,49	15,00	1,38	6,68	2,05	95,83
DEF 08-03	0,00	4,74	12,84	16,15	0,00	4,78	25,26	0,00	8,39	0,57	13,20	0,00	6,59	1,95	94,48
DEF 08-04	0,00	1,91	12,19	17,56	0,00	4,31	28,61	0,00	7,74	0,46	13,50	0,00	6,79	1,89	94,96
DEF 08-05	0,00	19,09	2,66	16,42	0,00	4,93	25,10	0,00	4,69	0,53	13,60	0,00	6,69	1,86	95,57
AA 08-11	0,00	10,34	5,58	16,74	0,00	3,58	26,77	0,00	9,28	0,47	13,30	0,00	6,70	2,39	95,16
AA 08-12	2,23	10,64	24,62	17,91	0,00	0,00	3,51	10,05	0,00	0,43	16,00	7,69	0,00	1,31	94,40
AA 08-13	0,00	7,33	0,00	17,04	1,25	6,46	32,91	0,00	3,76	0,47	15,70	0,00	7,81	1,66	94,39
AA 08-14	0,00	15,66	1,33	18,17	0,00	5,06	25,67	0,00	3,55	0,43	15,20	0,00	7,05	1,95	94,06
AA 08-15	5,32	7,98	24,62	17,06	0,00	0,00	8,93	8,34	0,00	0,45	15,00	7,08	0,00	1,20	95,98
AA 08-16	0,00	17,49	2,59	15,59	0,00	6,07	25,63	0,00	4,83	0,48	13,80	0,00	6,77	1,85	95,11
AA 08-17	0,00	17,20	3,59	15,60	0,00	5,39	27,15	0,00	4,71	0,60	13,20	0,00	6,84	1,81	96,08
AA 08-21	0,00	12,29	4,99	18,25	0,00	6,10	30,22	0,00	1,81	0,41	12,30	0,00	5,66	1,00	93,04
LEA 06-81	0,00	18,85	6,25	18,22	0,00	2,94	19,86	0,00	5,77	0,66	14,50	0,00	6,49	2,00	95,53
LEA 06-93	0,00	11,46	6,46	15,68	0,00	6,13	29,78	0,00	5,97	0,43	12,80	0,00	6,36	1,27	96,33

Table 7-4: CIPW norm of the different samples calculated in GCDkit 2.3.

Prøve id.	SiO2	Al2O3	Fe2O3	TiO2	MgO	CaO	Na2O	K2O	MnO	P2O5	Gl.tap	Sum Hoved	Mg#	Na2O+K2O	K2O/Na2O
*	[%]	[%]	[%]	[%]	[%]	[%]	[%]	[%]	[%]	[%]	[%]	[%]			
Alkaline Lamprophyres	42,5	13,7	12,0	2,9	7,1	10,3	3,0	2,0	0,2	0,74	5,1	99,5	37,2	5,0	0,7
Ultramafic Lamprophyres	32,3	6,7	13,6	3,1	15,0	14,0	1,0	1,9	0,22	1,0	10,0	98,82	52,4	2,9	1,9
GGU 269160	38,8	10,0	16,0	5,29	7,85	10,72	0,46	3,94	0,220	1,260	4,03	98,52	32,9	4,4	8,6
GGU 269176	39,1	9,7	15,9	5,75	7,63	12,57	2,08	2,13	0,240	1,450	2,98	99,52	32,5	4,2	1,0
a	43,1	10,2	11,5	4,07	8,18	13,09	2,25	2,07	0,220	1,350	3,66	99,73	41,5	4,3	0,9
b	42,0	9,5	12,7	3,53	7,78	12,99	3,15	2,00	0,000	0,950	4,51	99,07	38,0	5,2	0,6
c	35,5	7,4	15,1	3,93	10,60	14,17	2,47	2,39	0,000	1,350	4,84	97,69	41,3	4,9	1,0

Table 7-5: ”Alkaline Lamprophyres” and ”Ultramafic Lamprophyres” are average values of the respective rock types from Rock (1991). Samples GGU 269160 and GGU 269176 are lamprophyres from Revdal, Liverpool Land (Larsen et al., 1990). Samples a, b and c are tertiary dykes from the Scoresby Sund area and the Kangerdlugssuaq area (Larsen et al., 1990).

7.2 General Chemical Characteristics

The Liverpool Land lamprophyres are characterized by restricted concentrations of SiO_2 (35 - 40 wt%), Al_2O_3 (10 wt% - 13 wt%), FeO (12 - 16 wt%) and TiO_2 (3 - 5 wt%). The concentrations of MgO (6 – 11 wt%), CaO (11-16), Na_2O (1.26 – 2.56 wt%) and K_2O (0.323 – 3.23 wt%) are more variable. The two samples AA 08-12 and AA 08-15 are not lamprophyres and do not show the same chemical characteristics. All lamprophyre samples are ultrabasic and silica undersaturated in composition (Figure 7-1). On the total-alkali versus silica (TAS) diagram (Lebas et al., 1986) (Figure 7-1) AA 08-12 plots in the tephrite basanite field, AA 08-15 plots in the basalt field and the rest plot in the foidite field. In the same figure it can be seen that all samples are within the alkaline series with sample AA 08-15 plotting closest to the sub-alkaline series (Irvine and Baraghar, 1971). Figure 7-1 also show that all the samples plot within the alkaline lamprophyre field of Rock (1987), while samples AA 08-13 and AA 08-14 also plot within the ultramafic lamprophyre field. In Figure 7-2 one can see that samples AA 08-12, AA 08-15, DEF 08-01, DEF 08-03 and DEF 08-04 are definitely sodic while the others are on the border or in the potassic field. As can be seen from the CIPW norm in Table 7-4 all samples are nepheline normative except AA 08-12 and AA 08-15 which are quartz normative. Mg# vary from 23-47 which clearly indicate that they are not primary mantle melts (Kirstein et al., 2006).

Because of the restricted SiO_2 content any elements plotted against SiO_2 show no clear patterns and have not been included in this thesis. Elements plotted against Mg# have been included and will be discussed in section 7.3.

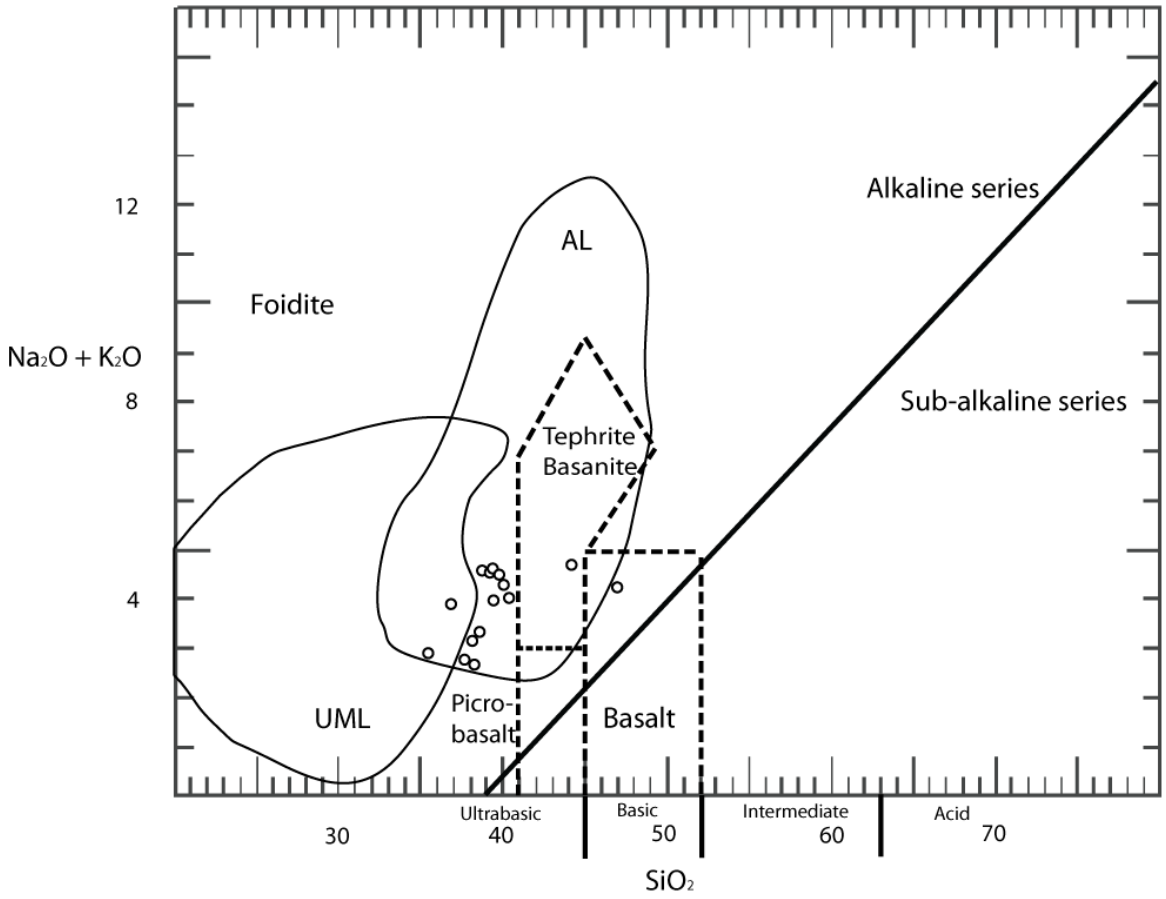

Figure 7-1: Diagram modified after: Total alkali – silica diagram of Le Bas (1986); Lamprophyre classification diagram of Rock (1987); Alkaline diagram of Irvine and Baragar (1971).

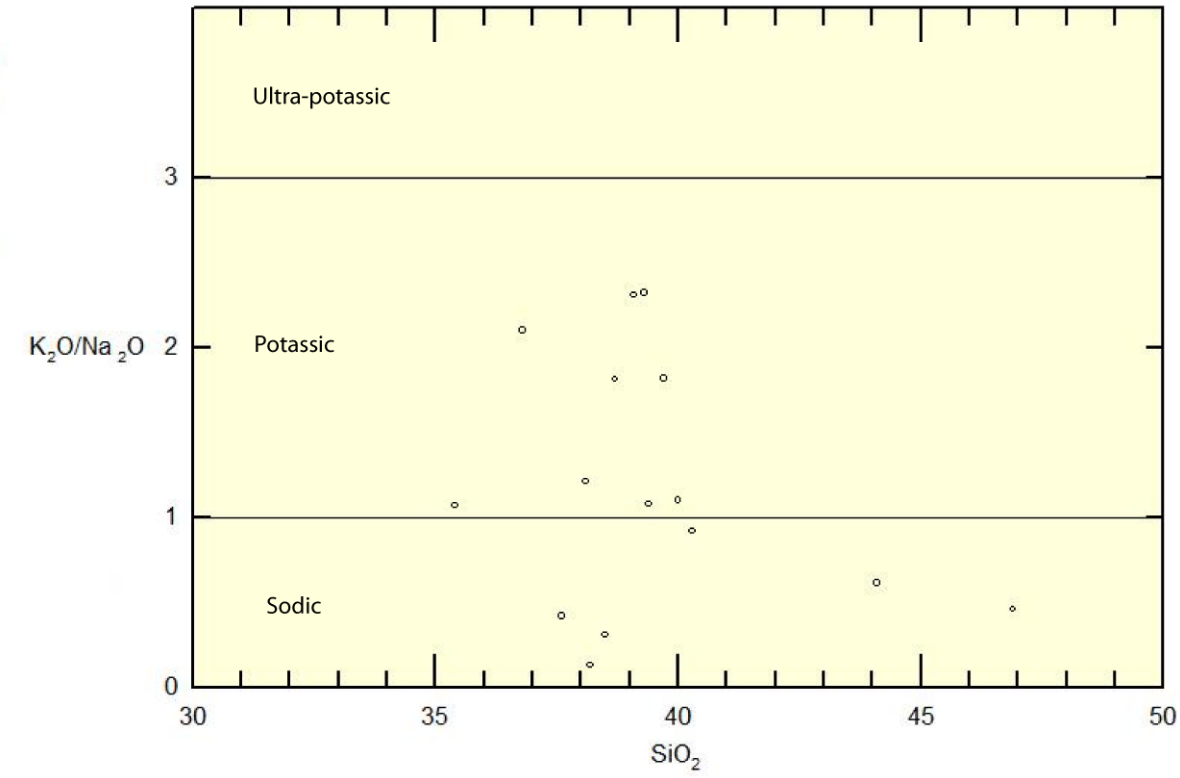

Figure 7-2: All samples plotted in the sodic-potassic diagram after (Irvine and Baraghar, 1971).

7.3 Bulk rock major element data

In these element-element diagrams different major elements have been plotted against Mg#. The Liverpool Land lamprophyres are shown in blue as group 1 while samples AA 08-12 and AA 08-15 has been excluded to avoid confusion. Group 2 are two lamprophyre samples from Revdal (Larsen et al., 1990) of believed Tertiary (K-Ar) age or Late Permian (interpretation from field relations). Group 3 are three Tertiary dykes; one trachybasalt from Kangerdlugssuaq, and one monchiquite and one alnöitic dyke from the Scoresby Sund area.

The Liverpool Land lamprophyres do not show any particular trends. There is often a larger spread in the major elements as Mg# decrease but this could be due to the larger number of samples with a low Mg#. Larsen et al. (1990) interpreted the Revdal lamprophyres to correlate well with other Tertiary dykes in Central East Greenland. From these major element plots they correlate better with the Liverpool Land lamprophyres. The Revdal lamprophyres were not analyzed for trace elements.

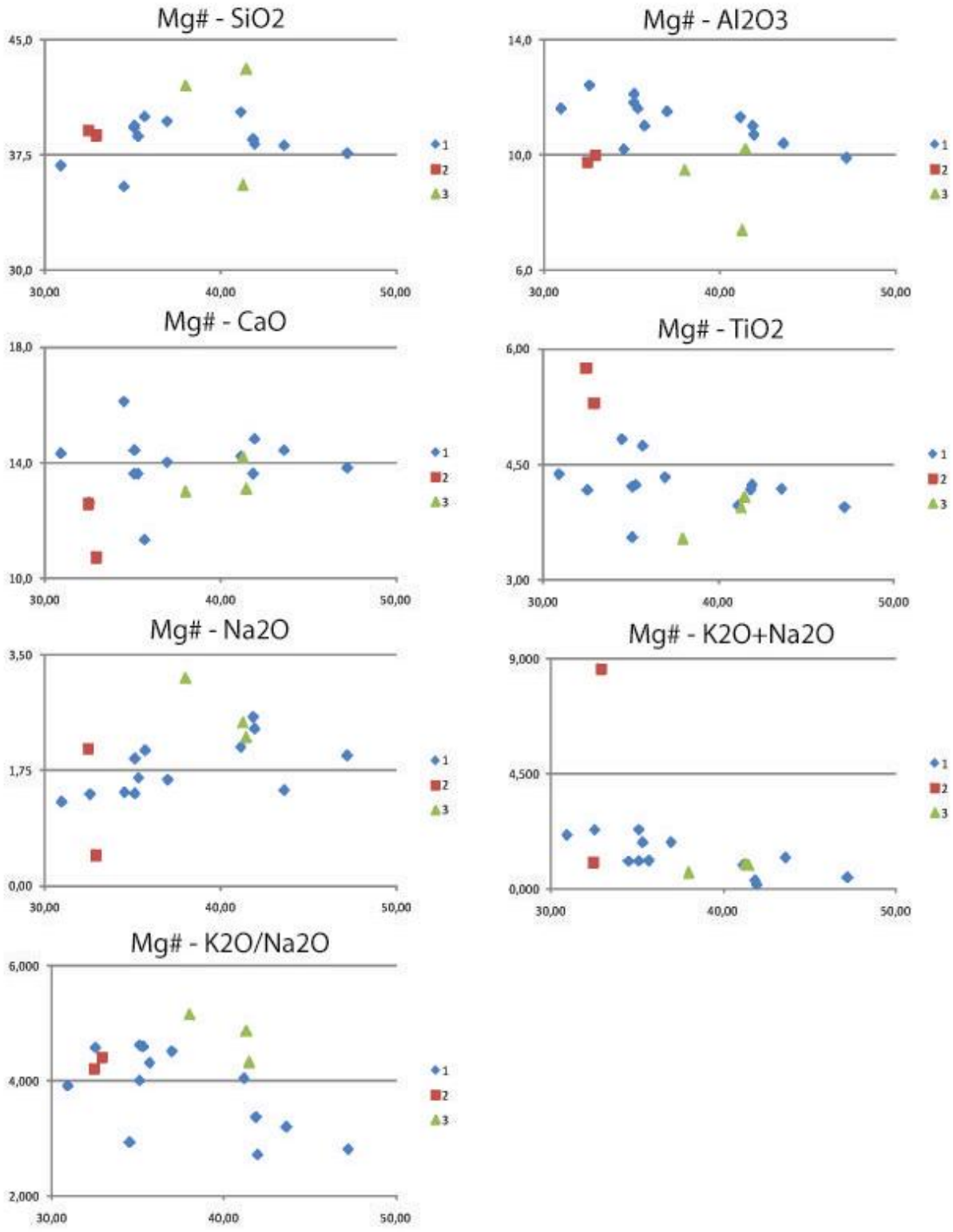

Figure 7-3: Major element plots of Mg# against SiO_2, Al_2O_3, Fe_{tot}, TiO_2, CaO, Na_2O, Na_2O+K_2O, and K_2O/Na_2O. Three groups have been plotted; group 1, Liverpool Land lamprophyres, group 2, Revdal Lamprophyres and group 3, tertiary dykes from Kangerdlugssuaq and the Scoresby Land area.

7.4 Trace Elements

Element – Element plots

In these element-element diagrams Rb, K, Ba, La, Nb and Y have been plotted against Th (Figure 7-4). The Liverpool Land lamprophyres are shown in blue as group 1 while samples AA 08-12 and AA 08-15 are shown as group 2. The two groups show no relation in the element – element plots. Trace element data does not exist for the Revdal lamprophyres. The plots with large-ion lithosphile (LIL) elements (Rb, K and Ba) show a large spread. The high field strength (HFS) elements (La, Nb and Y) show trends towards origo, but deviate slightly as seen from the lines in the figure.

Spider - Diagrams

Concentrations of Cs and Sm are within detection limit in a few samples and have been included – while Ob, Pr, Wu, Dy, Yb, and Lu are below detection limit and are left out of the spider diagram (Figure 7-5) modified after Sun and McDonough (1989). The diagram displays two groups, the lamprophyres and samples AA 08-12 and AA 08-15. Both groups can be considered coming from enriched sources but the blue group is clearly more enriched than the red one and has an ocean island basalt (OIB) signature (Sun and McDonough, 1989). A general trend of decrease from left to right can be seen in group 1 in the spider diagram normalized against PM which is normal when "typical" mantle undergo partial melting.

The LIL elements Rb and K show troughs and significant variation and samples DEF 08-01, DEF 08-03, and DEF 08-04 stand out with very low values. The other LIL elements Cs, Ba and Pb either show a large variation or are below detection limit. A through in Nb is also observed and Nb values are between 72 – 124 ppm.

In the REE spider-diagram after Sun and McDonough (1989) only show the elements La, Ce and Nd and all samples have been grouped as one. The REE data is insufficient and the diagram has been included to illustrate this.

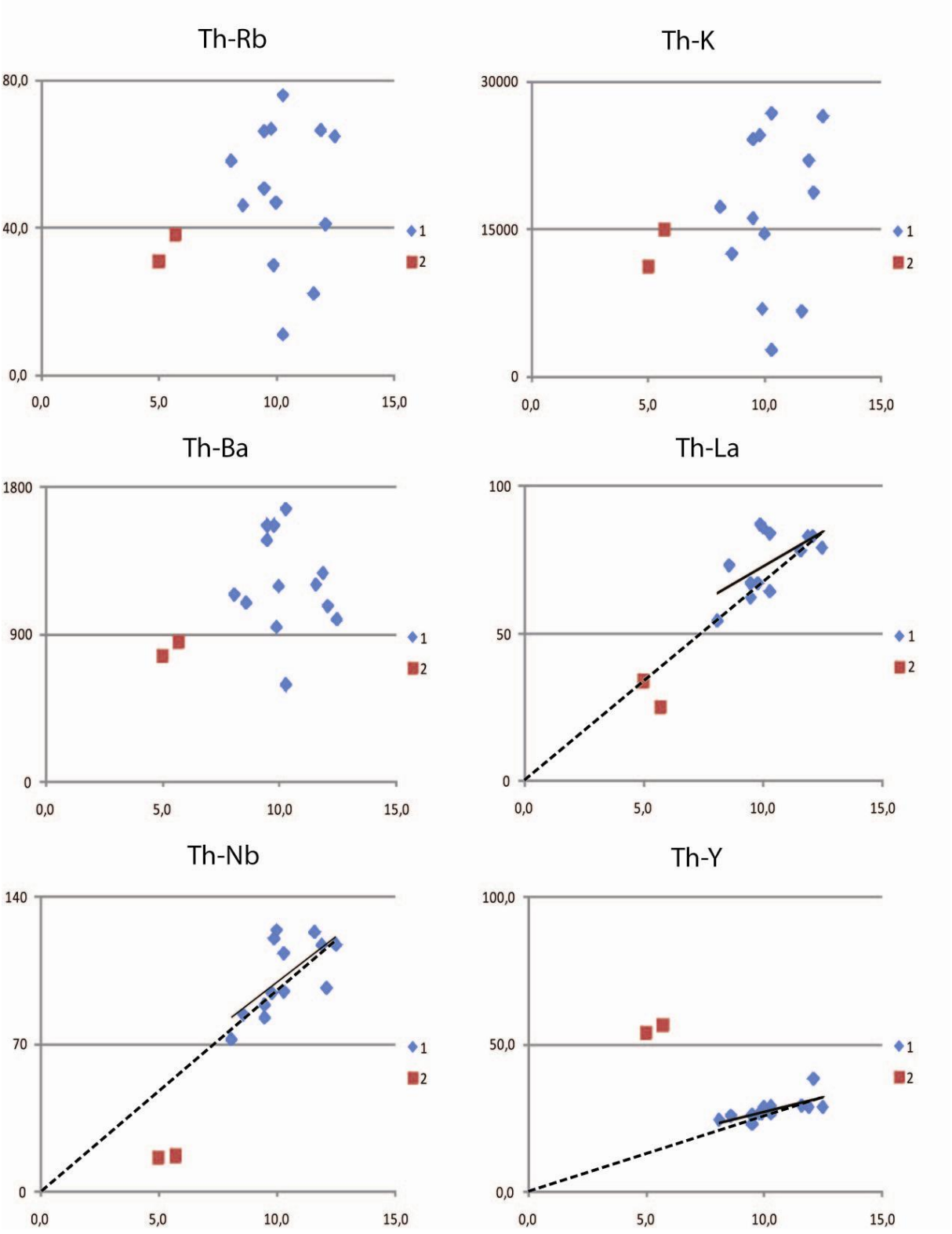

Figure 7-4: Trace element plots with thorium plotted against Rb, K, Ba, La, Nb, and Y. The Liverpool Land lamprophyres are shown as group 1 and samples AA 08-12 and AA 08-15 are shown as group 2. The dotted line is a linear trend line added in Excel while the dotted line is meant to show that they deviate from origo. The plot shows that there is no relation between the two groups.

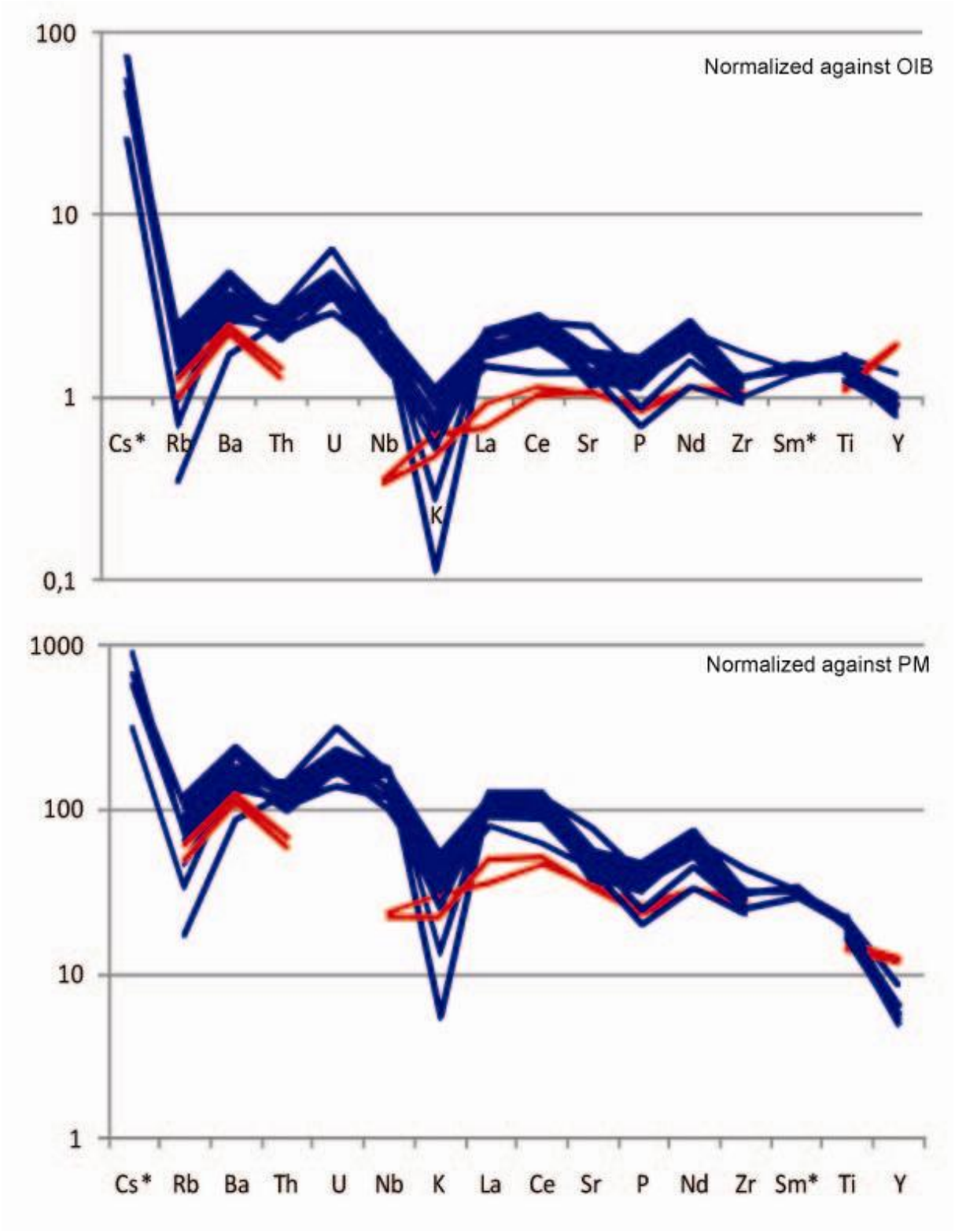

Figure 7-5: Spider-diagram modified after Sun and McDonough (1989) where Ob, Pr, Wu, Dy, Yb, and Lu has been left out.

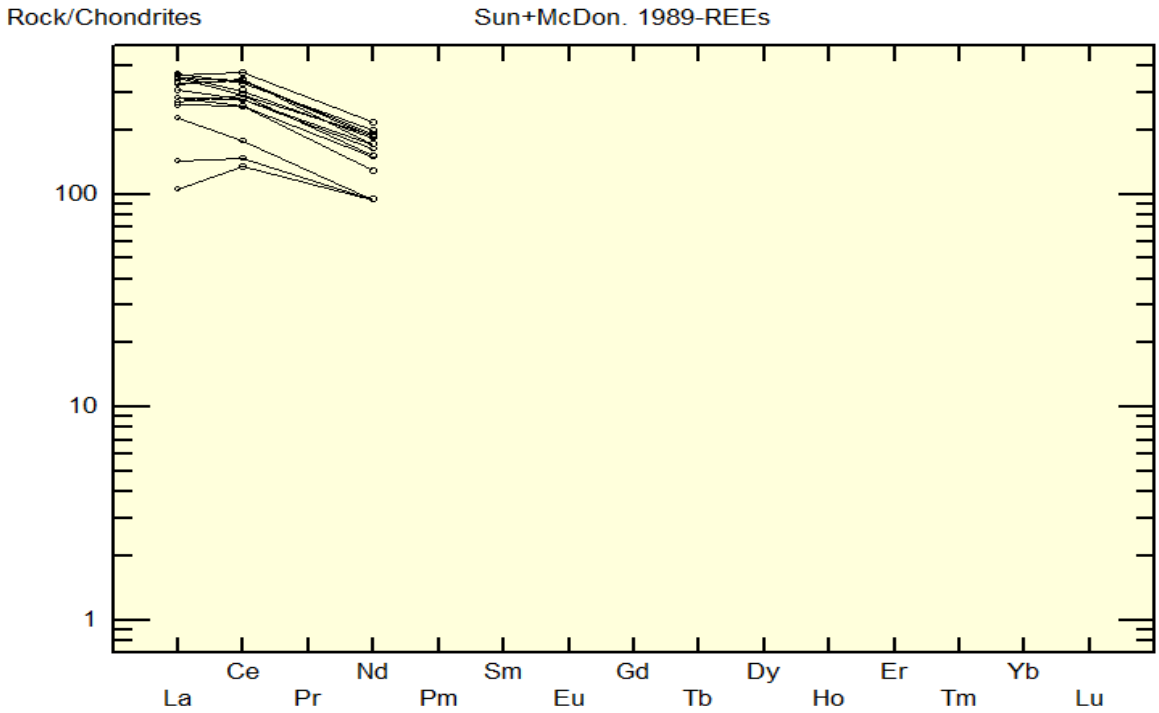

Figure 7-6: REE spider diagram after Sun and McDonough (1989) where La, Ce and Nd are the only elements above detection limit. All samples has been included in one group.

8 Mineral Chemistry

8.1 Introduction

To investigate variations in mineral chemistry from core to rim as well as inferred compositional changes across growth surfaces EMP spot analyses on selected minerals have been carried out at the Department of Geosciences. Samples for analysis have been selected because of their fresh appearance and phenocryst assemblage. Both phenocrysts and matrix of samples AA 08-17, AA 08-16, DEF 08-06, DEF 08-01, AA 08-13, AA 08-12, AA 08-15, AA 08-14 and LEA 06-81 have been analyzed for classification, comparison, and interpretation. Almost 300 single spot analyses have been taken from phenocrysts and matrix in the different thin-sections in addition to well over 400 profile analyses from CPX – and biotite phenocrysts.

The chemical formula from mineral analysis has been calculated according to normal procedures. For CPX and spinel the concentrations of Fe^{3+} has been calculated using stoichiometric criteria using Droops (1987) general equation. The weight percent of oxides has been recalculated based on the calculated cations. When advantageous the Mg# and different constituents of a mineral have also been calculated. Most of the analysis can be found in Appendix A. The CPX phenocryst profile analyses will be included in an Excel worksheet (named CPX phenocryst profile analyses).

In addition to single spot analyses, complete sections of phenocrysts from core to rim has been analyzed with approximately one spot analysis per 10 µm. Poor analyses results (CPX analyses above 101 wt% and below 98,8 wt% and biotite analyses below 93,5 wt%) have been replaced by calculated intermediate values of the neighboring analyses. These analyses strings will be referred to as "analyses profiles" in the following text. The analyses profiles are represented by white lines on the CPX - or biotite phenocryst in question in a BS-image (CPX phenocrysts in Figure 8-1 and biotite phenocrysts in Figure 8-20). From every profile element-element plots (e. g. Figure 8-2) and element-line plots (e. g. Figure 8-3) has been made to better see any chemical changes. The element-line plot is correlated with a close-up BS-image of the profile to see how chemical changes influence the phenocryst.

The profiles have been divided into zones on the basis of changes in color/composition on BS-images and changes in Mg#. Some zones have also been identified on the basis of some obvious change in one or more of the elements, TiO_2, Al_2O_3, Cr_2O_3, and Na_2O. This division also makes it easier to see changes in composition from core to rim and to refer to different parts of a phenocryst profile when necessary. In the element-element plots the different zones have been given different symbols and a legend for the zones can be seen in the upper right corner in every plot. The range in concentrations can be seen on the y-axis of every plot whereas the range in Mg# is shown on the x-axis of every plot. In the El-line plot the legend can be seen on the left side and shows which line represents which element. The different zones are divided by black lines from top to bottom through the lines and BS-picture and zone numbers can be seen on the BS-picture. To the left (y-axis) of every plot the range in concentrations can be seen, all in wt% while the x-axis show analysis number.

8.2 Observations and Results

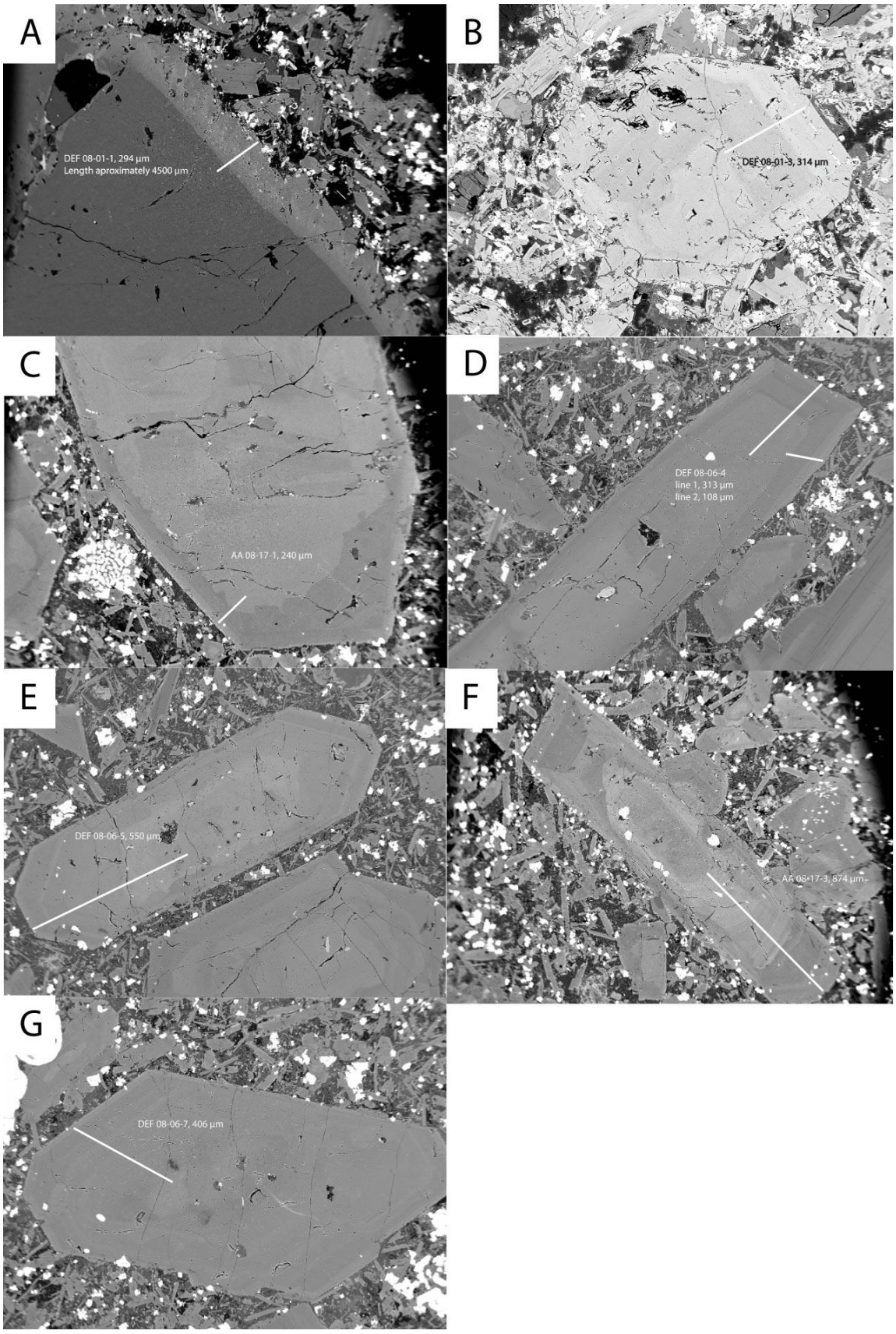

Figure 8-1: BS-pictures of CPX phenocryst profiles with sample name, profile length and profile line.

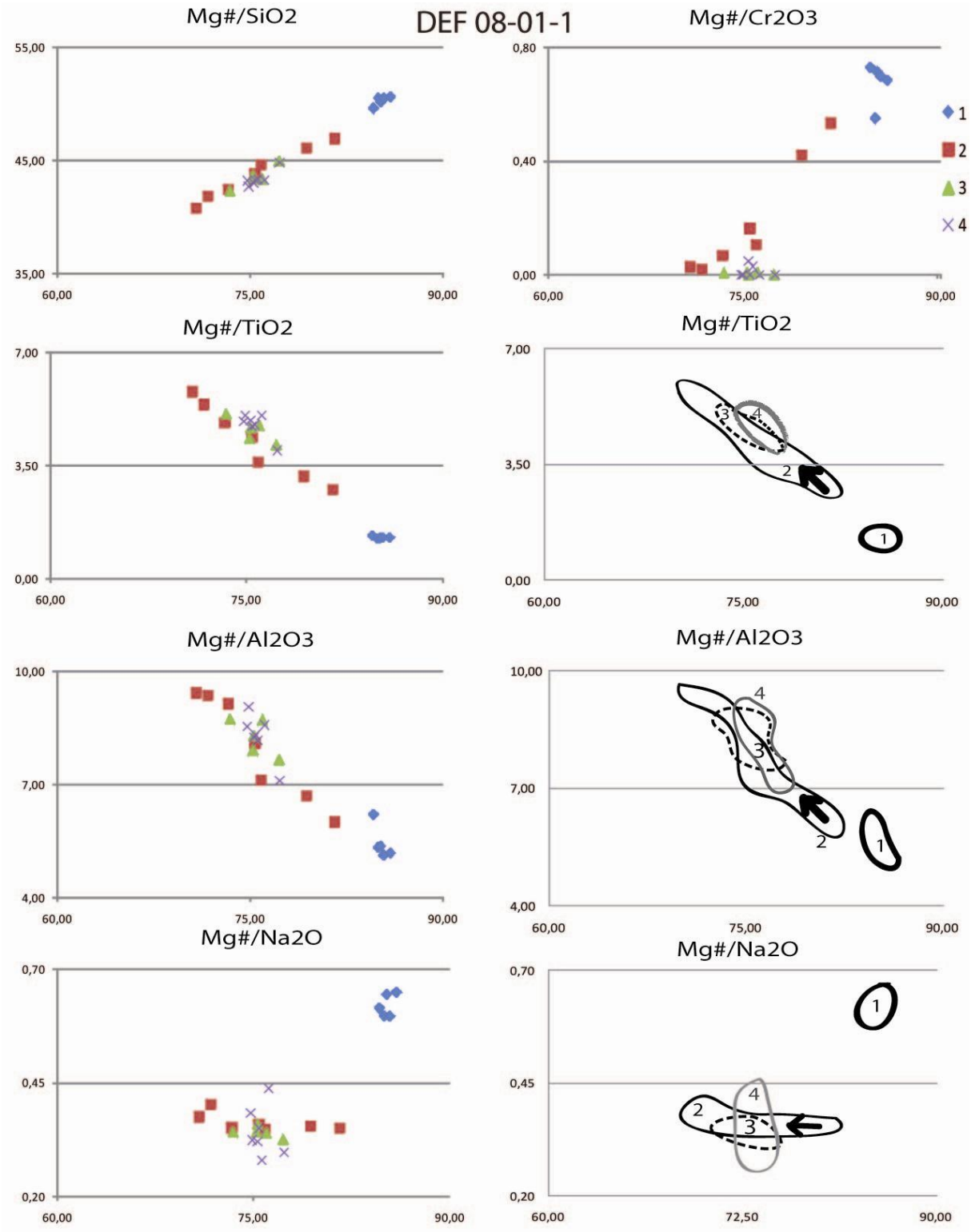

Figure 8-2: CPX phenocryst profile element - element plot from DEF 08-01-1.

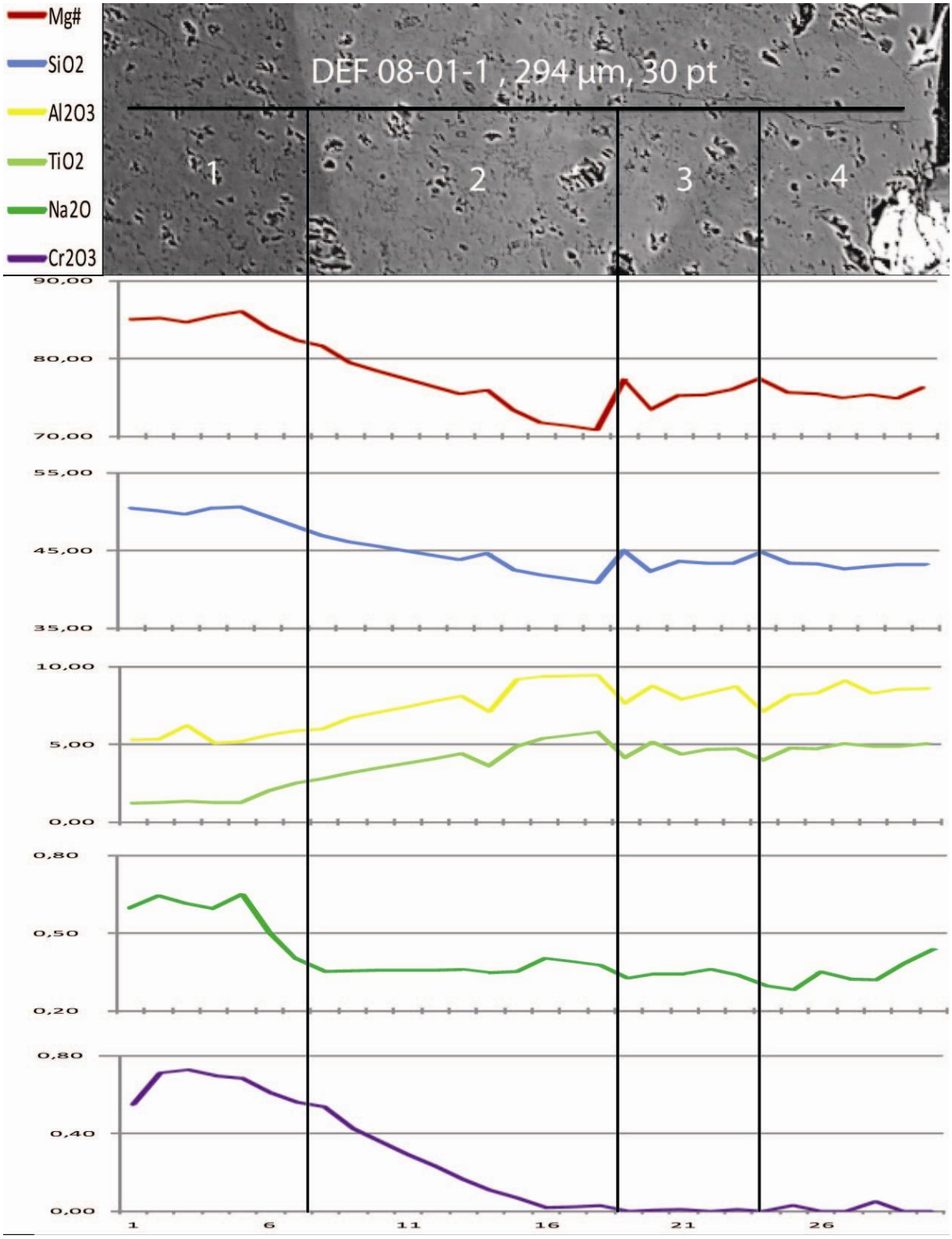

Figure 8-3: CPX phenocryst profile element – line plot from DEF 08-01-1 divided in zones correlated with phenocryst BS-image.

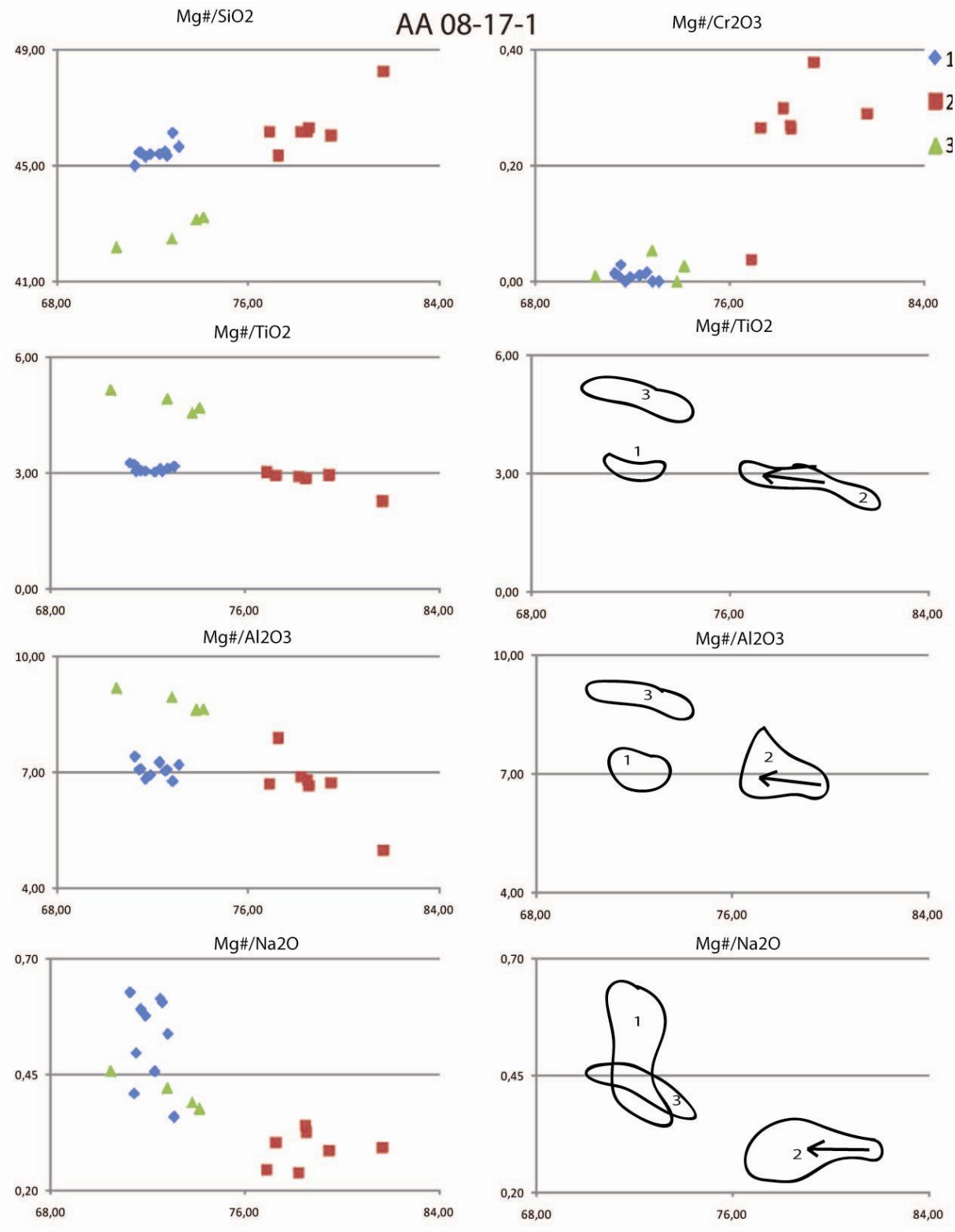

Figure 8-4: CPX phenocryst profile element - element plot from AA 08-17-1.

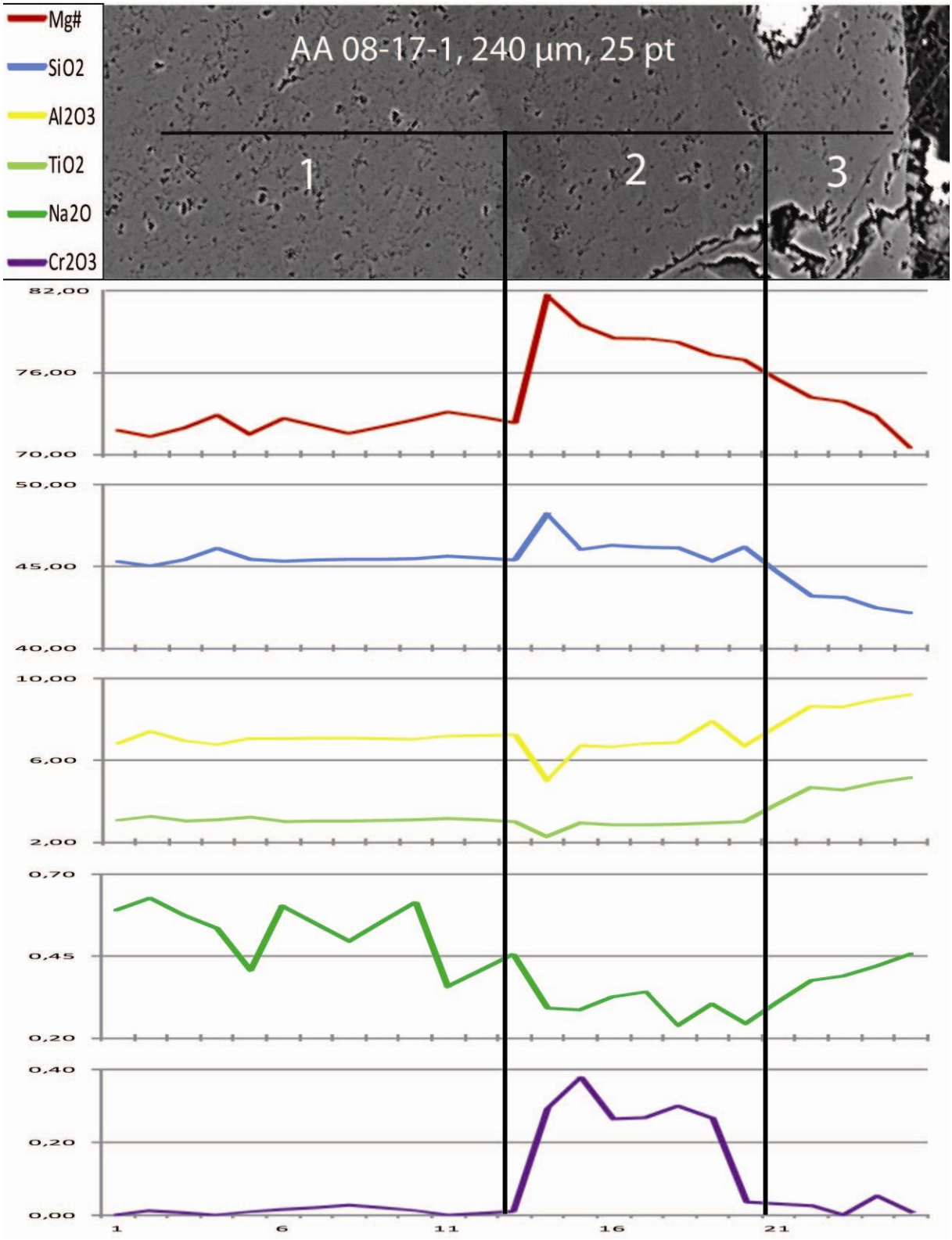

Figure 8-5: CPX phenocryst profile element – line plot from AA 08-17-1 divided in zones correlated with phenocryst BS-image.

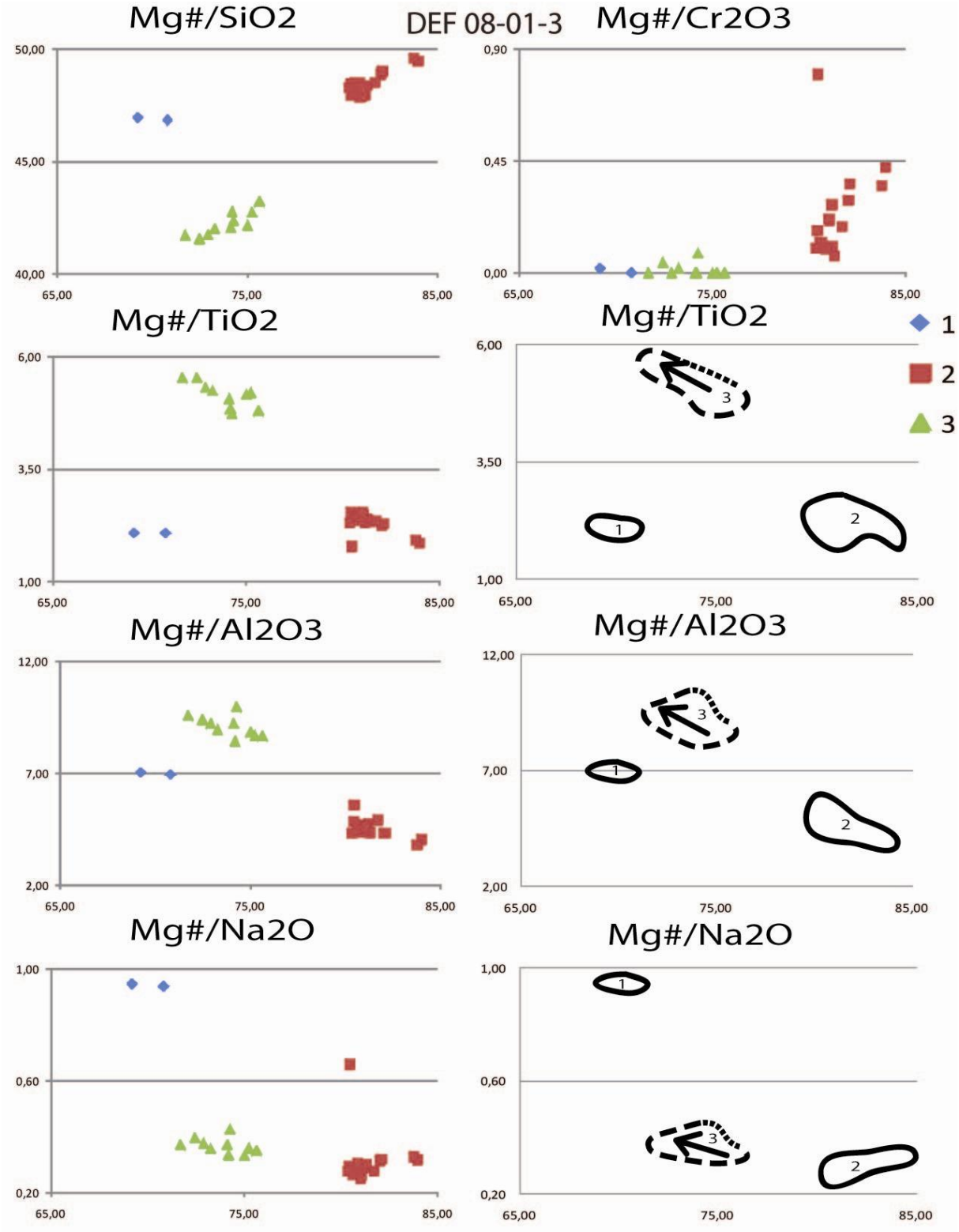

Figure 8-6: CPX phenocryst profile element - element plot from DEF 08-01-3.

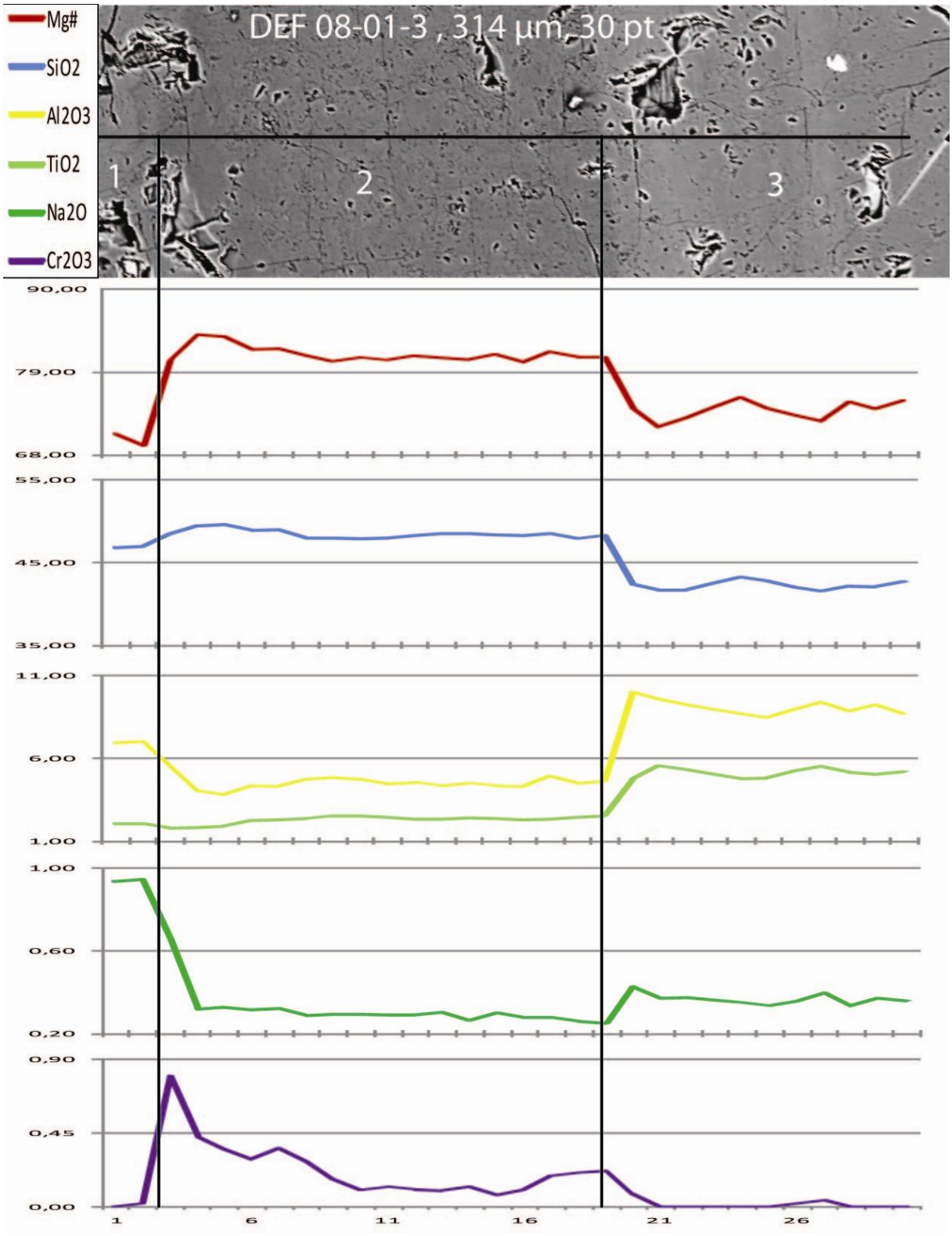

Figure 8-7: CPX phenocryst profile element – line plot from DEF 08-01-3 divided in zones correlated with phenocryst BS-image.

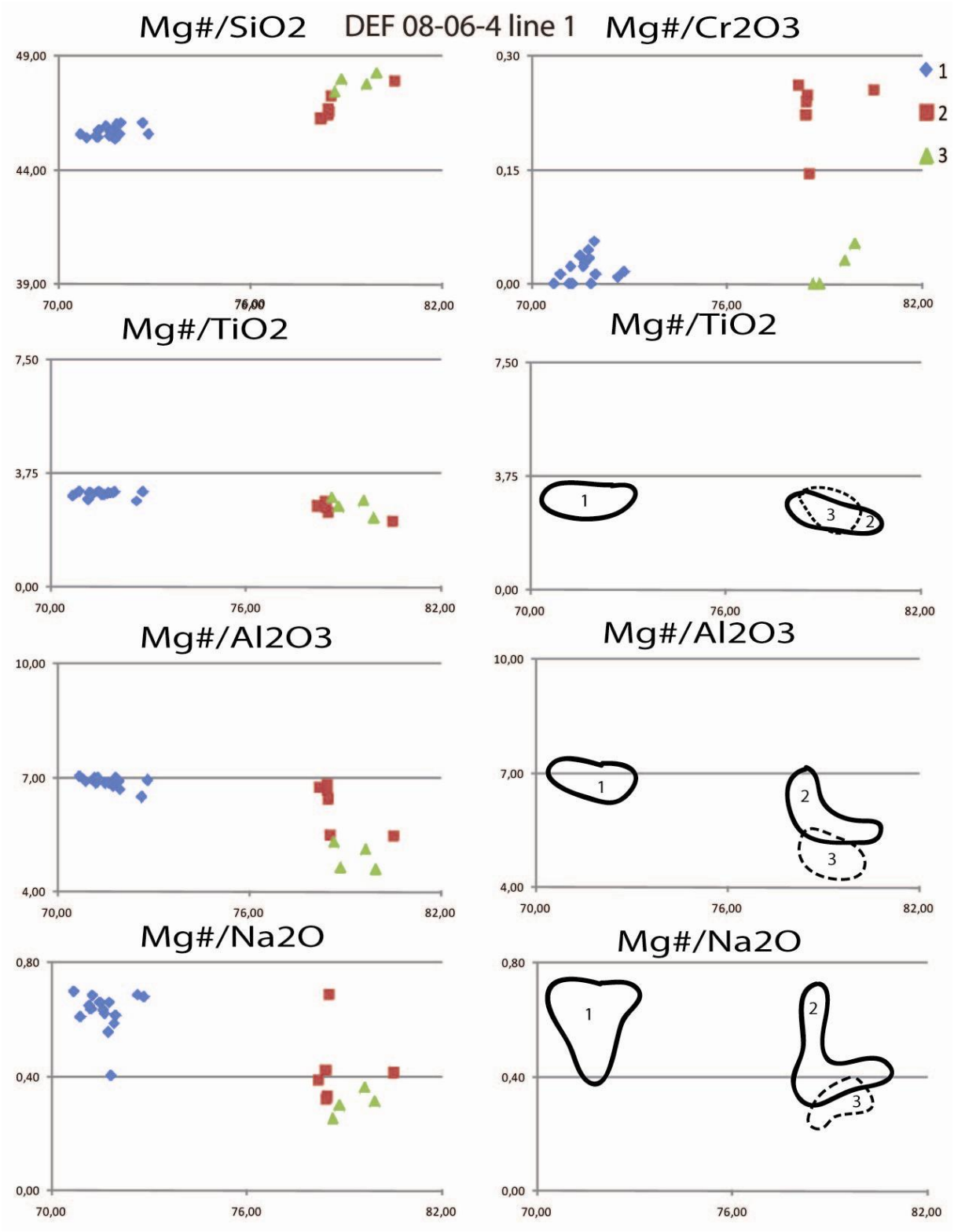

Figure 8-8: CPX phenocryst profile element - element plot from DEF 08-06-4 line 1.

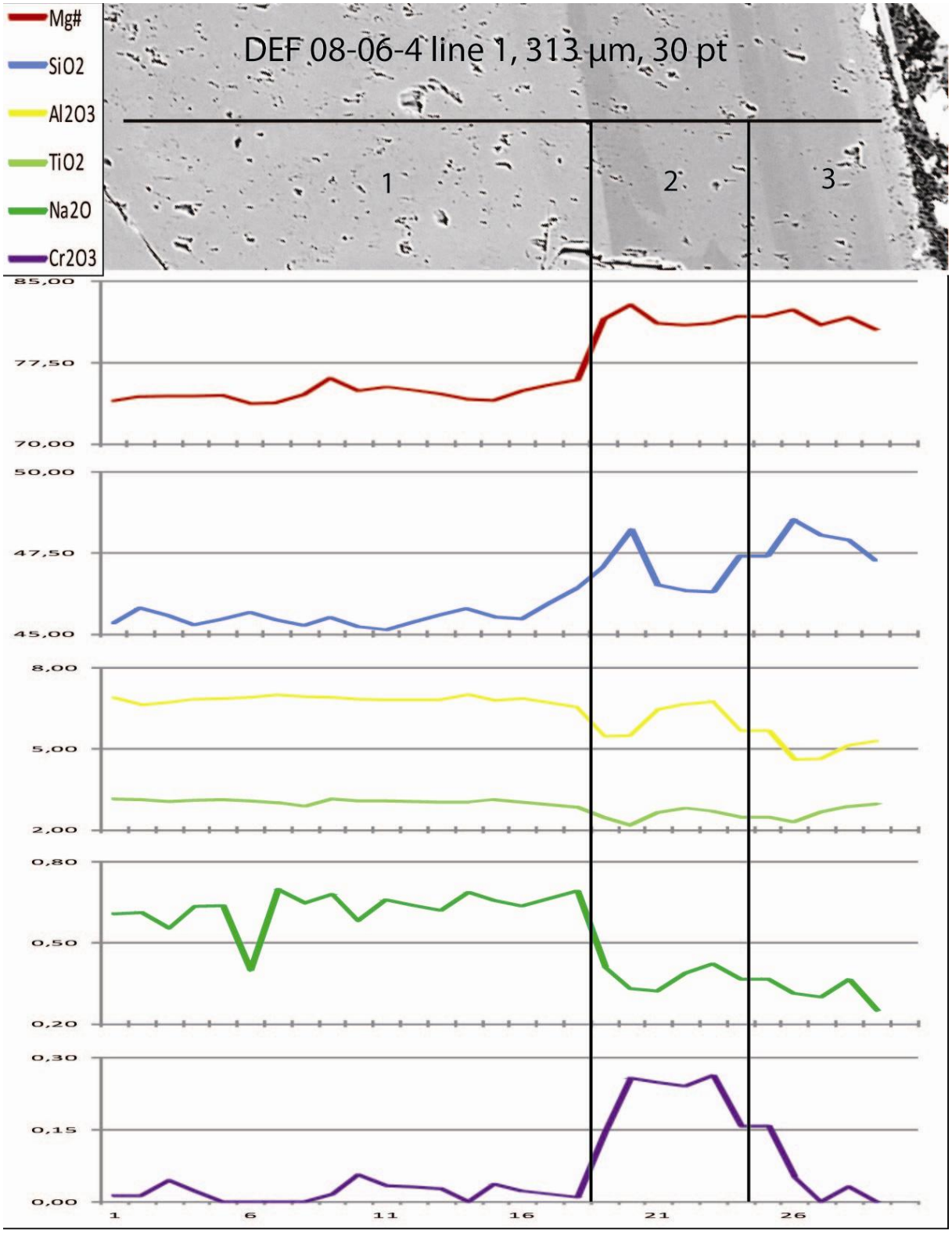

Figure 8-9: CPX phenocryst profile element – line plot from DEF 08-06-4 line 1 divided in zones correlated with phenocryst BS-image.

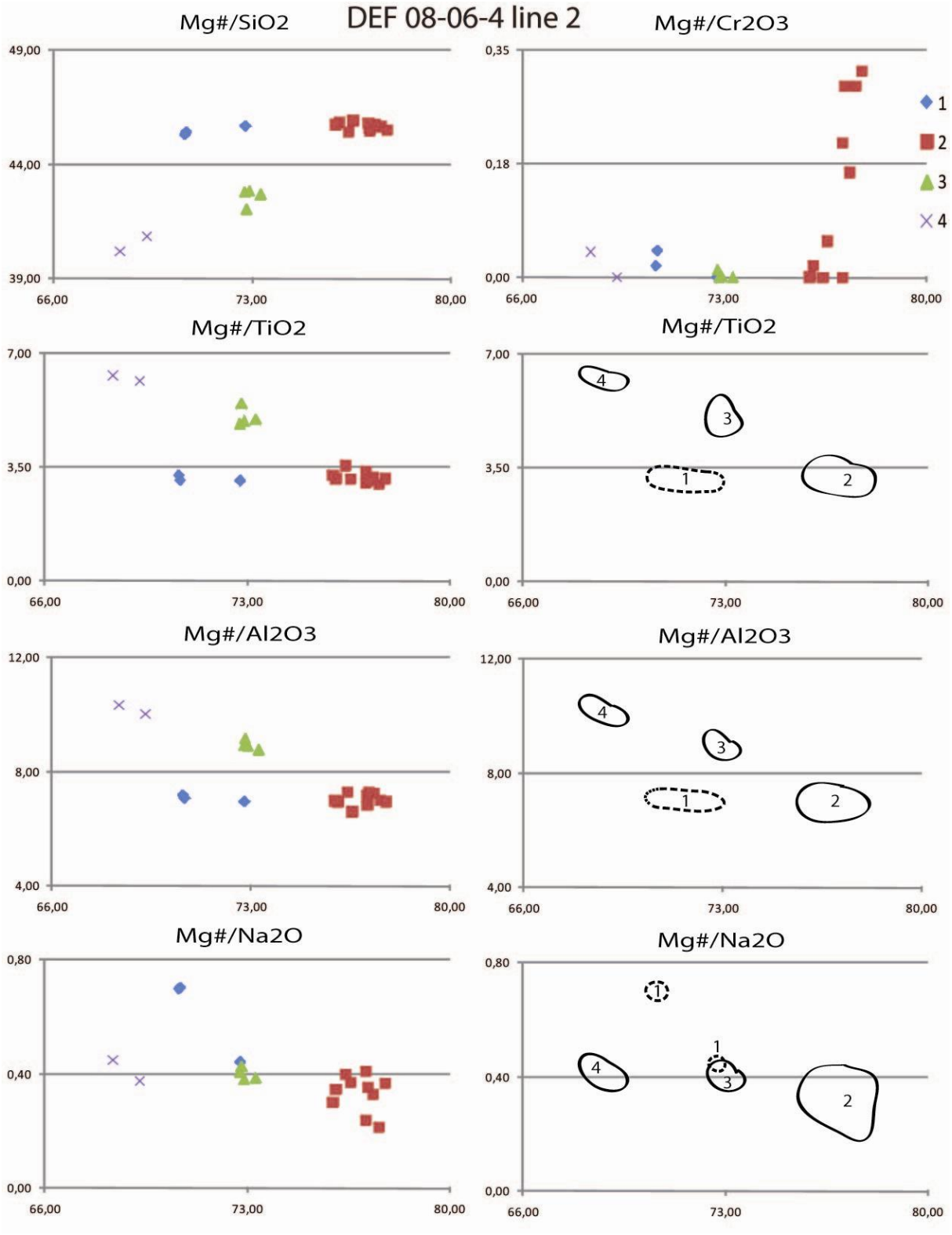

Figure 8-10: CPX phenocryst profile element - element plot from DEF 08-06-4 line 2.

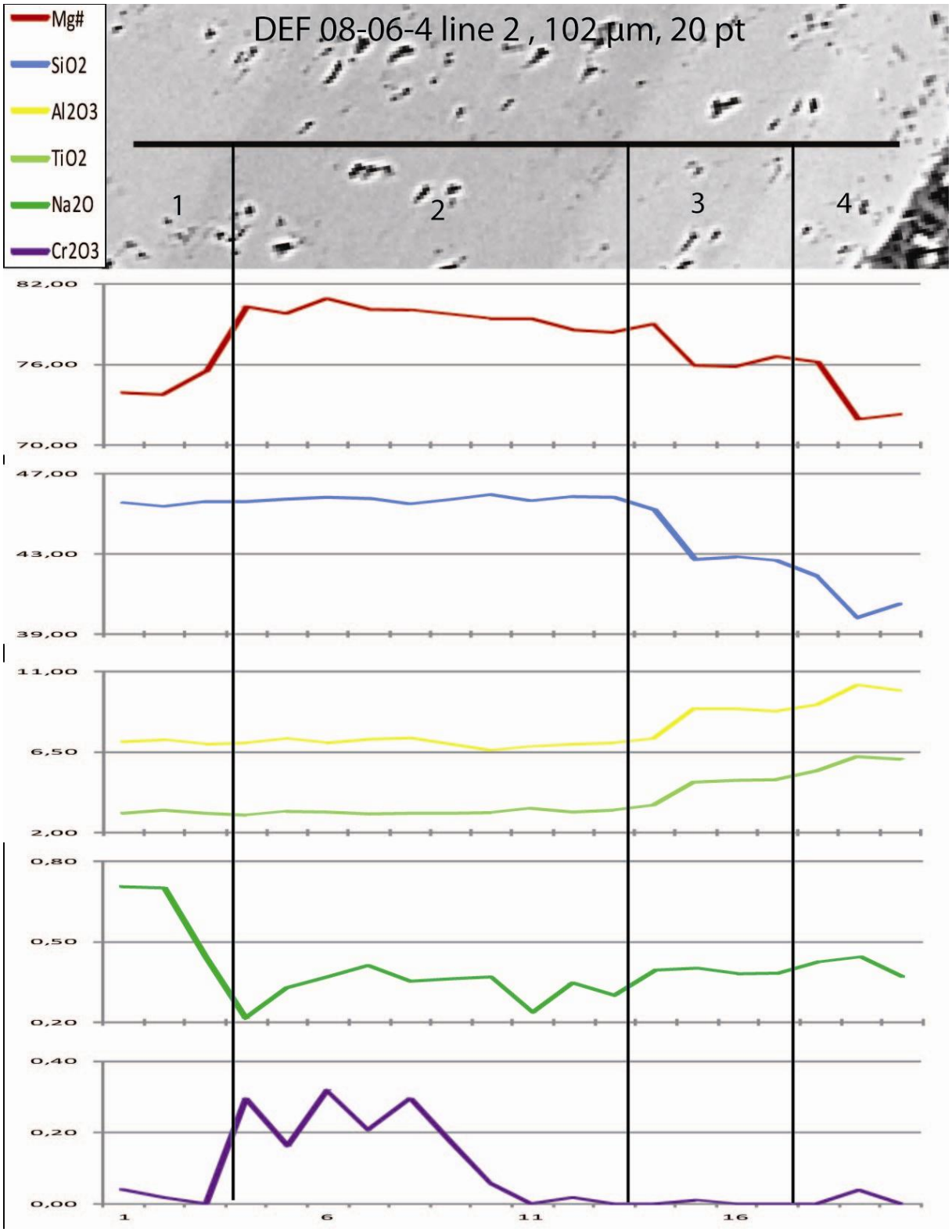

Figure 8-11: CPX phenocryst profile element – line plot from DEF 08-06-4 line 2 divided in zones correlated with phenocryst BS-image.

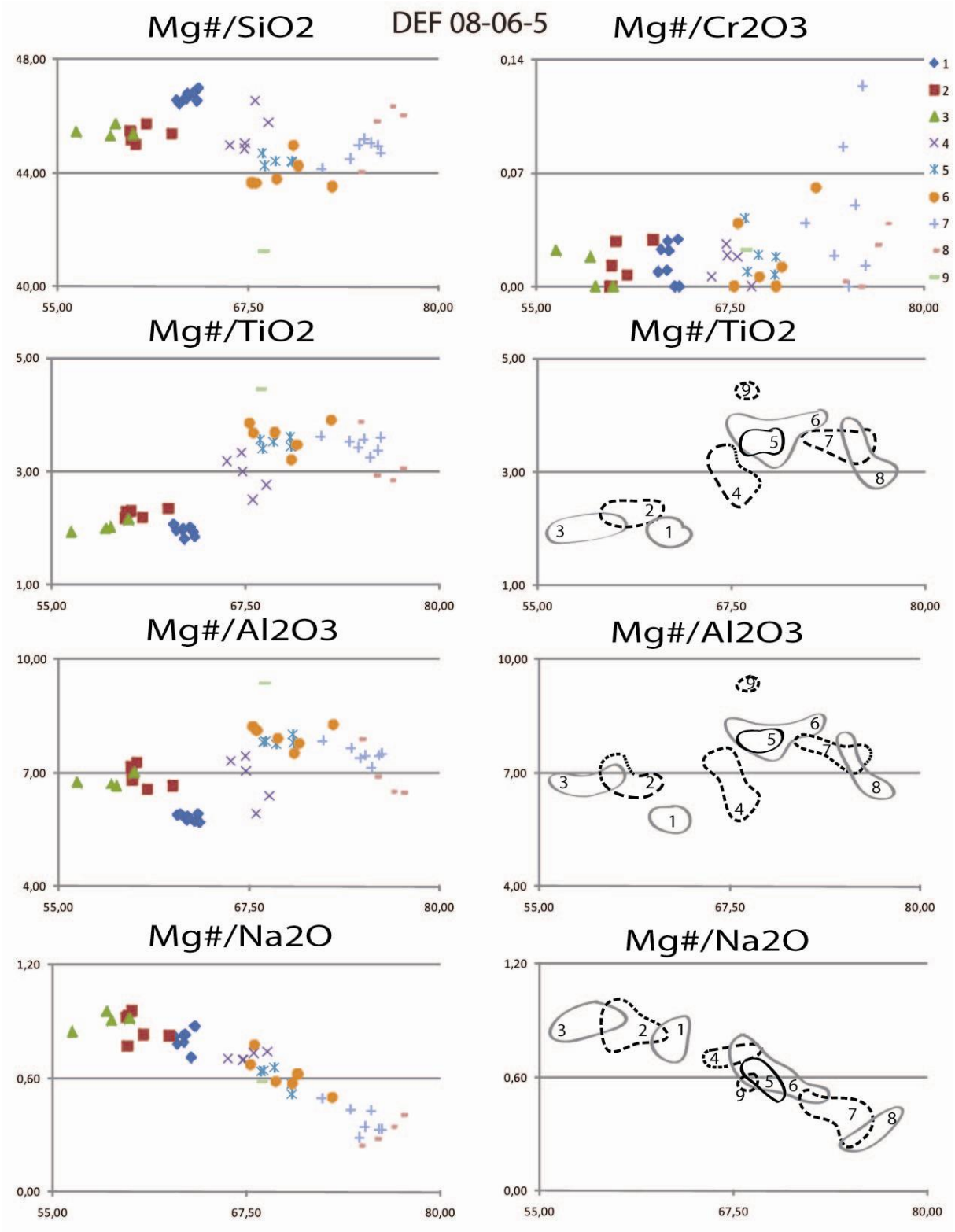

Figure 8-12: CPX phenocryst profile element - element plot from DEF 08-06-5.

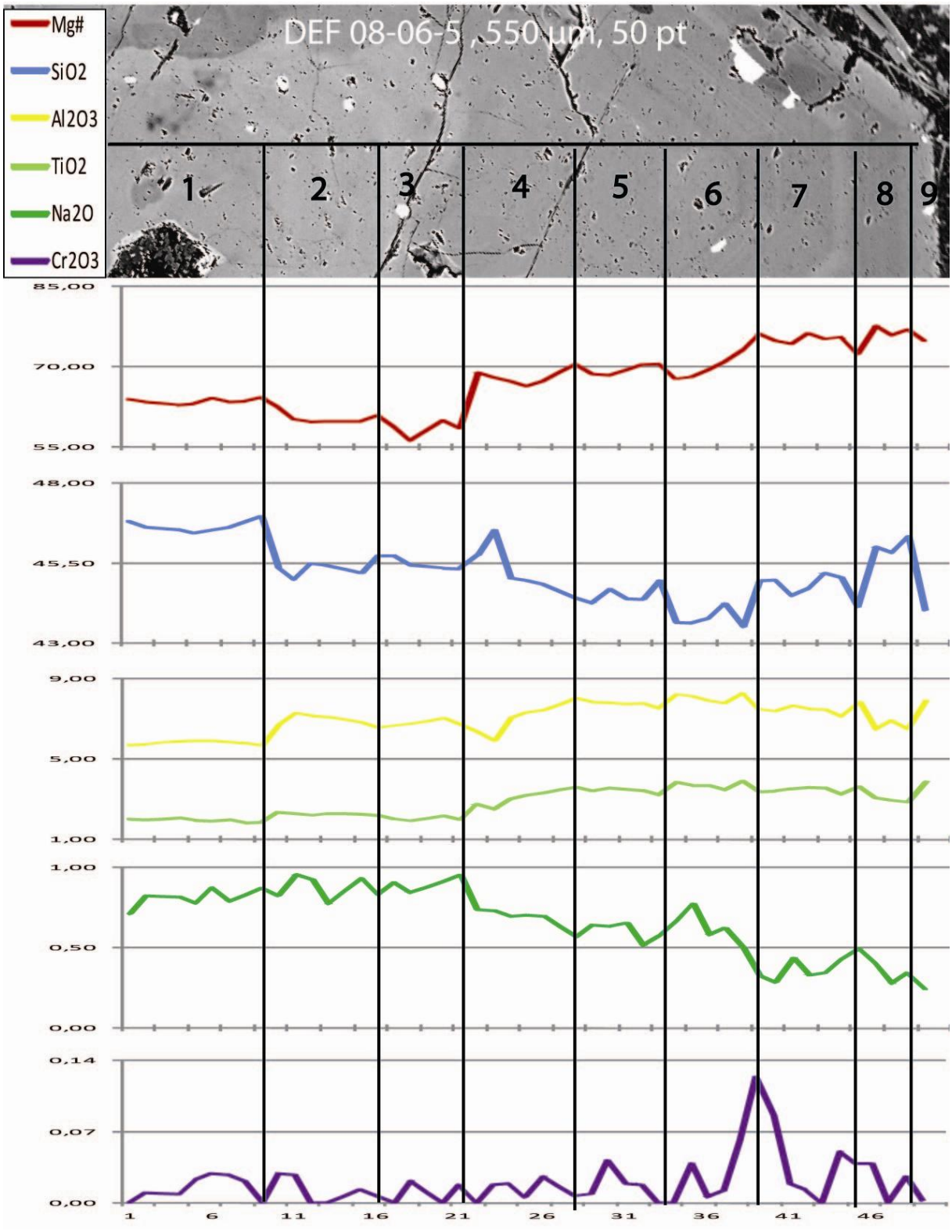

Figure 8-13: CPX phenocryst profile element – line plot from DEF 08-06-5 divided in zones correlated with phenocryst BS-image.

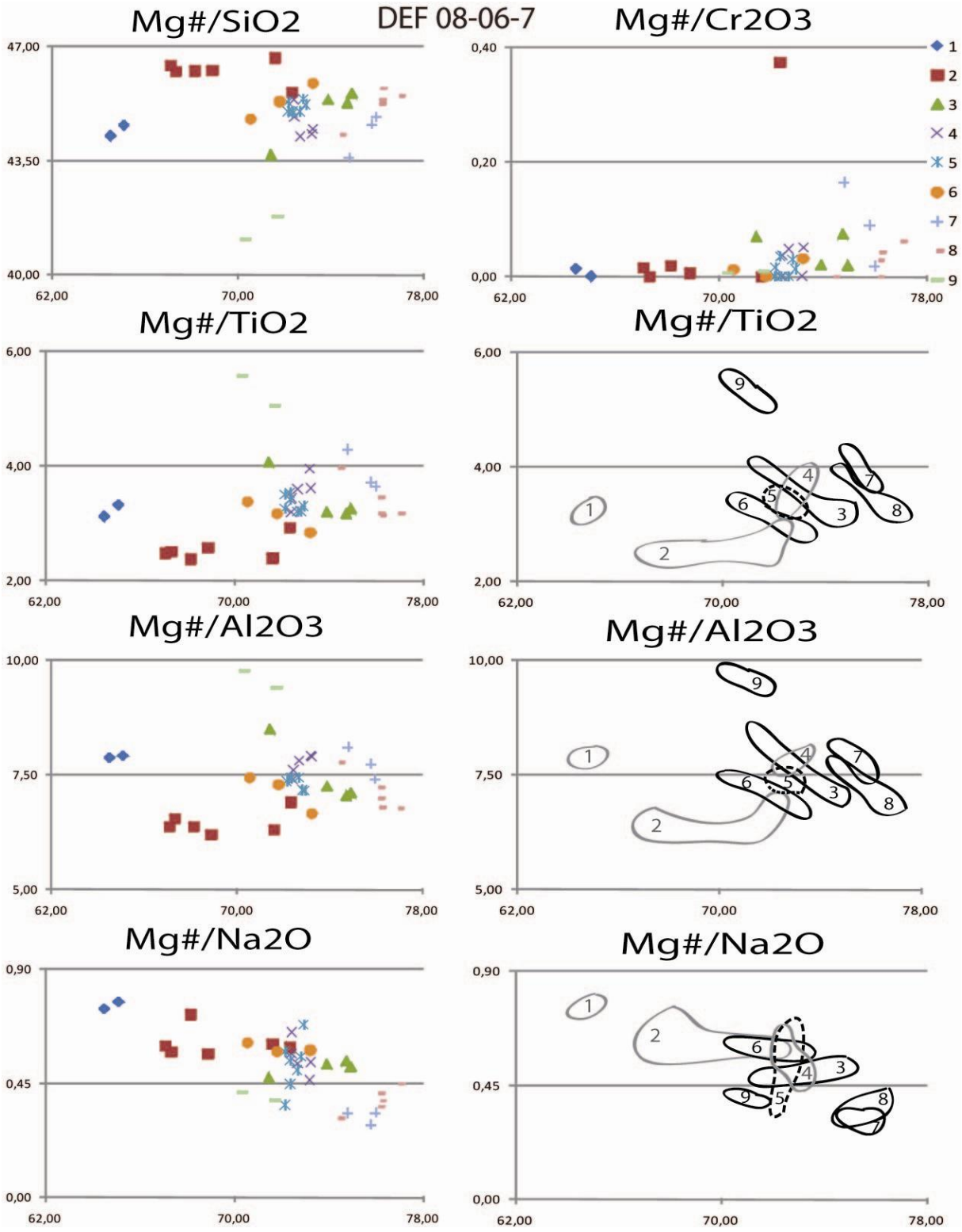

Figure 8-14: CPX phenocryst profile element - element plot from DEF 08-06-7.

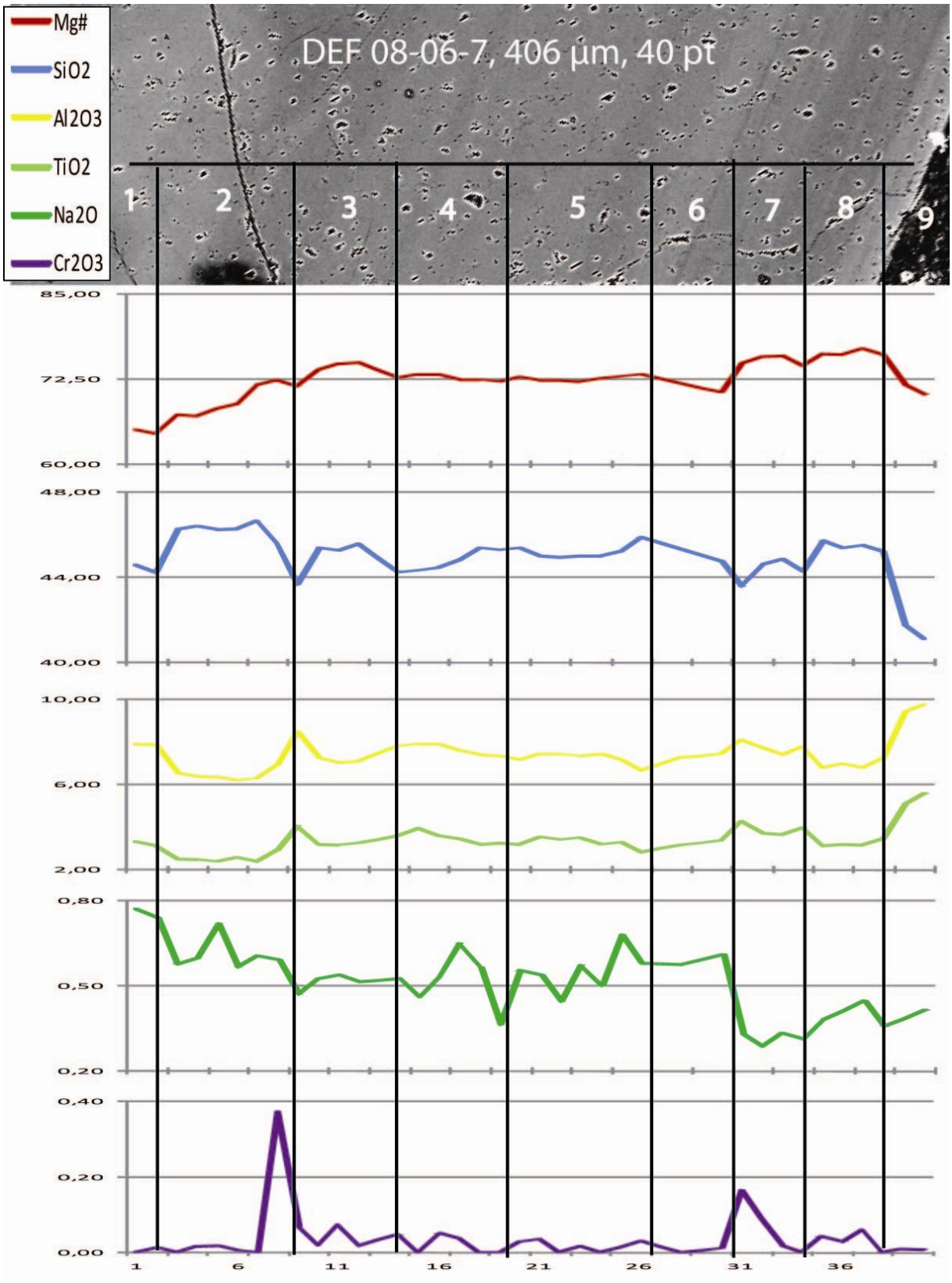

Figure 8-15: CPX phenocryst profile element – line plot from DEF 08-06-7 divided in zones correlated with phenocryst BS-image.

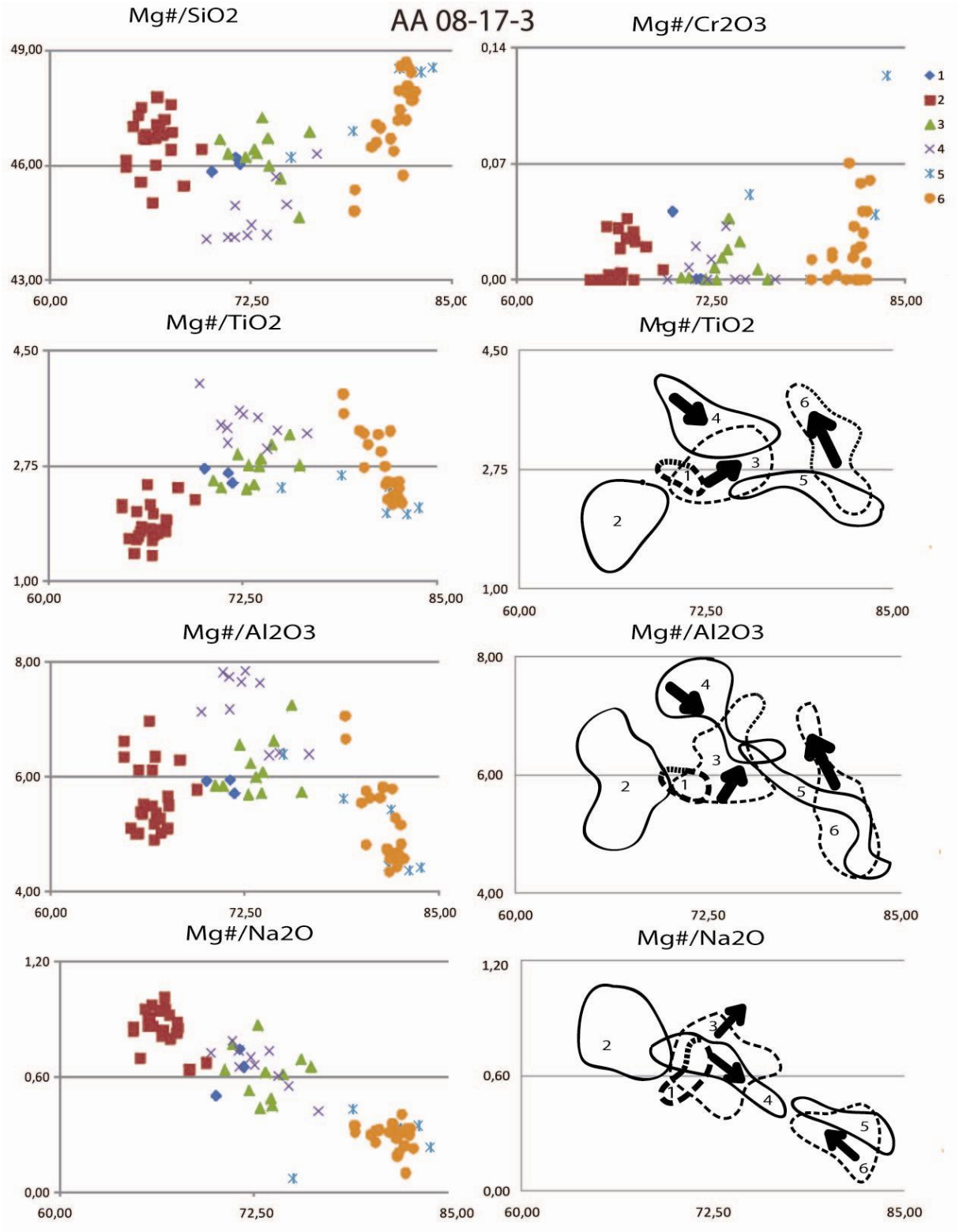

Figure 8-16: CPX phenocryst profile plot from AA 08-17-3.

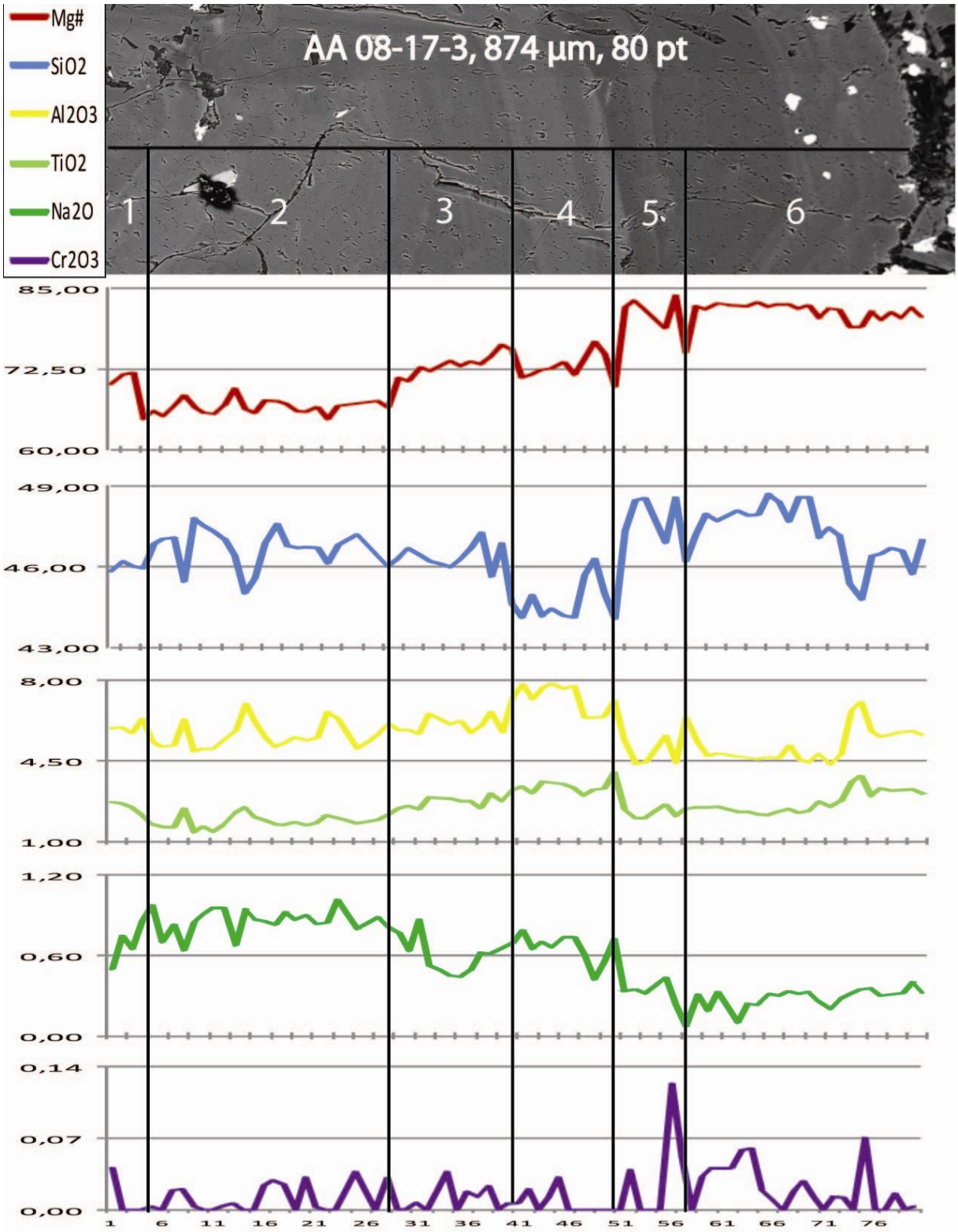

Figure 8-17: CPX phenocryst profile element – line plot from AA 08-17-1 divided in zones correlated with phenocryst BS-image.

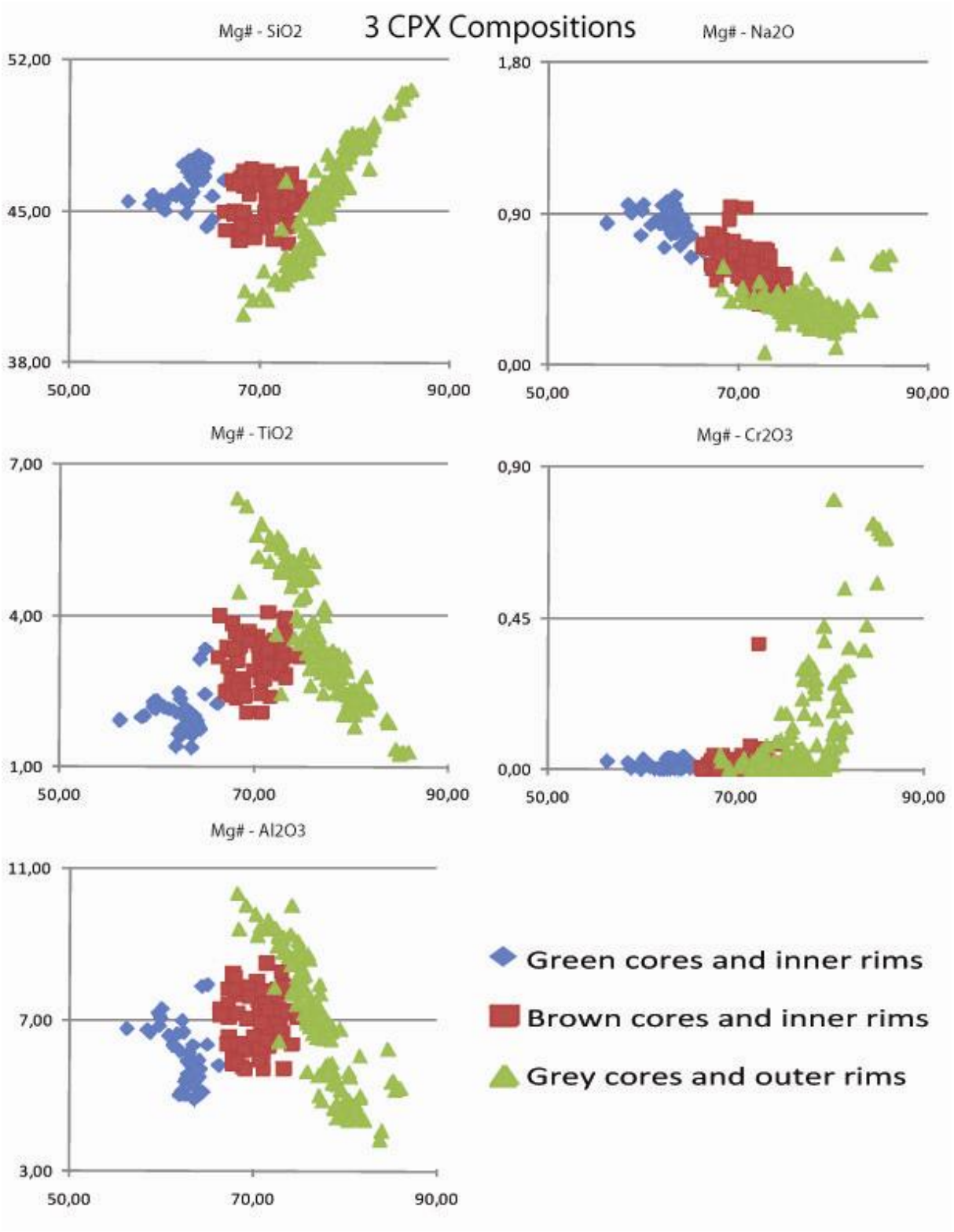

Figure 8-18: El-El plots with all analyses from all CPX phenocryst profiles divided in 3 groups. Green cores and inner rims are shown in blue, brown cores and inner rims are shown in red and grey cores and outer rims are shown in green. Matrix CPX grains have the same composition as brown cores and inner rims (red group) and the grey outer rims (green group).

Sample	DEF 08-01					AA 08-13			
Description	Core	Core	Core	Core	Core	Inner core	Core	Core	Core
Analysis	#74	#78	#80	#85	#91	#110	#111	#114	#120
SiO2	50,39	50,72	51,37	45,11	50,17	45,51	44,74	47,29	44,69
TiO2	1,03	1,00	1,01	2,24	0,54	2,98	1,82	1,39	1,96
Al2O3	4,83	4,58	4,60	8,33	2,48	7,57	7,51	6,66	8,63
Cr2O3	0,29	0,41	0,66	0,04	0,02	0,02	0,00	0,00	0,02
Fe2O3	3,18	2,43	0,72	6,51	4,14	4,63	8,24	6,30	6,89
FeO	2,26	2,74	3,87	5,48	7,33	2,85	5,31	5,15	6,27
MnO	0,14	0,10	0,09	0,27	0,32	0,14	0,37	0,38	0,49
MgO	15,71	15,68	16,06	8,92	11,41	12,24	8,36	9,45	7,99
CaO	21,46	21,68	21,02	21,66	22,90	23,60	22,33	21,71	21,63
Na2O	0,70	0,65	0,61	1,42	0,68	0,45	1,31	1,66	1,41
K2O	0,02	0,00	0,00	0,01	0,00	0,00	0,00	0,00	0,02
Total	100,00	100,00	100,00	100,00	100,00	100,00	100,00	100,00	100,00
Si	1,844	1,857	1,875	1,708	1,895	1,700	1,707	1,782	1,702
Al	0,208	0,197	0,198	0,372	0,110	0,333	0,338	0,296	0,387
Cr	0,008	0,012	0,019	0,001	0,001	0,000	0,000	0,000	0,001
Fe3+	0,088	0,067	0,020	0,185	0,118	0,130	0,237	0,179	0,197
Ti	0,028	0,028	0,028	0,064	0,015	0,084	0,052	0,039	0,056
Mg	0,857	0,856	0,874	0,503	0,642	0,682	0,476	0,531	0,453
Fe2+	0,069	0,084	0,118	0,174	0,232	0,089	0,169	0,162	0,200
Mn	0,004	0,003	0,003	0,009	0,010	0,004	0,012	0,012	0,016
Ca	0,842	0,850	0,822	0,879	0,927	0,944	0,913	0,877	0,883
Na	0,050	0,046	0,043	0,105	0,050	0,033	0,097	0,121	0,104
K	0,001	0,000	0,000	0,001	0,000	0,000	0,000	0,000	0,001
Mg	46,10	46,01	47,59	28,77	33,30	36,85	26,33	30,14	25,93
Fe	8,65	8,28	7,66	21,02	18,64	12,09	23,14	20,07	23,60
Ca	45,25	45,71	44,76	50,22	48,06	51,05	50,53	49,78	50,47
mg*	84,20	84,74	86,14	57,78	64,11	75,29	53,23	60,03	52,35

Table 8-1: Selected EMP spot analysis of CPX phenocrysts from samples DEF 08-01 (Figure 6-1) and AA 08-13 (Figure 6-2). The most extreme values are seen with high and low Mg#, Na_2O and Cr_2O_3.

Sample	AA 08-17					AA 08-14
Description	Core	Core	Inner Rim	Rim	Core	Core
Analysis	#9	#18	#19	#20	#21	#134
SiO2	46,73	39,32	47,39	36,45	49,50	43,85
TiO2	2,51	3,99	2,48	7,54	1,44	1,70
Al2O3	5,91	11,35	5,53	12,63	5,19	7,89
Cr2O3	0,01	0,00	0,04	0,00	0,17	0,05
Fe2O3	5,47	9,79	4,34	8,20	3,25	8,88
FeO	2,40	5,00	2,28	4,29	1,85	7,40
MnO	0,14	0,41	0,13	0,24	0,10	0,74
MgO	12,90	6,52	13,69	7,07	15,16	6,56
CaO	23,32	22,55	23,76	22,61	22,83	21,47
Na2O	0,60	1,05	0,36	0,93	0,49	1,47
K2O	0,01	0,01	0,00	0,03	0,01	0,00
Total	100,00	100,00	100,00	100,00	100,00	100,00
Si	1,743	1,519	1,761	1,408	1,818	1,693
Al	0,260	0,517	0,242	0,575	0,225	0,359
Cr	0,000	0,000	0,001	0,000	0,005	0,001
Fe3+	0,154	0,284	0,121	0,238	0,090	0,258
Ti	0,070	0,116	0,069	0,219	0,040	0,049
Mg	0,718	0,376	0,758	0,407	0,830	0,377
Fe2+	0,075	0,161	0,071	0,139	0,057	0,239
Mn	0,004	0,013	0,004	0,008	0,003	0,024
Ca	0,932	0,934	0,946	0,936	0,898	0,888
Na	0,043	0,079	0,026	0,070	0,035	0,110
K	0,000	0,000	0,000	0,001	0,000	0,000
Mg	38,12	21,25	39,90	23,55	44,19	21,12
Fe	12,38	25,97	10,33	22,28	7,98	29,16
Ca	49,50	52,79	49,77	54,17	47,83	49,72
mg*	75,48	45,00	79,44	51,39	84,71	42,01

Table 8-2: Selected EMP spot analysis of CPX phenocrysts from samples AA 08-17 (Figure 6-6) and AA 08-14 (Figure 6-3). The most extreme values are seen with high and low Mg#, Na_2O and Cr_2O_3.

	#68	#69	#70	#71
SiO2	53,07	53,08	44,97	46,45
TiO2	0,29	0,61	3,47	3,01
Al2O3	0,14	0,57	7,60	6,49
Cr2O3	0,00	0,00	0,02	0,13
Fe2O3	1,61	1,44	4,70	3,90
FeO	7,40	6,16	2,57	3,54
MnO	0,27	0,17	0,12	0,11
MgO	13,58	14,33	12,44	12,80
CaO	23,19	23,09	23,73	23,07
Na2O	0,46	0,54	0,36	0,47
K2O	0,00	0,03	0,00	0,02
Total	100,00	100,00	100,00	100,00
Si	1,983	1,970	1,681	1,733
Al	0,006	0,025	0,335	0,285
Cr	0,000	0,000	0,001	0,004
Fe3+	0,045	0,040	0,132	0,109
Ti	0,008	0,017	0,098	0,085
Mg	0,756	0,793	0,693	0,712
Fe2+	0,231	0,191	0,080	0,110
Mn	0,008	0,005	0,004	0,004
Ca	0,928	0,918	0,950	0,922
Na	0,034	0,039	0,026	0,034
K	0,000	0,001	0,000	0,001
Mg	38,40	40,71	37,26	38,33
Fe	14,47	12,15	11,64	12,02
Ca	47,14	47,14	51,10	49,65
mg*	72,64	77,01	76,20	76,12

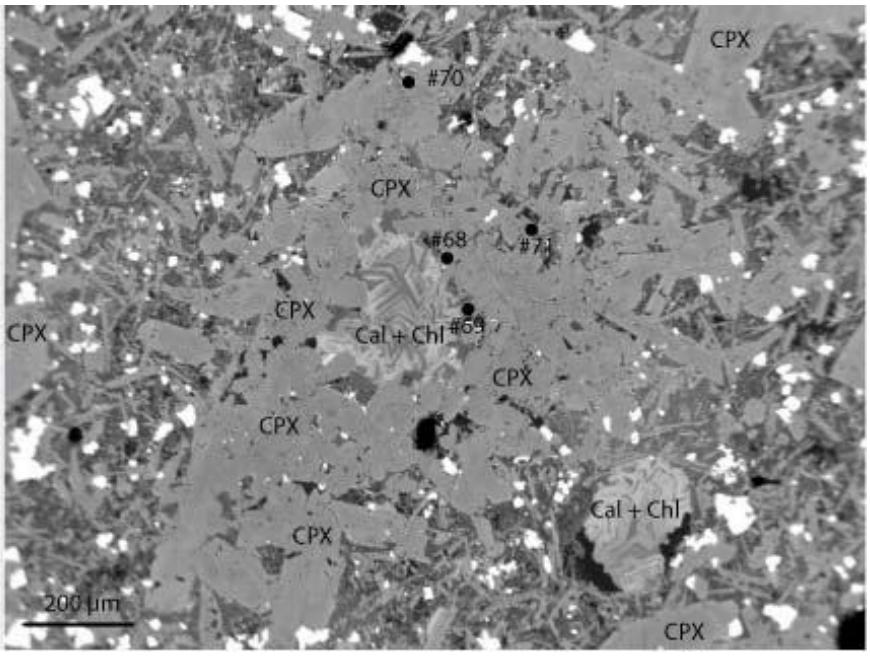

Figure 8-19: EMP spot analyses of CPX aggregate rimming a calcite/chlorite core. The composition of analyses #68 and #69 are unique in this rock. Analyses #70 and #71 are similar to grey outer rims of CPX phenocrysts (green group in Figure 8-18).

Clinopyroxene phenocryst chemistry

The clinopyroxene analyses are in general diopsidic in composition while a few analyses show a hedenbergite composition (E. g. analyses in Table 8-1 and Table 8-2). They commonly have a high TiO_2 (3-5 wt%) and Al_2O_3 (5-9 wt%) content which show an increase towards the rim. High concentrations of Na_2O (up to 1.6 wt%) and $Cr2O_3$ (up to 0.8 wt%) can be seen in some analyses. The SiO_2 content vary between ca 40 – 50 wt% and the Mg# values vary between 42 and 86.

In CPX phenocryst profiles (Figure 8-2 - Figure 8-17) concentrations of Al_2O_3 and TiO_2 show almost identical changes in many cases and show a correlation with the SiO_2 content. Green CPX cores have increased Na_2O concentrations compared to the rims. Cores with a high Mg# number (85 - 90) also have high Na_2O contents (0,61 - 0,70 wt%, analyses #74, #78 and #80 in Table 8-1 and zone 1 in phenocryst DEF 08-01-1, Figure 8-2 and Figure 8-3) compared to rims with a high Mg# number and plot outside the trend seen in the Mg# - Na2O plot (Figure 8-18). The Na_2O concentration appears to correlate with Mg# and show an increase with decreasing Mg#. Cr_2O_3 concentrations are very low but local highs are found with peaks ranging from 0.30 wt% to around 0.80 wt%. The highest Cr_2O_3 concentrations are found in parts of phenocrysts with the highest Mg# number.

Two analyses stand out from the rest with a high SiO_2 content (53 wt%) and low Al_2O_3 (0.14 - 0.57 wt%) and TiO_2 (0.3 - 0.6 wt%) contents. A BS-image of the analysis area of these anomalous CPX compositions can be seen in Figure 8-19.

Some phenocrysts and outer rims in general show a decrease in SiO_2, CaO and Cr_2O_3 together with an increase of TiO_2 and Al_2O_3, with decreasing Mg#. Na_2O show a correlation with Mg#. This type of zoning is referred to as normal zoning by Orejana et al. (2007) and can be seen in phenocryst DEF 08-

01-1 (Figure 8-2 and Figure 8-3). Most of the analyzed CPX phenocrysts do not show normal zoning throughout the whole crystal. Fe-rich cores are rimmed by Fe-poor rims, a phenomena referred to as reverse zoning by Orejana et al. (2007). These cores are either green with a low Mg# number (around 42 - 65) or brown with an intermediate Mg# number (around 50 – 75). Examples of reversely zoned CPX phenocrysts are AA 08-17-1, DEF 08-01-3, DEF 08-06-4, DEF 08-6-5, DEF 08-06-7 and AA 08-17-3.

In the element-element plots of some individual CPX phenocrysts (e. g. Figure 8-14 and Figure 8-16), the composition of the melt show what appears to be random patterns. The complex zoning observed in CPX phenocrysts appears to be reflected in the chemistry. Sector zoning is seen in phenocryst DEF 08-06-4 (Figure 8-1 D) and is documented by two profiles (Figure 8-8 - Figure 8-11).

In Figure 8-18 all CPX phenocryst profile analyses are plotted together and divided based on appearance. Green cores and inner rims are shown in blue color, brown cores and inner rims are shown in red color and the light cores and outer rims are green color. These compositions are not equally distributed in the different rock types, the aillikites are dominated by green cores and grey cores and outer rims while the sannaites show the whole range of compositions. Matrix CPX often exhibits a core and rim and show a great span in chemistry. Analyses of matrix CPX show that these grains have the same compositions as the brown cores and inner rims and the grey outer rims, they do not match the grey cores.

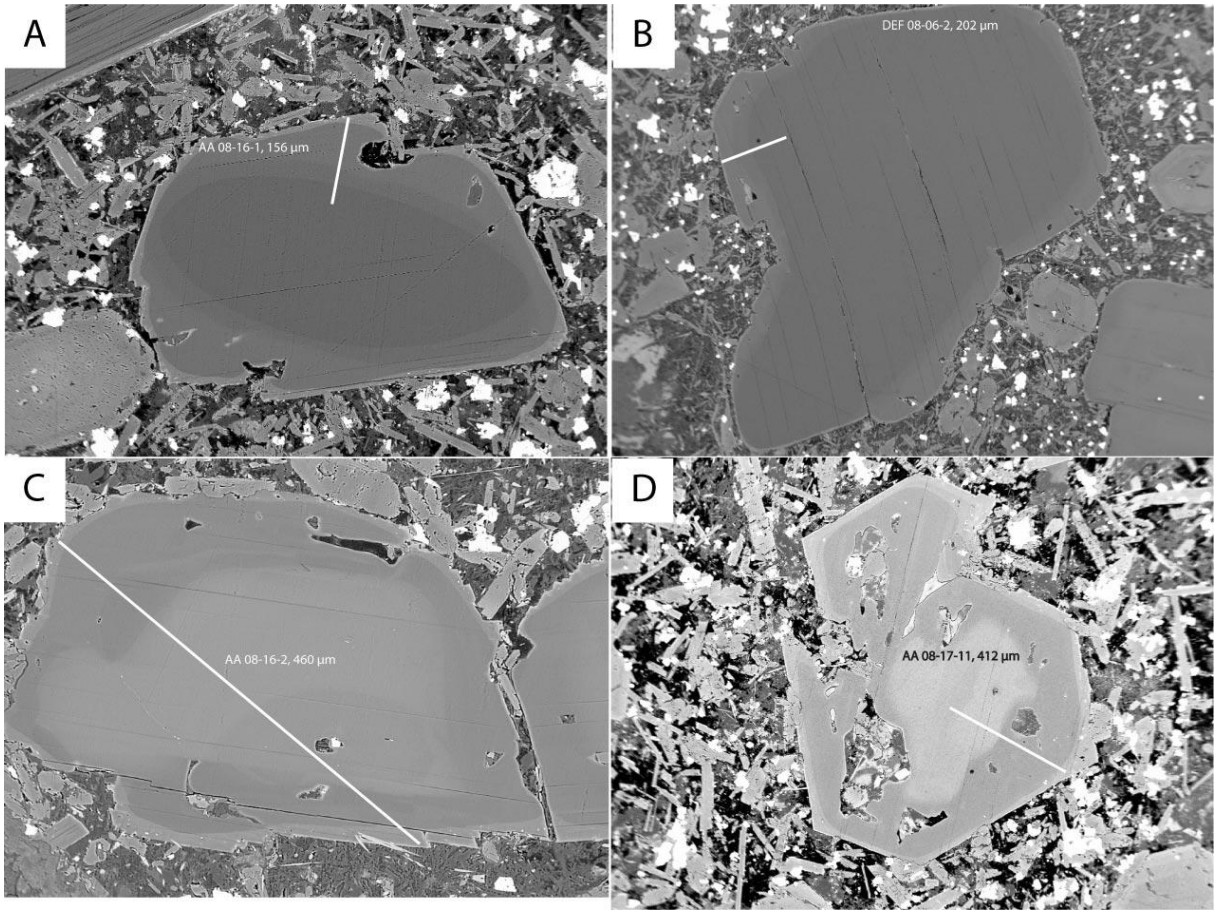

Figure 8-20: BS-pictures of biotite phenocryst profiles with sample name and profile length.

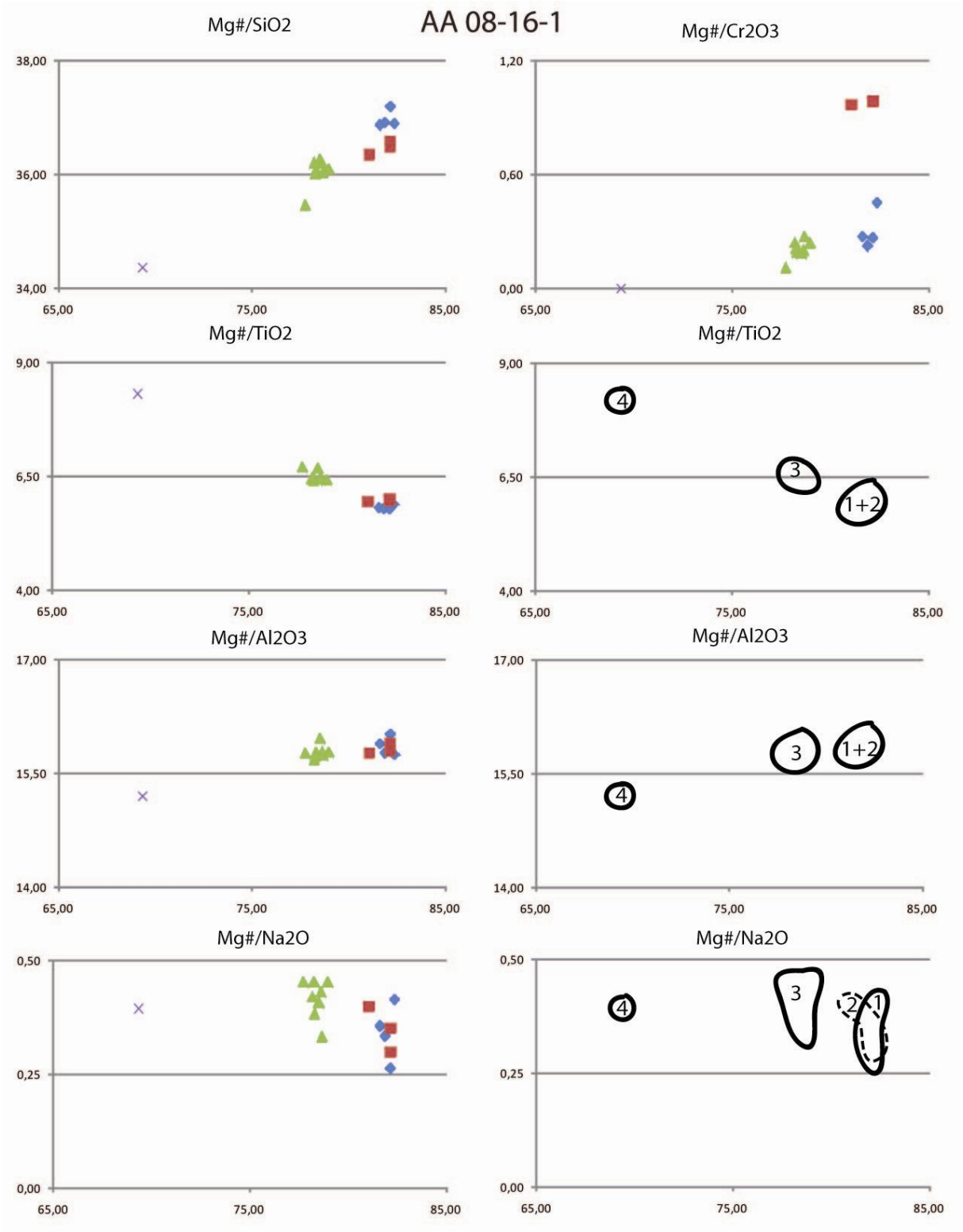

Figure 8-21 : Biotite phenocryst profile plot from AA 08-16-1.

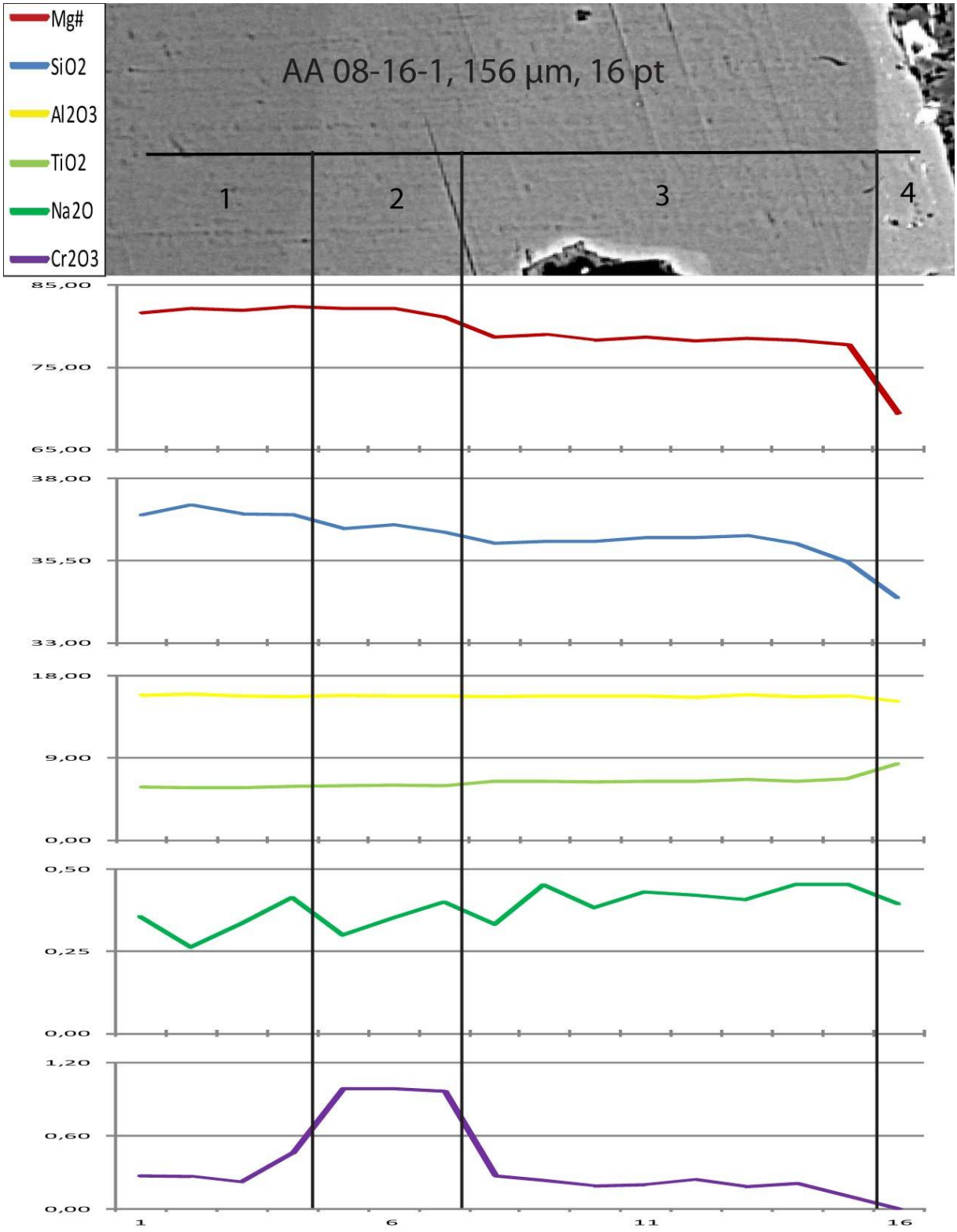

Figure 8-22: Element-line profile from biotite phenocryst AA 08-16-1 divided in zones correlated with phenocryst BS-image.

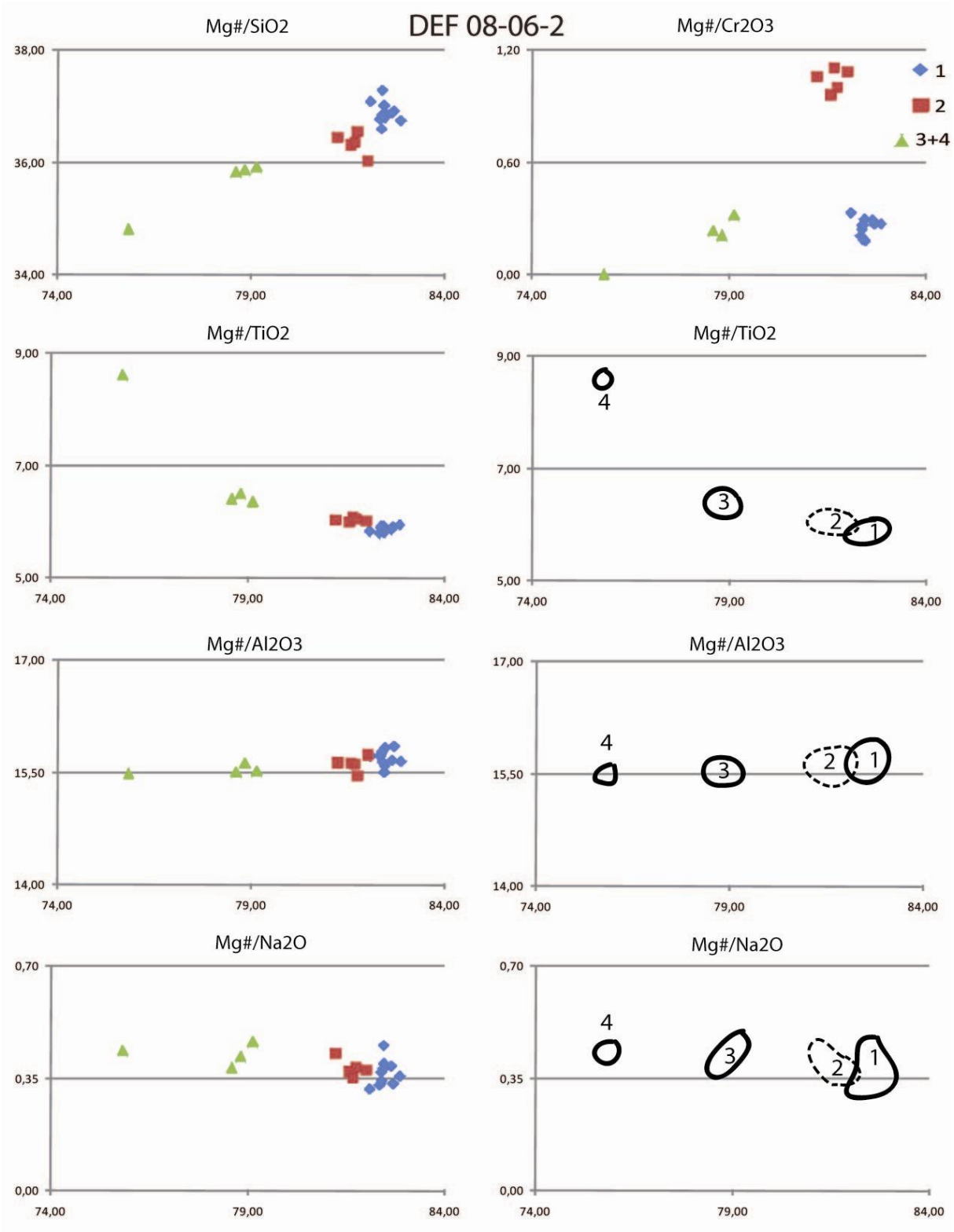

Figure 8-23: Biotite phenocryst profile plot from DEF 08-06-2.

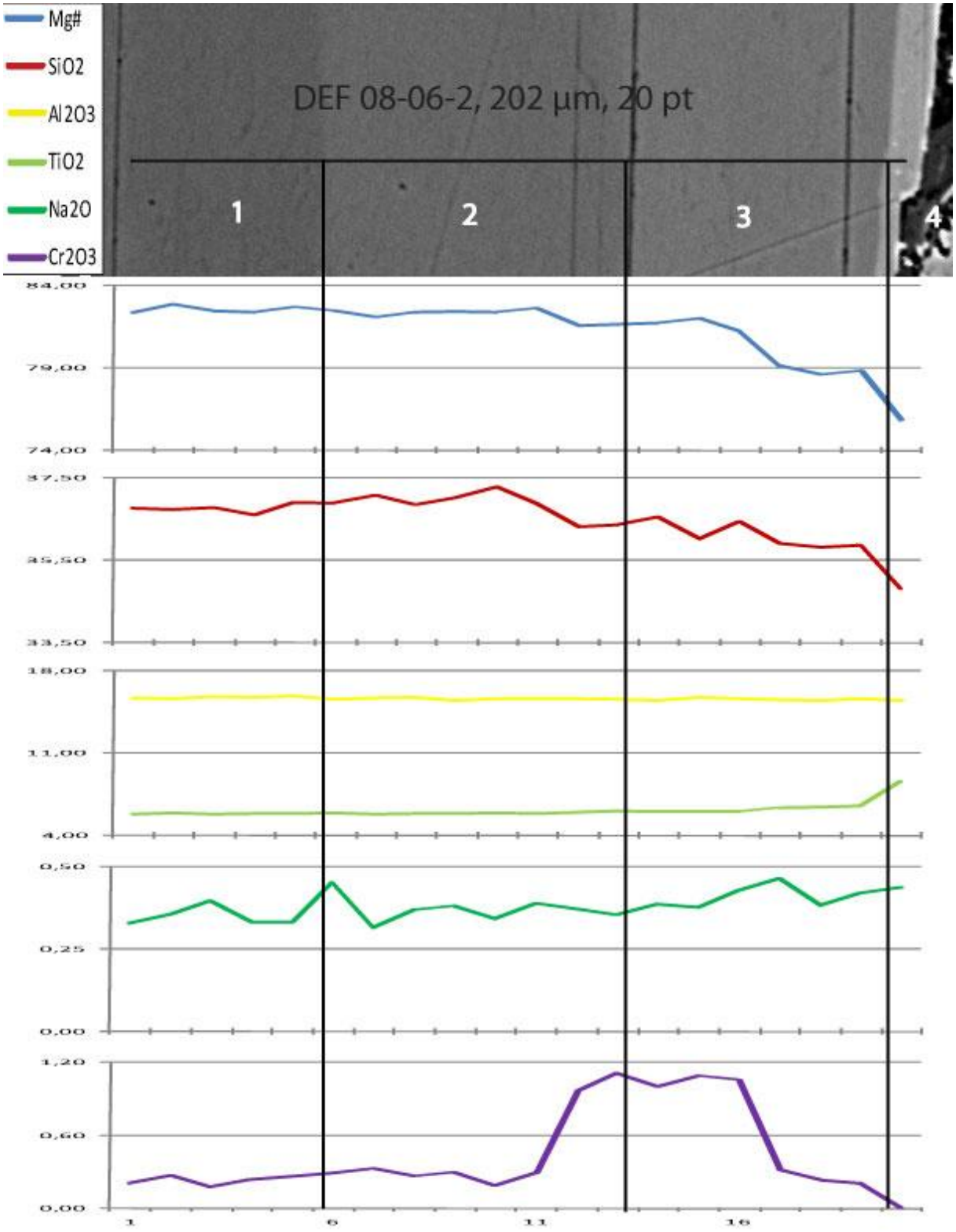

Figure 8-24: Element-line profile from CPX phenocryst DEF 08-06-2 divided in zones correlated with phenocryst BS-image.

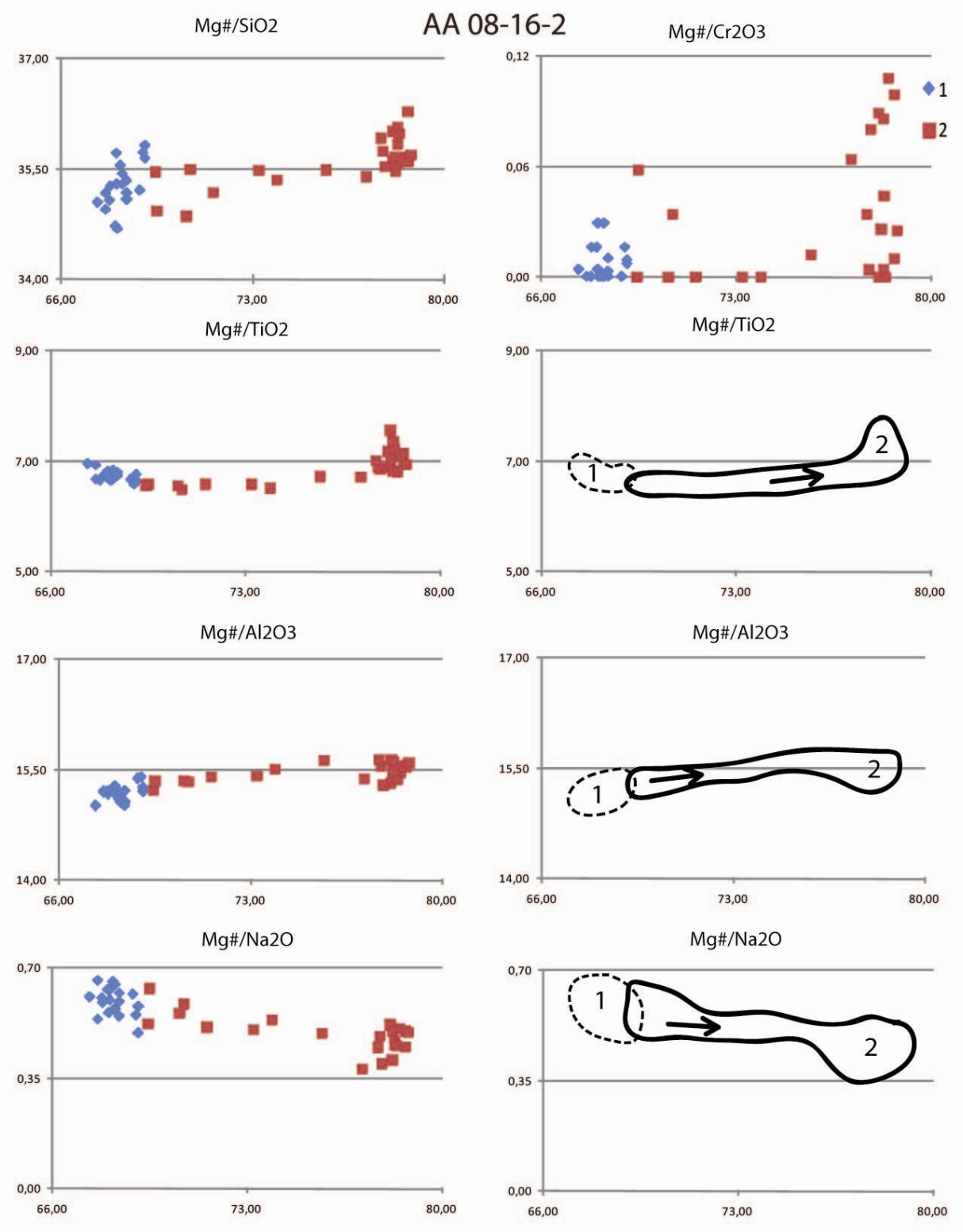

Figure 8-25: Biotite phenocryst profile plot from AA 08-16-2.

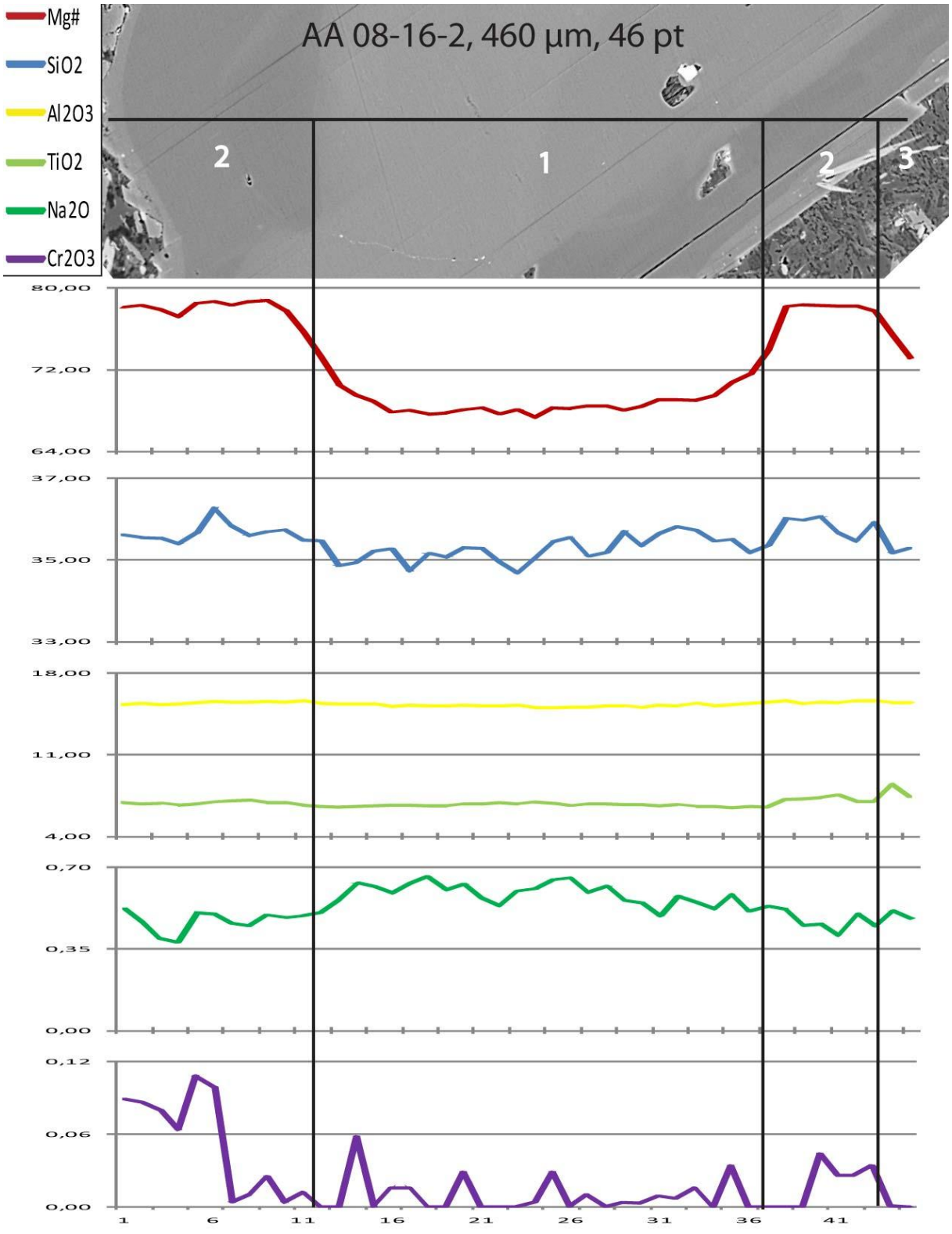

Figure 8-26: Element-line profile from CPX phenocryst AA 08-16-2 divided in zones correlated with phenocryst BS-image.

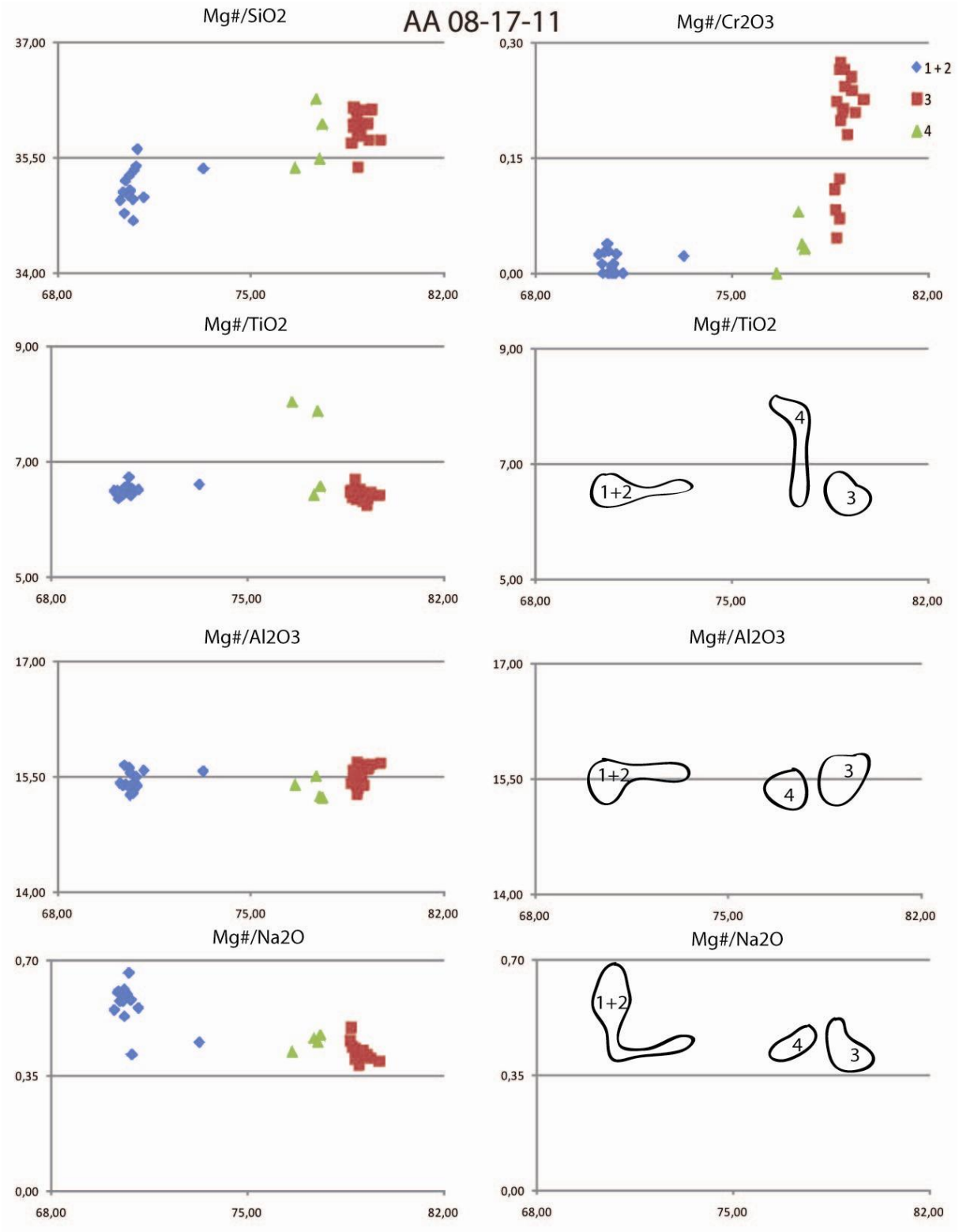

Figure 8-27: Biotite phenocryst profile plot from AA 08-17-11.

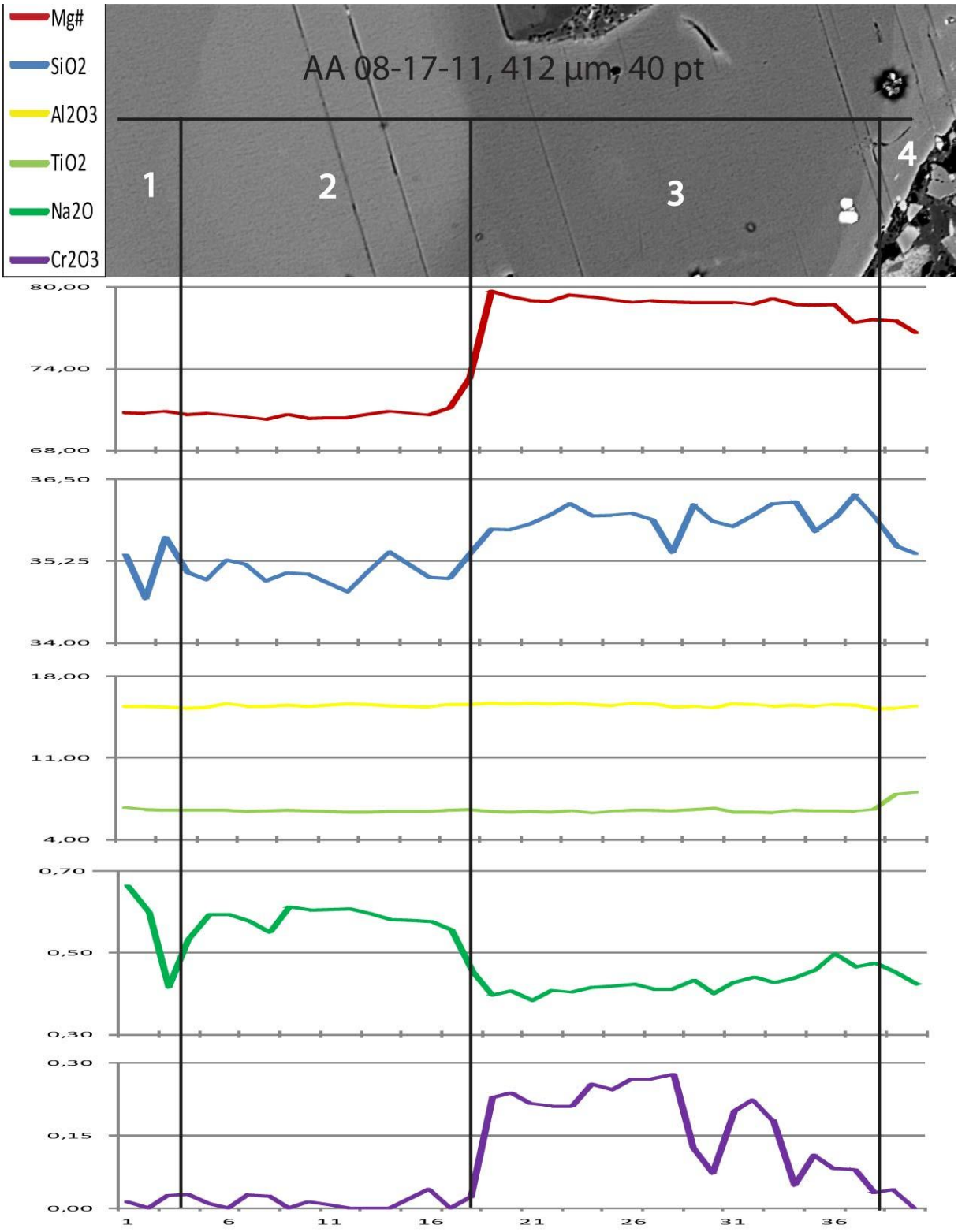

Figure 8-28: Element-line profile from CPX phenocryst AA 08-17-11 divided in zones correlated with phenocryst BS-image.

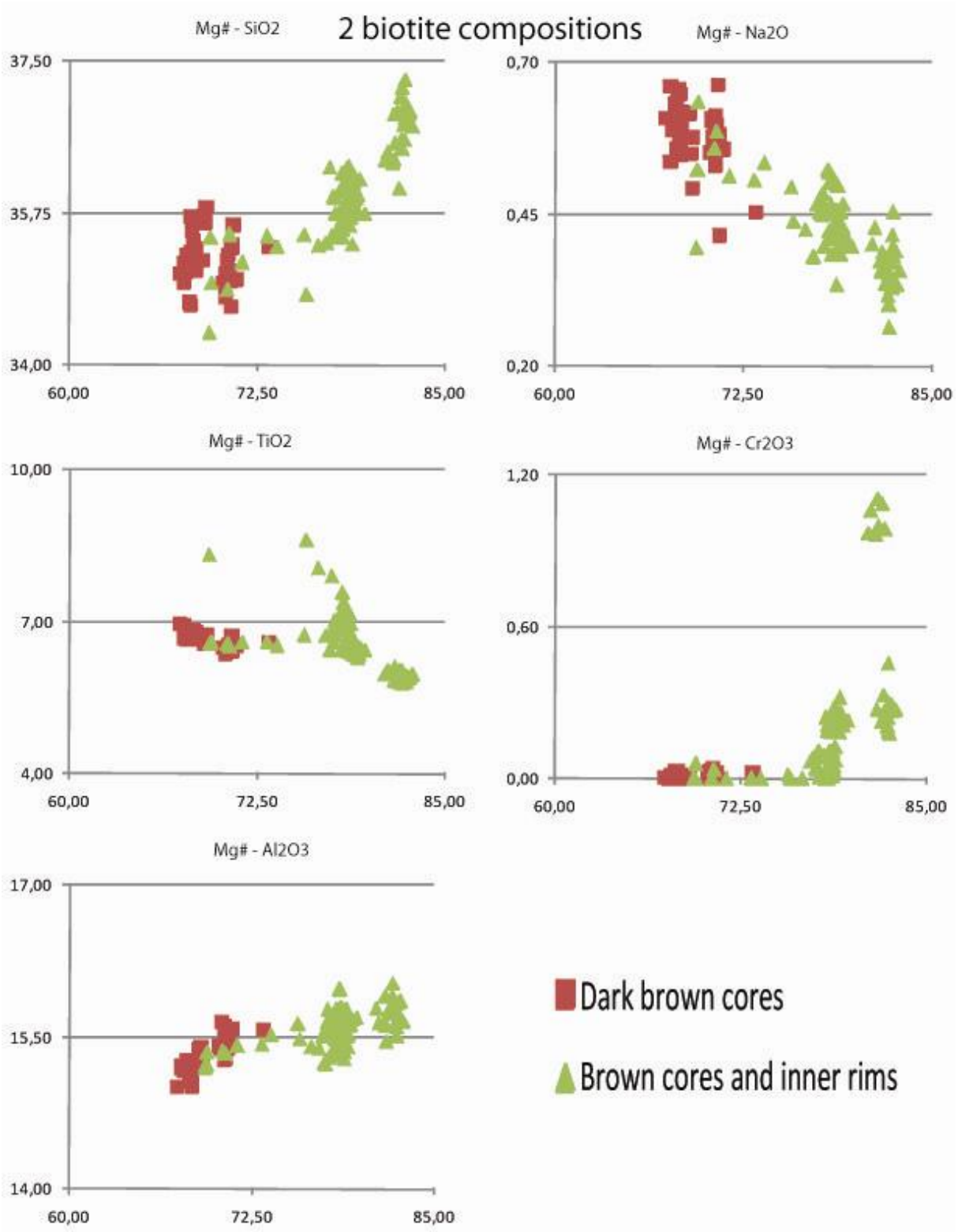

Figure 8-29: El-El plots with all analyses from all biotite phenocrysts divided in two groups. Dark brown cores are shown in red and brown cores and inner rims are shown in green. Matrix biotite has the same composition as brown cores and inner rims.

Biotite phenocryst chemistry

Biotite phenocrysts show high concentrations of TiO_2 (6 – 9 wt%) and can be classified as Ti-biotite – Ti-phlogopite (although named biotite to avoid confusion). With an FeO content of 7 - to 18 wt% and an MgO content of 10 – to 20 wt% the Mg# in biotite phenocrysts range from around 84-68 and the highest Mg# numbers are found in the cores of normally zoned phenocrysts.

In the biotite phenocryst profiles one can see that the Al_2O_3 and TiO_2 contents are very constant and the only significant variation happens in the rim (zone 4 in biotite phenocrysts DEF 08-06-2, AA 08-16-1 and AA 08-17-11) where TiO_2 shows an increase. The Mg# number and SiO_2 content are reasonably similar in evolution and show a general decrease towards the rim. In the element-line plots the Mg# values show defined plateaus while the SiO_2 line show more variation. The reversely zoned phenocrysts exhibit more chemical variation in the with respect to Mg# and SiO_2 than the normally zoned phenocrysts. Na_2O show a slightly increasing trend with decreasing Mg#. The highest Cr_2O_3 concentrations (>1 wt%) are found in the zones with the highest Mg# in the normally zoned phenocrysts. The reversely zoned phenocrysts show Cr_2O_3 peaks around 0.3 wt% in the high Mg# zone.

All the biotite phenocryst profile plots have been plotted in one element-element plot (Figure 8-29) and are divided in two groups, “dark brown cores” and “brown cores and inner rims”. Each group appears to plot in two groups with different Mg# numbers. Matrix biotite grains share chemical characteristics with the green group, brown cores and inner rims.

Spinel phenocryst chemistry

Spinel with a lot of chemical variation has been analyzed and the results can be found in Appendix A. Spinel rich in Cr, Mg, Al, Ti and Fe are found only in sample DEF 08-01 (aillikite, ultramafic lamprophyre) both as a phenocryst, as inclusions in phenocryst DEF 08-01-3 and as matrix. Sample DEF 08-01 has the highest bulk chemistry content of Cr_2O_3 of the lamprophyric samples and the inclusions of spinel rich in Cr, Mg, Al, Ti and Fe are found in a zone of a CPX phenocryst which has a high Cr_2O_3 content and a high Mg# value. In the sannaites (alkaline lamprophyres) Al, Ti and Fe-rich spinel dominate which only has a few wt% Cr_2O_3 and MgO. While Al, Ti and Fe-rich spinel can be found in cores and inclusions, the more Ti and Fe-rich spinel grains are found in inclusions, rims and matrix. The bulk of matrix spinel is dominated by Fe-rich magnetite in both the ultramafic and alkaline lamprophyres.

EMP analysis of spinel phenocrysts, inclusions, and rims

Sample	DEF 08-01-25			DEF 08-01-25			DEF 08-01-25					DEF 08-01-3		
Description	Core			Phenocryst rim			Matrix					Inclusion in CPX		Matrix
Analysis	#1	#2	#6	#3	#4	#5	#7	#8	#9	#10	#11	#19	#20	#33
SiO2	0,08	0,09	0,07	0,05	0,08	0,03	0,10	0,06	2,03	0,07	0,07	0,02	0,08	0,09
TiO2	2,88	2,84	2,83	14,39	10,68	16,23	17,20	17,59	9,12	18,34	17,35	4,39	8,46	3,48
Al2O3	19,94	19,73	19,36	1,95	4,94	3,66	1,05	1,40	1,28	0,97	0,79	16,91	11,86	25,45
Cr2O3	36,07	36,50	36,88	3,79	12,42	3,56	0,11	0,17	0,13	0,09	0,42	28,20	18,25	27,23
Fe2O3	9,87	9,86	9,69	31,58	27,57	26,77	29,98	29,03	38,13	28,28	29,72	17,02	23,51	11,58
FeO	17,40	17,02	17,58	43,94	40,18	46,38	48,17	48,49	46,92	48,61	48,31	21,93	27,28	18,03
MnO	0,24	0,26	0,24	1,34	1,43	2,02	2,61	2,61	1,44	2,81	2,61	0,29	0,38	0,22
MgO	13,34	13,53	13,11	2,41	2,22	0,76	0,00	0,00	0,06	0,00	0,00	11,07	9,97	13,87
CaO	0,00	0,00	0,00	0,07	0,09	0,14	0,31	0,12	0,58	0,21	0,19	0,16	0,21	0,05
V2O3	0,18	0,16	0,23	0,48	0,38	0,45	0,46	0,53	0,31	0,61	0,54	0,00	0,00	0,00
Total	100,00	100,00	100,00	100,00	100,00	100,00	100,00	100,00	100,00	100,00	100,00	100,00	100,00	100,00
				Number of ions on the basis of 32O in the framework										
Si	0,021	0,023	0,016	0,014	0,024	0,009	0,031	0,017	0,605	0,021	0,021	0,006	0,022	0,021
Al	5,845	5,783	5,699	0,674	1,682	1,268	0,371	0,492	0,448	0,344	0,280	5,108	3,695	7,276
Cr	7,094	7,176	7,281	0,878	2,838	0,826	0,027	0,040	0,030	0,022	0,099	5,714	3,816	5,222
Fe3+	1,848	1,845	1,821	6,968	5,997	5,922	6,757	6,534	8,543	6,374	6,710	3,284	4,678	2,115
Ti	0,540	0,531	0,532	3,174	2,323	3,589	3,875	3,959	2,042	4,132	3,916	0,846	1,682	0,635
V	0,035	0,031	0,046	0,113	0,088	0,106	0,111	0,128	0,075	0,147	0,131	0,000	0,000	0,000
Mg	4,946	5,016	4,881	1,051	0,956	0,331	0,000	0,000	0,029	0,000	0,000	4,232	3,930	5,015
Fe2+	3,620	3,540	3,671	10,773	9,712	11,401	12,066	12,129	11,681	12,178	12,119	4,702	6,032	3,658
Mn	0,052	0,054	0,052	0,333	0,351	0,502	0,663	0,661	0,362	0,713	0,663	0,063	0,085	0,044
Ca	0,000	0,000	0,000	0,021	0,029	0,046	0,098	0,038	0,186	0,068	0,061	0,044	0,060	0,013
Total	24,00	24,00	24,00	24,00	24,00	24,00	24,00	24,00	24,00	24,00	24,00	24,00	24,00	24,00

Figure 8-30: Analyses of spinel from an ultramafic lamprophyre – aillikite, sample DEF 08-01.

9 Ar^{40}/Ar^{39} Dating

Samples M-14C and M-21 previously mentioned in chapter 1, introduction, have been dated (Buchanan, 2008) by the Ar^{40}/Ar^{39} dating technique. The age plateau diagrams from Buchanan (2008) has been included and show lamprophyre crystallization ages of 262 Ma for sample M-14C and 264 Ma for sample M-21. These dykes were also sampled by Augland (2007) and samples LEA 06-93, LEA 06-81 and LEA 06-90 are from the same area.

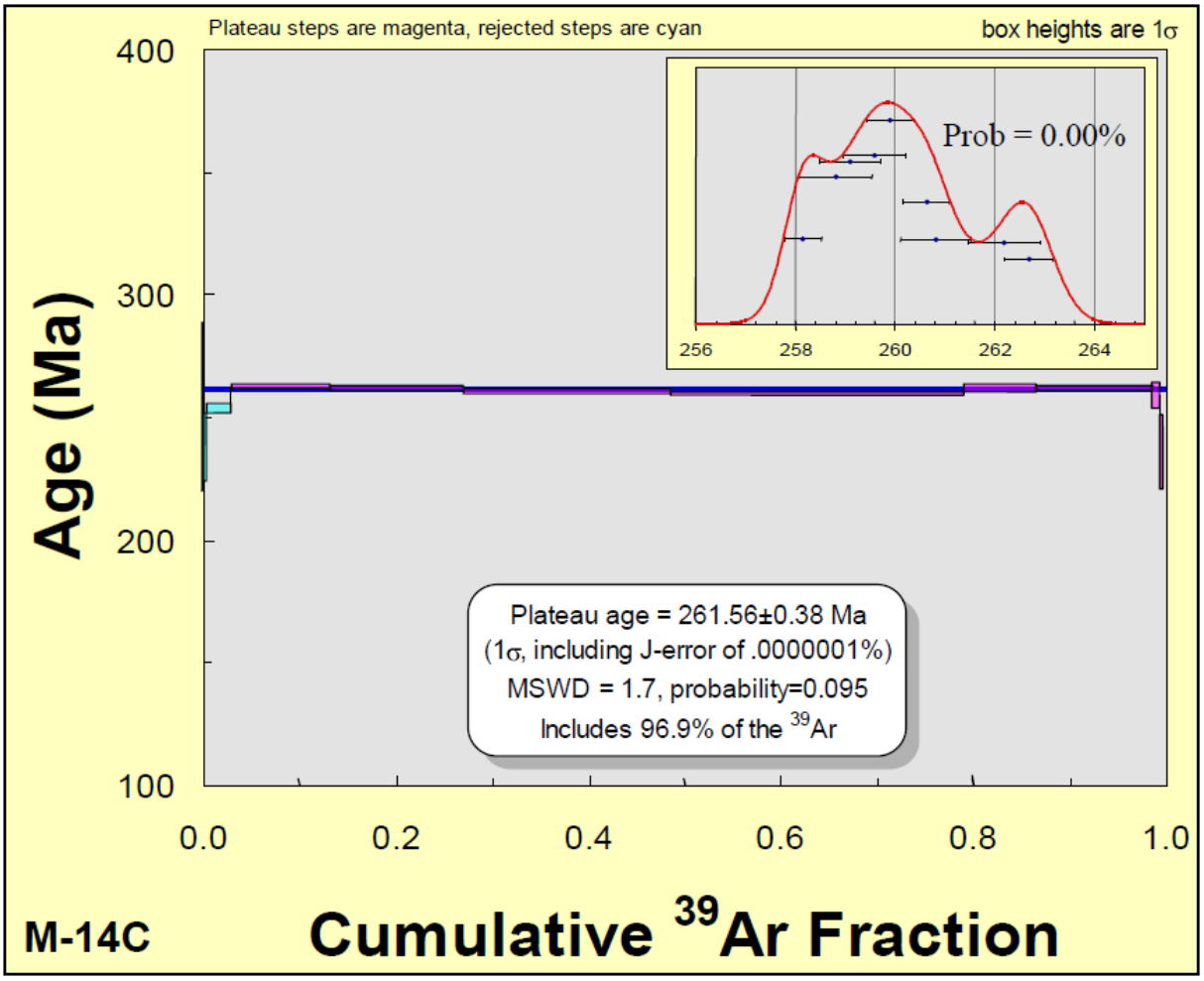

Figure 9-1: Plateau diagram produced from the incremental heating data collected from sample M-14C. *Inset:* Probability density diagram created from the SCTF data from sample M-14C. Individual crystal data represented as points with error bars (error bars are1σ). Prob. = the probability that the SCTF data could be part of a normal distribution.

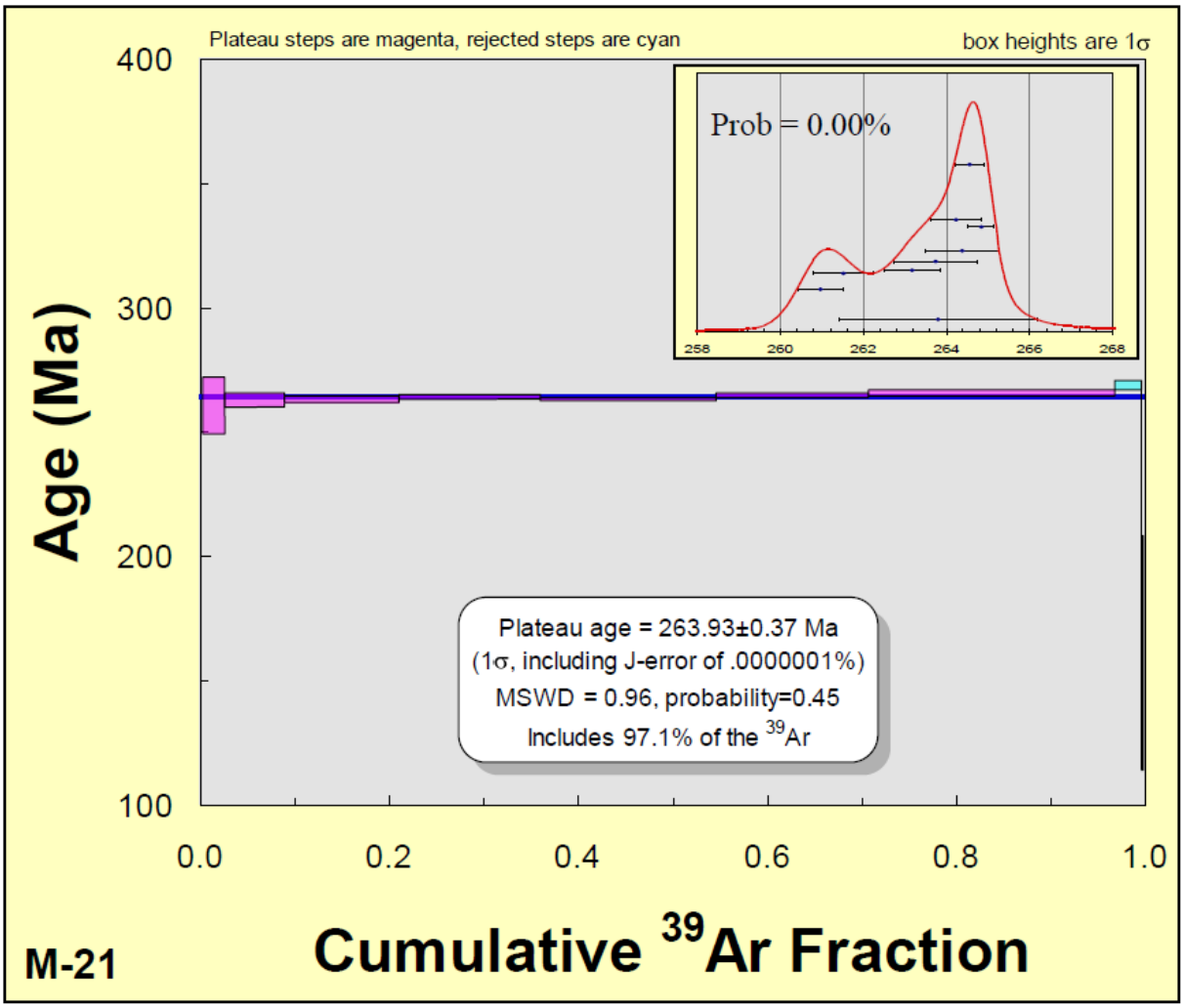

Figure 9-2: Plateau diagram produced from the incremental heating data collected from sample M-21. *Inset:* Probability density diagram created from the SCTF data from sample M-21. Individual crystal data represented as points with error bars (error bars are1σ). Prob. = the probability that the SCTF data could be part of a normal distribution.

10 Discussion

10.1 Magma Evolution

Two different branches of rocks have been identified, alkaline and ultramafic lamprophyres. Still, the bulk rock major element chemistry overlap and the trace element abundances are comparably high with similar normalized distributions (chapter 7, Bulk Rock Chemistry, Table 7-1 and Figure 7-5). This suggest that the parental magmas are related (Tappe et al., 2004). In addition, the mineral assemblages in the two different rocks appear related and also point towards a relation between the different rocks, a common source is proposed. Previous work has also revealed that ultramafic - and alkaline lamprophyres can form a compositional and geochemical continuum (Tappe et al., 2006). Tappe et al. (2006) conclude that ultramafic rocks grade into rocks with a felsic component higher than 10% and are clearly related by fractionation. Primary carbonate-rich UML magmas (proto aillikite) rarely reach upper crustal levels although they may be abundant early components of extension-related continental magmatism (Tappe et al., 2006). This would explain the uncertainties concerning classification, e. g. the fact that sample AA 08-14 appears to have a mafic component less than 90% but still has no feldspars and resemble the aillikites in many ways.

Magma mixing

Clinopyroxene phenocrysts, especially phenocrysts in the sannaites, display complex zoning, twinning and resorbtion, features which has been related to magma mixing in earlier work (Bedard et al., 1988; Dobosi and Fodor, 1992). These complex zoning patterns are illustrated in pictures in Chapter 6, Petrography and in plots in Chapter 8, Mineral Chemistry. In addition there are different types of CPX phenocryst zones which display different chemical compositions, green cores and inner rims, brown cores and inner rims, and grey cores and outer rims (Figure 8-18). Green CPX phenocryst cores has been discussed in many papers and three possible origins for green CPX cores were presented by Bedard (1988):

I) They are cognate but formed under a different pressure-temperature regime than did the mantling pyroxene (Frisch and Schmincke, 1969; Huckenholz, 1973; Scott, 1976; Wilkinson, 1975).

II) They are derived from a felsic magma generated through high-pressure differentiation of cogenetic or similar magmas (Brooks and Printzlau, 1978; Duda and Schmincke, 1985; Liotard et al., 1988; Lloyd, 1981).

III) They are accidental xenocrysts (Barton and Vanbergen, 1981; Wass, 1979).

Other variations of these explanations, e.g. increasing oxygen and/or water fugacity has also been proposed as an explanation of cognate green-core clinopyroxene phenocrysts with inverse zoning (Holm, 1982; Aurisicchio *et al.*, 1988). Dobosi and Fodor (1992) pointed out that identical Fe-rich diopside cores in two unrelated provinces is suspect. Also, the coincidence of Fe-rich diopside compositions that appear genetically unrelated to the main assemblages of green-core clinopyroxene may actually indicate that they are cognate and a normal part of the igneous processes that produce

green-core phenocrysts (Dobosi and Fodor, 1992). In Xu's model (2003), the green-core clinopyroxene phenocrysts are regarded as xenocrysts. They may have been entrained from disintegrated wall rocks during magma ascent (Barton and Vanbergen, 1981) or represent crystallization products of an evolved magma which subsequently mixed with a more primitive magma.

The brown cores and inner rims are generally observed in the sannaites and similar observations are not abundant in the literature. Orejana et al. (2007) described similar cores and concluded that they had crystallized from a distinct and more evolved magma after significant crystal fractionation.

The grey cores are characterized by a high Mg# (ca 85) and Cr (ca 1 wt%) indicate that they crystallized in a primitive, mantle derived melt (von Seckendorff et al., 2004). The cores are homogeneous and have a high Na_2O content, a trait which deviates from the normal trend seen in Figure 8-18. This could suggest that these cores formed under different conditions than the other cores and rims. The Na content is said to increase with pressure (Thompson, 1974; Wass, 1979). The solubility of Ti in clinopyroxene is said to increase as the pressure drops (Edgar et al., 1980) or temperature increases (Gamble and Taylor, 1980). These cores have high a high Na_2O content and a low TiO_2 content which could suggest that these cores formed at a higher pressure.

The grey outer rims are also characterized by a high Mg# and zones of high Cr_2O_3 (ca 1 wt%). This would suggest that mantle melts have been involved (von Seckendorff et al., 2004) and that there has been several pulses. The grey outer rims in general show a decrease in SiO_2, CaO and Cr_2O_3 together with an increase of TiO_2 and Al_2O_3, with decreasing Mg#. Na_2O show a correlation with Mg#. The fact that the grey cores are the most abundant and that similar rims are seen in all samples is interpreted to reflect that primitive mantle melts are the main source of these rocks.

Two different hypotheses were presented by Orejana et al. (2007) to explain changing geochemical characteristics in his CPX phenocrysts: 1) magma differentiation as a consequence of progressive cooling and crystallization, and 2) changes in pressure conditions during crystallization. Based on their data, Orejana et al. (2007) explain the depletion of Mg, Cr, Si and Ca and the enrichment of Al and incompatible trace elements with fractional crystallization of olivine, CPX and Cr-spinel. My observation of Cr-Mg-Al-Ti-Fe spinel and magnetite in my samples is a further indication of AFC processes and is compatible with the explanation presented by Orejana et al. (2007). Cr-spinel and olivine are the earliest phases in an aillikite magma to crystallize (Tappe et al., 2006). Since the rim compositions from all CPX phenocrysts are similar and plot within a restricted range, this is an indication that they all crystallized from the same magma, close to its subvolcanic emplacement level (Orejana et al., 2007).

The fact that the bulk rock chemistry SiO_2 content show such a limited range (35-40 wt%) is an indication that the SiO_2 content of the sum of fractionated phases lies close to 35-40 wt% and/or that AFC is a minor process. In the bulk chemistry, a relatively constant SiO_2 is accompanied by a slight increase in Al_2O_3 with decreasing Mg# (Figure 7-3). This fits with olivine fractionation, but indicates that spinel fractionation is of minor importance since Al_2O_3 increases with decreasing Mg#.

Without trace-element analyses from the different cores it is difficult to establish how they relate to each other; still, mixing of different magmas might not be necessary to explain the different cores. According to Couch (2001) mixing may occur between distinct magma batches or between different

zones of the same magma chamber, through a convective self-mixing process. Therefore, different magmas have not necessarily been involved.

Fluid-rich phenocrysts

While the ultramafic lamprophyre samples have an almost fluid-free phenocryst assemblage the alkaline lamprophyres include fluid-rich phenocrysts like biotite and calcite. Still, sample DEF 08-01 which does not contain either biotite or calcite has the highest L.O.I. (7.11 wt%) of all the samples.

The fact that calcite is only found as a phenocryst phase in the sannaites could be an implication that the CO_2/H_2O ratio was higher in the sannaites than in the aillikites (Tappe et al., 2004). In the Torngat ultramafic lamprophyres the different rock samples still have the same CaO content which Tappe et al. (2004) explain as CO_2 loss (degassing) of the rocks which are free of carbonate phenocrysts.

In the case of the Liverpool Land lamprophyres the alkaline lamprophyre samples that contain calcite as a phenocryst phase actually have a lower CaO bulk rock chemistry than the ultramafic lamprophyre samples that does not have calcite phenocrysts. There must be some other factor that controls the growth of calcite phenocrysts. Growth of biotite phenocrysts could increase the CO_2/H_2O ratio as H_2O was incorporated into biotite. If this is the case degassing might not be necessary in the Liverpool Land lamprophyres, it could be due to crystallization conditions that calcite phenocrysts did not develop. It must be noted that several samples contain either ocelli which are rich in calcite or late cracks filled with calcite. The ocelli could be where the CO_2 have taken place if not found as calcite phenocrysts.

10.2 Summary and Magmatic Model

Mantle melts are indicated by primitive high-pressure CPX phenocryst cores. Ultramafic melts are thus generated somewhere in the asthenosphere or the mantle lithosphere (Tappe et al., 2006). Emplacement is passive and controlled by extensional tectonics as indicated by field observations and documentation of several pulses of primitive magma in phenocrysts. A multi-stage veined mantle melting model for UML magma production beneath an incipiently rifted cratonic area (Tappe et al., 2006) is suggested. This model also opens for emplacement over tens of millions of years. The melts are at some point in the mantle enriched in fluids and incompatible elements (Neumann pers comm.). At lower crustal level the ultramafic melts reach a magma chamber and are later intruded by two distinctly more developed melts as indicated by resorbtion and addition of green and brown cores and inner rims. This is followed by one or more pulses of ultramafic melts as indicated by the primitive grey rims. Magma mixing and AFC dominate in the crustal magma reservoir and sannaites (AL) have been interpreted to be the most affected by these processes as indicated by spinel fractionation and compositional zoning in CPX - and biotite phenocrysts. Fluid-rich phenocryst phases are more abundant, and calcite appears as phenocrysts in the sannaites (AL). The calcite phenocrysts could indicate that the CO_2/H_2O ratio was higher in the sannaites than in the aillikites (Tappe et al., 2004). Xenoliths of the host rock (Hodal-Storefjord Monzodiorite) are abundant in the dykes.

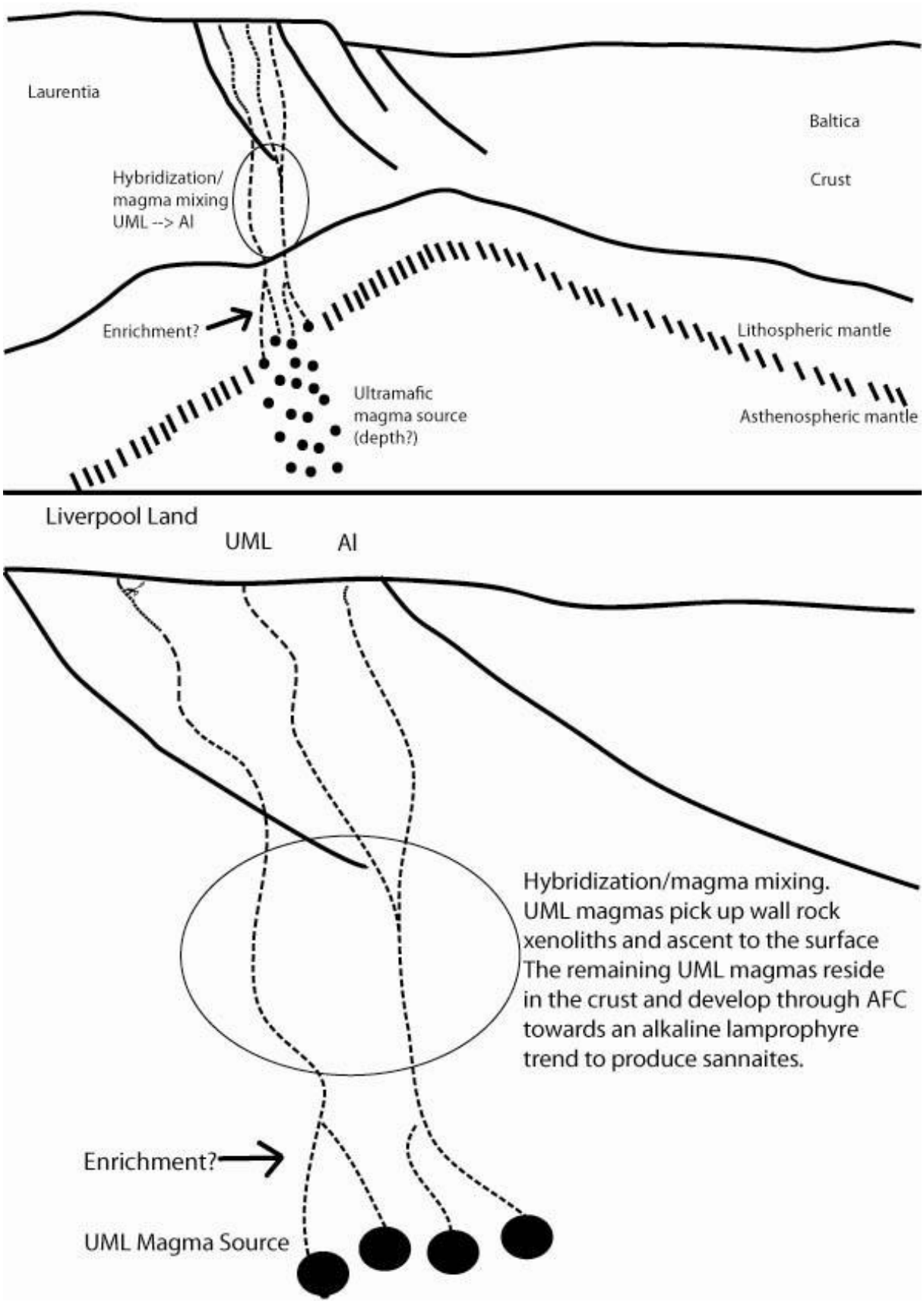
Laurentia
Baltica
Crust
Hybridization/
magma mixing
UML --> AI
Enrichment?
Lithospheric mantle
Ultramafic
magma source
(depth?)
Asthenospheric mantle
Liverpool Land
UML
AI
Hybridization/magma mixing.
UML magmas pick up wall rock
xenoliths and ascent to the surface
The remaining UML magmas reside
in the crust and develop through AFC
towards an alkaline lamprophyre
trend to produce sannaites.
Enrichment?
UML Magma Source

10.3 Comparison with Lamprophyres elsewhere in NE Greenland

There are three known reported lamprophyre dyke clusters in Central East Greenland. These are the Revdal lamprophyres, the Liverpool Land Lamprophyres and the Ole Rømer Land lamprophyres. Uncertainties concerning the age of these lamprophyres raise the interesting question of whether these different lamprophyres are related. The available data on the different dykes vary; there are XRF major element data on the Revdal dykes along with petrographic descriptions and field observations. For the 420 Ma lamprophyre dyke (Andresen 1995) there are no data besides the age.

Samples AA 08-12 and AA 08-15 have been interpreted to be unrelated to the lamprophyres from trace element analyses (Figure 7-4 and Figure 7-5) in addition to a different mineralogy. These dykes could perhaps be equivalents of the Tertiary dolerites described by (Augland, 2007; Coe and Cheeney, 1972).

The Revdal Lamprophyres

More than 15 lamprophyric dykes are observed in the Revdal area (Larsen et al., 1990; Stemmerik and Sørensen, 1980). Field observations by Stemmerik and Sørensen (1980) report a number of thin lamprophyric dykes cutting the Lower Permian sediments but only parts of the Upper Permian sequence. The dykes all terminate at the base of the Upper Permian Karstryggen Formation limestone. Whereas Stemmerik and Sørensen (1980) suggested a Late Permian intrusion age for the dykes, K-Ar age dating of three samples (whole-rock analyses, biotite and single biotite) gave ages around 48 and 35 Ma. Larsen et al. (1990) concludes that the dykes are of Tertiary age as indicated by K-Ar age dating but stressed that a closer look at rock fragments found above the dyke termination within sediments is needed for a definitive answer to the age of the dykes. Larsen et al. (1990) also note that paleomagnetic investigations of the dykes failed to give any consistent results even within single samples.

The dykes are described as subvertical, 0.1-0.5 m wide and strike between 116° and 154° N. They are described as monchiquites, alnöitic monchiquites and fourchites (Rock, 1987; Sørensen, 1974). From Figure 4-1 the nomenclature of lamprophyric rocks after Rock (1991) can be seen. Monchiquites and fourchites are alkaline lamprophyres but while fourchite is an obsolete rock name, monchiquite is still in use. An alnöite is an ultramafic melilite bearing lamprophyre. A petrographical description (Larsen et al., 1990) describe a phenocryst of Ti-rich clinopyroxene with a green salite or more sodic resorbed clinopyroxene core. Large fragments of diopside, often unzoned, occur in all samples and most samples contain pinkish Ti-augites that may be zoned. Phenocryst biotite is found in the alnöitic monchiquites. The ground mass is rich in clinopyroxene, flakes of biotite, apatite needles, equidimensional oxides, and is presumably feltspatoid rich. Some samples from the top of the dykes are rich in brown glass or palagonite. No evidence of major later thermal alteration is observed.

Geochemistry has been performed on two samples, GGU 269160 and GGU 269176 and the data have been compared to Tertiary rocks from the Kangerdlugssuaq area and the Scoresby Sund area. The bulk chemistry major element data from both Revdal lamprophyres and Tertiary rocks from the Kangerdlugssuaq area and the Scoresby area have been included in chapter 7, Bulk Rock Chemistry in Table 7-5 and Figure 7-3. Larsen et al. (1990) argued based on these data that the Revdal

lamprophyres correspond well with the Tertiary rocks of Kangerdlugssuaq area and the Scoresby area, I would argue that they correspond equally well with the Liverpool Land lamprophyres (Figure 7-3).

Liverpool Land Calc-Alkaline Lamprophyres

Lamprophyric dykes (M-14C and M-21) were sampled south of my samples but have been considered to belong to the same lamprophyre swarm. They have been dated to 262 Ma and 264 Ma (see Chapter 9) which is the age assumed for the Liverpool Land Lamprophyres as a group. They have been classified as kersanites and a petrographic description has been given by Buchanan (2008). The mineralogy is different, phlogopite and plagioclase as phenocrysts with fine grained phlogopite, sodium plagioclase and opaque minerals. Compositional zoning is ubiquitous in plagioclase phenocrysts. Calcite are seen filling late stage cracks in the matrix and the interior portions of some minerals (Buchanan, 2008).

Comparison

There are several similarities between the lamprophyres in Revdal and the ones I have investigated in Liverpool Land. They both include lamprophyres from the alkaline - and ultramafic lamprophyre group but include different rocks, sannaites and aillikites on Liverpool Land and monchiquites, alnöitic monchiquites and fourchites (the latter is an obsolete rock name) in Revdal. The description of a Ti-rich clinopyroxene phenocryst with a green salite or more sodic resorbed clinopyroxene core similar to what is seen in the Liverpool Land lamprophyres is an indication that similar processes have been active in both areas. Also the observation of unzoned diopside and pinkish Ti-augites that may be zoned can be seen in the Liverpool Land lamprophyres. Similarities in the ground mass are clinopyroxene, flakes of biotite, apatite needles and equidimensional oxides. The kersanites (CAL) described by Buchanan (2008) have a completely different mineralogy and do not fit into this picture.

There are differences as well, while the Revdal dykes strike NW-SE (116° - 154° N) the Liverpool Land Lamprophyres strike N-S (330° - 038° N) (Figure 10-1). The orientation of the Liverpool Land lamprophyres corresponds well with the regional extension at the time. The orientation of the Revdal dykes is not consistent with the interpreted regional extension at the time and would correspond better to a Late Devonian (NNE-SSW) extensional configuration. The Revdal dykes are furthermore thinner, 0.1 – 0.5 m wide while the Liverpool Land Lamprophyres are generally around 1 m although some are as thin as 20 cm.

The data on the Liverpool Land Lamprophyres give two possible explanations: 1) Either the classification into different groups is misleading – they are related and are similar in age. 2) The Liverpool Land Lamprophyres represent two separate events of lamprophyric magmatism: a calc-alkaline event at 264-262 Ma (Buchanan, 2008) and one ultramafic/alkaline event of unknown age. If the latter is correct, one could speculate if the ultramafic/alkaline event is related to the lamprophyric dykes in Revdal (Larsen et al., 1990).

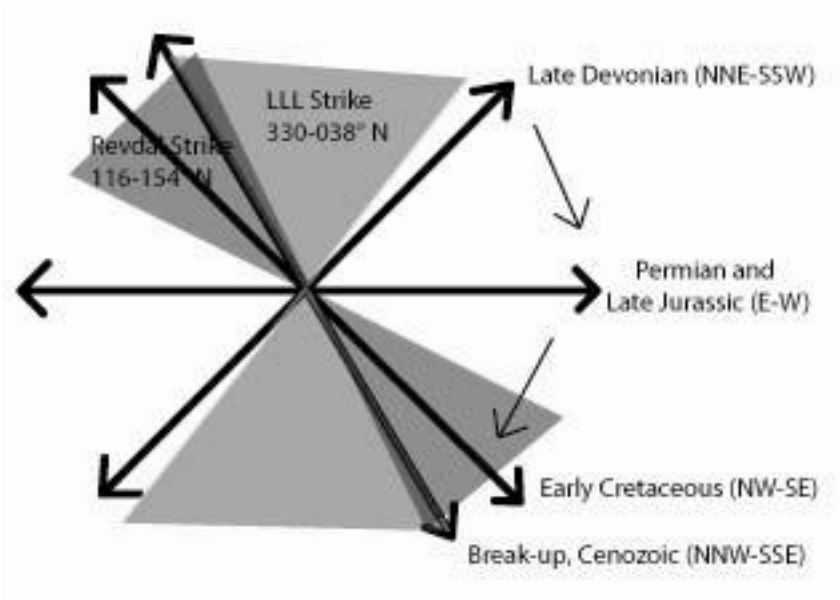

Figure 10-1: Simplified diagram illustrating the orientation/strike of the Liverpool Land - and Revdal lamprophyres (Larsen et al., 1990). The Revdal lamprophyres strike approximately NW-SE and correspond to Late Devonian extension. The Liverpool Land Lamprophyres strike approximately N-S and correspond to Late Jurassic Extension. The direction of extension was NNE-SSW in the Late Devonian, E-W Late Jurassic, NW-SE Early Cretaceous and NNW-SSE during break-up, Cenozoic (Lundin, 2008; Timmerman et al., 2009).

10.4 Regional Significance of Liverpool Land Lamprophyres

Emplacement in an Extensional Setting

The OIB signature, coast parallel N-S strike and signs of multiple primitive intrusions indicate that the Liverpool Land Lamprophyres were related to extensional tectonics. They thus fit into a complicated picture of regional extension and widespread magmatism in NW Europe in the Carboniferous-Permian.

The UK at c. 350 Ma in the Tournisian was a transtensional regime in the foreland of the Variscan Orogeny (Timmerman, 2004; Upton et al., 2004). Rifting was interrupted in the Late Carboniferous to Early Permian when the Lower Rotliegend group (300 – 288 Ma) experienced large scale dextral wrench-deformation of the lithosphere and upwelling of the asthenosphere triggering extensive melt generation (Maynard et al., 1997; Timmerman et al., 2009; Ziegler, 1990). In later Permian times wrench tectonics was succeeded by roughly E-W extension within the Fennoscandian craton north of the Variscan foreland basin (Timmerman et al., 2009). The craton was decoupled from the Northern Permian Basin, where the stress regime changed from right-lateral wrenching to a more NE-SW directed extensional stress regime during post magmatic thermal relaxation (Maynard et al., 1997; Timmerman et al., 2009; Ziegler, 1990). The wrenching and extension in the Northern – and Southern Permian Basin is interpreted to have created the Oslo Rift, Skagerrak-Kattegat rift area, Norwegian-Danish Basin, and the central North Sea. This is a good indication that the whole area was affected by the same regional tectono-magmatic phase (Heeremans and Faleide, 2004). The Carboniferous-

Permian alkaline magmatism in Scotland, the Oslo Rift, Scania and northern Germany is interpreted to be related to extension (Monaghan and Pringle, 2004; Neumann et al., 2004).

Permian and Triassic extension is however not restricted to the North Sea. Steltenpohl et al. (2004) found two pulses of post-orogenic continental rifting in north-central Norway, one during the Early Permian (ca. 272 Ma) and the other one during the Middle Triassic (ca. 236 Ma). A two stage extensional history has also been observed other places in and around the North Sea. Chadwick and Evans (1995) report Late Permian and Early Triassic extension from onshore Britain. Two stages of extension is also suspected in the Northern North Sea (Badley et al., 1988), similarly in the North Celtic Sea an Early Permian - and an Early Triassic phase has been suggested (Shannon et al., 1995).

As previously mentioned did Faerseth et al. (1976) map some lamprophyric dykes in Sunnhordland. The dykes are controlled by NNW-SSE trending faults which form part of a more general joint and fault system of a similar orientation which dominates the tectonic structure of western Norway. Færseth proposes that there must have been regional extension because of the coast-parallel normal faulting which would also explain the access to volcanic material to the surface. He also proposes that this alkaline igneous activity could be related to a larger tectonic system associated with the North Sea rift system. This corresponds with the sinistral translation of Greenland-Laurentia relative to Baltica during the Devonian (Mosar et al., 2002). The Liverpool Land lamprophyres are thus an indication that magmatism in the Permian was not constrained to the North Sea and that crustal extension involving the entire crust extended far into the North Atlantic region.

Plate tectonic setting of the Liverpool Land Lamprophyres

Apart from the lamprophyric occurrences earlier mentioned, Rock (1991) presents all confirmed calc-alkaline, alkaline, and ultramafic occurrences in the North Sea and North Atlantic in his book 'Lamprophyres'. All the lamprophyric occurrences above and from this thesis are presented in Figure 10-2. If Rock's (1991) sources are correct, Northeast Greenland is dominated by calc-alkaline Tertiary lamprophyres, most likely related to continent break-up. In addition, Late Caledonian lamprophyres are confirmed in Ole Rømer Land (Andresen et al., 1995) and Permian CAL in Liverpool Land (Buchanan, 2008). The lamprophyric occurrences in Norway are Permian, Triassic and Jurassic alkaline lamprophyres that are found in the south-west (Rock, 1991). Rock (1991) also presents a swarm of Late Caledonian calc-alkaline lamprophyre dykes and Permian alkaline lamprophyre dykes in the UK and Scotland concentrated along the Caledonian Orogen. The Permian alkaline lamprophyres from the UK and Scotland have been included in the map (Figure 10-2).

During the Vendian period (650 – 545 Ma), a tectonic event similar to the collapse of the Caledonian Orogeny and the insipient opening of the Norwegian – Greenland Sea occurred, when the supercontinent Rhodinia started to break up and the Proto-Atlantic formed. This event was accompanied by ultramafic lamprophyres and carbonatites (Tappe et al., 2004). Tappe et al. (2004) concludes that the volatile-rich, ultramafic potassic-to-carbonatitic magmatism (an association also mentioned by Rock (1991)) followed the major continental rifting stage and occurred when nearby oceanic rifting was already initiated. The maximum age of the alkaline rock suites coincides with the rift to drift transition (Torsvik et al., 1996) around 600 – 580 Ma followed by the opening of the Iapetus Ocean.

In the present case, there are no confirmed occurrences of carbonatites in the North Sea or North Atlantic region in the Permian, but the lamprophyres clearly have a link to the extensional tectonics that follow the Caledonian Orogen. The large spread in the ages of the dykes in the North Atlantic region, stretching from ca. 260 – 30 Ma, compared to the much shorter time span of lamprophyric magmatism in the Vendian, could reflect the 300 Ma (Lundin, 2008) period of episodic extension related to the break-up of the Atlantic.

Compared to the Late Caledonian calc-alkaline lamprophyres and the Permian alkaline lamprophyres in the UK and Scotland and the Tertiary calc-alkaline lamprophyres in NE Greenland (Rock, 1991) the Liverpool Land Lamprophyres are aberrant, they do not fit into a clear regional pattern as the other occurrences do. On a regional scale, the ca. 275 Ma (K-Ar) Sunnhordland dyke swarm (Faerseth et al., 1976) in W Norway represents the only known potential lamprophyric correlative. Although the AL on the Orkney Islands have been suggested to be 250 ± 10 Ma (K-Ar; (Baxter and Mitchell, 1984)), recent U-Pb dating indicate that they may be as old as 310 Ma (A.M. Lundmark, pers. comm. 2009). However, the 262 Ma (Torsvik et al., 1997) Sotra alkaline dyke is of the same age and has been related to extension in W Norway (Faerseth et al., 1976; Torsvik et al., 1997), indicating coeval extension in W Norway and Liverpool Land.

These isolated occurrences could reflect the difficulties related to field work on NE Greenland, which is still largely unexplored. More dykes may be revealed in the future to form a regional pattern, alternatively, the presently known dyke swarms are in fact isolated occurrences.

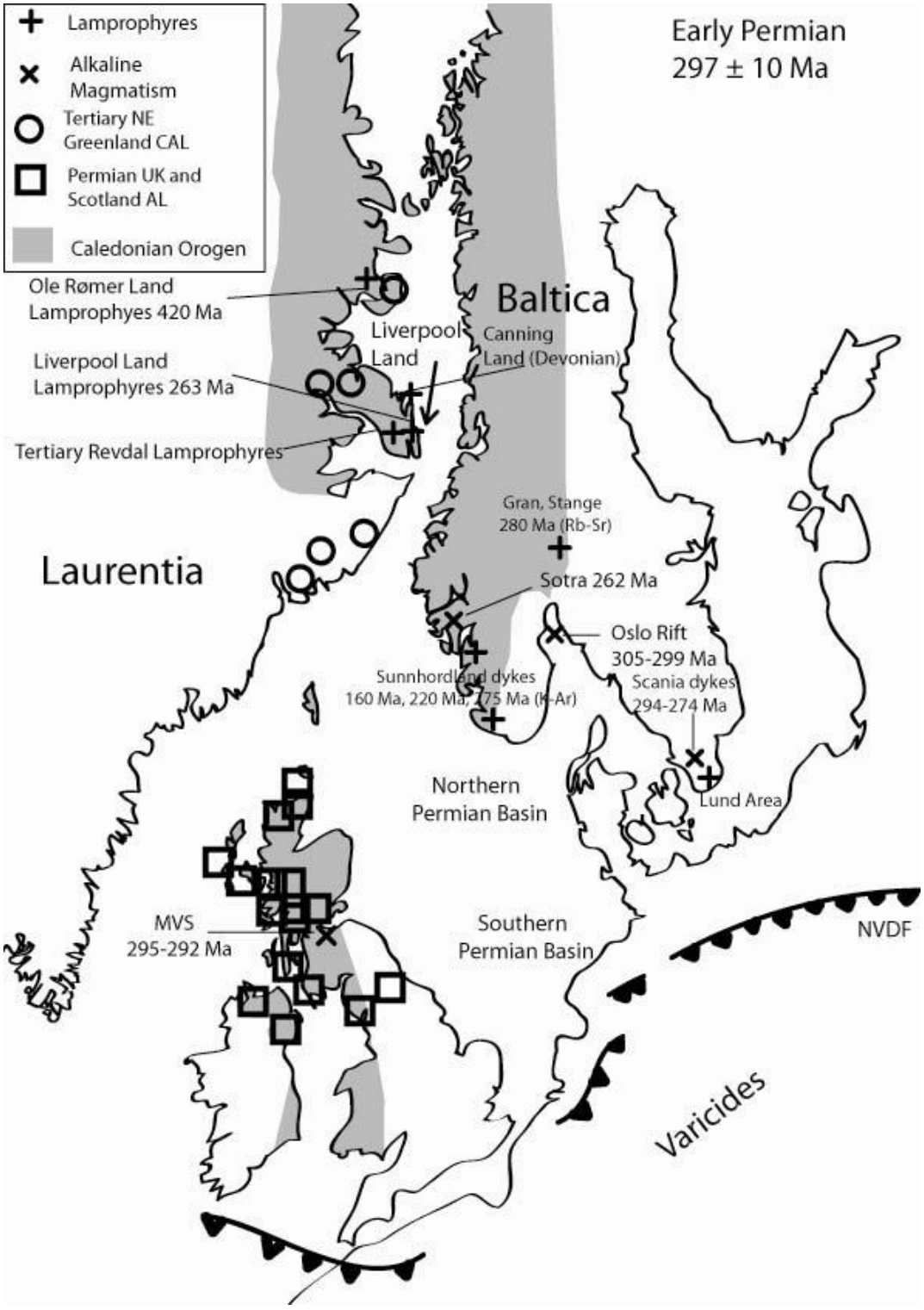

Figure 10-2: Simplified map of the North Atlantic prior to Tertiary opening showing the location of lamprophyric dykes and occurrences of extensive alkaline magmatism modified after Torsvik et al. (2008), Neumann et al. (2004), Stephens et al. (1984) and Heeremans and Faleide (2004). References: Midland Valley of Scotland (MVS) (Monaghan and Pringle, 2004), Tertiary Revdal lamprophyric dykes (Larsen et al., 1990), Sotra alkaline dykes, 262 Ma (Torsvik et al., 1997), Oslo Province Lamprophyres (Scott and Middleton, 1983), Sunnhordland alkaline dykes (including lamprophyres) (Faerseth, 1978; Faerseth et al., 1976), alkaline Scania dykes (Obst et al., 2004) and alkaline Oslo Rift dykes (Neumann et al., 2004), Tertiary North East Greenland calc-alkaline lamprophyre dykes (Rock, 1991), Permian Scotland and UK alkaline lamprophyre dykes (Rock, 1991).

11 Conclusion

Our data shows that according to lamprohyre classification schemes the Liverpool Land Lamprophyres consists of three different rock branches, alkaline and ultramafic lamprophyres in addition to the previously known calc-alkaline lamprophyres. Bulk rock chemistry, mineral chemistry and petrography of the alkaline and ultramafic lamprophyres are interpreted to reflect a common mantle source and a similar history of ascent, which include magma mixing and AFC.

Three geochemically different phases in CPX crystals are observed in the AL and UML in Liverpool land, which is compatible with mixing of different, potentially unrelated, melt batches. In addition, both ultramafic and alkaline lamprophyres show signs of crustal contamination. Magma mixing and/or crustal contamination is interpreted to have caused the ultramafic melts to develop towards a more 'alkaline lamprophyre' character. This means that no alkaline source magma was present. The classification of the lamprophyres into two different families, the AL and the UML, is therefore misleading in the sense that they do not represent different sources. This highlights the need for a revision of the classification of lamprophyric rocks.

The calc-alkaline lamprophyres have been dated to 261.6 ± 0.4 Ma and 263.9 ± 0.9. Petrographical data give no indication of a relationship between the AL and UML, on the one hand, and the CAL on the other. Therefore it should not be assumed that the two different groups are coeval, and the AL and UML should be dated separately. Given the geochemical and petrographical similarities between the AL/UML of Liverpool Land and the Tertiary Revdal suite, one may speculate that the two dyke swarms are related. Although there are uncertainties surrounding the age, the Liverpool Land Lamprophyres do not fit into a regional pattern of lamprophyric occurrences. Nevertheless the CAL proves that magmatism related to extension in the Permian was not constrained to the North Sea but extended far into the North Atlantic region.

12 References

Andresen, A., and Hartz, E.H., 1998, Basement-cover relationships and orogenic evolution in the Central East Greenland Caledonides: Gff, v. 120, p. 191-198.

Andresen, A., Hartz, E.H., and Vold, J., 1995, A late orogenic extensional origin for the intracrustal gneiss domes of the East Greenland Caledonides (72-74 degrees N): Strasbourg, France, p. 353-369.

Augland, L.E., 2007, The Gubbedalen shear zone; a terrane boundary in the East Greenland Caledonides: a structural and geochronological study: Oslo, UiO.

Azbej, T., Szabo, C., Bodnar, R.J., and Dobosi, G., 2006, Genesis of carbonate aggregates in lamprophyres from the northeastern Transdanubian Central Range, Hungary: Magmatic or hydrothermal origin?: Mineralogy and Petrology, v. 88, p. 479-497.

Badley, M.E., Price, J.D., Dahl, C.R., and Agdestein, T., 1988, The structural evolution of the northern Viking Graben and its bearing upon extensional modes of basin formation: Journal of the Geological Society, v. 145, p. 455-472.

Barton, M., and Vanbergen, M.J., 1981, Green clinopyroxenes and associated phases in a potassium-rich lava from the Leucite Hills, Wyoming: Contributions to Mineralogy and Petrology, v. 77, p. 101-114.

Baxter, A.N., and Mitchell, J.G., 1984, Camptonite-Monchiquite Dyke Swarms of Northern Scotland - Age Relationships and their Implications: Scottish Journal of Geology, v. 20, p. 297-308.

Bedard, J.H.J., Francis, D.M., and Ludden, J., 1988, Petrology and pyroxene chemistry of Monteregian dykes - The origin of concentric zoning and green cores in clinopyroxenes from alkali basalts and lamprophyres: Canadian Journal of Earth Sciences, v. 25, p. 2041-2058.

Brooks, C.K., and Printzlau, I., 1978, Magma mixing in mafic alkaline volcanic-rocks - Evidence from relict phenocryst phases and other inclusions: Journal of Volcanology and Geothermal Research, v. 4, p. 315-331.

Buchanan, J.W., 2008, Tectonic evolution of a Caledonian-aged continental basement eclogite terrane in Liverpool Land, East Greenland: Auburn, Auburn University.

Cameron, T.D.J., 1993, Triassic, Permian and Pre-permian (Central and Northern North Sea), 163 s. p.

Chadwick, R.A., and Evans, D.J., 1995, The timing and direction of Permo-Triassic extension in southern Britain: Geological Society, London, Special Publications, v. 91, p. 161-192.

Cocks, L.R.M., and Torsvik, T.H., 2005, Baltica from the late Precambrian to mid-Palaeozoic times: The gain and loss of a terrane's identity: Earth-Science Reviews, v. 72, p. 39-66.

Coe, K., and Cheeney, R.F., 1972, Preliminary results of mapping in Liverpool Land, East Greenland: Grønlands Geologiske Undersøkelse, p. 7-19.

Couch, S., Sparks, R.S.J., and Carroll, M.R., 2001, Mineral disequilibrium in lavas explained by convective self-mixing in open magma chambers: Nature, v. 411, p. 1037-1039.

Daviknes, H.K., 2009, Age and geochemistry of some intrusives from the East Greenland Caledonides: Oslo, The University of Oslo.

Dobosi, G., and Fodor, R.V., 1992, Magma fractionation, replenishment, and mixing as inferred from green-core clinopyroxenes in the Pliocene Basanite, Southern Slovakia: Lithos, v. 28, p. 133-150.

Dore, A.G., LUNDIN, E.R., JENSEN, L.N., BIRKELAND, Ø., ELIASSEN, P.E., and FICHLER, C., 1999, Principal tectonic events in the evolution of the northwest European Atlantic margin: Geological Society, London, Petroleum Geology Conference series, v. 5, p. 41-61.

Droop, G.T.R., 1987, A general equation for estimating Fe^{3+} concentrations in ferromagnesian silicates and oxides from microprobe analyses, using stoichiometric criteria: Mineralogical Magazine, v. 51, p. 431-435.

Duda, A., and Schmincke, H.U., 1985, Polybaric differentiation of alkali basaltic magmas - Evidence from green-core clinopyroxenes (Eifel, FRG): Contributions to Mineralogy and Petrology, v. 91, p. 340-353.
Edgar, A.D., Condliffe, E., Barnett, R.L., and Shirran, R.J., 1980, An experimental-study of an olivine ugandite magma and mechanisms for the formation of its K-enriched derivatives: Journal of Petrology, v. 21, p. 475-497.
Faerseth, R.B., 1978, Mantle-derived lherzolite xenoliths and megacrysts from Permo-Triassic dykes, Sunnhordland, Western Norway: Lithos, v. 11, p. 23-35.
Faerseth, R.B., Macintyre, R.M., and Naterstad, J., 1976, Mesozoic alkaline dykes in Sunnhordland Region, Western Norway - Ages, geochemistry and regional significance: Lithos, v. 9, p. 331-345.
Foley, S.F., 1984, Liquid immiscibility and melt segregation in alkaline lamprophyres from Labrador: Lithos, v. 17, p. 127-137.
Frisch, T., and Schmincke, H., 1969, Petrology of clinopyroxene-amphibole inclusions from the roque nublo volcanics, gran canaria, canary islands: Bulletin of Volcanology, v. 33, p. 1073-1088.
Gaina, C., Gernigon, L., and Ball, P., 2009, Palaeocene-Recent plate boundaries in the NE Atlantic and the formation of the Jan Mayen microcontinent: Journal of the Geological Society, v. 166, p. 601-616.
Gamble, R.P., and Taylor, L.A., 1980, Crystal/liquid partitioning in augite: effects of cooling rate: Earth and Planetary Science Letters, v. 47, p. 21-33.
Glennie, K.W., 1998, Lower Permian - Rotliegend, *in* Glennie, K.W., ed., Petroleum geology of the North Sea: basic concepts and recent advances, Volume 4: Oxford, Blackwell Science, p. 137-173.
Hamilton, W.B., 1994, Subduction systems and magmatism: Geological Society, London, Special Publications, v. 81, p. 3-28.
Hartz, E., and Andresen, A., 1995, Caledonian sole thust of Central East Greenland - A crustal-scale extensional detachment: Geology, v. 23, p. 637-640.
Heeremans, M., and Faleide, J.I., 2004, Late Carboniferous-Permian tectonics and magmatic activity in the Skagerrak, Kattegat and the North Sea: Geological Society, London, Special Publications, v. 223, p. 157-176.
Heeremans, M., Timmerman, M.J., Kirstein, L.A., and Faleide, J.I., 2004, New constraints on the timing of late Carboniferous-early Permian volcanism in the central North Sea: Geological Society, London, Special Publications, v. 223, p. 177-193.
Higgins, A.K., Elvevold, S., Escher, J.C., Frederiksen, K.S., Gilotti, J.A., Henriksen, N., Jepsen, H.F., Jones, K.A., Kalsbeek, F., Kinny, P.D., Leslie, A.G., Smith, M.P., Thrane, K., and Watt, G.R., 2004, The foreland-propagating thrust architecture of the East Greenland Caledonides 72{degrees}-75{degrees}N: Journal of the Geological Society, v. 161, p. 1009-1026.
Huckenholz, H.G., 1973, Origin of fassaitic augite in alkali basalt suite of Hocheifel Area, Western Germany: Contributions to Mineralogy and Petrology, v. 40, p. 315-326.
Irvine, T.N., and Baraghar, W.R.A., 1971, A guide to the chemical classification of the common volcanic rocks: Can. J. Earth Sci., p. 523-548.
Kalsbeek, F., Higgins, A.K., Jepsen, H.F., and Nutman, A.P., 2008, Granites and granites in the North Atlantic Caledonides, *in* Higgins, A.K., Gilotti, J.A., and Smith, M.P., eds., The Greenland Caledonides: evolution of the northeast margin of Laurentia
Boulder, Colo., Geological Society of America, p. 227-249.
Kirstein, L.A., Davies, G.R., and Heeremans, M., 2006, The petrogenesis of Carboniferous-Permian dyke and sill intrusions across northern Europe: Contributions to Mineralogy and Petrology, v. 152, p. 721-742.
Larsen, P.H., Stemmerik, L., Nielsen, T.F.D., and Rex, D.C., 1990, Lamprophyric dykes in Revdal, Scoresby Land, East Greenland: conflicting field observations and K-Ar age determinations: Bulletin of the Geological Society of Denmark, v. 38, p. 1-10.

Le Maitre, R.W., 1989, A Classification of Igneous Rocks and Glossary of Terms, Cambridge : Cambridge University Press.
—, 2002, Igneous rocks : a classification and glossary of terms : recommendations of the International Union of Geological Sciences, Subcommission on the Systematics of Igneous Rocks, Cambridge : Cambridge University Press.
Lebas, M.J., 1989, Nephelinitic and Basanitic Rocks: Journal of Petrology, v. 30, p. 1299-1312.
Lebas, M.J., Lemaitre, R.W., Streckeisen, A., and Zanettin, B., 1986, A chemical classification of volcanic-rocks based on the total alkali silica diagram: Journal of Petrology, v. 27, p. 745-750.
Liotard, J.M., Briot, D., and Boivin, P., 1988, Petrological and geochemical relationships between pyroxene megacrysts and associated alkali-basalts from Massif-Central (France): Contributions to Mineralogy and Petrology, v. 98, p. 81-90.
Lloyd, F.E., 1981, Upper-mantle metasomatism beneath a continental rift - Clinopyroxenes in alkali mafic lavas and nodules from south west Uganda: Mineralogical Magazine, v. 44, p. 315-323.
Lovlie, R., and Mitchell, J.G., 1982, Complete remagnetization of some Permian dykes from Western Norway induced during burial/uplift: Physics of the Earth and Planetary Interiors, v. 30, p. 415-421.
Lundin, E.R., 2008, Late Mesozoic and Cenozoic tectonic evolution of the mid-Norwegian margin: a NE Atlantic perspective: Oslo, University of Oslo.
Malpas, J., Foley, S.F., and King, A.F., 1986, Alkaline mafic and ultramafic lamprophyres from the Aillik Bay area, Labrador: Canadian Journal of Earth Sciences, v. 23, p. 1902-1918.
Martin, C.A.L., Stewart, S.A., and Doubleday, P.A., 2002, Upper Carboniferous and Lower Permian tectonostratigraphy on the southern margin of the Central North Sea: Journal of the Geological Society, v. 159, p. 731-749.
Matte, P., 1989, Accretionary history and crustal evolution of the Variscan Belt in Western-Europe: Washington, Dc, Elsevier Science Bv, p. 309-337.
Maynard, J.R., Hofmann, W., Dunay, R.E., Bentham, P.N., Dean, K.P., and Watson, I., 1997, The Carboniferous of western Europe: the development of a petroleum system: Petroleum Geoscience, v. 3, p. 97-115.
Mitchell, J.G., and Roberts, D., 1986, Ages of lamprophyre dykes from Ytterøy and Lerkehaug, near Steinkjer, Central Norwegian Caledonides: Norsk geologisk tidsskrift, p. 255-261.
Mitchell, R.H., 1994, The Lamprophyre Facies: Mineralogy and Petrology, v. 51, p. 137-146.
—, 1995, Kimberlites, orangeites, and related rocks: New York, Plenum Press, XIV, 410 s. p.
Monaghan, A.A., and Pringle, M.S., 2004, 40Ar/39Ar geochronology of Carboniferous-Permian volcanism in the Midland Valley, Scotland: Geological Society, London, Special Publications, v. 223, p. 219-241.
Mosar, J., Eide, E.A., Osmundsen, P.T., Sommaruga, A., and Torsvik, T.H., 2002, Greenland - Norway separation: A geodynamic model for the North Atlantic: Norwegian Journal of Geology, v. 82, p. 281-298.
Neumann, E.-R., Wilson, M., Heeremans, M., Spencer, E.A., Obst, K., Timmerman, M.J., and Kirstein, L., 2004, Carboniferous-Permian rifting and magmatism in southern Scandinavia, the North Sea and northern Germany: a review: Geological Society, London, Special Publications, v. 223, p. 11-40.
Obst, K., Solyom, Z., and Johansson, L., 2004, Permo-Carboniferous extension-related magmatism at the SW margin of the Fennoscandian Shield: Geological Society, London, Special Publications, v. 223, p. 259-288.
Orejana, D., Villaseca, C., and Paterson, B.A., 2007, Geochemistry of mafic phenocrysts from alkaline lamprophyres of the Spanish Central System: implications on crystal fractionation, magma mixing and xenoliths entrapment within deep magma chambers: European Journal of Mineralogy, v. 19, p. 817-832.
Phillips, W.J., 1973, Interpretation of crystalline spheroidal structures in igneous rocks: Lithos, v. 6, p. 235-244.

Rock, N., 1977, Nature and origin of lamprophyres - Definitions, distinctions, and derivations: Earth-Science Reviews, v. 13, p. 123-169.
Rock, N.M.S., 1985, The nature and origin of ultramafic lamprophyres - alnoites and allied rocks: Journal of Petrology, v. 27, p. 155-196.
—, 1987, The nature and origin of lamprophyres: an overview: Geological Society, London, Special Publications, v. 30, p. 191-226.
—, 1991, Lamprophyres: Birmingham, Van Nostrand Reinhold.
Scott, P.W., 1976, Crystallization trends of pyroxenes from alkaline volcanic-rocks of Tenerife, Canary-Islands: Mineralogical Magazine, v. 40, p. 805-816.
Scott, P.W., and Middleton, R., 1983, Camptonite and Maenaite sills near Gran, Hadeland, Oslo Region: Norges Geologiske Undersokelse Bulletin, p. 1-26.
Shand, P., Gaskarth, J.W., Thirlwall, M.F., and Rock, N.M.S., 1994, Late Caledonian lamprophyre dyke swarms of South-Eastern Scotland: Mineralogy and Petrology, v. 51, p. 277-298.
Shannon, P.M., Williams, B.P.J., and Sinclair, I.K., 1995, Tectonic controls on Upper Jurassic to Lower Cretaceous reservoir architecture in the Jeanne d'Arc Basin, with some comparisons from the Porcupine and Moray Firth Basins: Geological Society, London, Special Publications, v. 93, p. 467-490.
Steltenpohl, M.G., Hames, W.E., and Andresen, A., 2004, The Silurian to Permian history of a metamorphic core complex in Lofoten, northern Scandinavian Caledonides: Tectonics, v. 23, p. 23.
Stemmerik, L., and Sørensen, M., 1980, Upper Permian dykes in southern Scoresby Land, East Greenland: Grønlands Geologiske Undersøkelse, v. 100, p. 108.
Stephens, M.B., Swinden, H.S., and Slack, J.F., 1984, Correlation of massive sulfide deposits in the Appalachian-Caledonian orogen on the basis of the paleotectonic setting: Economic Geology, v. 79, p. 1442-1478.
Sun, S.-s., and McDonough, W.F., 1989, Chemical and isotopic systematics of oceanic basalts: implications for mantle composition and processes: Geological Society, London, Special Publications, v. 42, p. 313-345.
Sørensen, H., 1974, Glossary of alkaline and related rocks, *in* Sørensen, H., ed., The Alkaline Rocks, John Wiley & Sons, p. 558-577.
Tappe, S., Foley, S.F., Jenner, G.A., Heaman, L.M., Kjarsgaard, B.A., Romer, R.L., Stracke, A., Joyce, N., and Hoefs, J., 2006, Genesis of ultramafic lamprophyres and carbonatites at Aillik Bay, Labrador: A consequence of incipient lithospheric thinning beneath the North Atlantic craton: Journal of Petrology, v. 47, p. 1261-1315.
Tappe, S., Foley, S.F., Jenner, G.A., and Kjarsgaard, B.A., 2005, Integrating ultramafic lamprophyres into the IUGS classification of igneous rocks: Rationale and implications: Journal of Petrology, v. 46, p. 1893-1900.
Tappe, S., Jenner, G.A., Foley, S.F., Heaman, L., Besserer, D., Kjarsgaard, B.A., and Ryan, B., 2004, Torngat ultramafic lamprophyres and their relation to the North Atlantic Alkaline Province: Lithos, v. 76, p. 491-518.
Tegner, C., Brooks, C.K., Duncan, R.A., Heister, L.E., and Bernstein, S., 2008, Ar-40-Ar-39 ages of intrusions in East Greenland: Rift-to-drift transition over the Iceland hotspot: Lithos, v. 101, p. 480-500.
Thompson, R.N., 1974, Some high-pressure pyroxenes: Mineralogical Magazine, v. 39, p. 768-787.
Timmerman, M.J., 2004, Timing, geodynamic setting and character of Permo-Carboniferous magmatism in the foreland of the Variscan Orogen, NW Europe: Geological Society, London, Special Publications, v. 223, p. 41-74.
Timmerman, M.J., Heeremans, M., Kirstein, L.A., Larsen, B.T., Spencer-Dunworth, E.A., and Sundvoll, B., 2009, Linking changes in tectonic style with magmatism in northern Europe during the late Carboniferous to latest Permian: Tectonophysics, v. 473, p. 375-390.
Torsvik, T.H., Andersen, T.B., Eide, E.A., and Walderhaug, H.J., 1997, The age and tectonic significance of dolerite dykes in western Norway: Journal of the Geological Society, v. 154, p. 961-973.

Torsvik, T.H., Smethurst, M.A., Burke, K., and Steinberger, B., 2008, Long term stability in deep mantle structure: Evidence from the similar to 300 Ma Skagerrak-Centered Large Igneous Province (the SCLIP): Earth and Planetary Science Letters, v. 267, p. 444-452.

Torsvik, T.H., Smethurst, M.A., Meert, J.G., Van der Voo, R., McKerrow, W.S., Brasier, M.D., Sturt, B.A., and Walderhaug, H.J., 1996, Continental break-up and collision in the Neoproterozoic and Palaeozoic -- A tale of Baltica and Laurentia: Earth-Science Reviews, v. 40, p. 229-258.

Tronnes, R.G., Planke, S., Sundvoll, B., and Imsland, P., 1999, Recent volcanic rocks from Jan Mayen: Low-degree melt fractions of enriched northeast Atlantic mantle: Journal of Geophysical Research-Solid Earth, v. 104, p. 7153-7168.

Upton, B.G.J., Stephenson, D., Smedley, P.M., Wallis, S.M., and Fitton, J.G., 2004, Carboniferous and Permian magmatism in Scotland: Geological Society, London, Special Publications, v. 223, p. 195-218.

von Seckendorff, V., Timmerman, M.J., Kramer, W., and Wrobel, P., 2004, New 40Ar/39Ar ages and geochemistry of late Carboniferous-early Permian lamprophyres and related volcanic rocks in the Saxothuringian Zone of the Variscan Orogen (Germany): Geological Society, London, Special Publications, v. 223, p. 335-359.

Wass, S.Y., 1979, Multiple origins of clinopyroxenes in alkali basaltic rocks: Lithos, v. 12, p. 115-132.

Wilkinson, J.F.G., 1975, Ultramafic inclusions and high-pressure megacrysts from a nephelinite sill, Nandewar Mountains, Northeastern New-South-Wales, and their bearing on origin of certain ultramafic inclusions in alkaline volcanic-rocks: Contributions to Mineralogy and Petrology, v. 51, p. 235-262.

Wilson, M., Neumann, E.-R., Davies, G.R., Timmerman, M.J., Heeremans, M., and Larsen, B.T., 2004, Permo-Carboniferous magmatism and rifting in Europe: introduction: Geological Society, London, Special Publications, v. 223, p. 1-10.

Woolley, A.R., Bergman, S.C., Edgar, A.D., LeBas, M.J., Mitchell, R.H., Rock, N.M.S., and Smith, B.H.S., 1996, Classification of lamprophyres, lamproites, kimberlites, and the kalsilitic, melilitic, and leucitic rocks: Canadian Mineralogist, v. 34, p. 175-186.

Xu, Y.G., Huang, X.L., Menzies, M.A., and Wang, R.C., 2003, Highly magnesian olivines and green-core clinopyroxenes in ultrapotassic lavas from western Yunnan, China: evidence for a complex hybrid origin: European Journal of Mineralogy, v. 15, p. 965-975.

Ziegler, P.A., 1990, Geological atlas of Western and Central Europe: [den Haag], Shell International Petroleum Maatschappij BV.

13 Appendix A

EMP analysis of feldspars in AA 08-15, AA 08-12, LEA 06-81, AA 08-14, AA 08-17, and AA 08-13

Sample	AA 08-15													
Analysis	#1	#2	#3	#4	#5	#6	#7	#8	#9	#10	#11	#12	#13	#14
SiO2	65,85	67,08	66,97	67,57	66,25	54,04	67,82	63,44	53,21	63,30	62,37	57,08	66,59	55,95
TiO2	0,00	0,00	0,00	0,00	0,00	0,11	0,04	0,05	0,17	0,03	0,08	0,08	0,01	0,18
Al2O3	21,61	20,68	20,69	20,71	21,15	27,62	20,37	18,22	28,46	18,39	18,18	26,25	21,11	26,86
FeO	0,05	0,03	0,05	0,08	0,24	0,91	0,21	0,13	0,88	0,24	0,31	0,75	0,20	0,82
MgO	0,00	0,00	0,01	0,00	0,01	0,12	0,01	0,00	0,14	0,00	0,01	0,08	0,04	0,07
CaO	2,30	1,32	1,51	1,13	2,06	11,42	0,93	0,00	12,56	0,01	0,01	9,32	1,62	10,01
Na2O	10,34	10,75	11,13	11,17	10,82	5,00	11,48	0,29	4,57	0,24	0,26	6,31	10,97	5,65
K2O	0,07	0,04	0,07	0,02	0,11	0,35	0,05	16,35	0,32	15,94	15,54	0,55	0,08	0,45
Total	100,23	99,90	100,43	100,69	100,63	99,55	100,90	98,48	100,31	98,14	96,74	100,42	100,63	99,99
					Number of ions on the basis of 8O in the framework									
Si	2,889	2,948	2,919	2,939	2,888	2,457	2,940	2,979	2,406	2,985	2,985	2,554	2,900	2,525
Ti	0,000	0,000	0,000	0,000	0,000	0,004	0,001	0,002	0,006	0,001	0,003	0,003	0,000	0,006
Al	1,117	1,071	1,063	1,062	1,086	1,480	1,041	1,008	1,516	1,022	1,026	1,384	1,084	1,429
Fe2+	0,002	0,001	0,002	0,003	0,009	0,034	0,007	0,005	0,033	0,009	0,012	0,028	0,007	0,031
Mg	0,000	0,000	0,001	0,000	0,001	0,008	0,001	0,000	0,010	0,000	0,000	0,005	0,002	0,005
Ca	0,108	0,062	0,071	0,053	0,096	0,556	0,043	0,000	0,608	0,001	0,000	0,447	0,076	0,484
Na	0,880	0,916	0,941	0,942	0,914	0,441	0,964	0,026	0,401	0,022	0,024	0,547	0,926	0,494
K	0,004	0,002	0,004	0,001	0,006	0,020	0,003	0,980	0,019	0,959	0,949	0,032	0,004	0,026
Total	5,00	5,00	5,00	5,00	5,00	5,00	5,00	5,00	5,00	5,00	5,00	5,00	5,00	5,00
Ab	88,68	93,43	92,68	94,57	89,92	43,34	95,46	2,62	39,00	2,26	2,44	53,35	92,04	49,22
An	10,92	6,34	6,96	5,30	9,46	54,69	4,27	0,00	59,20	0,06	0,04	43,58	7,53	48,22
Or	0,41	0,23	0,36	0,13	0,62	1,97	0,28	97,38	1,81	97,68	97,52	3,07	0,43	2,56

EMP analysis of feldspars in AA 08-15, AA 08-12, LEA 06-81, AA 08-14, AA 08-17, and AA 08-13

Sample	AA 08-15			AA 08-12	LEA 06-81	AA 08-14	AA 08-17		AA 08-13		
Analysis	#15	#16	#25	#36	#47	#54	#29	#38	#24	#25	#52
SiO2	62,99	65,15	62,79	63,97	64,04	64,22	64,47	64,57	65,17	63,42	63,31
TiO2	0,06	0,02	0,00	0,01	0,05	0,00	0,05	0,01	0,00	0,06	0,04
Al2O3	18,36	21,26	18,18	18,21	18,72	17,55	18,52	19,33	18,30	19,55	19,09
FeO	0,22	0,26	0,06	0,11	0,45	0,84	0,25	0,26	0,39	0,28	0,84
MgO	0,00	0,00	0,02	0,01	0,01	0,00	0,00	0,02	0,00	0,02	0,00
CaO	0,07	2,44	0,00	0,00	0,02	0,09	0,06	0,02	0,07	0,06	0,03
Na2O	0,30	10,71	0,29	0,20	0,30	0,33	0,69	0,72	0,22	0,17	0,57
K2O	15,69	0,06	15,87	16,21	16,18	16,42	16,19	16,02	16,87	16,99	16,14
Total	97,69	99,90	97,22	98,72	99,76	99,45	100,23	100,96	101,01	100,54	100,01
				Number of ions on the basis of 8O in the framework							
Si	2,983	2,860	2,987	3,000	2,971	2,993	2,968	2,949	2,987	2,914	2,924
Ti	0,002	0,001	0,000	0,000	0,002	0,000	0,002	0,000	0,000	0,002	0,001
Al	1,025	1,100	1,019	1,006	1,023	0,964	1,005	1,041	0,988	1,058	1,039
Fe2+	0,009	0,010	0,003	0,004	0,017	0,033	0,010	0,010	0,015	0,011	0,032
Mg	0,000	0,000	0,002	0,000	0,000	0,000	0,000	0,001	0,000	0,001	0,000
Ca	0,003	0,115	0,000	0,000	0,001	0,004	0,003	0,001	0,003	0,003	0,001
Na	0,028	0,911	0,027	0,018	0,027	0,030	0,062	0,064	0,020	0,015	0,051
K	0,948	0,004	0,963	0,970	0,958	0,976	0,951	0,934	0,986	0,996	0,951
Total	5,00	5,00	5,00	5,00	5,00	5,00	5,00	5,00	5,00	5,00	5,00
Ab	2,83	88,50	2,71	1,86	2,69	2,97	6,08	6,37	1,97	1,52	5,05
An	0,34	11,15	0,00	0,00	0,12	0,44	0,28	0,10	0,32	0,27	0,13
Or	96,83	0,34	97,29	98,14	97,19	96,59	93,64	93,53	97,71	98,21	94,82

EMP analysis of matrix analcite in DEF 08-01

	#1	#2	#3
SiO2	53,929	54,017	54,218
Al2O3	22,828	22,503	22,643
FeO	0,178	0,054	0,233
MgO	0,005	0,022	0,032
CaO	0,146	0,088	0,179
Na2O	13,385	13,302	13,368
K2O	0,075	0,128	0,102
Total	90,546	90,114	90,775

Numbers of ions on the basis of 96 O in the framework			
Si	32,04674	32,215831	32,1442
Al	15,98767	15,817397	15,82154
Fe2+	0,088458	0,0269332	0,115524
Mg	0,004429	0,0195601	0,028282
Ca	0,092958	0,0562334	0,113706
Na	15,4215	15,381642	15,36641
K	0,056857	0,0973884	0,077147

EMP analysis of unknown mineral DEF 08-01-9

Analysis	#5	#6
Na2O	0	0,009
K2O	0,007	0,023
SiO2	37,497	38,007
Al2O3	11,577	11,835
CaO	1,791	1,713
FeO	15,171	15,512
TiO2	0,012	0,03
MgO	19,313	20,187
Total	85,368	87,316

EMP analysis of spinel phenocrysts, inclusions, and rims

Sample	DEF 08-01-25			DEF 08-01-25			DEF 08-01-25					DEF 08-01-3		
Description	Core			Phenocryst rim			Matrix					Inclusion in CPX		Matrix
Analysis	#1	#2	#6	#3	#4	#5	#7	#8	#9	#10	#11	#19	#20	#33
SiO2	0,08	0,09	0,07	0,05	0,08	0,03	0,10	0,06	2,03	0,07	0,07	0,02	0,08	0,09
TiO2	2,88	2,84	2,83	14,39	10,68	16,23	17,20	17,59	9,12	18,34	17,35	4,39	8,46	3,48
Al2O3	19,94	19,73	19,36	1,95	4,94	3,66	1,05	1,40	1,28	0,97	0,79	16,91	11,86	25,45
Cr2O3	36,07	36,50	36,88	3,79	12,42	3,56	0,11	0,17	0,13	0,09	0,42	28,20	18,25	27,23
Fe2O3	9,87	9,86	9,69	31,58	27,57	26,77	29,98	29,03	38,13	28,28	29,72	17,02	23,51	11,58
FeO	17,40	17,02	17,58	43,94	40,18	46,38	48,17	48,49	46,92	48,61	48,31	21,93	27,28	18,03
MnO	0,24	0,26	0,24	1,34	1,43	2,02	2,61	2,61	1,44	2,81	2,61	0,29	0,38	0,22
MgO	13,34	13,53	13,11	2,41	2,22	0,76	0,00	0,00	0,06	0,00	0,00	11,07	9,97	13,87
CaO	0,00	0,00	0,00	0,07	0,09	0,14	0,31	0,12	0,58	0,21	0,19	0,16	0,21	0,05
V2O3	0,18	0,16	0,23	0,48	0,38	0,45	0,46	0,53	0,31	0,61	0,54	0,00	0,00	0,00
Total	100,00	100,00	100,00	100,00	100,00	100,00	100,00	100,00	100,00	100,00	100,00	100,00	100,00	100,00
						Number of ions on the basis of 32O in the framework								
Si	0,021	0,023	0,016	0,014	0,024	0,009	0,031	0,017	0,605	0,021	0,021	0,006	0,022	0,021
Al	5,845	5,783	5,699	0,674	1,682	1,268	0,371	0,492	0,448	0,344	0,280	5,108	3,695	7,276
Cr	7,094	7,176	7,281	0,878	2,838	0,826	0,027	0,040	0,030	0,022	0,099	5,714	3,816	5,222
Fe3+	1,848	1,845	1,821	6,968	5,997	5,922	6,757	6,534	8,543	6,374	6,710	3,284	4,678	2,115
Ti	0,540	0,531	0,532	3,174	2,323	3,589	3,875	3,959	2,042	4,132	3,916	0,846	1,682	0,635
V	0,035	0,031	0,046	0,113	0,088	0,106	0,111	0,128	0,075	0,147	0,131	0,000	0,000	0,000
Mg	4,946	5,016	4,881	1,051	0,956	0,331	0,000	0,000	0,029	0,000	0,000	4,232	3,930	5,015
Fe2+	3,620	3,540	3,671	10,773	9,712	11,401	12,066	12,129	11,681	12,178	12,119	4,702	6,032	3,658
Mn	0,052	0,054	0,052	0,333	0,351	0,502	0,663	0,661	0,362	0,713	0,663	0,063	0,085	0,044
Ca	0,000	0,000	0,000	0,021	0,029	0,046	0,098	0,038	0,186	0,068	0,061	0,044	0,060	0,013
Total	24,00	24,00	24,00	24,00	24,00	24,00	24,00	24,00	24,00	24,00	24,00	24,00	24,00	24,00

EMP analysis of spinel phenocrysts, inclusions, and rims

Sample	AA 08-17-14					AA 08-17-14			DEF 08-06	AA 08-13-4	AA 08-13-4	AA 08-13-11	AA 08-13-08	AA 08-13-9
Description	Core		Rim			Matrix			Aggregate	Matrix, skeletal		Phenocryst	Matrix	Matrix
Analysis	#12	#13	#14	#15	#16	#17	#18	#19	#37	#14	#38	#47	#28	#37
SiO2	0,10	0,08	0,77	1,15	1,24	3,51	3,07	0,10	0,37	0,19	0,95	0,35	0,51	0,10
TiO2	17,02	17,30	14,55	12,81	12,74	7,38	7,97	16,77	16,47	16,34	18,64	15,53	0,31	93,51
Al2O3	5,28	5,16	3,38	2,95	3,64	2,25	2,45	4,01	6,26	6,79	1,58	8,34	0,41	0,03
Cr2O3	0,10	0,10	0,25	0,28	0,37	0,14	0,09	0,12	0,55	0,08	0,02	0,08	0,00	0,00
Fe2O3	29,55	29,24	31,08	33,10	32,33	37,25	37,10	28,11	29,38	27,80	26,22	28,18	51,51	
FeO	39,87	40,17	46,36	46,45	46,64	47,18	46,84	46,96	38,24	44,25	50,78	41,69	47,17	1,14
MnO	0,49	0,62	1,51	1,52	1,61	1,21	1,18	2,90	0,76	1,05	1,44	0,45	0,00	0,00
MgO	7,06	6,87	1,12	0,68	0,57	0,17	0,19	0,29	7,84	3,45	0,08	5,36	0,00	0,00
CaO	0,04	0,04	0,51	0,56	0,41	0,48	0,70	0,29	0,12	0,05	0,29	0,02	0,09	0,26
V2O3	0,50	0,43	0,46	0,49	0,45	0,43	0,42	0,46	0,00	0,00	0,00	0,00	0,00	0,00
Total	100,00	100,00	100,00	100,00	100,00	100,00	100,00	100,00	100,00	100,00	100,00	100,00	100,00	95,05
					Number of ions on the basis of 32O in the framework									
Si	0,027	0,021	0,227	0,339	0,364	1,034	0,903	0,028	0,103	0,055	0,282	0,097	0,155	0,034
Al	1,732	1,697	1,168	1,022	1,259	0,783	0,850	1,390	2,031	2,272	0,552	2,731	0,147	0,013
Cr	0,022	0,021	0,059	0,066	0,086	0,032	0,020	0,028	0,121	0,018	0,006	0,017	0,000	0,000
Fe3+	6,194	6,140	6,850	7,332	7,144	8,260	8,224	6,228	6,090	5,938	5,869	5,891	11,696	
Ti	3,566	3,632	3,206	2,836	2,814	1,636	1,766	3,713	3,413	3,489	4,170	3,246	0,070	23,538
V	0,112	0,096	0,107	0,115	0,106	0,101	0,099	0,108	0,000	0,000	0,000	0,000	0,000	0,000
Mg	2,933	2,858	0,491	0,298	0,249	0,075	0,084	0,128	3,220	1,458	0,035	2,219	0,000	0,001
Fe2+	9,288	9,376	11,357	11,434	11,450	11,626	11,538	11,563	8,808	10,503	12,630	9,685	11,902	0,320
Mn	0,116	0,146	0,374	0,380	0,401	0,301	0,295	0,722	0,178	0,253	0,363	0,106	0,000	0,000
Ca	0,011	0,013	0,162	0,178	0,128	0,151	0,220	0,092	0,037	0,015	0,093	0,006	0,030	0,094
Total	24,00	24,00	24,00	24,00	24,00	24,00	24,00	24,00	24,00	24,00	24,00	24,00	24,00	24,00

EMP analysis of spinel phenocrysts, inclusions, and rims

Sample	AA 08-17-12	DEF 08-01-11	AA 08-13-01		AA 08-15-1		AA 08-12-2
Description	Late melt	Inclusion	Inclusion		Matrix		Matrix
Analysis	#40	#24	#7	#8	#19	#20	#35
SiO2	1,54	0,05	0,14	0,09	0,78	0,82	1,60
TiO2	16,02	9,11	13,88	16,18	1,91	1,06	2,32
Al2O3	3,50	6,15	6,64	7,30	0,10	0,11	0,15
Cr2O3	0,67	3,72	0,10	0,05	0,02	0,00	0,05
Fe2O3	27,38	36,13	33,64	30,54	49,69	50,56	48,12
FeO	47,58	40,98	37,10	35,34	47,14	47,08	47,37
MnO	1,64	1,06	0,40	0,62	0,06	0,05	0,08
MgO	1,13	2,63	7,49	9,38	0,00	0,03	0,02
CaO	0,55	0,17	0,61	0,49	0,30	0,30	0,27
V2O3	0,00	0,00	0,00	0,00	0,00	0,00	0,00
Total	100,00	100,00	100,00	100,00	100,00	100,00	100,00
	Number of ions on the basis of 32O in the framework						
Si	0,450	0,015	0,039	0,026	0,234	0,248	0,482
Al	1,202	2,083	2,159	2,334	0,034	0,039	0,053
Cr	0,155	0,844	0,021	0,011	0,006	0,000	0,012
Fe3+	6,009	7,809	6,984	6,233	11,283	11,476	10,892
Ti	3,515	1,969	2,881	3,302	0,433	0,240	0,525
V	0,000	0,000	0,000	0,000	0,000	0,000	0,000
Mg	0,489	1,125	3,082	3,792	0,001	0,013	0,011
Fe2+	11,604	9,843	8,559	8,016	11,895	11,875	11,916
Mn	0,405	0,259	0,093	0,142	0,016	0,012	0,021
Ca	0,171	0,053	0,181	0,143	0,098	0,097	0,087
Total	24,00	24,00	24,00	24,00	24,00	24,00	24,00

Single CPX EMP spot analyses

	#1	#2	#3	#4	#5	#6	#7	#8	#9	#10	#11	#12	#13	#14
SiO2	42,91	47,40	45,60	45,25	45,96	48,56	42,43	39,30	46,73	45,90	47,95	45,41	47,54	39,84
TiO2	4,88	2,32	2,98	2,94	2,37	1,83	4,83	6,13	2,51	2,11	2,01	3,05	2,51	6,29
Al2O3	8,66	5,58	6,88	7,47	7,70	5,25	8,70	10,85	5,91	6,16	4,74	6,92	5,06	10,50
Cr2O3	0,01	0,29	0,00	0,02	0,00	0,31	0,00	0,00	0,01	0,00	0,03	0,00	0,03	0,03
Fe2O3	5,00	4,35	5,41	5,62	5,23	3,64	6,15	7,40	5,47	6,81	5,08	5,54	4,41	6,57
FeO	2,79	2,03	3,03	2,45	2,51	2,31	1,73	3,17	2,40	4,47	1,65	2,47	2,20	1,94
MnO	0,12	0,08	0,10	0,11	0,07	0,13	0,13	0,23	0,14	0,40	0,12	0,10	0,11	0,09
MgO	11,78	14,05	11,89	12,21	12,55	14,57	11,82	8,80	12,90	10,29	14,08	12,32	14,05	10,76
CaO	23,46	23,60	23,50	23,37	23,04	23,01	23,84	23,28	23,32	22,93	23,99	23,71	23,84	23,55
Na2O	0,38	0,30	0,61	0,55	0,58	0,39	0,36	0,73	0,60	0,92	0,34	0,47	0,27	0,43
K2O	0,01	0,01	0,00	0,01	0,00	0,01	0,00	0,12	0,01	0,01	0,00	0,00	0,00	0,00
Total	100,00	100,00	100,00	100,00	100,00	100,00	100,00	100,00	100,00	100,00	100,00	100,00	100,00	100,00
Si	1,613	1,759	1,709	1,692	1,711	1,794	1,596	1,501	1,743	1,738	1,780	1,699	1,766	1,507
Al	0,384	0,244	0,304	0,329	0,338	0,229	0,386	0,488	0,260	0,275	0,207	0,305	0,222	0,468
Cr	0,000	0,009	0,000	0,001	0,000	0,009	0,000	0,000	0,000	0,000	0,001	0,000	0,001	0,001
Fe3+	0,141	0,122	0,153	0,158	0,146	0,101	0,174	0,213	0,154	0,194	0,142	0,156	0,123	0,187
Ti	0,138	0,065	0,084	0,083	0,066	0,051	0,137	0,176	0,070	0,060	0,056	0,086	0,070	0,179
Mg	0,660	0,777	0,664	0,681	0,696	0,802	0,662	0,501	0,718	0,581	0,779	0,687	0,778	0,607
Fe2+	0,088	0,063	0,095	0,077	0,078	0,071	0,054	0,101	0,075	0,141	0,051	0,077	0,068	0,061
Mn	0,004	0,002	0,003	0,004	0,002	0,004	0,004	0,007	0,004	0,013	0,004	0,003	0,003	0,003
Ca	0,945	0,938	0,943	0,936	0,919	0,911	0,961	0,953	0,932	0,930	0,954	0,951	0,949	0,955
Na	0,028	0,022	0,045	0,040	0,042	0,028	0,027	0,054	0,043	0,068	0,025	0,034	0,019	0,032
K	0,001	0,000	0,000	0,000	0,000	0,000	0,000	0,006	0,000	0,000	0,000	0,000	0,000	0,000
Mg	35,91	40,85	35,74	36,70	37,80	42,46	35,70	28,23	38,12	31,25	40,37	36,65	40,49	33,48
Fe	12,67	9,83	13,49	12,85	12,32	9,35	12,53	18,11	12,38	18,73	10,20	12,63	10,14	13,87
Ca	51,42	49,32	50,76	50,46	49,89	48,19	51,77	53,67	49,50	50,02	49,43	50,72	49,38	52,65
mg*	73,91	80,60	72,59	74,07	75,43	81,96	74,02	60,92	75,48	62,52	79,83	74,38	79,97	70,71

	#15	#16	#17	#18	#19	#20	#21	#22	#23	#24	#25	#26	#27	#28	#29
SiO2	45,34	45,66	47,96	39,32	47,39	36,45	49,50	49,39	45,27	47,10	44,31	47,17	42,23	38,02	45,24
TiO2	3,05	3,00	2,39	3,99	2,48	7,54	1,44	1,39	3,32	2,58	4,07	2,94	5,26	6,23	3,18
Al2O3	7,23	6,83	4,66	11,35	5,53	12,63	5,19	5,33	7,27	5,68	7,73	5,32	9,10	11,90	6,83
Cr2O3	0,00	0,01	0,05	0,00	0,04	0,00	0,17	0,21	0,23	0,01	0,02	0,01	0,01	0,00	0,05
Fe2O3	5,60	5,30	4,34	9,79	4,34	8,20	3,25	3,42	4,55	4,67	4,85	4,14	5,30	7,79	5,87
FeO	2,39	3,20	1,98	5,00	2,28	4,29	1,85	1,74	2,37	1,97	2,54	2,24	2,95	5,90	1,35
MnO	0,14	0,17	0,09	0,41	0,13	0,24	0,10	0,09	0,10	0,11	0,12	0,13	0,11	0,29	0,08
MgO	12,32	11,92	14,40	6,52	13,69	7,07	15,16	15,26	12,73	13,58	12,26	13,91	11,19	6,55	13,07
CaO	23,38	23,28	23,87	22,55	23,76	22,61	22,83	22,69	23,86	23,94	23,71	23,83	23,31	22,30	24,00
Na2O	0,55	0,62	0,26	1,05	0,36	0,93	0,49	0,48	0,31	0,37	0,39	0,28	0,50	1,02	0,34
K2O	0,01	0,00	0,00	0,01	0,00	0,03	0,01	0,01	0,00	0,00	0,00	0,03	0,04	0,01	0,00
Total	100,00	100,00	100,00	100,00	100,00	100,00	100,00	100,00	100,00	100,00	100,00	100,00	100,00	100,00	100,00
Si	1,695	1,711	1,779	1,519	1,761	1,408	1,818	1,813	1,690	1,751	1,660	1,753	1,592	1,470	1,688
Al	0,319	0,302	0,204	0,517	0,242	0,575	0,225	0,230	0,320	0,249	0,341	0,233	0,404	0,542	0,300
Cr	0,000	0,000	0,001	0,000	0,001	0,000	0,005	0,006	0,007	0,000	0,001	0,000	0,000	0,000	0,001
Fe3+	0,158	0,150	0,121	0,284	0,121	0,238	0,090	0,094	0,128	0,131	0,137	0,116	0,150	0,227	0,165
Ti	0,086	0,085	0,067	0,116	0,069	0,219	0,040	0,038	0,093	0,072	0,115	0,082	0,149	0,181	0,089
Mg	0,687	0,666	0,796	0,376	0,758	0,407	0,830	0,835	0,708	0,752	0,685	0,771	0,629	0,378	0,727
Fe2+	0,075	0,100	0,061	0,161	0,071	0,139	0,057	0,053	0,074	0,061	0,080	0,070	0,093	0,191	0,042
Mn	0,004	0,005	0,003	0,013	0,004	0,008	0,003	0,003	0,003	0,003	0,004	0,004	0,003	0,009	0,003
Ca	0,937	0,935	0,949	0,934	0,946	0,936	0,898	0,892	0,954	0,954	0,951	0,949	0,941	0,924	0,960
Na	0,040	0,045	0,019	0,079	0,026	0,070	0,035	0,034	0,023	0,027	0,028	0,020	0,036	0,077	0,024
K	0,000	0,000	0,000	0,000	0,000	0,001	0,000	0,000	0,000	0,000	0,000	0,001	0,002	0,001	0,000
Mg	36,91	35,89	41,26	21,25	39,90	23,55	44,19	44,46	37,93	39,57	36,89	40,37	34,62	21,84	38,34
Fe	12,73	13,75	9,60	25,97	10,33	22,28	7,98	8,03	10,96	10,27	11,86	9,92	13,57	24,71	11,06
Ca	50,35	50,37	49,14	52,79	49,77	54,17	47,83	47,51	51,11	50,16	51,25	49,71	51,81	53,45	50,60
mg*	74,35	72,30	81,12	45,00	79,44	51,39	84,71	84,71	77,58	79,39	75,67	80,27	71,84	46,91	77,62

	#30	#35	#36	#37	#38	#39	#40	#41	#42	#43	#43	#45	#46	#47
SiO2	42,31	43,88	47,29	48,10	39,33	47,93	44,48	48,41	45,77	46,56	46,56	47,13	45,66	48,35
TiO2	3,98	3,75	2,53	2,25	6,49	1,69	2,73	2,22	2,75	3,15	3,15	2,93	2,97	2,14
Al2O3	7,74	8,39	6,09	4,85	11,07	5,12	8,01	4,57	6,31	5,79	5,79	5,23	6,87	4,76
Cr2O3	0,01	0,01	0,18	0,02	0,03	0,02	0,01	0,00	0,00	0,00	0,00	0,00	0,01	0,16
Fe2O3	8,36	5,78	3,37	4,34	6,09	4,31	6,11	3,46	5,42	4,34	4,34	4,25	5,51	3,94
FeO	4,26	3,05	2,99	2,14	3,58	6,13	5,06	3,67	3,97	2,71	2,71	2,74	3,01	2,28
MnO	0,24	0,15	0,09	0,13	0,11	0,40	0,31	0,11	0,12	0,10	0,10	0,10	0,10	0,11
MgO	9,20	11,04	13,62	14,24	9,48	10,91	9,55	13,84	11,89	13,59	13,59	13,80	12,07	14,28
CaO	23,07	23,24	23,56	23,53	23,25	22,64	22,87	23,41	23,29	23,45	23,45	23,48	23,12	23,63
Na2O	0,83	0,68	0,28	0,38	0,54	0,83	0,87	0,31	0,44	0,32	0,32	0,31	0,65	0,35
K2O	0,01	0,03	0,01	0,01	0,02	0,01	0,00	0,01	0,03	0,00	0,00	0,03	0,02	0,02
Total	100,00	100,00	100,00	100,00	100,00	100,00	100,00	100,00	100,00	100,00	100,00	100,00	100,00	100,00
Si	1,619	1,651	1,756	1,783	1,497	1,807	1,687	1,800	1,721	1,735	1,735	1,755	1,710	1,792
Al	0,349	0,372	0,266	0,212	0,497	0,228	0,358	0,200	0,280	0,254	0,254	0,229	0,303	0,208
Cr	0,000	0,000	0,005	0,001	0,001	0,001	0,000	0,000	0,000	0,000	0,000	0,000	0,000	0,005
Fe3+	0,241	0,163	0,094	0,121	0,174	0,122	0,174	0,097	0,153	0,122	0,122	0,119	0,155	0,110
Ti	0,114	0,106	0,071	0,063	0,186	0,048	0,078	0,062	0,078	0,088	0,088	0,082	0,084	0,060
Mg	0,525	0,619	0,754	0,787	0,538	0,613	0,540	0,767	0,667	0,755	0,755	0,766	0,674	0,789
Fe2+	0,136	0,096	0,093	0,066	0,114	0,193	0,160	0,114	0,125	0,085	0,085	0,085	0,094	0,071
Mn	0,008	0,005	0,003	0,004	0,004	0,013	0,010	0,003	0,004	0,003	0,003	0,003	0,003	0,003
Ca	0,946	0,937	0,937	0,935	0,948	0,914	0,929	0,933	0,938	0,936	0,936	0,937	0,928	0,938
Na	0,061	0,050	0,020	0,027	0,040	0,061	0,064	0,022	0,032	0,023	0,023	0,022	0,047	0,025
K	0,001	0,002	0,001	0,000	0,001	0,001	0,000	0,001	0,002	0,000	0,000	0,001	0,001	0,001
Mg	28,28	34,01	40,07	41,14	30,26	33,04	29,75	40,08	35,32	39,73	39,73	40,10	36,34	41,29
Fe	20,75	14,52	10,10	10,02	16,42	17,69	19,01	11,20	14,95	11,02	11,02	10,87	13,63	9,61
Ca	50,98	51,46	49,83	48,85	53,32	49,28	51,24	48,72	49,73	49,26	49,26	49,04	50,03	49,09
mg*	57,68	70,08	79,88	80,42	64,82	65,13	61,02	78,16	70,27	78,29	78,29	78,67	72,72	81,12

	#48	#49	#50	#51	#52	#53	#54	#55	#56	#57	#58	#59	#60	#61	#62
SiO2	46,05	46,80	46,44	44,84	45,89	40,05	46,70	42,65	47,06	45,06	42,49	43,80	46,39	45,79	47,92
TiO2	2,84	2,97	1,97	3,13	3,02	6,25	2,33	4,74	2,44	3,46	4,85	3,32	2,96	2,24	2,56
Al2O3	6,60	5,20	6,22	7,23	6,81	10,25	6,16	8,80	5,70	7,43	8,95	7,88	6,07	6,41	4,58
Cr2O3	0,32	0,00	0,00	0,01	0,03	0,01	0,00	0,04	0,06	0,01	0,01	0,01	0,00	0,00	0,01
Fe2O3	4,78	4,91	5,81	6,44	4,78	6,34	5,02	5,72	4,94	4,88	5,58	7,21	4,87	6,76	4,15
FeO	2,04	2,04	5,48	2,36	2,44	2,90	3,88	2,00	2,42	3,46	2,24	3,17	2,30	3,63	2,56
MnO	0,08	0,16	0,37	0,17	0,10	0,11	0,20	0,10	0,19	0,09	0,12	0,24	0,10	0,30	0,09
MgO	13,15	13,67	10,26	11,72	12,92	10,24	11,98	11,83	12,94	11,66	11,52	10,52	13,23	10,98	14,24
CaO	23,79	23,94	22,47	23,40	23,61	23,31	23,08	23,75	23,72	23,33	23,85	23,03	23,67	23,06	23,58
Na2O	0,35	0,29	0,95	0,64	0,39	0,50	0,64	0,36	0,53	0,61	0,37	0,82	0,40	0,81	0,30
K2O	0,00	0,02	0,02	0,05	0,01	0,04	0,01	0,02	0,00	0,00	0,02	0,00	0,00	0,03	0,00
Total	100,00	100,00	100,00	100,00	100,00	100,00	100,00	100,00	100,00	100,00	100,00	100,00	100,00	100,00	100,00
Si	1,716	1,744	1,756	1,684	1,712	1,520	1,750	1,602	1,754	1,690	1,598	1,656	1,729	1,727	1,780
Al	0,290	0,228	0,277	0,320	0,299	0,458	0,272	0,390	0,251	0,328	0,397	0,351	0,267	0,285	0,201
Cr	0,009	0,000	0,000	0,000	0,001	0,000	0,000	0,001	0,002	0,000	0,000	0,000	0,000	0,000	0,000
Fe3+	0,134	0,138	0,165	0,182	0,134	0,181	0,142	0,162	0,139	0,138	0,158	0,205	0,137	0,192	0,116
Ti	0,080	0,083	0,056	0,088	0,085	0,178	0,066	0,134	0,069	0,098	0,137	0,094	0,083	0,064	0,072
Mg	0,730	0,759	0,579	0,656	0,718	0,579	0,669	0,663	0,719	0,652	0,646	0,593	0,735	0,617	0,788
Fe2+	0,064	0,064	0,173	0,074	0,076	0,092	0,122	0,063	0,075	0,108	0,070	0,100	0,072	0,114	0,079
Mn	0,003	0,005	0,012	0,005	0,003	0,004	0,006	0,003	0,006	0,003	0,004	0,008	0,003	0,010	0,003
Ca	0,950	0,956	0,910	0,941	0,943	0,948	0,927	0,956	0,947	0,938	0,961	0,933	0,945	0,932	0,939
Na	0,026	0,021	0,070	0,047	0,028	0,037	0,046	0,026	0,038	0,044	0,027	0,060	0,029	0,059	0,022
K	0,000	0,001	0,001	0,002	0,001	0,002	0,000	0,001	0,000	0,000	0,001	0,000	0,000	0,001	0,000
Mg	38,84	39,52	31,45	35,28	38,30	32,12	35,88	35,89	38,12	35,46	35,12	32,25	38,86	33,09	40,95
Fe	10,64	10,74	19,06	14,07	11,38	15,34	14,45	12,34	11,66	13,55	12,63	17,02	11,19	16,95	10,29
Ca	50,52	49,75	49,49	50,64	50,32	52,54	49,67	51,78	50,23	50,99	52,25	50,73	49,96	49,97	48,75
mg*	78,49	78,64	62,27	71,49	77,09	67,68	71,29	74,42	76,58	72,35	73,55	65,46	77,65	66,13	79,91

	#64	#65	#66	#67	#68	#69	#70	#71	#72	#73	#74	#75	#77	#78
SiO2	43,29	45,45	47,18	46,23	53,07	53,08	44,97	46,45	47,31	45,20	50,39	47,12	42,27	50,72
TiO2	4,33	3,24	2,89	2,91	0,29	0,61	3,47	3,01	3,06	3,38	1,03	2,60	5,05	1,00
Al2O3	8,67	6,76	5,49	6,57	0,14	0,57	7,60	6,49	5,38	6,13	4,83	5,75	8,91	4,58
Cr2O3	0,00	0,00	0,01	0,00	0,00	0,00	0,02	0,13	0,00	0,02	0,29	0,38	0,03	0,41
Fe2O3	5,33	5,23	3,61	4,53	1,61	1,44	4,70	3,90	3,47	5,68	3,18	4,32	5,69	2,43
FeO	2,74	3,64	3,28	3,71	7,40	6,16	2,57	3,54	3,22	4,03	2,26	1,74	2,24	2,74
MnO	0,10	0,18	0,12	0,18	0,27	0,17	0,12	0,11	0,11	0,28	0,14	0,08	0,08	0,10
MgO	11,83	11,63	13,36	11,75	13,58	14,33	12,44	12,80	13,53	11,34	15,71	13,81	11,76	15,68
CaO	23,26	23,20	23,75	23,45	23,19	23,09	23,73	23,07	23,51	23,30	21,46	23,81	23,64	21,68
Na2O	0,41	0,65	0,30	0,66	0,46	0,54	0,36	0,47	0,34	0,53	0,70	0,37	0,34	0,65
K2O	0,02	0,02	0,00	0,00	0,00	0,03	0,00	0,02	0,07	0,11	0,02	0,02	0,00	0,00
Total	100,00	100,00	100,00	100,00	100,00	100,00	100,00	100,00	100,00	100,00	100,00	100,00	100,00	100,00
Si	1,625	1,708	1,758	1,732	1,983	1,970	1,681	1,733	1,761	1,707	1,844	1,749	1,590	1,857
Al	0,384	0,299	0,241	0,290	0,006	0,025	0,335	0,285	0,236	0,273	0,208	0,251	0,395	0,197
Cr	0,000	0,000	0,000	0,000	0,000	0,000	0,001	0,004	0,000	0,001	0,008	0,011	0,001	0,012
Fe3+	0,151	0,148	0,101	0,128	0,045	0,040	0,132	0,109	0,097	0,161	0,088	0,121	0,161	0,067
Ti	0,122	0,092	0,081	0,082	0,008	0,017	0,098	0,085	0,086	0,096	0,028	0,073	0,143	0,028
Mg	0,662	0,651	0,742	0,656	0,756	0,793	0,693	0,712	0,751	0,638	0,857	0,764	0,659	0,856
Fe2+	0,086	0,114	0,102	0,116	0,231	0,191	0,080	0,110	0,100	0,127	0,069	0,054	0,070	0,084
Mn	0,003	0,006	0,004	0,006	0,008	0,005	0,004	0,004	0,003	0,009	0,004	0,002	0,003	0,003
Ca	0,936	0,934	0,948	0,941	0,928	0,918	0,950	0,922	0,938	0,943	0,842	0,947	0,953	0,850
Na	0,030	0,047	0,022	0,048	0,034	0,039	0,026	0,034	0,024	0,039	0,050	0,027	0,025	0,046
K	0,001	0,001	0,000	0,000	0,000	0,001	0,000	0,001	0,003	0,005	0,001	0,001	0,000	0,000
Mg	36,03	35,14	39,11	35,53	38,40	40,71	37,26	38,33	39,75	33,97	46,10	40,47	35,72	46,01
Fe	13,06	14,48	10,93	13,51	14,47	12,15	11,64	12,02	10,63	15,85	8,65	9,38	12,67	8,28
Ca	50,91	50,38	49,96	50,96	47,14	47,14	51,10	49,65	49,63	50,18	45,25	50,15	51,61	45,71
mg*	73,40	70,82	78,15	72,45	72,64	77,01	76,20	76,12	78,90	68,19	84,20	81,19	73,82	84,74

	#79	#80	#81	#82	#83	#84	#85	#86	#87	#88	#89	#90	#91	#92	#93
SiO2	42,82	51,37	47,36	46,53	48,48	41,55	45,11	46,74	44,96	47,75	42,27	39,66	50,17	42,92	47,94
TiO2	5,19	1,01	2,83	2,16	2,30	5,41	2,24	3,14	3,70	2,44	4,92	6,10	0,54	4,86	2,71
Al2O3	8,40	4,60	5,61	7,41	4,45	9,38	8,33	5,45	7,33	4,74	9,19	10,47	2,48	8,38	5,02
Cr2O3	0,01	0,66	0,10	0,00	0,08	0,04	0,04	0,00	0,11	0,18	0,12	0,05	0,02	0,00	0,01
Fe2O3	5,53	0,72	3,45	5,15	3,66	6,07	6,51	4,37	4,76	4,66	5,67	7,09	4,14	5,69	3,10
FeO	1,53	3,87	3,01	3,74	2,37	2,03	5,48	2,31	2,67	1,63	2,18	1,68	7,33	1,72	4,00
MnO	0,14	0,09	0,11	0,13	0,06	0,09	0,27	0,13	0,11	0,11	0,08	0,08	0,32	0,08	0,12
MgO	11,92	16,06	13,56	11,61	14,47	11,41	8,92	13,60	12,60	14,34	11,68	10,81	11,41	12,19	13,73
CaO	23,98	21,02	23,62	22,27	23,83	23,59	21,66	23,97	23,30	23,81	23,47	23,72	22,90	23,77	23,01
Na2O	0,50	0,61	0,35	0,96	0,28	0,41	1,42	0,29	0,42	0,32	0,40	0,35	0,68	0,38	0,37
K2O	0,00	0,00	0,00	0,03	0,00	0,01	0,01	0,00	0,03	0,01	0,02	0,00	0,00	0,00	0,00
Total	100,00	100,00	100,00	100,00	100,00	100,00	100,00	100,00	100,00	100,00	100,00	100,00	100,00	100,00	100,00
Si	1,607	1,875	1,761	1,738	1,796	1,566	1,708	1,741	1,681	1,772	1,589	1,502	1,895	1,610	1,784
Al	0,371	0,198	0,246	0,326	0,194	0,417	0,372	0,239	0,323	0,207	0,407	0,467	0,110	0,371	0,220
Cr	0,000	0,019	0,003	0,000	0,002	0,001	0,001	0,000	0,003	0,005	0,004	0,001	0,001	0,000	0,000
Fe3+	0,156	0,020	0,096	0,145	0,102	0,172	0,185	0,122	0,134	0,130	0,160	0,202	0,118	0,161	0,087
Ti	0,147	0,028	0,079	0,061	0,064	0,153	0,064	0,088	0,104	0,068	0,139	0,174	0,015	0,137	0,076
Mg	0,667	0,874	0,751	0,647	0,799	0,641	0,503	0,755	0,702	0,793	0,654	0,610	0,642	0,682	0,761
Fe2+	0,048	0,118	0,094	0,117	0,074	0,064	0,174	0,072	0,083	0,050	0,068	0,053	0,232	0,054	0,125
Mn	0,004	0,003	0,003	0,004	0,002	0,003	0,009	0,004	0,003	0,003	0,002	0,003	0,010	0,003	0,004
Ca	0,964	0,822	0,941	0,892	0,946	0,952	0,879	0,957	0,933	0,947	0,945	0,962	0,927	0,956	0,917
Na	0,036	0,043	0,026	0,069	0,020	0,030	0,105	0,021	0,031	0,023	0,029	0,025	0,050	0,028	0,027
K	0,000	0,000	0,000	0,001	0,000	0,000	0,001	0,000	0,001	0,001	0,001	0,000	0,000	0,000	0,000
Mg	36,25	47,59	39,85	35,84	41,57	34,96	28,77	39,53	37,83	41,23	35,74	33,33	33,30	36,75	40,20
Fe	11,33	7,66	10,26	14,74	9,23	13,06	21,02	10,39	11,89	9,56	12,63	14,07	18,64	11,72	11,36
Ca	52,42	44,76	49,89	49,42	49,20	51,98	50,22	50,08	50,27	49,21	51,63	52,59	48,06	51,53	48,44
mg*	76,19	86,14	79,52	70,86	81,84	72,81	57,78	79,19	76,08	81,17	73,88	70,31	64,11	75,81	77,97

	#94	#95	#96	#97	#98	#99	#100	#101	#102	#103	#104	#105	#106	#107
SiO2	47,25	47,10	47,65	45,49	46,17	45,93	46,74	42,40	41,99	49,29	43,11	46,42	46,38	40,91
TiO2	2,93	3,28	2,73	2,90	2,55	2,88	2,49	4,99	5,00	1,90	4,51	2,50	3,08	5,48
Al2O3	4,86	5,03	3,70	7,71	7,01	7,48	6,78	9,38	9,30	4,75	8,90	7,06	5,99	9,93
Cr2O3	0,00	0,02	0,00	0,00	0,03	0,00	0,03	0,00	0,00	0,02	0,02	0,00	0,00	0,03
Fe2O3	4,43	4,43	5,30	4,92	5,11	4,13	4,07	4,57	6,35	2,56	5,24	4,53	4,54	6,43
FeO	2,31	1,70	3,20	2,97	2,42	3,74	3,26	3,55	1,83	3,86	2,07	2,98	2,34	2,00
MnO	0,09	0,20	0,30	0,06	0,08	0,09	0,12	0,11	0,13	0,07	0,16	0,14	0,15	0,07
MgO	13,87	13,69	12,34	12,08	12,92	11,85	12,78	11,16	11,24	14,11	11,66	12,41	13,11	10,80
CaO	23,95	24,09	24,11	23,28	23,22	23,29	23,25	23,49	23,60	22,98	23,90	23,41	24,10	23,89
Na2O	0,28	0,45	0,65	0,57	0,49	0,59	0,47	0,34	0,54	0,46	0,44	0,54	0,33	0,39
K2O	0,02	0,02	0,02	0,00	0,00	0,00	0,02	0,00	0,02	0,00	0,00	0,01	0,01	0,06
Total	100,00	100,00	100,00	100,00	100,00	100,00	100,00	100,00	100,00	100,00	100,00	100,00	100,00	100,00
Si	1,759	1,752	1,790	1,700	1,720	1,717	1,741	1,597	1,581	1,824	1,617	1,731	1,730	1,546
Al	0,213	0,220	0,164	0,339	0,308	0,330	0,297	0,417	0,413	0,207	0,393	0,310	0,263	0,442
Cr	0,000	0,000	0,000	0,000	0,001	0,000	0,001	0,000	0,000	0,001	0,001	0,000	0,000	0,001
Fe3+	0,124	0,124	0,150	0,138	0,143	0,116	0,114	0,130	0,180	0,071	0,148	0,127	0,127	0,183
Ti	0,082	0,092	0,077	0,082	0,072	0,081	0,070	0,142	0,142	0,053	0,127	0,070	0,086	0,156
Mg	0,770	0,759	0,691	0,673	0,717	0,661	0,710	0,627	0,631	0,778	0,652	0,690	0,729	0,608
Fe2+	0,072	0,053	0,101	0,093	0,075	0,117	0,101	0,112	0,058	0,119	0,065	0,093	0,073	0,063
Mn	0,003	0,006	0,009	0,002	0,002	0,003	0,004	0,003	0,004	0,002	0,005	0,004	0,005	0,002
Ca	0,955	0,960	0,970	0,932	0,927	0,933	0,928	0,948	0,952	0,911	0,960	0,935	0,963	0,967
Na	0,020	0,032	0,048	0,042	0,036	0,043	0,034	0,025	0,039	0,033	0,032	0,039	0,024	0,029
K	0,001	0,001	0,001	0,000	0,000	0,000	0,001	0,000	0,001	0,000	0,000	0,001	0,000	0,003
Mg	40,01	39,91	35,96	36,61	38,46	36,11	38,23	34,44	34,58	41,34	35,63	37,29	38,42	33,36
Fe	10,34	9,62	13,52	12,68	11,85	12,91	11,81	13,46	13,24	10,24	11,90	12,14	10,80	13,61
Ca	49,65	50,47	50,52	50,71	49,69	50,99	49,96	52,11	52,18	48,41	52,48	50,57	50,78	53,03
mg*	79,46	80,58	72,68	74,28	76,44	73,67	76,40	71,90	72,31	80,14	74,97	75,44	78,06	71,02

	#108	#109	#110	#111	#112	#113	#114	#115	#116	#117	#118	#119	#120	#121	#122
SiO2	45,78	42,72	45,51	44,74	42,89	46,44	47,29	47,20	46,71	47,08	46,19	46,80	44,69	45,50	43,04
TiO2	2,75	4,66	2,98	1,82	4,84	2,94	1,39	2,59	2,99	2,90	2,56	2,52	1,96	3,15	4,58
Al2O3	7,30	9,21	7,57	7,51	9,01	5,97	6,66	5,57	5,88	5,60	7,24	6,61	8,63	7,27	9,11
Cr2O3	0,00	0,02	0,02	0,00	0,00	0,01	0,00	0,00	0,00	0,03	0,07	0,03	0,02	0,05	0,03
Fe2O3	5,29	5,24	4,63	8,24	4,88	4,71	6,30	4,25	4,31	4,27	4,73	3,98	6,89	4,60	4,83
FeO	2,76	2,20	2,85	5,31	2,67	2,21	5,15	2,68	2,85	2,10	3,34	3,17	6,27	2,87	2,56
MnO	0,11	0,08	0,14	0,37	0,12	0,09	0,38	0,13	0,14	0,10	0,10	0,08	0,49	0,14	0,16
MgO	11,79	11,75	12,24	8,36	11,54	13,32	9,45	13,39	12,96	13,73	12,26	12,92	7,99	12,53	11,67
CaO	23,51	23,77	23,60	22,33	23,60	23,99	21,71	23,84	23,67	23,80	22,87	23,47	21,63	23,48	23,60
Na2O	0,71	0,36	0,45	1,31	0,45	0,31	1,66	0,34	0,44	0,36	0,64	0,41	1,41	0,38	0,38
K2O	0,00	0,00	0,00	0,00	0,00	0,00	0,00	0,00	0,04	0,03	0,01	0,00	0,02	0,04	0,03
Total	100,00	100,00	100,00	100,00	100,00	100,00	100,00	100,00	100,00	100,00	100,00	100,00	100,00	100,00	100,00
Si	1,712	1,603	1,700	1,707	1,611	1,731	1,782	1,757	1,742	1,749	1,724	1,743	1,702	1,700	1,615
Al	0,322	0,407	0,333	0,338	0,399	0,262	0,296	0,244	0,258	0,245	0,318	0,290	0,387	0,320	0,403
Cr	0,000	0,001	0,000	0,000	0,000	0,000	0,000	0,000	0,000	0,001	0,002	0,001	0,001	0,001	0,001
Fe3+	0,149	0,148	0,130	0,237	0,138	0,132	0,179	0,119	0,121	0,119	0,133	0,112	0,197	0,129	0,136
Ti	0,077	0,131	0,084	0,052	0,137	0,082	0,039	0,073	0,084	0,081	0,072	0,071	0,056	0,089	0,129
Mg	0,657	0,657	0,682	0,476	0,646	0,740	0,531	0,743	0,721	0,761	0,682	0,717	0,453	0,698	0,653
Fe2+	0,086	0,069	0,089	0,169	0,084	0,069	0,162	0,084	0,089	0,065	0,104	0,099	0,200	0,090	0,080
Mn	0,003	0,002	0,004	0,012	0,004	0,003	0,012	0,004	0,004	0,003	0,003	0,003	0,016	0,004	0,005
Ca	0,942	0,955	0,944	0,913	0,950	0,958	0,877	0,951	0,946	0,948	0,915	0,936	0,883	0,940	0,949
Na	0,051	0,026	0,033	0,097	0,033	0,022	0,121	0,025	0,032	0,026	0,046	0,030	0,104	0,027	0,028
K	0,000	0,000	0,000	0,000	0,000	0,000	0,000	0,000	0,002	0,001	0,000	0,000	0,001	0,002	0,001
Mg	35,76	35,87	36,85	26,33	35,47	38,90	30,14	39,10	38,31	40,11	37,14	38,41	25,93	37,49	35,80
Fe	12,98	11,97	12,09	23,14	12,39	10,72	20,07	10,87	11,40	9,91	13,08	11,41	23,60	12,01	12,17
Ca	51,26	52,16	51,05	50,53	52,15	50,37	49,78	50,02	50,29	49,98	49,78	50,18	50,47	50,51	52,02
mg*	73,36	74,98	75,29	53,23	74,12	78,39	60,03	78,24	77,07	80,18	73,95	77,10	52,35	75,74	74,63

	#123	#124	#125	#126	#127	#128	#129	#130	#131	#132	#134	#135	#136
SiO2	42,03	49,17	47,61	46,79	46,89	45,06	47,90	42,35	45,68	41,67	43,96	46,13	47,61
TiO2	4,99	1,79	2,43	2,75	2,75	2,86	2,26	4,65	3,57	5,13	1,70	3,22	2,01
Al2O3	9,23	2,73	4,12	4,97	4,14	7,80	5,82	9,29	6,04	9,54	7,91	6,18	6,19
Cr2O3	0,02	0,02	0,03	0,12	0,00	0,02	0,00	0,00	0,00	0,00	0,05	0,00	0,07
Fe2O3	5,83	1,06	3,13	3,44	3,79	4,66	2,52	5,00	4,10	5,37	6,41	4,15	3,75
FeO	2,46	13,86	10,13	9,12	9,11	3,41	4,12	3,42	3,99	3,48	9,66	3,10	3,13
MnO	0,10	0,49	0,32	0,32	0,24	0,12	0,10	0,09	0,14	0,15	0,74	0,12	0,10
MgO	11,36	11,82	12,87	13,26	12,13	11,78	13,34	11,03	12,66	10,68	6,57	13,04	13,39
CaO	23,56	18,76	18,85	18,81	20,54	23,83	23,57	23,77	23,48	23,48	21,53	23,66	23,07
Na2O	0,37	0,00	0,00	0,00	0,00	0,02	0,00	0,04	0,05	0,14	0,00	0,06	0,04
K2O	0,03	0,30	0,52	0,41	0,42	0,44	0,37	0,35	0,28	0,36	1,47	0,34	0,62
Total	100,00	100,00	100,00	100,00	100,00	100,00	100,00	100,00	100,00	100,00	100,00	100,00	100,00
Si	1,584	1,879	1,806	1,770	1,784	1,691	1,782	1,599	1,716	1,578	1,710	1,725	1,770
Al	0,410	0,123	0,184	0,222	0,185	0,345	0,255	0,414	0,267	0,426	0,362	0,272	0,271
Cr	0,001	0,001	0,001	0,004	0,000	0,001	0,000	0,000	0,000	0,000	0,001	0,000	0,002
Fe3+	0,165	0,030	0,089	0,098	0,109	0,132	0,070	0,142	0,116	0,153	0,187	0,117	0,105
Ti	0,141	0,051	0,069	0,078	0,079	0,081	0,063	0,132	0,101	0,146	0,050	0,091	0,056
Mg	0,638	0,673	0,728	0,748	0,688	0,659	0,740	0,621	0,709	0,602	0,381	0,727	0,742
Fe2+	0,078	0,443	0,321	0,289	0,290	0,107	0,128	0,108	0,125	0,110	0,314	0,097	0,097
Mn	0,003	0,016	0,010	0,010	0,008	0,004	0,003	0,003	0,004	0,005	0,024	0,004	0,003
Ca	0,951	0,768	0,766	0,762	0,837	0,958	0,940	0,962	0,945	0,952	0,897	0,948	0,919
Na	0,027	0,000	0,000	0,000	0,000	0,001	0,000	0,003	0,003	0,010	0,000	0,004	0,003
K	0,001	0,015	0,025	0,020	0,021	0,021	0,018	0,017	0,014	0,018	0,073	0,016	0,030
Mg	34,77	34,88	38,00	39,22	35,62	35,44	39,32	33,83	37,33	33,05	21,12	38,42	39,76
Fe	13,40	25,34	21,99	20,81	21,03	13,03	10,73	13,78	12,93	14,70	29,16	11,48	11,01
Ca	51,82	39,78	40,01	39,97	43,35	51,53	49,95	52,39	49,75	52,25	49,72	50,10	49,23
mg*	72,18	57,92	63,35	65,33	62,88	73,11	78,57	71,06	74,28	69,22	42,01	76,99	78,32

Biotite Phenocryst EMP Profile Analyses

	#1	#2	#3	#4	#5	#6	#7	#8	#9	#10	#11	#12	#13
SiO2	36,76	36,74	36,79	36,59	36,91	36,89	37,08	36,84	37,01	37,28	36,88	36,32	36,36
TiO2	5,79	5,94	5,80	5,88	5,90	5,92	5,83	5,89	5,85	5,91	5,86	5,99	6,09
Al2O3	15,72	15,64	15,82	15,75	15,85	15,59	15,72	15,78	15,50	15,64	15,66	15,63	15,61
Cr2O3	0,21	0,27	0,18	0,24	0,27	0,29	0,33	0,26	0,30	0,19	0,29	0,96	1,11
FeO	7,17	6,96	7,10	7,27	7,13	7,17	7,34	7,16	7,12	7,15	7,09	7,46	7,43
MnO	0,03	0,07	0,03	0,04	0,01	0,00	0,03	0,02	0,07	0,05	0,04	0,03	0,02
MgO	18,84	19,06	18,82	19,18	19,14	18,90	18,95	18,86	18,93	18,90	19,04	18,61	18,64
CaO	0,06	0,04	0,04	0,07	0,05	0,04	0,05	0,08	0,05	0,04	0,07	0,04	0,05
Na2O	0,33	0,36	0,40	0,33	0,33	0,45	0,32	0,37	0,38	0,34	0,39	0,37	0,35
K2O	10,00	9,82	10,01	9,99	9,98	9,95	10,00	9,93	10,08	9,91	10,04	9,94	10,03
Total	94,90	94,88	94,98	95,35	95,57	95,18	95,63	95,18	95,27	95,39	95,35	95,34	95,68
Si	4,865	4,856	4,863	4,825	4,848	4,867	4,871	4,859	4,881	4,899	4,859	4,805	4,797
Al	2,451	2,437	2,465	2,449	2,453	2,424	2,434	2,452	2,409	2,422	2,431	2,437	2,427
Cr	0,577	0,590	0,576	0,583	0,583	0,587	0,576	0,585	0,580	0,584	0,581	0,597	0,604
Ti	0,793	0,769	0,785	0,802	0,783	0,791	0,806	0,790	0,785	0,786	0,781	0,825	0,820
Mg	0,004	0,008	0,004	0,005	0,002	0,000	0,003	0,002	0,007	0,005	0,004	0,003	0,003
Fe2+	3,717	3,755	3,708	3,771	3,748	3,717	3,711	3,708	3,722	3,702	3,739	3,670	3,666
Mn	0,021	0,028	0,019	0,025	0,028	0,030	0,034	0,027	0,031	0,019	0,030	0,101	0,115
Ca	0,008	0,005	0,005	0,010	0,007	0,005	0,007	0,011	0,007	0,005	0,010	0,005	0,007
Na	0,084	0,091	0,101	0,085	0,085	0,116	0,080	0,094	0,097	0,087	0,099	0,095	0,090
K	1,688	1,655	1,688	1,681	1,673	1,674	1,676	1,670	1,695	1,661	1,688	1,678	1,687
mg*	82,34	82,86	82,46	82,38	82,69	82,45	82,10	82,39	82,44	82,40	82,64	81,58	81,67

	#14	#15	#16	#17	#18	#19	#20	#21	#22	#23	#24	#25	#26
SiO2	36,55	36,03	36,44	35,91	35,82	35,86	34,80	36,88	37,19	36,91	36,90	36,49	36,59
TiO2	6,05	6,01	6,03	6,35	6,40	6,50	8,61	5,81	5,78	5,79	5,88	5,99	6,02
Al2O3	15,45	15,74	15,63	15,51	15,50	15,62	15,48	15,89	16,02	15,77	15,74	15,89	15,79
Cr2O3	1,00	1,09	1,06	0,32	0,24	0,21	0,00	0,27	0,27	0,22	0,45	0,99	0,99
FeO	7,26	7,32	7,54	8,37	8,70	8,56	9,18	7,39	7,37	7,43	7,16	7,11	7,09
MnO	0,07	0,00	0,04	0,07	0,06	0,05	0,09	0,09	0,00	0,06	0,02	0,07	0,03
MgO	18,41	18,71	18,41	17,97	18,05	17,98	16,33	18,69	19,09	19,02	18,84	18,55	18,39
CaO	0,03	0,04	0,05	0,04	0,05	0,09	0,12	0,07	0,06	0,11	0,05	0,06	0,07
Na2O	0,39	0,38	0,43	0,47	0,38	0,42	0,44	0,36	0,26	0,33	0,41	0,30	0,35
K2O	9,91	9,86	9,89	9,50	9,59	9,56	9,26	9,94	9,93	9,88	9,89	9,82	9,66
Total	95,11	95,16	95,51	94,51	94,78	94,85	94,31	95,38	95,96	95,52	95,34	95,27	94,97
Si	4,841	4,774	4,814	4,802	4,785	4,782	4,688	4,859	4,862	4,856	4,859	4,816	4,838
Al	2,412	2,458	2,434	2,445	2,440	2,456	2,457	2,468	2,469	2,444	2,444	2,472	2,461
Cr	0,603	0,599	0,599	0,639	0,644	0,652	0,872	0,576	0,568	0,573	0,583	0,594	0,599
Ti	0,804	0,811	0,833	0,936	0,971	0,955	1,034	0,815	0,806	0,817	0,788	0,785	0,784
Mg	0,007	0,000	0,004	0,008	0,007	0,005	0,011	0,010	0,000	0,007	0,002	0,008	0,003
Fe2+	3,634	3,697	3,625	3,581	3,594	3,575	3,279	3,670	3,720	3,730	3,700	3,651	3,624
Mn	0,105	0,114	0,110	0,034	0,025	0,022	0,000	0,028	0,027	0,023	0,047	0,103	0,103
Ca	0,005	0,005	0,007	0,006	0,007	0,013	0,017	0,010	0,008	0,015	0,007	0,009	0,010
Na	0,099	0,097	0,109	0,121	0,099	0,108	0,114	0,091	0,067	0,085	0,106	0,077	0,090
K	1,674	1,666	1,667	1,620	1,634	1,627	1,592	1,670	1,656	1,659	1,661	1,653	1,630
mg*	81,75	82,01	81,23	79,14	78,61	78,84	75,84	81,64	82,19	81,91	82,40	82,16	82,16

	#27	#28	#29	#30	#31	#32	#33	#34	#35	#36	#37	#38	#39
SiO2	36,35	36,03	36,10	36,08	36,20	36,20	36,27	36,01	35,46	34,37		35,61	35,56
TiO2	5,95	6,45	6,43	6,42	6,45	6,46	6,69	6,49	6,72	8,31		6,89	6,83
Al2O3	15,77	15,73	15,78	15,78	15,79	15,68	15,96	15,72	15,77	15,20		15,32	15,42
Cr2O3	0,97	0,27	0,24	0,19	0,20	0,24	0,18	0,21	0,11	0,00		0,09	0,09
FeO	7,64	8,57	8,51	8,70	8,75	8,91	8,69	8,81	8,91	11,45		8,74	8,64
MnO	0,02	0,02	0,03	0,04	0,05	0,07	0,08	0,07	0,10	0,14		0,07	0,07
MgO	18,38	17,80	18,01	17,71	18,18	18,08	18,01	17,95	17,66	14,72		17,65	17,62
CaO	0,09	0,08	0,07	0,08	0,09	0,10	0,07	0,08	0,07	0,18		0,17	0,13
Na2O	0,40	0,33	0,45	0,38	0,43	0,42	0,41	0,45	0,45	0,39		0,52	0,47
K2O	9,63	9,54	9,66	9,57	9,56	9,56	9,53	9,53	9,45	9,13		9,60	9,44
Total	95,20	94,84	95,26	94,95	95,69	95,71	95,89	95,31	94,70	93,86		94,65	94,25
Si	4,811	4,800	4,791	4,804	4,784	4,789	4,780	4,782	4,746	4,704		4,771	4,775
Al	2,460	2,470	2,468	2,476	2,459	2,444	2,479	2,461	2,487	2,451		2,419	2,441
Cr	0,592	0,647	0,642	0,643	0,642	0,643	0,663	0,648	0,676	0,856		0,695	0,690
Ti	0,845	0,955	0,944	0,969	0,967	0,985	0,958	0,978	0,997	1,310		0,979	0,970
Mg	0,002	0,002	0,003	0,004	0,005	0,008	0,009	0,008	0,012	0,016		0,008	0,008
Fe2+	3,627	3,536	3,563	3,516	3,582	3,565	3,538	3,553	3,524	3,003		3,526	3,528
Mn	0,101	0,029	0,025	0,020	0,021	0,025	0,019	0,022	0,011	0,000		0,009	0,009
Ca	0,012	0,012	0,010	0,012	0,013	0,014	0,010	0,012	0,010	0,026		0,024	0,019
Na	0,102	0,086	0,117	0,099	0,110	0,108	0,104	0,117	0,118	0,105		0,136	0,121
K	1,626	1,621	1,635	1,626	1,612	1,613	1,602	1,615	1,613	1,594		1,641	1,617
mg*	81,06	78,70	78,99	78,32	78,65	78,21	78,54	78,29	77,74	69,37		78,12	78,29

	#40	#41	#42	#43	#44	#45	#46	#47	#48	#49	#50	#51	#52
SiO2	35,53	35,40	35,66	36,28	35,83	35,60	35,69	35,74	35,49	35,48	34,86	34,93	35,21
TiO2	6,86	6,71	6,80	6,96	7,07	7,15	6,94	6,89	6,72	6,58	6,55	6,58	6,66
Al2O3	15,29	15,38	15,45	15,56	15,54	15,53	15,59	15,54	15,62	15,42	15,35	15,34	15,37
Cr2O3	0,08	0,06	0,11	0,10	0,00	0,01	0,03	0,00	0,01	0,00	0,00	0,06	0,00
FeO	8,76	9,13	8,50	8,53	8,51	8,35	8,43	8,76	9,77	10,55	11,49	11,98	12,14
MnO	0,07	0,04	0,08	0,07	0,09	0,08	0,07	0,09	0,12	0,14	0,12	0,15	0,15
MgO	17,41	17,37	17,55	17,81	17,40	17,44	17,70	17,37	17,27	16,41	15,62	15,51	15,26
CaO	0,15	0,19	0,27	0,15	0,11	0,11	0,09	0,10	0,07	0,09	0,07	0,06	0,04
Na2O	0,40	0,38	0,51	0,50	0,46	0,45	0,50	0,48	0,49	0,51	0,56	0,63	0,62
K2O	9,40	9,25	9,38	9,49	9,47	9,63	9,59	9,46	9,50	9,22	9,25	9,19	9,23
Total	93,94	93,92	94,32	95,45	94,49	94,36	94,62	94,46	95,05	94,39	93,87	94,44	94,67
Si	4,789	4,777	4,783	4,802	4,793	4,773	4,771	4,789	4,753	4,795	4,768	4,760	4,785
Al	2,429	2,446	2,443	2,428	2,450	2,454	2,457	2,455	2,466	2,456	2,475	2,464	2,462
Cr	0,695	0,682	0,687	0,693	0,712	0,721	0,698	0,695	0,677	0,669	0,674	0,675	0,681
Ti	0,987	1,031	0,954	0,944	0,952	0,936	0,942	0,982	1,094	1,193	1,314	1,366	1,379
Mg	0,008	0,005	0,009	0,008	0,010	0,009	0,008	0,011	0,013	0,016	0,013	0,017	0,017
Fe2+	3,498	3,495	3,510	3,514	3,470	3,486	3,528	3,470	3,447	3,306	3,184	3,151	3,091
Mn	0,009	0,007	0,011	0,010	0,000	0,001	0,003	0,000	0,001	0,000	0,000	0,006	0,000
Ca	0,022	0,027	0,039	0,022	0,016	0,016	0,013	0,015	0,009	0,013	0,010	0,009	0,006
Na	0,103	0,099	0,132	0,128	0,120	0,117	0,128	0,125	0,128	0,132	0,148	0,168	0,162
K	1,616	1,593	1,606	1,603	1,616	1,648	1,636	1,618	1,623	1,589	1,614	1,597	1,600
mg*	77,85	77,15	78,48	78,68	78,30	78,68	78,79	77,76	75,69	73,23	70,57	69,50	68,89

	#53	#54	#55	#56	#57	#58	#59	#60	#61	#62	#63	#64	#65
SiO2	35,27	34,73	35,17	35,08	35,30	35,29	34,95	34,69	35,05	35,44	35,55	35,09	35,18
TiO2	6,69	6,72	6,66	6,65	6,78	6,81	6,92	6,81	6,95	6,83	6,64	6,79	6,80
Al2O3	15,17	15,25	15,19	15,21	15,27	15,18	15,21	15,27	15,01	15,06	15,12	15,06	15,21
Cr2O3	0,02	0,02	0,00	0,00	0,03	0,00	0,00	0,00	0,00	0,03	0,00	0,01	0,00
FeO	12,57	12,44	12,57	12,68	12,53	12,51	12,53	12,47	12,69	12,32	12,50	12,30	12,32
MnO	0,17	0,22	0,19	0,16	0,15	0,18	0,14	0,14	0,19	0,15	0,15	0,16	0,14
MgO	15,06	15,10	14,96	15,15	15,14	15,31	14,86	15,09	14,91	15,03	15,21	15,13	15,14
CaO	0,09	0,06	0,05	0,06	0,07	0,32	0,15	0,11	0,10	0,09	0,08	0,11	0,08
Na2O	0,59	0,63	0,66	0,60	0,63	0,57	0,54	0,60	0,61	0,65	0,66	0,59	0,62
K2O	9,20	9,14	9,16	9,22	9,15	9,00	9,11	9,07	9,12	9,24	9,29	9,20	9,33
Total	94,81	94,30	94,60	94,80	95,04	95,17	94,42	94,24	94,63	94,83	95,19	94,43	94,81
Si	4,796	4,753	4,794	4,776	4,785	4,778	4,773	4,747	4,781	4,812	4,813	4,788	4,783
Al	2,431	2,460	2,440	2,441	2,440	2,421	2,448	2,463	2,414	2,411	2,412	2,423	2,437
Cr	0,684	0,692	0,683	0,681	0,692	0,693	0,711	0,701	0,714	0,698	0,677	0,697	0,695
Ti	1,429	1,424	1,432	1,444	1,420	1,416	1,431	1,427	1,447	1,399	1,415	1,403	1,401
Mg	0,020	0,025	0,021	0,018	0,017	0,021	0,016	0,016	0,022	0,017	0,017	0,018	0,016
Fe2+	3,053	3,080	3,040	3,076	3,060	3,090	3,026	3,078	3,032	3,044	3,069	3,079	3,068
Mn	0,002	0,002	0,000	0,000	0,003	0,000	0,000	0,000	0,000	0,003	0,000	0,001	0,000
Ca	0,013	0,008	0,008	0,008	0,010	0,046	0,022	0,016	0,014	0,013	0,012	0,017	0,012
Na	0,156	0,167	0,174	0,159	0,165	0,149	0,142	0,159	0,161	0,170	0,172	0,157	0,163
K	1,596	1,596	1,592	1,601	1,583	1,555	1,588	1,584	1,587	1,601	1,605	1,601	1,619
mg*	67,81	68,00	67,65	67,79	68,04	68,25	67,64	68,07	67,35	68,26	68,18	68,41	68,41

	#66	#67	#68	#69	#70	#71	#72	#73	#74	#75	#76	#77	#78
SiO2	35,71	35,34	35,64	35,81	35,72	35,46	35,50	35,18	35,35	36,01	35,97	36,07	35,66
TiO2	6,76	6,73	6,63	6,76	6,57	6,56	6,49	6,58	6,51	7,17	7,21	7,36	7,56
Al2O3	15,17	15,02	15,26	15,20	15,40	15,22	15,33	15,41	15,51	15,63	15,36	15,55	15,47
Cr2O3	0,00	0,00	0,01	0,01	0,02	0,00	0,03	0,00	0,00	0,00	0,00	0,04	0,03
FeO	12,45	12,42	12,10	12,13	12,27	12,16	11,62	11,20	10,24	8,65	8,55	8,53	8,58
MnO	0,22	0,17	0,13	0,15	0,10	0,14	0,12	0,09	0,12	0,09	0,09	0,08	0,05
MgO	15,13	15,28	15,33	15,40	15,45	15,67	15,91	15,93	16,46	17,53	17,57	17,43	17,39
CaO	0,08	0,06	0,06	0,10	0,08	0,10	0,07	0,09	0,07	0,10	0,08	0,08	0,06
Na2O	0,56	0,55	0,49	0,58	0,55	0,52	0,59	0,51	0,53	0,52	0,45	0,46	0,41
K2O	9,32	9,32	9,37	9,19	9,48	9,32	9,31	9,29	9,30	9,42	9,55	9,51	9,53
Total	95,39	94,87	95,02	95,32	95,62	95,15	94,98	94,27	94,10	95,13	94,85	95,10	94,74
Si	4,821	4,802	4,821	4,826	4,808	4,795	4,796	4,780	4,789	4,785	4,797	4,792	4,763
Al	2,415	2,405	2,432	2,414	2,442	2,426	2,442	2,467	2,476	2,448	2,414	2,435	2,435
Cr	0,687	0,688	0,675	0,685	0,665	0,668	0,659	0,673	0,663	0,717	0,723	0,736	0,759
Ti	1,406	1,411	1,369	1,367	1,381	1,374	1,313	1,273	1,160	0,962	0,954	0,948	0,958
Mg	0,025	0,019	0,015	0,017	0,011	0,016	0,014	0,010	0,014	0,010	0,011	0,009	0,006
Fe2+	3,045	3,095	3,092	3,093	3,099	3,159	3,205	3,227	3,324	3,473	3,493	3,453	3,462
Mn	0,000	0,000	0,001	0,001	0,002	0,000	0,004	0,000	0,000	0,000	0,000	0,005	0,003
Ca	0,011	0,008	0,009	0,014	0,012	0,015	0,010	0,013	0,010	0,014	0,011	0,011	0,008
Na	0,146	0,144	0,129	0,151	0,144	0,137	0,153	0,135	0,140	0,133	0,117	0,117	0,106
K	1,604	1,615	1,617	1,580	1,628	1,607	1,605	1,610	1,607	1,597	1,625	1,613	1,623
mg*	68,04	68,40	69,08	69,08	69,01	69,44	70,72	71,56	73,89	78,14	78,36	78,31	78,21

	#79	#80	#81	#82	#83	#84	#85	#86	#87	#88	#89	#90	#91
SiO2	35,46	35,92	35,17	35,29	35,35	34,68	35,61	35,08	34,96	35,26	35,20	34,94	35,07
TiO2	7,03	7,01	8,48	7,41	6,73	6,58	6,53	6,53	6,53	6,51	6,43	6,49	6,55
Al2O3	15,61	15,64	15,47	15,50	15,40	15,42	15,39	15,27	15,29	15,61	15,40	15,42	15,55
Cr2O3	0,03	0,03	0,00	0,00	0,01	0,00	0,03	0,03	0,01	0,00	0,03	0,03	0,00
FeO	8,64	8,89	9,33	10,62	11,39	11,58	11,49	11,48	11,46	11,64	11,69	11,62	11,56
MnO	0,06	0,08	0,06	0,10	0,11	0,14	0,12	0,14	0,11	0,12	0,13	0,16	0,16
MgO	17,51	17,53	16,13	16,36	15,63	15,89	15,85	15,67	15,68	15,85	15,82	15,61	15,81
CaO	0,08	0,12	0,09	0,11	0,04	0,01	0,00	0,03	0,03	0,03	0,03	0,03	0,02
Na2O	0,50	0,45	0,52	0,48	0,66	0,60	0,42	0,53	0,59	0,59	0,58	0,55	0,61
K2O	9,51	9,66	9,16	8,63	9,16	9,18	9,12	9,03	9,06	9,06	8,95	8,97	9,14
Total	94,42	95,31	94,40	94,48	94,48	94,07	94,55	93,78	93,72	94,67	94,27	93,81	94,48
Si	4,756	4,776	4,727	4,751	4,792	4,736	4,818	4,792	4,782	4,773	4,785	4,775	4,761
Al	2,467	2,450	2,451	2,459	2,462	2,482	2,453	2,459	2,465	2,491	2,467	2,483	2,488
Cr	0,709	0,701	0,858	0,750	0,686	0,676	0,665	0,672	0,672	0,662	0,658	0,667	0,669
Ti	0,968	0,988	1,049	1,195	1,292	1,323	1,300	1,311	1,311	1,318	1,329	1,328	1,313
Mg	0,006	0,009	0,007	0,012	0,012	0,016	0,013	0,016	0,013	0,014	0,015	0,018	0,018
Fe2+	3,501	3,474	3,232	3,283	3,159	3,234	3,196	3,191	3,198	3,197	3,207	3,181	3,201
Mn	0,003	0,004	0,000	0,000	0,001	0,000	0,003	0,003	0,001	0,000	0,003	0,003	0,000
Ca	0,011	0,016	0,013	0,015	0,005	0,002	0,000	0,004	0,004	0,004	0,005	0,004	0,003
Na	0,130	0,115	0,134	0,126	0,174	0,158	0,109	0,141	0,157	0,156	0,152	0,146	0,161
K	1,627	1,638	1,571	1,483	1,585	1,599	1,574	1,574	1,580	1,564	1,552	1,564	1,584
mg*	78,22	77,70	75,37	73,12	70,78	70,73	70,88	70,62	70,73	70,59	70,46	70,26	70,63

	#92	#93	#94	#95	#96	#97	#98	#99	#100	#101	#102	#103	#104
SiO2	35,05	34,91	34,78	35,08	35,39	35,20	35,01	34,99	35,36	35,74	35,73	35,81	35,95
TiO2	6,49	6,42	6,35	6,38	6,41	6,42	6,42	6,51	6,60	6,42	6,35	6,40	6,39
Al2O3	15,39	15,52	15,65	15,57	15,50	15,44	15,38	15,58	15,57	15,68	15,61	15,67	15,62
Cr2O3	0,01	0,01	0,00	0,00	0,00	0,02	0,04	0,00	0,02	0,23	0,24	0,22	0,21
FeO	11,67	11,63	11,58	11,43	11,27	11,42	11,58	11,43	10,60	8,24	8,32	8,47	8,41
MnO	0,12	0,13	0,14	0,14	0,14	0,11	0,08	0,09	0,05	0,01	0,04	0,03	0,05
MgO	15,71	15,68	15,65	15,61	15,56	15,62	15,68	15,91	16,39	18,17	17,94	17,92	17,79
CaO	0,03	0,05	0,07	0,04	0,02	0,02	0,02	0,04	0,04	0,02	0,01	0,03	0,04
Na2O	0,60	0,61	0,61	0,59	0,58	0,58	0,58	0,56	0,45	0,40	0,41	0,38	0,41
K2O	8,89	8,93	8,97	9,03	9,09	9,08	9,08	9,09	9,29	9,46	9,62	9,57	9,48
Total	93,98	93,88	93,79	93,87	93,96	93,91	93,85	94,19	94,37	94,36	94,25	94,50	94,35
Si	4,779	4,77	4,755	4,79	4,817	4,80	4,782	4,759	4,780	4,779	4,791	4,790	4,811
Al	2,474	2,50	2,521	2,50	2,486	2,48	2,476	2,498	2,481	2,471	2,467	2,470	2,463
Cr	0,666	0,66	0,653	0,66	0,657	0,66	0,660	0,666	0,671	0,646	0,640	0,644	0,644
Ti	1,331	1,33	1,324	1,30	1,283	1,30	1,323	1,300	1,198	0,921	0,933	0,947	0,941
Mg	0,013	0,01	0,016	0,02	0,016	0,01	0,009	0,010	0,006	0,001	0,004	0,004	0,006
Fe2+	3,194	3,19	3,190	3,17	3,158	3,18	3,193	3,226	3,303	3,623	3,585	3,573	3,550
Mn	0,001	0,00	0,000	0,00	0,000	0,00	0,004	0,000	0,002	0,024	0,025	0,023	0,022
Ca	0,005	0,01	0,010	0,01	0,002	0,00	0,002	0,006	0,005	0,003	0,001	0,004	0,005
Na	0,160	0,16	0,161	0,16	0,153	0,15	0,153	0,147	0,119	0,102	0,106	0,099	0,106
K	1,547	1,56	1,564	1,57	1,577	1,58	1,582	1,576	1,602	1,613	1,645	1,633	1,618
mg*	70,37	70,39	70,42	70,63	70,85	70,71	70,57	71,12	73,28	79,71	79,28	78,98	78,94

	#105	#106	#107	#108	#109	#110	#111	#112	#113	#114	#115	#116	#117
SiO2	36,13	35,95	35,96	35,98	35,88	35,38	36,12	35,85	35,78	35,94	36,13	36,15	35,70
TiO2	6,47	6,26	6,41	6,53	6,52	6,49	6,60	6,70	6,36	6,39	6,33	6,51	6,49
Al2O3	15,67	15,60	15,50	15,69	15,63	15,34	15,40	15,28	15,63	15,56	15,39	15,50	15,42
Cr2O3	0,21	0,26	0,24	0,27	0,27	0,28	0,12	0,07	0,20	0,22	0,18	0,05	0,11
FeO	8,21	8,24	8,54	8,39	8,38	8,33	8,52	8,55	8,52	8,56	8,34	8,53	8,54
MnO	0,07	0,04	0,01	0,09	0,04	0,10	0,01	0,05	0,07	0,07	0,07	0,05	0,03
MgO	17,90	17,73	18,08	17,74	17,77	17,66	17,82	17,98	17,98	17,92	17,86	17,82	17,72
CaO	0,02	0,01	0,05	0,00	0,05	0,06	0,02	0,04	0,00	0,01	0,01	0,05	0,05
Na2O	0,40	0,42	0,42	0,42	0,41	0,41	0,43	0,40	0,43	0,44	0,43	0,44	0,46
K2O	9,52	9,50	9,41	9,36	9,54	9,49	9,56	9,51	9,55	9,27	9,52	9,58	9,48
Total	94,60	94,00	94,60	94,46	94,48	93,52	94,61	94,42	94,52	94,38	94,25	94,67	93,98
Si	4,816	4,824	4,801	4,806	4,798	4,786	4,823	4,801	4,787	4,806	4,838	4,824	4,802
Al	2,461	2,468	2,439	2,469	2,463	2,446	2,423	2,411	2,465	2,453	2,429	2,438	2,445
Cr	0,649	0,632	0,643	0,656	0,656	0,660	0,663	0,675	0,640	0,643	0,638	0,653	0,656
Ti	0,915	0,924	0,953	0,937	0,937	0,942	0,951	0,957	0,953	0,957	0,934	0,952	0,961
Mg	0,008	0,004	0,001	0,010	0,005	0,011	0,001	0,005	0,008	0,008	0,008	0,005	0,004
Fe2+	3,557	3,547	3,598	3,532	3,541	3,561	3,547	3,589	3,587	3,573	3,566	3,544	3,554
Mn	0,022	0,027	0,026	0,028	0,028	0,029	0,013	0,008	0,021	0,024	0,019	0,005	0,012
Ca	0,003	0,002	0,007	0,000	0,007	0,009	0,003	0,006	0,000	0,001	0,001	0,008	0,007
Na	0,104	0,108	0,108	0,110	0,107	0,108	0,112	0,104	0,111	0,114	0,111	0,113	0,119
K	1,618	1,627	1,603	1,594	1,628	1,637	1,629	1,624	1,630	1,582	1,626	1,631	1,627
mg*	79,40	79,25	79,03	78,85	79,00	78,89	78,84	78,85	78,87	78,73	79,11	78,74	78,66

	#118	#119	#120	#121	#122
SiO2	35,91	36,27	35,93	35,48	35,37
TiO2	6,50	6,43	6,58	7,89	8,04
Al2O3	15,59	15,51	15,23	15,24	15,39
Cr2O3	0,08	0,08	0,03	0,04	0,00
FeO	8,52	9,02	9,00	8,81	8,91
MnO	0,08	0,09	0,08	0,11	0,06
MgO	17,83	17,49	17,64	17,25	16,49
CaO	0,04	0,06	0,05	0,09	0,08
Na2O	0,50	0,47	0,47	0,45	0,42
K2O	9,40	9,42	9,41	9,14	9,09
Total	94,45	94,82	94,42	94,50	93,85
Si	4,802	4,838	4,819	4,751	4,766
Al	2,457	2,438	2,407	2,405	2,444
Cr	0,654	0,646	0,664	0,794	0,815
Ti	0,953	1,006	1,009	0,987	1,005
Mg	0,009	0,011	0,009	0,012	0,007
Fe2+	3,555	3,477	3,528	3,443	3,313
Mn	0,009	0,008	0,003	0,004	0,000
Ca	0,006	0,009	0,007	0,013	0,012
Na	0,129	0,120	0,123	0,118	0,111
K	1,603	1,602	1,610	1,562	1,562
mg*	78,71	77,38	77,60	77,51	76,62

Biotite Single Spot EMP Analyses

	#1	#2	#3	#4	#5	#6	#7	#8	#9	#10	#11	#12	#13
SiO2	36,7	35,31	33,14	35,25	35,55	34,76	37,8	37,01	36,51	35,92	35,24	36	34,37
TiO2	5,86	8,19	8,34	6,72	6,41	7,77	5,78	6	6,45	8,05	6,98	7,2	8,82
Al2O3	16,23	15,41	14,96	15,42	15,61	15,21	16,15	15,74	15,63	15,29	15,19	15,63	15,57
Cr2O3	0,1	0	0	0,04	0,22	0,01	0,25	1,1	0,18	0,02	0,02	0	0,04
FeO	8,11	8,55	17,82	11,42	8,47	9,73	7,25	7,24	8,65	9,05	12,49	8,66	9,51
MnO	0,03	0,1	0,33	0,14	0,07	0,11	0,03	0,05	0,04	0,07	0,14	0,06	0,1
MgO	18,32	16,83	10,12	15,87	17,74	16,66	19,47	18,74	17,93	16,81	15,04	17,78	16,04
CaO	0	0,08	0,06	0,02	0,07	0,07	0,09	0,05	0,07	0,09	0,05	0,16	0,14
Na2O	0,4	0,49	0,44	0,61	0,35	0,51	0,31	0,39	0,43	0,49	0,64	0,47	0,5
K2O	9,7	9,15	8,89	8,97	9,51	9,21	9,79	9,78	9,54	9,12	9,22	9,58	9,03
Total	95,44	94,1	94,09	94,46	93,99	94,04	96,9	96,1	95,44	94,9	95	95,54	94,11
Si	4,838	4,743	4,678	4,777	4,783	4,71	4,881	4,842	4,83	4,786	4,782	4,768	4,648
Al	2,521	2,44	2,489	2,463	2,476	2,428	2,458	2,426	2,438	2,401	2,429	2,439	2,48
Ti	0,581	0,827	0,886	0,686	0,649	0,792	0,561	0,591	0,642	0,807	0,713	0,718	0,897
Fe2+	0,894	0,96	2,103	1,294	0,953	1,102	0,782	0,792	0,958	1,008	1,417	0,959	1,075
Mn	0,003	0,011	0,04	0,016	0,008	0,012	0,003	0,005	0,004	0,008	0,016	0,007	0,011
Mg	3,6	3,371	2,129	3,206	3,557	3,365	3,747	3,654	3,537	3,34	3,043	3,511	3,234
Cr	0,01	0	0	0,004	0,023	0,001	0,026	0,114	0,019	0,002	0,002	0	0,004
Ca	0	0,011	0,008	0,003	0,01	0,01	0,012	0,007	0,01	0,013	0,007	0,023	0,02
Na	0,102	0,127	0,12	0,159	0,09	0,134	0,077	0,099	0,111	0,126	0,169	0,122	0,13
K	1,631	1,568	1,6	1,551	1,632	1,593	1,613	1,632	1,611	1,55	1,596	1,619	1,558
Mg#	80	77,6	49,8	71	78,7	75,1	82,7	82,1	78,6	76,7	68	78,4	74,9

	#14	#15	#16	#17	#18	#19	#20	#21	#22	#23	#24	#25	#26
SiO2	36,81	36,51	35,3	36,69	36,16	35,75	34,5	35,1	35,6	35,36	35,19	34,58	36,41
TiO2	6,06	6,09	8,45	5,95	6,08	6,53	8,37	6,8	6,91	8,21	7,45	7,6	5,85
Al2O3	16,1	16,03	15,42	15,74	15,67	15,55	14,99	15,43	16,06	15,34	15,3	15,22	16,05
Cr2O3	0,13	0,13	0	0,29	1,02	0,24	0,01	0,01	0,03	0	0	0,05	0,06
FeO	8,21	7,78	9,07	7,06	7,32	8,53	9,42	11,84	8,73	9,65	7,79	8,29	7,62
MnO	0,07	0,05	0,07	0,03	0	0,04	0,05	0,12	0,06	0,11	0,07	0,11	0,06
MgO	18,55	18,48	16,65	18,94	18,89	18,14	16,29	16,09	17,7	16,51	17,91	17,71	18,44
CaO	0,08	0,09	0,61	0,03	0,02	0,04	0,4	0,01	0,09	0,08	0,05	0,04	0
Na2O	0,41	0,42	0,46	0,36	0,44	0,41	0,47	0,67	0,44	0,48	0,46	0,45	0,42
K2O	9,55	9,77	8,95	9,91	9,58	9,61	9,26	9,04	9,16	9,14	8,96	9	9,77
Total	95,96	95,34	94,97	94,99	95,18	94,84	93,76	95,09	94,78	94,87	93,17	93,06	94,68
Si	4,828	4,819	4,711	4,848	4,782	4,771	4,69	4,739	4,743	4,735	4,751	4,698	4,834
Al	2,488	2,494	2,426	2,452	2,442	2,446	2,402	2,455	2,521	2,421	2,435	2,437	2,512
Ti	0,598	0,605	0,848	0,592	0,605	0,655	0,856	0,691	0,692	0,827	0,757	0,777	0,584
Fe2+	0,9	0,859	1,012	0,78	0,81	0,952	1,071	1,337	0,972	1,08	0,879	0,942	0,847
Mn	0,007	0,005	0,008	0,004	0	0,004	0,006	0,013	0,007	0,012	0,008	0,012	0,007
Mg	3,627	3,638	3,313	3,73	3,725	3,609	3,302	3,238	3,516	3,296	3,606	3,587	3,65
Cr	0,013	0,014	0	0,031	0,107	0,025	0,001	0,001	0,003	0	0	0,005	0,007
Ca	0,012	0,012	0,087	0,004	0,003	0,005	0,059	0,001	0,013	0,011	0,008	0,006	0
Na	0,105	0,106	0,119	0,091	0,112	0,106	0,124	0,176	0,113	0,125	0,12	0,12	0,107
K	1,597	1,645	1,523	1,67	1,617	1,637	1,606	1,557	1,557	1,562	1,543	1,559	1,655
Mg#	80	80,8	76,5	82,6	82,1	79,1	75,4	70,6	78,2	75,1	80,3	79	81,1

	#27	#28	#29	#30	#31	#32	#33	#34
SiO2	35,06	34,34	34,27	35,71	35,11	34,7	35,22	36,25
TiO2	6,94	7,03	7,31	6,91	6,93	7,18	6,32	5,75
Al2O3	15,69	15,74	16,09	15,68	16,1	16,23	15,34	16
Cr2O3	0	0,01	0	0,02	0	0	0,02	0,02
FeO	8,37	9,15	8,65	8,2	9,52	8,95	13,18	9,43
MnO	0,07	0,08	0,06	0,12	0,11	0,09	0,27	0,05
MgO	17,73	16,87	17,11	17,99	17,3	17,21	14,37	17,45
CaO	0,06	0,08	0,06	0,1	0,04	0,08	0,02	0,07
Na2O	0,53	0,53	0,49	0,5	0,53	0,52	0,4	0,46
K2O	9,23	9,03	8,9	9,02	9,38	8,96	9,14	9,45
Total	93,67	92,86	92,93	94,25	95,01	93,92	94,26	94,93
Si	4,73	4,694	4,663	4,771	4,697	4,676	4,826	4,835
Al	2,494	2,535	2,58	2,469	2,539	2,578	2,476	2,515
Ti	0,705	0,723	0,748	0,694	0,697	0,728	0,651	0,577
Fe2+	0,944	1,046	0,984	0,916	1,065	1,009	1,51	1,051
Mn	0,008	0,01	0,007	0,014	0,012	0,01	0,031	0,006
Mg	3,565	3,438	3,47	3,584	3,451	3,457	2,934	3,47
Cr	0	0,001	0	0,002	0	0	0,002	0,002
Ca	0,009	0,011	0,009	0,015	0,006	0,011	0,003	0,01
Na	0,138	0,14	0,129	0,13	0,138	0,137	0,105	0,118
K	1,588	1,574	1,546	1,537	1,601	1,54	1,597	1,608
Mg#	78,9	76,5	77,8	79,4	76,2	77,2	65,6	76,6